ENGINEERING A PLATFORM TO HARNESS PLURIPOTENT STEM CELL-DERIVED PARACRINE FACTORS

A Dissertation
Presented to
The Academic Faculty

by

Jenna L. Wilson

In Partial Fulfillment
Of the Requirements for the Degree
Doctor of Philosophy in Bioengineering

Georgia Institute of Technology

December 2015

ENGINEERING A PLATFORM TO HARNESS PLURIPOTENT STEM CELL-DERIVED PARACRINE FACTORS

Approved by:

Dr. Todd McDevitt, Advisor
Gladstone Institute of Cardiovascular Disease
Gladstone Institutes

Dr. Athanassios Sambanis
School of Chemical & Biomolecular Engineering
Georgia Institute of Technology

Dr. Edward Botchwey
Department of Biomedical Engineering
Georgia Institute of Technology

Dr. Edmund Waller
Department of Hematology & Oncology
Emory University

Dr. Krishnendu Roy
Department of Biomedical Engineering
Georgia Institute of Technology

Date Approved: 10/26/2015

To my family – parents Tim and Julie, sister Zoe, boyfriend Chris,
and four-legged personal therapists – for their encouragement and support

ACKNOWLEDGEMENTS

I would like to begin by thanking my advisor, Dr. Todd McDevitt, for being there for me along every step of my Ph.D. journey. Though he was ironically not on my radar when I initially applied to Georgia Tech, Todd was scheduled as my final faculty interview during my recruitment visit, and the extra time afforded by this last time slot provided ample time to speak with each other (even though it made me late to dinner). I had been through 10-15 similar meetings at while visiting Georgia Tech and other schools, but this one felt different -- perhaps it is appropriate that my final interview was the end of a winding road that led me to my Ph.D. advisor. I have a vivid memory of getting on the plane from Atlanta back to Oregon and just *knowing* that Georgia Tech, and more specifically the McDevitt lab, was where I was going to be. Looking back five and a half years later, there are no regrets – though I clearly had no idea what I was getting myself into. I couldn't have foreseen the anxiety that comes with the expectation to act independently when I still felt so unprepared, the expectation to write research grants and review papers less than one year into graduate school, the expectation to take no published data at face value. On the other hand, I also couldn't have anticipated the way in which these stresses and pressures would shape me into an independent scientist and provide me with the confidence to tackle diverse challenges. In addition to growing as a scientist, I also have to credit Todd for constantly improving my technical writing. I'll admit that the first document I received his edits on was a blow to my pride – never had I seen so many edits and comments! With time, however, I began to appreciate how lucky I was to have an advisor who really would read every single word (usually multiple times) and provide

helpful feedback so that we could present the best product possible. In addition to being a fantastic scientific mentor, Todd has really developed into a true friend, and I will be forever grateful for his company (as well as the company of his amazing wife Meg!) when I moved out to San Francisco one month ahead of the rest of the research group. The lab is now at an interesting transition point, and I'm so excited to see how Todd will shape the research focus moving forward.

I would also like to thank the members of my thesis committee for their insight into my project. Dr. Edward Botchwey has always shown great enthusiasm for the overall concept of my project, and the expertise his lab has in working with hematopoietic stem and progenitor cells was essential for the completion of my project. I have to specifically thank his post-doc Dr. Molly Ogle for her help with my studies. I know that she has many projects that she's working on, and it means a great deal that she was still happy to help me out. I was also lucky to have the mentorship of Dr. Krishnendu Roy, and I really appreciate his many questions and suggestions, both at the broad, high level and at the level of technical details. I am very grateful that Dr. Athanassios Sambanis agreed to be on my thesis committee even though he was away from Georgia Tech and had to go out of his way to teleconference in to our discussions. I took two courses from Dr. Sambanis during grad school, including my favorite course (Stem Cell Bioprocessing), and I sincerely appreciate his emphasis on critical thinking and strong engineering principles. Finally, I am very appreciative that Dr. Edmund Waller took time out of his extremely busy clinical and research schedule to help shape my thesis. Not only was he an incredible source of knowledge regarding clinical translation, but he also continually pushed the biological emphasis of my project which resulted in more interesting scientific findings.

My research also would not have been possible with the great support of many others. In the Bioengineering program, I'm very thankful for the help of Dr. Andres Garcia along with Laura Paige and the late Chris Ruffin. I'm also grateful for my interactions with Sally Gerrish and Shannon Sullivan in the BME department. Through my participation in BBUGS, BGSAC, and the Petit Scholars program, I truly appreciate all of the work that Colly Mitchell and Meg McDevitt in IBB do to keep these programs afloat in addition to their many other responsibilities. I also have to thank Sandra Powell in IBB for helping me with the many financial issues I've had over the years (particularly after moving to San Francisco) and ensuring that I always eventually received a paycheck. The managers of the core facilities in IBB, particularly Andrew Shaw, Aqua Asberry, and Steve Woodard, were also instrumental for allowing me to advance my research. With the move to Gladstone, I also have to thank Daryl Jones for his assistance with the transition and helping me figure out how to navigate a new system.

Of course, I have to especially thank the people I spent every day with for the past several years – the other members of the McDevitt lab. When I first rotated in the lab in the summer of 2010, I was paired with graduate student Melissa Kinney – and how lucky I was! Melissa, two years my elder, seemed to be an all-knowing font of information and helped me to expand my extremely rudimentary initial understanding of stem cells. Throughout my time with her in grad school, I never stopped turning to her for both her excellent scientific mind and as a true friend. She continues to be such a great role model for me, and I know that our friendship with persist throughout life. Anh Nguyen joined the lab at the same time as me, and I was tremendously lucky to have her as a friend throughout grad school. As an expert on the Atlanta food scene, Anh was the one who introduced me

to many of the delicious eats of Buford Highway, and we continue to meet for delicious food today! Doug White also joined the lab as a member of my entering class and continually re-shaped my concept of the intersection between stem cell biology and computational modeling through his (always) entertaining lab meeting presentations. Doug was also a great friend outside the lab, particularly for the two years I was a quasi-roommate of his at Pirate House. The additional faces in the lab when I first joined were Carolyn Sargent (who kindly let me squish next to her desk for my first few months), Rich Carpenedo, Alyssa Kitchel, Andres Bratt-Leal, Ken Sutha, Barbara Nsiah, Priya Baraniak, and Ankur Singh. My time with these founding lab members ranged from a few months to a few years, and all of them acted as tremendous role models while providing valuable early input into my project. The summer following my first year of grad school, Denise Sullivan and Josh Zimmermann had the luck (or unluck?) to work with me during their initial rotation in the lab, and they became some of my closest friends and scientific confidantes. Marian Hettiaratchi and Melissa Goude also joined that fall, and it has been great to work with both of them. In particular, the motivation behind Marian's project is along a similar vein of my own, so it's been great to collaborate with her. Olivia Burnsed, Alex McKinley, and Emily Jackson joined the lab next, along with Katy Lassahn (who had really been there all along but was now an official grad student!), Jessie Butts, Liane Tellier, and Chad Glen, and I feel so fortunate to have interacted with all of them. Additionally, post-doctoral fellows Yun Wang, Krista Fridley, Tracy Hookway, Lindsay Fitzpatrick, Sarah Griffiths, and Tobias Miller joined the lab during this time, and their experience brought valuable fresh perspective to the lab. I'm also grateful for the research support staff we've had throughout the years, particularly Marissa Cooke, Jesse McClellan,

Alex Ortiz, Elizabeth Peijnenburg, and Christian Mandrycky. With the transition of our lab from Georgia Tech to The Gladstone Institutes in January 2015, it was extremely difficult to "split up the family" and I've truly missed the constant interactions with Denise, Marian, Olivia, Emily, Katy, Liane, and Chad. Video-conferenced lab meetings just aren't the same! On the other hand, I've been very fortunate to strengthen my relationships with the other brave souls who made the move – Josh, Jessie, Yun, and Tracy. Josh in particular has been a truly amazing friend during this time, and I'm so appreciative of his support. We've also grown to include new lab members, and I'm very grateful for the interactions I've had with Dylan McCreedy, Oriane Matthys, Ashley Libby, Ariel Kauss, and Amy Foley. I'm so excited to see how these new faces in new places are going to shape the research of the lab.

I am also extremely grateful to the undergraduate researchers I've had the opportunity to mentor. In particular, Mohamad Ali Najia and Sraeyes Sridhar have been enormously helpful in the completion of this thesis work. I "inherited" Mohamad from previous grad student Barbara, and I'm not sure how I was chosen to be the lucky one! Mohamad worked with me as a Petit Scholar to develop the microencapsulation system and continued to work independently alongside me for several years following. Sraeyes was also selected as a Petit Scholar and was a very dedicated researcher who helped to develop the packed bed perfusion bioreactor. He also continued to work on the project once I moved to San Francisco and enabled our continued collaboration with the Botchwey lab. I am so grateful to both Mohamad and Sraeyes for their hard work and great ideas, and I know they have tremendous futures ahead of them. In additional, I am appreciative of

several other undergraduates (Daniela Villa Moreno, Jessica Lin, and Rabbia Saeed) that worked with me for short periods of time.

During my first year at Georgia Tech, I was awarded a spot in the new Stem Cell Biomanufacturing IGERT training grant, and I am very thankful for the additional knowledge and connections I gained through this program. The other IGERT trainees in my class (Doug White, Jen Lei, Amy Clark, and Alison Douglas) as well as the trainees of later classes provided a unique interdisciplinary group for discussions, and I really benefited from our interactions. Working with Dr. Robert Nerem was one of the highlights of the IGERT program, and I am particularly grateful for our many conversations over breakfast while attending the Advanced Course in Regenerative Medicine Manufacturing in Portugal in 2013. I am also thankful that I was able to participate in the Stem Cell Ethics and Policy course taught by Aaron Levine, and I really enjoyed thinking about stem cell biology from a social science perspective. During my fourth year of grad school, I had the privilege (or burden?) of acting as the TA for 40 graduate students from six institutions in the Stem Cell Engineering class, and I was able to learn many valuable skills regarding course structure and organization. I also benefited from my time as a fellow on the Center for Drug Discovery, Development, and Delivery GAANN program, and I am grateful for the mentorship of Dr. Mark Prausnitz and Dr. Andreas Bommarius during the course and discussion meetings.

It would have been impossible to make it through graduate school without the moral support of my friends and colleagues. I was lucky in that my entering class of BIOE and BME students was comprised of many passionate and fun-loving people, and I'm so grateful to all of them -- but particularly to Chris, Phil, Eli, Doug, Kristin, Jessie, Kyle,

John, Anh, and Lauren. Outside of the program, I'm also thankful for the continual friendship of Laura, Diana, and Megan. My participation in the BBUGS and BGSAC/BGA student groups also enabled the formation of many friendships, and it was great to get out of the lab for an ice cream social, potluck, or some Frisbee golf! The quals practices through BGSAC were not only extremely beneficial preparation (Patricia was tougher than any of my committee members!) but also became a real bonding experience for everyone in the BIOE program, and I really enjoyed being on the other side of the table (especially alongside Timothy) to make new BIOEs sweat (and learn, of course). Since moving to Gladstone, it's been great to meet new people, and I'm particularly thankful to my friendships with Alex and Sean and our frequent gaming group.

Going back in time a bit, I never would have even considered graduate school without the fantastic mentors I had as an undergraduate. My first experience with research was in the lab of Dr. Greg Rorrer at Oregon State, and I was lucky to have an extremely influential first graduate student mentor in Tavi Cruz-Uribe. I was also fortunate to work with new faculty Dr. Ganti Murthy at Oregon State, which was my first experience with the challenges of setting up a new lab. Dr. Murthy was very patient with me as a beginning researcher, and I'm grateful that he didn't kick me out after a dropped and shattered the hemocytometer on my first day. I spent the summer of 2008 working as an Amgen Scholar at UCLA in the lab of Dr. Rachelle Crosbie, which was my first taste of biomedical research. I learned so much working with my graduate student mentor Jamie Marshall that summer, including how to run PCR (which I then performed ad nauseum), how to deal with a finicky cryostat, and how to make perfect gels for Western blots. Back at Oregon State, I performed the work for my undergraduate thesis with Dr. Adam Higgins, a graduate

of the Georgia Tech bioengineering program. Without his push, I wouldn't have even considered applying to Georgia Tech, so I am very grateful to him for persuading me to apply. While in his lab, I worked with his graduate student Allyson Fry Davidson, and she was a great friend and mentor to me who I was excited to re-connect with when I moved out to the Bay Area. Even though they all told me I shouldn't bother with grad school, I also want to thank everyone I worked with at Bend Research, Inc. for the valuable background knowledge I gained in bioreactor development and bioprocessing. In addition, I want to generally thank all of the teachers and professors I have ever had, as all of you impacted my desire to pursue an advanced degree.

Finally, I am forever indebted to my family for their unwavering support. My parents, Tim and Julie, are such fantastic role models for me. With their work as educators, they always emphasized the importance of asking questions, trying your best even when things (like Algebra II) got tough, and never thinking of learning as a chore. They like to claim that they had no role in their daughter getting a Ph.D. in engineering, but they of course had everything to do with it. I'm grateful that they encouraged me to go to school in Georgia even when it was so far from home and meant I would only see them once or twice a year. It's been so great to be back on the West coast this year so that I can spend more time with them! I also want to acknowledge my sister Zoe for her friendship and encouragement. Though we work in completely different fields, the passion and creativity she has for everything she does is such an inspiration for me. Essentially family at this point is my boyfriend Christopher Quinto, who entered the BME program with me. We began dating during the fall of our first year in grad school and never looked back. He's been my constant support, from the beginning when I was stressing over IBS take-home

exams, to that awful fall semester when I was in over my head with coursework, to taking on the role of “animal wrangler” for six months while I was in San Francisco before he moved out, to becoming my “house husband” while I was preparing this dissertation. I’m so happy to spend every day with him and his stupid jokes, endless energy, and positive attitude. Our little family also includes our sweet dog Lana and our sometimes sweet cats Martin and Roxanne, who have acted as constant therapy for me. On a distinctly personal note, I would also like to acknowledge Caraway, Radaya, Cinnia, Inga, and Myali for providing me with a creative outlet during the past few years of grad school, and the band Real Estate for providing the soundtrack for my thesis writing. To everyone who has provided me with assistance, mentoring, encouragement, love, and laughter, I thank you! This dissertation is a consequence of your support, and I am forever grateful.

TABLE OF CONTENTS

LIST OF TABLES

LIST OF FIGURES

LIST OF SYMBOLS AND ABBREVIATIONS

AFP	Alpha fetoprotein
APA	Alginate-poly-L-lysine-alginate
BMP	Bone morphogenetic protein
CFSE	Carboxyfluorescein succinimidyl ester
CFU	Colony forming unit
CM	Conditioned media
DAPI	4',6-diamidino-2-phenylindole
ECM	Extracellular matrix
EB	Embryoid body
EGF	Epithelial growth factor
eGFP	Enhanced green fluorescent protein
ELISA	Enzyme-linked immunosorbent assay
ESC	Embryonic stem cell
FGF	Fibroblast growth factor
HGF	Hepatocyte growth factor
HLA	Human leukocyte antigen
IGF	Insulin-like growth factor
IGFBP	Insulin-like growth factor binding protein
iPSC	Induced pluripotent stem cell
G-CSF	Granulocyte-colony stimulating factor
GM-CSF	Granulocyte-macrophage colony-stimulating factor
HARV	High aspect ratio vessel
High G	High guluronic acid content

High M	High mannuronic acid content
HSC	Hematopoietic stem cell
ID	Inner diameter
IPA	Ingenuity Pathway Analysis
KO N2B27	Knock-out media supplemented with N2 and B27
IL	Interleukin
Lin	Lineage
LT-HSC	Long-term hematopoietic stem cell
MAPK	Mitogen-activated protein kinase
M-CSF	Macrophage colony-stimulating factor
mEF	Mouse embryonic fibroblast
MSC	Mesenchymal stem cell
MWCO	Molecular weight cut-off
NSC	Neural stem cell
OD	Outer diamter
PBS	Phosphate buffered saline
PCR	Polymerase chain reaction
PDMS	Polydimethylsiloxane
Pe	Peclet number
PLL	Poly-L-lysine
PSC	Pluripotent stem cell
Re	Reynolds number
Sc	Schmidt number
SC	Satellite cell
SCF	Stem cell factor

SDF	Stromal cell-derived factor
ST-HSC	Short-term hematopoietic stem cell
TGF	Transforming growth factor
TPO	Thrombopoietin
VEGF	Vascular endothelial growth factor
Wnt	Wingless type

SUMMARY

Stem cells have exploded onto the scene of regenerative medicine in the past two decades and have been touted as a sort of medical panacea with uses ranging from modeling early developmental processes to enabling better *in vitro* platforms for drug testing. However, the majority of applications initially focused on exploiting the differentiation capacity of stem cells for the replacement of damaged tissues. Despite the continued excitement surrounding cell replacement therapies, the results of initial *in vivo* transplantation studies have indicated that many of the observed functional improvements were due to the transient paracrine actions of the transplanted stem cells, rather than the stem cells permanently engrafting and replacing the damaged cellular material. Thus, research on the identity and potency of paracrine factors secreted by stem cells has become an increased area of focus in the regenerative medicine field. However, the secretory properties of pluripotent stem cells, including embryonic stem cells (ESCs), have been largely neglected in favor of research on the paracrine actions of multipotent adult stem cells. Due to the mitogenic and morphogenic roles of ESCs during the early stages of development, they are an underexplored cell population with a unique and potent secretome.

A potential application for the milieu of mitogens and morphogens produced by pluripotent stem cells is the restoration of the proliferative and regenerative capacity of adult stem cell populations. While the self-renewal capacities of adult stem cell populations *in vivo* are well-documented, similar success has not been achieved in attempts to expand the cell populations *ex vivo*. For example, hematopoietic stem cells (HSCs) cultured *ex vivo*

exhibit extremely limited expansion potential and rapidly lose the capacity for self-renewal, while muscle satellite cell populations demonstrate a decreased capacity for re-engraftment and regeneration following expansion *ex vivo*. Due to insufficient and unreliable expansion with traditional cytokines, increased emphasis is being placed on the use of developmental factors, such as Wnt proteins, Notch ligand, bone morphogenetic proteins (BMPs), and fibroblast growth factors (FGFs), to expand adult stem cell populations *ex vivo*. Additionally, the regulation of adult stem cell populations *in vivo* is critically dependent on the surrounding microenvironment, and the loss of stem cell function in response in disease or aging has been attributed to a failure of the niche to adequately support cell function. For example, systemic factors from young animals restore the regenerative capacity of aged animals, indicating that the diminished function of aged stem cell populations arises more from the aged microenvironment than from cell intrinsic changes. Therefore, identifying and applying signals capable of restoring functionality to deteriorated stem cell niches would be a significant development for the translation of regenerative therapies.

To take advantage of the stimulatory potential of pluripotent cell-derived signals, the goal of this project was to develop a controlled means of harnessing and delivering soluble factors derived from pluripotent stem cells. The traditional use of conditioned media is limited by the need for a bolus delivery, likely product degradation, and the relatively dilute concentrations of cell-secreted factors. Therefore, a novel upstream bioreactor for ESC culture was developed that can be continuously perfused to deliver secreted factors to downstream cell populations. In order to facilitate densely packed cultures, prevent agglomeration of stem cell aggregates, and protect cells from damage by

hydrodynamic forces, a microencapsulation-based approach was investigated for ESC culture **(Chapter 3)**. A number of microencapsulation configurations were examined, but ultimately the encapsulation of pre-formed ESC aggregates led to the highest cell viability and degree of reproducibility. ESC aggregates encapsulated in alginate microbeads exhibited diminished cell growth and a delayed loss of pluripotency in comparison to unencapsulated aggregates, though similar levels of viability were observed. Altering the composition of alginate from a stiffer, more highly crosslinked composition ("High G") to a softer, less crosslinked structure ("High M") promoted greater concentrations of growth factors in the conditioned media and induced the enclosed ESC aggregates to differentiate toward a mesendodermal lineage. Given the establishment of the microencapsulation method, a bioreactor was then designed to extract secreted factors from a high density culture of microencapsulated ESCs **(Chapter 4)**. The development of a packed bed configuration allowed for continuous perfusion of medium, which both enables direct one-way delivery to downstream cell populations and leads to increased concentration of ESC-secreted growth factors in comparison to density-matched static controls, perhaps through the removal of a system of negative feedback inhibition. Depending on the flow rate of perfusion through the reactor, a peak yield of growth factor could be achieved.

The development the efficient and tightly engineered bioreactor system to deliver trophic factors from pluripotent stem cells enabled a number of downstream investigations. Because many of the morphogens and growth factors produced by ESCs are generally present in low concentrations, previous attempts to characterize the composition of ESC conditioned media have encountered technical challenges. However, the concentration of factors obtained through perfusion culture enabled thorough characterization of ESC

secreted factors at the gene and protein levels **(Chapter 5)**. Using antibody arrays containing 96 cytokines and growth factors, many mitogenic and morphogenic proteins were detected in media conditioned by ESCs, and the quantity of secreted factors was increased with perfusion culture (in comparison to static culture) for essentially all detected species. To determine the influence of perfusion culture on ESC phenotype, a custom gene expression array of 96 proteins was designed. Dramatic differences in gene expression profile were observed between ESCs, mouse embryonic fibroblasts, and mesenchymal stem cells, emphasizing that pluripotent stem cells are a unique source of factors even in comparison to other traditional supportive cell populations. In addition, a global increase in gene expression was observed in ESCs cultured in the perfusion bioreactor, suggesting that the culture platform may be affecting protein expression at the level of transcriptional regulation.

Finally, the impact of ESC secreted factors on adult stem cell populations *ex vivo* was established using three different cell populations that were studied in both co-culture with ESCs and with ESC conditioned media **(Chapter 6)**. Cultures of bone marrow-derived mesenchymal stem cells (MSCs) were examined in addition to more heterogeneous primary cells isolated from murine bone marrow and skeletal muscle. Conditioned media collected from ESCs at different stages of differentiation and ESCs cultured under different environmental settings were also directly compared to determine the impact of a shifting composition of paracrine factors. Mesenchymal stem cell populations and hematopoietic progenitors exhibited increased growth in response to ESC conditioned media, and the hematopoietic progenitors also demonstrated increased differentiation capacity, particularly to lymphoid populations. The presence of ESC conditioned medium in

heterogeneous cultures of primary skeletal muscle cells led to enrichment of myocytes over fibroblasts and reduced the differentiation of myocytes to multinucleated myotubes. Overall, the studies demonstrated the potent mitogenic nature of pluripotent stem cell-derived factors across multiple adult stem cell niches.

The development of platforms which efficiently harness stem cell paracrine factors will be essential for the translation of future therapies in regenerative medicine, whether through delivery the of regenerative factors to a dysfunctional location *in vivo* or by enabling expansion of multipotent stem cell populations for cell therapy applications. Through the integration of concepts in biomaterials and bioprocess engineering with stem cell biology and regenerative medicine, this project incorporated technology development with critical biological questions regarding the identity and performance of embryonic morphogens for expanding adult stem cell populations *ex vivo*. Ultimately, this project established pluripotent stem cells as a unique source of potent growth factors and cytokines which can be regulated and concentrated using engineering design parameters to enable multiple applications in the field of regenerative medicine.

CHAPTER 1

INTRODUCTION

A reduced capacity for regeneration often accompanies illness, injury, or aging, a decline that is associated with the diminished function of adult stem cell populations. Increasing evidence indicates that the decreased ability of adult stem cell populations to properly maintain and repair deteriorating tissues reflects a failure of the surrounding microenvironment to provide adequate support. For example, systemic factors from young animals restore the regenerative capacity of aged animals, indicating that the diminished function stems more from the aged microenvironment than from cell intrinsic changes. Therefore, identifying and applying signals capable of restoring functionality to dysfunctional stem cell niches would be a significant development for the translation of regenerative therapies. In addition, knowledge regarding mitogenic cues can enable the development of *ex vivo* expansion protocols to generate adequate cell numbers of adult stem cells for allogeneic or autologous cell therapies.

Pluripotent embryonic stem cells (ESCs), the "youngest" cellular state, stimulate tissue specification and morphogenesis by secreting growth factors, cytokines, chemokines, and mitogens. The regenerative capacity of fetal tissue, such as its ability for scarless wound-healing, can be related to endogenous secreted signals during the growth and maturation of developing mammals. Developmental morphogenic factors involved in multipotent stem cell ontogeny—such as members of the wingless-type (Wnt), sonic hedgehog, Notch, fibroblast growth factor, bone morphogenetic protein, and insulin-like growth factor pathways—may enhance the function of adult stem cells. In addition, initial

studies transplanting stem cells *in vivo* suggest that many of the observed functional improvements were due to the transient paracrine actions of the transplanted stem cells, rather than the stem cells actively engrafting and replacing the damaged cellular material. Thus, in combination, embryonic signals may recapitulate the supportive *in vivo* environment. Therefore, the paracrine actions of ESC trophic factors are an unexplored source of paracrine cues to stimulate adult stem cells to regain a more "youthful" proliferative and/or regenerative capability. However, ESC-based therapies present significant challenges, such as the difficulty of controlling ESC differentiation and the potential for teratoma formation by transplanted ESCs. Therefore, an engineered platform that provides a defined environment to control ESC morphogen secretion and subsequently delivers ESC-derived trophic factors without cell transplantation would be a truly transformative regenerative therapy.

The ***long term goal*** that motivated the work of this dissertation is to engineer strategies for the delivery of trophic factors derived from pluripotent stem cells as a means to regenerate aged, diseased, or injured tissue. The ***overall objective*** of this project was to develop an engineered platform for the delivery of pluripotent factors to enable factor identification and to stimulate adult stem cell populations *ex vivo*. The ***general hypothesis*** was that providing a defined environment via encapsulation and bioreactor parameters will allow the trophic secretion of ESCs to be controlled and concentrated such that exposure of adult stem cell populations to soluble factors derived from pluripotent microenvironments will promote cell survival, proliferation, and function. The rationale for this hypothesis was based upon the morphogenic role of ESCs during development which suggests that they are a potent source of secreted factors capable of providing

powerful rejuvenative signals to stimulate adult stem cell populations. The primary objective was completed and the central hypothesis investigated through the following specific aims:

Specific Aim 1. Develop a microencapsulation-based platform for ESC culture. The *working hypothesis* was that varying encapsulation parameters, such as the configuration of cells and the composition of alginate beads, would lead to defined environments for ESC culture. The impact of alginate composition on encapsulated single ESCs and ESC aggregates was assessed via cell viability, cell proliferation, aggregate morphology, and gene/protein expression for pluripotent and lineage-specific markers. The *outcome* of this aim was the establishment of a robust culture platform which enabled well-defined, high density cultures of encapsulated ESC aggregates.

Specific Aim 2. Investigate strategies for high density ESC culture to facilitate concentration and delivery of paracrine factors. The *working hypothesis* was that ESC factor secretion could be controlled via environmental conditions while trophic factors were concentrated through culture in a high density bioreactor. A packed bed perfusion bioreactor was designed, fabricated, and validated for culture of encapsulated ESCs and trophic factor concentration. The impact of external influences, including alginate composition, hypoxic culture, directed mesoderm differentiation, and perfusion culture, on encapsulated ESC secretion profiles was assessed via gene and protein expression. The *outcomes* of this aim were the development and validation of a novel culture platform to

enable delivery of a morphogen-riche perfusate and the characterization of a unique secretory milieu that is distinct from other supportive cell populations.

Specific Aim 3. Explore the effects of ESC trophic factors on adult stem populations *ex vivo*. The *working hypothesis* is that delivery of pluripotent stem cell-derived morphogens will improve the survival, proliferation, and function of adult stem cell populations, including mesenchymal stem cells, hematopoietic progenitors, and skeletal muscle myoblasts, in an *ex vivo* setting. Following exposure to ESC-derived factors, mesenchymal stem cells were assessed for growth and morphology, hematopoietic progenitors were evaluated for proliferation, lineage commitment, and differentiation potential, and myoblasts were examined for growth and differentiation. The *outcome* of this aim is the establishment of pluripotent cell-derived factors as a novel mitogenic source for the *ex vivo* culture of adult stem cell populations.

This project is ***innovative*** because the delivery of the complex potent milieu of concentrated trophic factors produced by pluripotent stem cells using a novel high-density perfusion reactor is a novel method to stimulate the growth and enhance the function of adult stem cells. Additionally, the development of the microencapsulation-based bioreactor platform for stem cell culture and trophic factor concentration is an original approach that can be used to study heterotypic paracrine cell interactions. The results of this project have a direct translational impact for expansion and transplantation of bone marrow and skeletal muscle-derived multipotent stem cell populations and yield novel scientific insights that

could lead to a more mechanistic understanding of the influence of embryonic-derived signals on the regeneration of adult stem populations.

CHAPTER 2

BACKGROUND[1,2]

2.1 Pluripotent stem cells

2.1.1 Origin and characteristics

Stem cells are now known to be found in nearly all tissues throughout the body and are defined by the signature characteristics of self-renewal and differentiation capacity. Pluripotent stem cells (PSCs) include embryonic stem cells (ESCs), derived from the inner cell mass of the pre-implantation blastocyst [1–3], and induced pluripotent stem cells (iPSCs), obtained by reprogramming somatic cells to a pluripotent state [4,5]. Both ESCs and iPSCs can expand indefinitely *in vitro* and differentiate into all three germ lineages (endoderm, mesoderm and ectoderm), consequently giving rise to cells from all tissue types. Pluripotent cells differ functionally from multipotent stem cells that are more restricted in their differentiation capacity. Common multipotent stem cells include mesenchymal stem cells (MSCs), which can be derived from multiple sources including bone marrow [6] and adipose tissue [7], and hematopoietic stem cells (HSCs), found in bone marrow [8] and cord blood [9]. Because most multipotent stem cells can be readily

---

[1]Modified from: Wilson JL, McDevitt TC. Stem cell microencapsulation for phenotypic control, bioprocessing, and transplantation. Biotechnol Bioeng 2013;110:667-82.

[2]Modified from: Wilson JL, McDevitt TC. Biofunctional Hydrogels for Three-Dimensional Stem Cell Culture. Biology and Engineering of Stem Cell Niches (eds. Ajaykumar Vishwakarma and Jeffrey Karp, Designing Smart Biomaterials to Mimic & Control Stem Cell Niche section), Elsevier Press.

obtained from adults, autologous and allogeneic cell therapies are feasible for several clinical applications; however, *ex vivo* expansion of multipotent stem cells is limited when compared to the capacity for indefinite self-renewal that defines pluripotent stem cells. Thus, ESCs and iPSCs may represent a more practical solution for large-scale production of a broader range of cell therapy products.

2.1.2 Three-dimensional stem cell culture

There are significant differences between the native environment of stem cell populations and the artificial *in vitro* culture platforms used by the majority of scientists today. For example, pluripotent stem cells exist transiently in the pre-implantation blastocyst constituting the inner cell mass, a tightly packed cluster of cells which is encased in a layer of epithelial trophoblast and surrounded by the fluid of the blastocoel cavity [2]. In contrast, bone marrow mesenchymal stem/stromal cells are encompassed in a semi-solid matrix consisting of various collagens, proteoglycans, and glycosaminoglycans [10,11]. Despite these distinct yet similarly complex microenvironments, *in vitro* studies of ESCs and MSCs are generally conducted in the same manner: as two-dimensional (2D) cell monolayers on plastic surfaces.

In typical 2D culture, cells are specifically polarized by attachment to a plastic surface on one side and contact with liquid culture medium on the other. Interactions between neighboring cells occur laterally within a single plane, if at all, and the three-dimensional physical cues presented by interstitial extracellular matrices are absent entirely. Since cell-matrix and cell-cell interactions dictate much of a cell's behavior, it is logical that the attenuation of these cues can lead to cell dysfunction, and this has been observed in cell types ranging from liver hepatocytes to ovarian and colorectal cancer cells

[12–14]. Therefore, a greater emphasis on three-dimensional (3D) culture platforms for stem cell culture may provide more accurate insights into *in vivo* cell physiological function as well as enable more advanced applications, such as tissue-engineered constructs, biomanufacturing approaches, and platforms for drug discovery and toxicity testing.

There are several standard approaches for 3D culture of stem cells, including seeding of cells onto porous scaffolds or decellularized ECM from native tissues [15] and culture of cells within hydrogel scaffolds [16]. Additionally, material-free approaches exist, including the formation of scaffold-free microtissues, often in the form of spheroids or aggregates. Spherical aggregates are used in pluripotent stem cell cultures to promote spontaneous differentiation through recapitulation of developmental processes. Embryoid bodies (EBs), pluripotent stem cell aggregates, play pivotal roles in many differentiation protocols and can be used as a platform for directed differentiation [17]. Traditional methods for embryoid body formation include hanging drop, static and stirred suspension formation, methylcellulose culture, and microwell forced aggregation [18,19]. Once formed, aggregates can be cultured in suspension, allowing for straightforward translation to scalable bioreactors. In the last five years, three-dimensional aggregates of pluripotent stem cells have been gently coaxed to self-organize into organoid structures resembling a number of functional tissues, including optic cup [20,21], anterior pituitary [21], intestine [22], thyroid [23], and cerebral brain [24], among others. Therefore, three-dimensional culture of pluripotent stem cells can instigate complex morphogenic processes which likely coincide with the production of relevant morphogenic cues.

2.1.3 Paracrine actions

Early studies in delivering stem cells to sites of injury have exhibited improved tissue function, which was originally attributed to differentiation of the stem cells and replacement of the damaged tissue. However, a recent paradigm shift has emerged suggesting that the beneficial effects observed following stem cell transplantation may be due to the cells' transient paracrine actions more so than their engraftment and subsequent differentiation [25–29] (**Figure 2.1)**. Injection of ESCs into embryos with multiple cardiac defects has improved the embryonic cardiac phenotype, a finding attributed to secretion of insulin-like growth factor 1 (IGF-1) and Wnt5a [30]. ESC transplantation has also reduced myocardial dysfunction in a rat model of surgically induced global ischemia, presumably by increasing the secretion of VEGF and interleukin-10 [31]. Additionally, *in vitro* studies have utilized ESC co-culture for expanding cardiomyocytes and corneal epithelial cells [32–34], observing improved proliferation and function in both cases. Conditioned media from ESCs was also found to improve proliferation of aged satellite cells and myoblasts while inhibiting differentiation [35] as well as improve survival of hematopoietic progenitors [36]. In addition to stem cell-derived factors, evidence suggests that systemic molecules present in younger animals can improve function in aged animals, as has been observed using the parabiotic mouse model for enhanced wound healing [37,38], improvement in muscle satellite cell function [39–41], rejuvenation of neural cells and cognitive function [42–45], and reversal of cardiac hypertrophy [46]. As pluripotent ESCs represent the ultimate "young" state, similar effects may be observed with the delivery of pluripotent stem cell-derived factors. Therefore, ESCs represent a comprehensive cell source capable of stimulating adult stem cell populations though the secretion of a complex milieu of morphogenic factors.

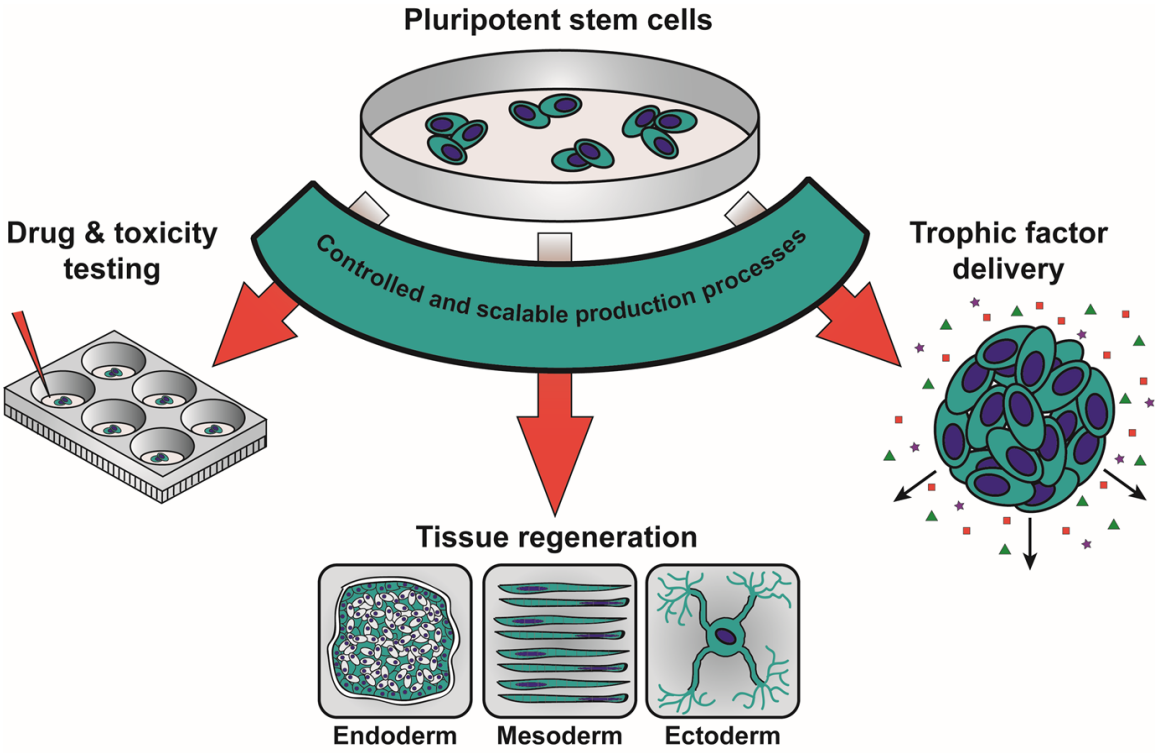

Figure 2.1. Applications of pluripotent stem cells. Pluripotent stem cells enable many downstream applications, including advanced drug screening platforms, differentiation into cell types from all three germ lineages (endoderm, mesoderm, and ectoderm), and secretion of paracrine trophic factors. The translation of all applications is dependent on the development of robust processes for expanding pluripotent stem cells and harnessing their unique abilities.

2.2 Stem cell bioprocessing

2.2.1 Microencapsulation

In the early 1960s, Thomas M. S. Chang drew inspiration from naturally-occurring aqueous partitions, such as cells and organelles, to develop a method for microencapsulation of biological material in natural polymers [47]. Since that time, cell microencapsulation has been widely researched, particularly in the field of cell transplantation for the treatment of endocrine disorders, such as diabetes, in which a continual regulation and response to physiologic stimuli is required. Encapsulation facilitates allogeneic and xenogeneic cell transplantation because the semi-permeable membrane of the capsule protects the enclosed cells from the host immune system. In addition to the benefits of microencapsulation for transplantation, the technology offers several potential advantages for stem cell expansion and differentiation. The modification of encapsulation material properties, such as the polymer species, type of coating, mechanics, and permeability, can be used to control the stem cell microenvironment, allowing for either the maintenance of potency or directed differentiation toward a desired lineage. In addition, encapsulated stem cells can be expanded in scalable suspension bioreactor systems without being damaged by the presence of hydrodynamic shear forces. Consequently, microencapsulation can play an important role throughout the pipeline of production and delivery of stem cell therapies **(Figure 1.2)**.

The general encapsulation process involves the formation of cell-containing droplets, the crosslinking of droplets, and often the coating of droplets with a stabilizing membrane. Hydrogels are the most common material used in encapsulation for several reasons. First, hydrogels generally have high porosity, leading to high permeability and

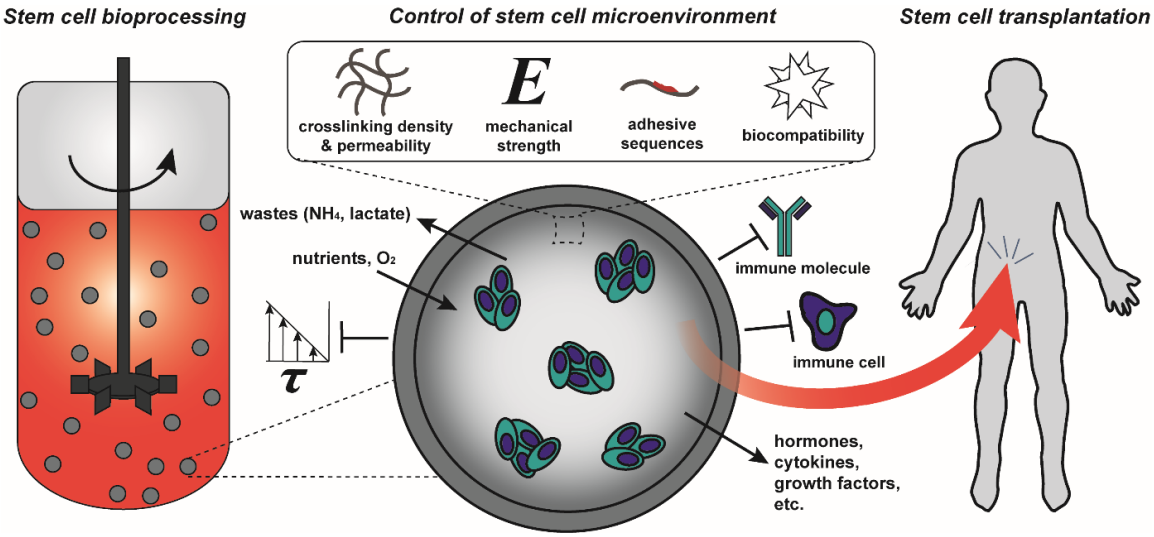

Figure 2.2. Stem cell microencapsulation approaches. Microencapsulation of stem cells permits mass transport of nutrients and secretory products while restricting the passage of immune molecules and cells and shielding from physical forces. Modification of various capsule parameters can modulate stem cell response(s) while simultaneously enabling expansion in scalable suspension bioreactors for bioprocessing and transplantation *in vivo*.

minimal mass transfer limitations. Second, hydrogel materials tend to be soft and flexible, reducing mechanical friction on adjacent tissues upon transplantation. Third, the high water content leads to hydrophilic interactions, which reduce interfacial tension, protein adsorption, and cellular adhesion while enhancing biocompatibility. Natural polymeric materials are used more often than synthetic polymers because they are more biocompatible and require milder crosslinking processes (i.e. those that take place under aqueous and physiological conditions without the presence of reactive species). However, a reduction in the stability of the microcapsule can occur using natural polymers when compared to results obtained with synthetic polymers [48].

The general formulations of microcapsules include solid matrix beads, solid matrix beads with an external coating, liquid core capsules, and direct conformal coating. Liquid core capsules are fashioned by liquefying the center of a solid matrix bead as the outer membrane is stabilized by a thin polyion coating [49]. Conformal coated microcapsules are

formed by constructing a thin membrane surrounding individual cells or pre-formed cell aggregates, thereby minimizing the empty capsule volume [50]. In some cases, encapsulated single cells will aggregate into spheroids within a capsule. The fashion in which cells form aggregates within microcapsules is based on the mechanical restriction of the hydrogel [51]. In solid matrix beads, encapsulated cells are more physically constrained and therefore proliferate to form smaller spheroids with multiple foci. In liquid core capsules, cell movement and proliferation are less restricted, and the cells can therefore aggregate and proliferate as a single large spheroid [52]. As cells proliferate in liquid core capsules, the capsules tend to swell, but excessive swelling can be restricted with the addition of a polymeric surface coating [53].

2.2.2 Alginate as a biomaterial for microencapsulation

Alginate, a natural polymer purified from brown seaweed, is the most common material used for microencapsulation due to its abundance, biocompatibility, and gentle cross-linking procedure. Alginate is made up of two anionic monomers, α-L-guluronic acid (G) and β-D-mannuronic acid (M), which are arranged in both homopolymeric regions (GG blocks and MM blocks) and mixed monomeric regions (MG blocks) [54]. Alginate can be cross-linked by several different divalent cations, including calcium and barium. Calcium (Ca^{2+}) crosslinks only G residues, therefore, alginates with higher G content and longer GG blocks produce stiffer, more durable capsules when crosslinked with Ca^{2+} than alginates with greater M content. Alternatively, barium crosslinks alginate by binding to both G and M residues, thus yielding stronger and more uniform crosslinking than Ca^{2+} alone can provide [55]. The molecular weight of alginate also impacts its physical properties, with higher molecular weight alginate leading to capsules with greater

mechanical stability than lower molecular weight alginate [48]. However, the relative impact on the mechanical stability with increasing molecular weight is not as profound as increasing either the G content or concentration of alginate [52]. The stability of alginate capsules generally weakens over time due to exposure to certain species in the cell culture medium or in vivo, including chelating agents (e.g. sodium citrate, EDTA, phosphate) or monovalent ions (e.g. sodium), which can displace the ionic interactions created by the divalent cross-linkers [56]. Although alginate has many favorable properties for cell encapsulation, native isoforms are not able to directly interact with cells since alginate lacks adhesive moieties. Therefore, it is primarily the mechanical properties of native alginate that impact its relationship with cells. The mechanical properties (e.g. elastic modulus, viscosity, osmotic tolerance/swelling) are generally based on the chemical properties of the alginate (e.g. G vs. M composition, molecular weight, concentration). Thus, when deciding on an alginate for microencapsulation, the physiochemical properties should be carefully considered depending on the intended function(s) of the system.

Alginate encapsulation alone is usually insufficient to completely shield cells from the immune system *in vivo* because of mechanical and chemical instability in addition to poor resistance to osmotic swelling, which often results in cell escape. Therefore, coating the exterior of alginate capsules to reduce the permeability to immune cells and proteins material while simultaneously increasing the mechanical stability and biocompatibility of the capsule is often performed by polyelectrolyte complexation, where two oppositely charged polymers are complexed to form a thin membrane layer with a thickness on the order of 10-100 μm [57]. Since alginate is a polyanion, the coating materials are usually polycations, with poly-L-lysine (PLL) being the most common since Lim and Sun

introduced the alginate-PLL system in 1980 [58]. PLL binds to both the M and G blocks through ionic interactions, though it typically binds more tightly to alginate with higher M content as there are more alginate moieties available for binding, creating a coating that is thicker and less permeable [59]. To improve biocompatibility, the positive PLL charges on the exterior of the capsule are sometimes neutralized through incubation with additional alginate, forming "APA" (alginate-PLL-alginate) beads. Chitosan, polyethylene glycol (PEG), and other polycations are sometimes used as alternatives to PLL; however PLL remains the most commonly used polymer due to its historical prevalence and creation of mechanically resistant capsules [60].

The two most common methods for hydrogel bead formation are emulsification and extrusion. The emulsification process involves creating a dispersion of a polymeric aqueous phase in an immiscible phase (often oil), followed by gelation through addition of a cross-linking agent or cooling of the mixture. There are several challenges with this approach, including the presence of shear forces during mixing that may harm cells and the insolubility of some gelling agents (e.g. $CaCl_2$) in the immiscible phase. The extrusion process involves forcing a cell-polymer solution through a small aperture, such as a needle or an area of small-diameter tubing, into a solution containing the cross-linker to stabilize bead formation. Solely adding droplets to a cross-linking bath generates large particles (on the order of millimeters) and is feasible only for low viscosity solutions. In order to form smaller, more uniform beads with higher viscosity solutions, a voltage gradient between the needle and cross-linking solution can be applied to overcome droplet surface tension and therefore produce large quantities of smaller beads [61]. Alternatively, a constant vibration can be applied to a laminar liquid jet to produce small, uniform capsules [62,63].

A coaxial gas flow can also be used to form beads by shearing droplets with compressed gas that flows around the needle exit. An additional extrusion approach is the co-flowing of two immiscible liquid streams in a coaxial tube, one in the aqueous phase containing the cells/polymer and the other a liquid paraffin solution [64]. The paraffin solution, present in the outer coaxial tube, shears the polymer drops as they are extruded through a nozzle. Recently, microfluidics and microlithography have been introduced as systematic processes for more homogeneous and controlled capsule formation, though they currently have lower throughput than the aforementioned macro-scale methods [49].

2.2.3 Microencapsulation of pluripotent stem cells

Microencapsulation approaches have been explored as an approach to maintain the viability and pluripotency of microencapsulated ESCs. Agarose microencapsulation prevents embryoid body (EB) agglomeration in culture, allowing for higher density cultures without the formation of aggregates with large necrotic cores [65]. Murine ESCs (mESCs) were observed to retain >90% viability after 20 days in alginate-PLL capsules [66], with liquid core capsules leading to enhanced proliferation and viability compared to unliquefied capsules [67]. An altered liquid core configuration in which smaller alginate microcapsules containing mESCs were encapsulated in larger agarose capsules, followed by liquefaction of the alginate core, found that the enclosed mESCs formed EB-like spheroids and stained heterogeneously for alkaline phosphatase, suggesting a mixture of undifferentiated cells and differentiated progeny [68]. An additional study found that expression of the pluripotency markers OCT-4, SSEA-1, and alkaline phosphatase were maintained by mESCs for two weeks in vitro in APA liquid core capsules, though a decrease in pluripotency marker expression was observed once the capsules were

implanted in vivo [67]. Human ESCs (hESCs) have also been maintained in alginate-gelatin microcapsules for up to 260 days without experiencing significant decreases in viability or pluripotency [69] or as aggregates [70], thereby supporting future endeavors in the large-scale production of hESCs.

2.2.4 Bioreactor platforms

Several bioreactor systems have been employed for experimental studies of microencapsulated stem cells, including spinner flasks, which simulate larger-volume stirred tank bioreactors. *Ex vivo* expansion of APA encapsulated bone marrow HSCs using spinner flasks with continuous media exchange yielded a 12-24 fold multilineage expansion within 19 days [71]. In addition to *ex vivo* expansion of HSCs, the differentiation of mESCs to hematopoietic progenitors while encapsulated in agarose microcapsules was also performed in spinner flasks [65]. Cardiac differentiation protocols, which usually require an EB suspension culture step, have likewise been developed for microencapsulated mESCs in spinner flasks [72,73]. Spinner flask culture of microencapsulated hESCs found that while encapsulation of single hESCs led to poor viability, encapsulation of hESC aggregates and hESCs on microcarriers allowed for maintenance of viability and pluripotency for up to two weeks in suspension culture [70]. In addition to stirred tank bioreactors, other reactor configurations have been investigated, including the high aspect ratio vessel (HARV), a rotary microgravity reactor that operates under the laminar flow regime to lessen the impact of mechanical forces, which was used with mESC-containing alginate microcapsules to create mineralized constructs for bone tissue engineering [74]. A fixed bed reactor in which CellBeads, a commercially available product consisting of hMSC aggregates in alginate microcapsules, were packed and

perfused with culture medium was able to maintain viability and induce adipogenic differentiation with similar results to stirred suspension controls [75]. Other bioreactor configurations have been developed for the direct assembly of tissue engineered constructs, including a tubular perfusion system of aggregated alginate beads containing hMSCs [76,77]. The initial results obtained from bioreactor studies suggest that the development of novel bioreactor systems may lead to improved bioprocess efficiency through better maintenance of viability or more efficient directed differentiation than can be obtained with static cultures.

2.3 Adult stem cell niche regulation

2.3.1 Function of stem cell niches

Multipotent stem cell populations, including hematopoietic stem cells, mesenchymal stem cells, satellite cells, and neural stem cells, exist throughout life and act to maintain and repair many tissue types. Almost 40 years ago, the concept of a stem cell niche was proposed as a fixed region responsible for maintaining the self-renewal capacity of the resident stem cell pool [78]. While the standard description and purpose of the stem cell niche has not changed considerably since its initial definition, the complexity and number of components seems to be ceaselessly increasing as our understanding of stem cell anatomy and behavior improve. In general, the niche consists of specific soluble molecules, a particular extracellular matrix composition, and direct or indirect interactions with other cell types that all function at the structural, topographical, environmental, and chemical level [79–81].

Hematopoietic stem cells, which were the first stem cells to be identified and transplanted, give rise to all blood and immune cells and are responsible for continually replenishing these cell populations for functions ranging from oxygen transport throughout the body (via erythrocytes) to adaptive immune responses (via T cells and B cells). Though the mature cells derived from HSCs through the process of hematopoiesis are found throughout circulation in the body, the HSCs themselves are housed primarily along the endosteal surface of trabecular bone. This anatomical location permits easy access to circulation for both the HSCs themselves and their differentiated progeny [82,83]. The bone marrow niche exists as a semi-solid matrix consisting of various collagens, proteoglycans, glycosaminoglycans, and calcium minerals to house the resident HSCs [10,11,84,85]. Many other cell types also reside within the bone marrow niche, including mesenchymal stem/stromal cells (MSCs), endothelial progenitor cells, osteoblasts, adipocytes, nerve cells, and Cxcl12-abundant reticular (CAR) cells [86]. High levels of regulatory cytokines (e.g. SDF-1, SCF, interleukins, TPO) are present within the niche in addition to ligands of the Notch and Wnt signaling pathways [82,84,87–89]. It is worth noting that though the bone marrow is the anatomical location for post-natal adult HSCs, the HSC niche during development shifts between multiple tissue regions, including the aorta-gonad-meonephros region, the yolk sac, the placenta, the fetal liver, and the spleen [90]. Therefore, recapitulating cues found in these early transient environments might be a novel approach to rejuvenate HSC function.

Similar to HSCs and other adult stem cell populations, skeletal muscle satellite cells do not act autonomously and require structural and biochemical signals along with support from their niche. Satellite cells are generally located along myofibers underneath the

surrounding basal lamina and outside the plasma membrane of the myofiber [91]. Many soluble cues, including Wnts, FGFs, IGFs, HGF, EGFs, SDF-1α, and Notch ligand, are exchanged between satellite cells and the surrounding myofibers, interstitial cells, and endothelial cells, and the identities and concentrations of the paracrine factors are responsible for maintaining quiescence, prompting self-renewal, and instigating differentiation [92–97]. In addition to the niches of HSCs and satellite cells, stem cell niches have also been identified for a number of tissue specific stem cells, including those of the intestine [98,99], skin [100], and nervous system [101].

2.3.2 Targeting dysregulated stem cell niches

The elegant and specified functionalities of stem cell niches are perhaps most appreciated when compared to systems in which the niche function has gone awry. In fact, there is mounting evidence linking dysregulated stem cell niches with many pathological occurrences, including aging [40,102–104], tissue degeneration [105], and tumor formation [106–108]. Certain diseases are also associated with improper niche function, such as is the case with the skin disorder epidermolysis bullosa in which the extracellular matrix composition of the basement membrane does not support the resident epidermal stem cells [109,110]. Therefore, targeting stem cell niches in order to promote endogenous regeneration is a promising strategy for a number of distinct applications.

There have been several clinical therapeutics based on the concept of targeting the stem cell niche, with many in particularly focusing on the bone marrow compartment [111]. The co-delivery of parathyroid hormone with transplanted umbilical cord blood was hypothesized to stimulate the resident osteoblasts in order to increase the number of HSCs, as activated osteoblasts have increased expression of Notch ligand which can in turn

stimulate HSC proliferation. Despite promising results observed in mice, no significant human patient outcomes were observed [112]. Several parallel approaches have been investigated for treating bone marrow failure due to severe aplastic anemia. Treatment with eltrombopag, a mimic of the stimulatory cytokine thrombopoietin, was recently observed to improve hematopoiesis in patients with refractory aplastic anemia [113], while immunosuppression with agents including antithymocyte globulin and cyclosporine are currently approved to target the immune cells in the niche [114]. To induce mobilization of HSCs from the niche for isolation and subsequent transplantation, the cytokines G-CSF and GM-CSF, or the small molecule inhibitor AMD3100, are used to inhibit the CXCR4/CXCL12 chemotaxis pathway normally active in the bone marrow niche [115]. These clinical examples of targeting different aspects of the bone marrow niche in order to induce a given response are not successful in every patient, which may be due to patient-to-patient variability in the niche composition and response.

2.3.3 *Ex vivo* expansion of adult stem cells

Unlike pluripotent stem cells, multipotent stem cells are not capable of extensive self-renewal *in vitro*. There is tremendous need for expansion protocols for multipotent adult stem cell populations, either for autologous cell therapies in which a patient's own stem cell pool must be expanded, or for allogeneic cell therapies in which large banks of cells are desired.

For example, while HSCs are by far the most common stem cells to be clinically transplanted, HSC transplants are primarily dependent on the availability of allogeneic donors with matching HLA types. Umbilical cord blood represents an additional source of HSCs, but there are not enough cells in a single cord for an adult patient, necessitating the

pooling of the cells from multiple cords. The ability to expand HSCs *ex vivo* would therefore reduce the dependence on finding a donor match and improve availability of cells to patients. Unfortunately, attempts at expansion of HSCs, even with the addition of purified growth factors known to regulate HSCs, have had limited success [116–118], as HSCs must be expanded quickly or risk losing their proliferative and blood lineage potential. Expansion of ST-HSCs rather than the desired LT-HSCs is a common issue, as is favoring expansion of lymphoid over myeloid progenitors [119,120]. Some success has been observed when HSCs are co-cultured with MSCs [121–124], since MSCs are stromal cells that are a natural part of the HSC microenvironment. However, compared with pluripotent stem cells, MSCs are not as amenable to scalable culture due to their reduced capacity for growth *in vitro* and significant donor-to-donor variability [125,126]. Classical cytokines, such as stem cell factor (SCF), thrombopoietin (TPO), interleukins (ILs), and Flt3-ligand (Flt3L), have been used previously to stimulate expansion. However, due to insufficient and unreliable HSC expansion with traditional cytokines, new emphasis is being placed on the use of developmental factors, such as Wnt proteins, Notch ligand, bone morphogenetic proteins (BMPs), and fibroblast growth factors (FGFs) [117,120,127,128].

Similar challenges with *ex vivo* expansion are observed with primary muscle populations, with a decreased capacity for re-engraftment and regeneration observed in satellite cell-derived myoblasts following expansion *ex vivo* [129–132]. Current strategies to expand mouse myoblasts cultured *in vitro* include the presentation of Notch-ligand [133] and the use of hydrogel culture substrates with a low elastic modulus that better mimics the native physiological environment [134], while recent advances in expanding human muscle stem cells has been achieved through inhibition of p38 MAPK [135]. To overcome

the current limitations, an increased understanding of the components and interactions in the stem cell niche will likely translate to more effective protocols for the maintenance and expansion of adult stem cell populations *ex vivo*.

CHAPTER 3

ALGINATE ENCAPSULATION PARAMETERS INFLUENCE MICROENCAPSULATED EMBRYONIC STEM CELL PHENOTYPE[3]

3.1 Introduction

Stem cells, including pluripotent embryonic stem cells (ESCs), have tremendous potential as tools for regenerative medicine and drug discovery. However, there are many challenges to overcome before stem cell-derived therapies can be made broadly available, including the lack of processes to manufacture viable and homogenous cell populations of sufficient numbers [136]. Currently, the large scale production of mammalian cells typically occurs in suspension bioreactors, which impart hydrodynamic forces that can adversely affect stem cell viability and influence their phenotype [137–140]. Stem cells are very sensitive to environmental stimuli, as external signals in the culture environment provide cues that determine whether stem cells continue to self-renew or differentiate into specific cell types. Because most current bioprocesses are designed around suspension culture systems, investigation into systems to culture anchorage-dependent stem cells in suspension is critical for translating process technology and for achieving the high cell densities required for therapeutic doses [141,142]. In addition, the ability to culture stem

---

[3]Modified from: Wilson JL, Najia M, Saeed R, McDevitt TC. Alginate encapsulation parameters influence the differentiation of microencapsulated embryonic stem cell aggregates. Biotechnol Bioeng 2014;111:618-31.

cells at high density would enable concentration of cell secreted factors to support paracrine-based therapies.

One approach to the challenge of scalable bioprocessing is to encapsulate stem cells in hydrogels, such as alginate, to better control microenvironmental cues and enable suspension culture. Microencapsulation has been used for decades to protect enclosed cells from the host immune system upon transplantation, but it can also shield cells from hydrodynamic shear forces found in bioreactor environments and prevent agglomeration of stem cell aggregates while permitting diffusion of nutrients and oxygen through the encapsulation material [143]. Several investigations of ESC microencapsulation, mostly with single cells, have been previously performed with alginate capsule formulations [67,69,70], and directed differentiation has been achieved, in most cases through soluble factor addition, toward osteogenic [74,144], cardiac [72,73], hematopoietic [145,146], neural [147], pancreatic [148,149], and hepatocytic lineages [66,150]. Although most previous studies have examined the encapsulation of single ESCs, aggregates of ESCs are important to investigate in addition to single cells for a number of reasons. First, using pre-formed aggregates provides a consistent initial size that can be compared directly to unencapsulated controls, which can also be cultured in suspension. Though microencapsulation-based protocols have been developed to form multicellular aggregates [67,68,151], using microwell formation [19] may provide more consistency so that the impact of encapsulation parameters on cell phenotype is not confounded by the additional parameters of aggregate size or the aggregation kinetics [152]. Furthermore, microencapsulation of aggregates has been previously determined to improve cell viability [70], as ESCs generally require maintenance of intercellular adhesions for optimal survival

[153]. Finally, culture as 3D aggregates can initiate differentiation of ESCs as embryoid bodies (EBs) [17,154], providing a platform to study the impact of microencapsulation parameters on differentiation trajectory.

While encapsulation has been explored as a tool for stem cell expansion and directed differentiation, the impact of alginate encapsulation parameters on stem cell phenotype has not been systematically examined. Alginate is a biocompatible polymer purified from brown seaweed that is commonly used to encapsulate mammalian cells due to its relative abundance and mild cross-linking requirements. Alginate is composed of two anionic monomers, α-L-guluronic acid (G) and β-D-mannuronic acid (M), which are arranged in both homopolymeric regions (GG blocks and MM blocks) and mixed monomeric regions (MG blocks) [54]. Cross-linking occurs at G residues through binding of divalent cations such as calcium, therefore alginates with higher G content and longer GG blocks produce stiffer, more porous beads due to greater cross-linking than alginates with higher M content. Because native alginate is non-adhesive and therefore cannot interact directly with cells, the physical and chemical properties of the polymer dictate the interactions with the enclosed cells. A handful of studies have examined the impact of G and M content on cell proliferation, metabolism, and secretion. Experiments with murine insulinoma βTC3 cells found that alginates with high G content inhibited cell growth, leading to decreased metabolic and secretory activity [155]. Alternatively, studies of encapsulated neural stem cells observed improved secretion of neurotrophic factors when the cells were cultured in alginate with high G content, citing poor capsule stability in alginate with high M content [156]. Despite such examples of reported differences based on G and M content, most studies do not specify the composition of alginate species used,

thus provoking questions about the potential influence of the encapsulation material utilized on the phenotype of the enclosed cells.

An additional microencapsulation property that can be varied is the presence of a coating surrounding the capsule, typically with a polycation like poly-L-lysine (PLL), which has historically served as an added barrier to the host immune system upon transplantation by decreasing the permeability of larger molecules, such as antibodies, into and out of the bead [58]. However, coating with PLL also confers additional mechanical stability [57,60,157,158] which can be beneficial for maintaining capsule integrity over time. Many studies have described problems with single cells escaping or leaking out of the capsules [53,73,159,160], an issue which may be ameliorated through PLL coating. However, the issue of cell escape may be increased when encapsulating pre-formed aggregates due to their large size and potential proximity to the bead edge, and it has yet to be determined whether addition of PLL is sufficient to prevent escape in this context, a question also relevant for the encapsulation of other aggregated cells.

Overall, the inconsistency in the composition of alginate and use of a coating layer in previous studies with microencapsulated cells raises questions about whether disparate results ensue from differing material compositions. The potential impacts of microencapsulation material on cell phenotype are particularly relevant for the culture of ESCs due to their increased sensitivities to the surrounding physical microenvironment [161]. Thus, the objective of this study was to systematically examine the impact of varying alginate compositions on microencapsulated ESC expansion and phenotype. Single cells and pre-formed aggregates of murine ESCs were encapsulated in alginate microbeads composed of a high or low ratio of G to M residues, with and without a PLL coating.

Characterization of the mass transport and mechanical properties of each bead composition was performed, as well as analysis of encapsulated cell viability, morphology, and phenotype via gene and protein expression. The results of this study revealed distinctions in the growth rate, morphology, differentiation trajectories, and secretion activities of ESCs in each of the encapsulated formats over 14 days of culture, suggesting that alginate bead composition is an important parameter to consider when designing microencapsulation-based expansion and directed differentiation protocols.

3.2 Materials and methods

3.2.1 Microbead and microcapsule formation

Two different medium viscosity alginates were used: ultrapure MVG (Pronova) which contains greater than 60% G residues (High G) and ultrapure MVM (Pronova) which contains greater than 50% M residues (High M). Alginate solutions were prepared at 1.5 wt% in calcium-free DMEM (Gibco) and autoclaved for sterilization no more than one day before use. An electrostatic bead generator (Nisco) was utilized for encapsulation. The alginate solution was extruded through a 400 μm nozzle using a syringe pump at a flow rate of 6 mL/hour and a voltage of 10 kV to produce beads that were dropped into a stirred bath of 100 mM calcium chloride (EMD) to crosslink the polymer droplet solution. The beads were washed three times with serum-free media (5 mL per mL of alginate beads) prior to downstream culture. To add a poly-L-lysine (PLL) coating, the beads were coated with variable concentrations of PLL (MW 15,000-30,000; Sigma) (1 mL per mL of alginate beads) for 2 minutes prior to three additional media rinses. This low concentration and short incubation time facilitated dissolution of the beads at a later time point, whereas

longer incubation times or higher concentrations prevented the retrieval of encapsulated cells. Non-coated beads were dissolved with a 5 minute incubation with 55 mM sodium citrate, while the PLL-coated beads required a 10 minute incubation with TrypLE^{TM} (Invitrogen) prior to the 5 minute incubation with 55 mM sodium citrate. To form solid-core PLL-coated beads, the beads were incubated with 0.1% PLL for 10 minutes followed by incubation with 0.15% alginate for 10 minutes. To form liquid-core PLL-coated beads, the solid-core beads were additionally incubated with 55 mM sodium citrate for five minutes to liquefy the center. The solid-core and liquid-core beads could not be easily dissolved post-formation. An additional technique to form liquid-core beads was also examined, was adapted from Zhao et al in which a "shell" of 2% alginate with 250 mM mannitol in PBS was pushed through the outer region (21 gauge) of a coxial nozzle, while a 1% carboxymethyl cellulose with 0.25 M mannitol in PBS was simultaneously pushed through the inner region (28 gauge) of the coaxial nozzle [162].

3.2.2 Embryonic stem cell culture

Murine ESCs (D3 cell line) were cultured on tissue culture treated polystyrene dishes (Corning) adsorbed with 0.1% gelatin (EmbryoMax). Undifferentiated ESC culture media consisted of Dulbecco's modified Eagle's medium (DMEM) (Mediatech) supplemented with 15% fetal bovine serum (Hyclone), 100 U/mL penicillin, 100 µg/mL streptomycin, and 0.25 µg/mL amphotericin (Mediatech), 2 mM L-glutamine (Mediatech), 1x MEM non-essential amino acid solution (Mediatech), 0.1 mM 2-mercaptoethanol (Fisher Scientific), and 10^3 U/mL of leukemia inhibitory factor (LIF) (ESGRO). Cultures were replenished with fresh media every other day (complete media exchance) and passaged prior to reaching 70% confluence.

3.2.3 ESC aggregate formation and culture

A single cell suspension of undifferentiated ESCs was obtained through dissociation of monolayer cultures with 0.05% trypsin-EDTA (Mediatech). Defined, serum-free N2B27 media [163] was used for all aggregate cultures and consisted of DMEM/F12 (50/50) medium (Gibco) supplemented with N2 (Gibco), 25 μg/L bovine serum albumin (BSA), 100 U/mL penicillin, 100 μg/mL streptomycin, and 0.25 μg/mL amphotericin (Mediatech), 2 mM L-glutamine (Mediatech), all combined 1:1 with Neurobasal medium (Gibco) supplemented with B27 (Gibco). N2B27 basal media has been widely used by several groups for a number of different applications, including undifferentiated ESC culture [164], differentiation of ESCs to insulin-producing cells [149], and hematopoietic differentiation of ESCs [146]. Additionally, neural ectoderm differentiation is considered the "default" pathway for ESC differentiation [165] in the absence of any exogenous factors, thus N2B27 media is an appropriate choice for basal media to examine ESC differentiation. Aggregation of ESCs was achieved by centrifugation (200 rcf) of ESCs into 400 μm square polydimethylsiloxane (PDMS) micro-wells (Aggrewell™, Stem Cell Technologies) as previously reported [19,152]. The cell seeding density yielded approximately 500 cells per individual well. The ESCs were incubated in the wells for approximately 20 hours in serum-free N2B27 culture media to allow for aggregate formation. The resulting aggregate population was either immediately transferred to suspension culture (approximately 1500 aggregates in 10 mL of serum-free culture media) for the unencapsulated condition or transferred after subsequent encapsulation. Aggregates were cultured in sterile 100 x 15 mm bacteriological grade polystyrene Petri dishes (BD) and maintained on rotary orbital shakers [166] at ~45 rpm.

A 90% media exchange was performed every three days following gravity-induced sedimentation of the aggregates in 15 mL conical tubes. Suspension cultures were maintained for up to 14 days of differentiation.

3.2.4 Single cell and aggregate microencapsulation

Single cells were resuspended in 1.5% sterile alginate warmed to 37° at a density of 5 x 10^6 cell/mL of alginate, while aggregates were re-suspended at a density of 12,000 aggregates per mL (approximately 6 x 10^6 cells/mL), as this density balanced the number of empty beads with beads containing multiple aggregates. Alginate beads were formed using the electrostatic bead generator and processed as described in section 3.2.1. All encapsulated cells were cultured in serum-free N2B27 media on a rotary orbital shaker as previously described in section 3.2.3.

3.2.5 Mass transport characterization

To assess the diffusion of molecules out of the alginate beads, fluorescent dextran molecules of 3 kDa, 10 kDa, and 70 kDa (Life Technologies) were utilized. Alginate beads of varying compositions were incubated with 100 µM dextran solutions for 2 hours. After the 2 hour incubation, the beads were removed from the dextran solution using a cell strainer and added to a volume of fresh PBS. Samples of the PBS solution were taken every 30 seconds for 20 minutes in addition to 25 minute, 30 minute, and 40 minute time points. The collected samples were read on a Synergy H4 plate reader (Biotek) at the appropriate excitation and emission wavelengths and related to concentration based on standard curves created from known concentrations of fluorescent dextran.

3.2.6 Mechanical characterization

Alginate beads of both High G and High M were formed (without cells) and coated with PLL as described in section 3.2.1. The beads were maintained in serum-free (N2B27) media on a rotary orbital shaker to simulate conditions experienced during culture. At days 1, 7, and 14 following formation, the mechanical properties were assessed through micron-scale parallel-plate compression using a CellScale MicroSquisher and the associated SquisherJoy software [167]. The upper compression plate of a 302.8 μm cantilever compressed the samples at 40% strain over a period of 40 seconds, held at constant deformation for 10 seconds, and released over a period of 40 seconds to document the magnitude of hysteresis. To determine the Young's modulus, Hertzian theory for non-adhesive elastic contact was used to fit a linear regression line to 30 data points above and below the 20% strain data point on the plot of force (F) vs. deformation$^{2/3}$ (d). The resultant slope in addition to the initial radius (R) of the bead was used to calculate the Young's modulus of the sample (E), as described by the following standard expression:

$$F = \frac{4}{3} E \times R^{1/2} \times d^{2/3}$$

During testing, all samples were held in a PBS fluid bath (pH 7.4 with 0.1 g/L Ca^{2+} and 0.1 g/L Mg^{2+}).

3.2.7 Cell viability staining and imaging

Cell viability was assessed using a LIVE/DEAD kit (Molecular Probes Inc., Eugene, OR). Samples were incubated in PBS containing 0.1 μM calcein AM and 8 μM ethidium homodimer-1 at 4°C for 1 hour. The samples were washed with PBS, transferred to a glass-bottomed 24-well plate, and immediately imaged using a Zeiss LSM 700-405 confocal microscope (Carl Zeiss Inc.).

3.2.8 Cell number quantification

Samples were collected from each group at days 4, 7, 10, and 14 of differentiation. Encapsulated aggregates were released from beads through 10 minute incubation with TrypLE™ (Invitrogen) for PLL-coated beads only, trituration, and 5 minute incubation with 55 mM sodium citrate (Sigma) for all beads, as previously described [73]. The cells were centrifuged at 200 rcf for 5 minutes and rinsed 3x with PBS. Cells from all conditions were pelleted at 375 rcf for 4 minutes followed by supernatant removal and storage at -20°C. A CyQUANT Cell Proliferation Assay Kit (Molecular Probes Inc., Eugene, OR) was used to determine cell number, with a standard curve created using undifferentiated ESCs that were counted using a hemocytometer. The fluorescence (480 nm excitation, 520 nm emission) indicating DNA content was read using a Synergy H4 plate reader (Biotek). The net growth rate (μ_{net}) was determined by examining change in cell density (X) over given periods of time (t) using the following standard expression:

$$\frac{dX}{dt} = \mu_{net} X$$

3.2.9 Histological analysis

Encapsulated and unencapsulated aggregates were sampled at days 4, 7, and 14 of differentiation, rinsed with PBS, fixed in 4% paraformaldehyde for 30 minutes with rotation at room temperature, rinsed with PBS, and stored at 4°C. Fixed aggregates were embedded in Histogel (Richard-Allen Scientific, Kalamazoo, MI), processed via a series of graded ethanol and xylene rinses, and embedded in paraffin. Paraffin-embedded samples were sectioned at a thickness of 5 μm using a rotary microtome (Microtom HM310). For histological analysis, sections were de-paraffinized through a series of xylene and graded

ethanol concentrations, followed by staining with hematoxylin and eosin (H&E). Stained sections were imaged using a Nikon Eclipse 80i equipped with a SpotFlex digital camera (Diagnostic Instruments).

3.2.10 Quantitative real time PCR

Encapsulated aggregates were released from beads through 10 minute incubation with TrypLE^{TM} (Invitrogen) for PLL-coated capsules only, trituration, and 5 minute incubation with 55 mM sodium citrate (Sigma) for all beads. The cells were centrifuged at 200 rcf and rinsed 3x with PBS to remove residual PLL. RNA was extracted from the aggregates with the RNeasy Mini kit (Qiagen Inc, Valencia, CA). The RNA (300 ng/sample) was converted to complementary DNA using the iScript cDNA synthesis kit (Bio-Rad, Hercules, CA) and analyzed using real time PCR (MyIQ cycler, Bio-Rad). Forward and reverse primers for *18s*, *Oct4*, *Nanog*, *Pax6*, *AFP*, *MLC-2v*, and *Flk1* were designed with Beacon Designer software (sequences and conditions are given in **Table 3.1**) and purchased from Invitrogen. *Oct4* and *Nanog* gene expression were calculated with respect to undifferentiated ESC expression levels as previously described [168]. *Pax6*, *AFP*, *MLC-2v*, and *Flk1* concentrations were determined using a standard curve and normalized to *18s* expression levels.

Table 3.1. Primer sequences for quantitative real-time PCR analysis

Gene	Forward sequence	Reverse sequence	Melt temperature (°C)
18s	CTCTAGTGATCCCTGAGAAGTTCC	ACTCGCTCCACCTCATCCTC	60.0
Oct4	CCGTGTGAGGTGGAGTCTGGAG	GCGATGTGAGTGATCTGCTGTAGG	60.0
Nanog	GAAATCCCTTCCCTCGCCATC	CTCAGTAGCAGACCCTTGTAAGC	60.0
Pax6	ACGGCATGTATGATAAACTAAG	GCTGAAGTCGCATCTGAG	58.0
AFP	CACACCCGCTTCCCTCATCC	TTCTTCTCCGTCACGCACTGG	59.0
MLC-2v	GACCATTCTCAACGCATTCAAG	CTTCTCCGTGGGTAATGATGTG	59.0
Flk1	GGCGGTGGTGACAGTATC	TGACAGAGGCGATGAATGG	64.3

3.2.11 Immunofluorescent staining

Encapsulated and unencapsulated aggregates were sampled at days 4, 7, and 14 of differentiation, rinsed with PBS, fixed in 4% paraformaldehyde for 30 minutes with rotation at room temperature, rinsed with PBS, and stored at 4°C. For whole mount imaging, the fixed aggregates were washed 3x with block buffer (2% donkey serum, 0.1% Tween-20 in PBS) prior to permeabilization in 1.5% Triton-X 100 for 30 minutes. The aggregates were then re-fixed in 4% paraformaldehyde for 15 minutes, blocked for 1-3 hours at room temperature, and incubated with primary antibodies against OCT-4 (Santa Cruz Biotechnology sc-8628; goat polyclonal; 1:100) and SSEA-1 (Santa Cruz Biotechnology sc-21702; mouse monoclonal; 1:100) overnight at 4°C. The following day, the aggregates were washed 3x with block buffer and incubated with secondary antibodies (1:200 Alexa Fluor 555 donkey anti-goat, 1:200 Alexa Fluor 488 donkey anti-mouse) and Hoechst (Life Technologies; 1:100) for 4 hours at room temperature prior to 3x washes in block buffer and imaging. For histological sectioning, fixed aggregates were embedded in Histogel (Richard-Allen Scientific, Kalamazoo, MI) and subject to graded sucrose and OCT infiltration prior to rapid freezing in a dry ice-ethanol bath and storage at -80°C. OCT-embedded samples were sectioned at a thickness of 10 μm using a CryoStar NX70 cryostat and allowed to dry at room temperature. Each section was surrounded using a PAP hydrophobic barrier pen and rinsed with PBS 3x for 5 minutes. The slides were blocked and permeabilized with 3% donkey serum and 0.05% Triton X-100 for 45 minutes at room temperature. After rinsing with PBS 2x for 5 minutes, primary antibody solution diluted in blocking buffer (3% donkey serum in PBS) was added and incubated overnight at 4°C. Primary antibodies against OCT-4 (Santa Cruz Biotechnology sc-8628; goat polyclonal;

1:100), AFP (Dako A000829-2; rabbit polyclonal; 1:100), and α-SMA (Dako M0851; mouse monoclonal; 1:100) were used. Following overnight incubation, slides were rinsed with PBS 3x for 5 minutes and incubated with secondary solutions diluted in blocking buffer (1:1000 AlexaFluor®488 donkey anti-goat, 1:1000 Alexa Fluor 488 donkey anti-rabbit, and 1:1000 Alexa Fluor 488 donkey anti-mouse) for 1 hour at room temperature. Slides were rinsed with PBS 3x for 5 minutes and incubated with Hoechst dye (1:100) for 10 minutes at room temperature. Following a final PBS rinse, coverslips were mounted with Fluoromount-G (SouthernBiotch) and sealed with clear nail polish. The slides were imaged using a Zeiss LSM 700-405 confocal microscope (Carl Zeiss Inc.).

3.2.12 Conditioned media analysis

Spent media was collected from unencapsulated and encapsulated ESC aggregates cultured in hypoxia (3% oxygen) after 72 hours of culture between day 4 and day 7 of differentiation. The conditioned media was centrifuged at 3000 rcf for 5 minutes to remove cellular debris, and the supernatant was transferred to a new 15 mL conical tube for storage at -20°C. Enzyme-linked immunosorbent assay (ELISA) kits (DuoSet, R&D) were used to quantify the amount of VEGF and BMP-4 present in the conditioned media. Capture antibody was adsorbed onto 96 well MaxiSorp Immunoplates (Nunc), blocked with 1% BSA in PBS, incubated with standards and samples, and bound with detection antibody. The concentration of protein was determined using a colorimetric reaction of peroxidase and tetramethylbenxidine and a plate reader to measure the absorbance at 450 nm. The absorbance values for the conditioned media samples were compared to a standard curve to determine the protein concentration, which was normalized to cell number (as described in 3.2.8) and reported as pg of protein per mL or pg of protein per one million cells.

3.2.13 Statistics

All experiments were performed with replicate samples from independent conditions. The data is represented as the mean of the independent replicates, and the error bars represent the standard error of the mean. Before performing statistical analysis, data were normalized using a Box–Cox power transformation to normalize data variance. One-way and two-way ANOVAs were calculated between different conditions and time points as appropriate, followed by post hoc Tukey analysis to determine significant differences ($p < 0.05$). All statistical analyses were performed using MatLab and SYSTAT software.

3.3 Results

3.3.1 Characterization of microcapsule properties

A variety of alginate microbead and microcapsule configurations were initially examined as platforms for ESC culture. The concentration (i.e. wt%) and composition (i.e. higher or lower ratios of guluronic acid – High M and High G) of alginate were varied along with the presence or absence of a poly-L-lysine (PLL) coating **(Figure 3.1)**. In addition to uncoated beads **(Figure 3.1d)**, three different configurations of PLL-coated beads were explored: (1) coating with 0.05% PLL for 2 min, providing a thin barrier; (2) coating with 0.1% PLL for 10 minutes and 0.15% alginate for 10 minutes, providing a thicker barrier (termed "solid core") **(Figure 3.1e)**; and (3) coating with 0.1% PLL for 10 minutes and 0.15% alginate for 10 minutes, followed by liquefaction of the center through 5 minute incubation with the chelating agent sodium citrate (termed "liquid core") **(Figure 3.1f)**. An additional liquid core arrangement was investigated in which a shell of alginate was formed around a core of methylcellulose **(Figure 3.1g)**; however, the formation of

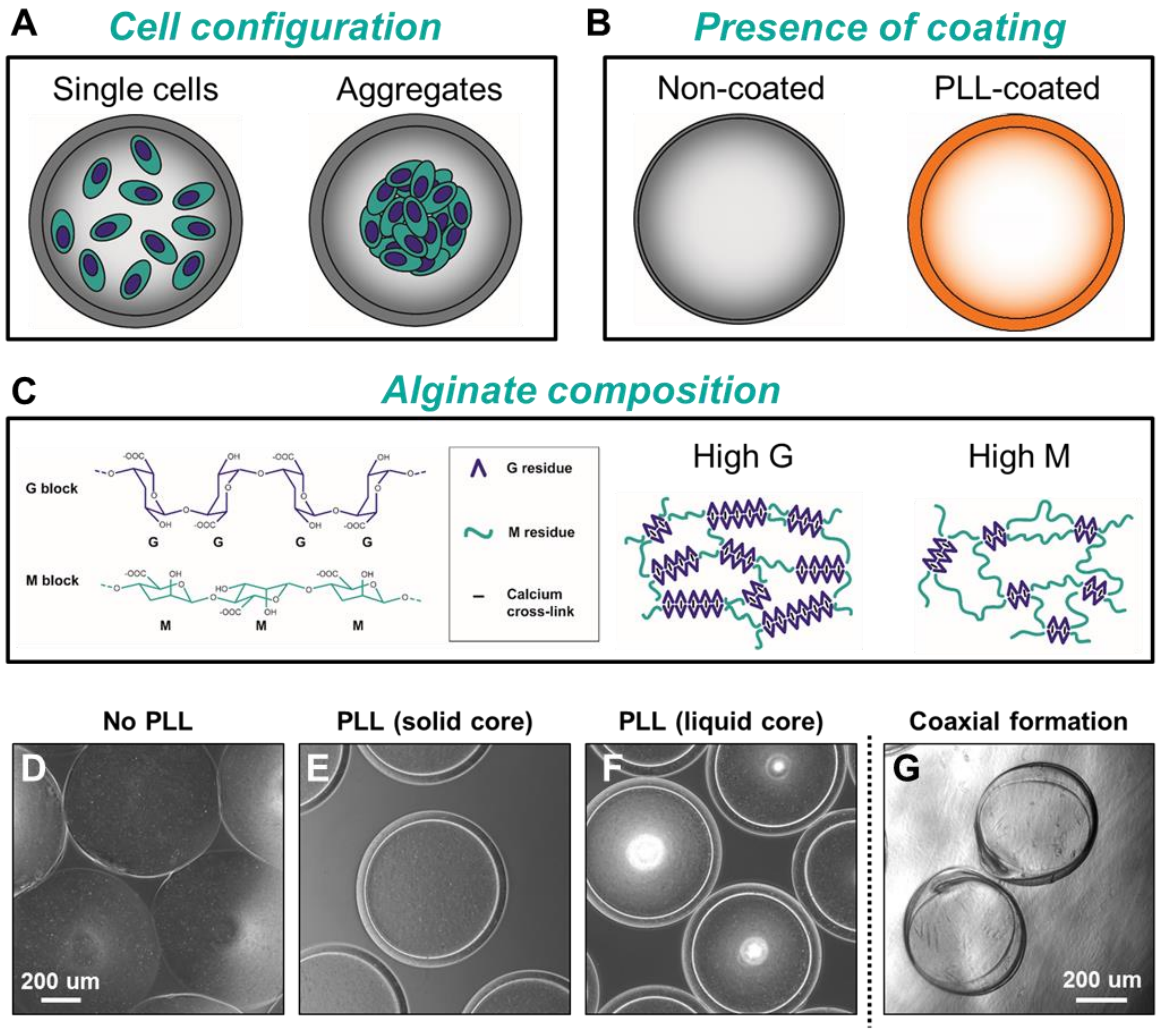

Figure 3.1. Configurations of alginate beads. ESCs were encapsulated as either single cells or as pre-formed 500 cell aggregates **(A)** in alginate composed of either a higher ratio of guluronic acid (G) residues or a higher ratios of mannuronic acid (M) residues **(C)**. The beads were maintained in a non-coated state or coated with poly-L-lysine to promote mechanical stability (**B)** and allow for liquefaction of the center core. Phase images of non-coated **(D),** PLL-coated **(E-F)**, and coaxial-formed **(G)** beads display the general size and form. Scale bar = 200 µm.

beads in this manner was inconsistent, with only a fraction (~10%) of the capsules containing a single aggregate.

Because the ultimate goal of the alginate encapsulation system requires diffusion of stem cell secreted molecules out of the beads, assessment of mass transport properties of different bead compositions was performed. To perform the experiments, alginate beads were incubated with dextran solutions (3 kDa, 10 kDa, 70 kDa) for two hours, assumed to be sufficient time for the dextran molecules to diffuse into the alginate and reach a steady state. Fairly instantaneous diffusion was observed with 3 kDa and 10 kDa dextran molecules in uncoated beads, while a more gradual diffusion profile was observed with the 70 kDa dextran, thus the larger size was used for future evaluations **(Figure 3.2a-c)**. Alginate beads composed of High G and High M were formed at two different concentrations (1.5 and 2.5% by weight) and with or without the presence of a PLL coating (with 1.5% alginate only). The PLL coating appeared to block initial transport of the 70 kDa dextran molecules into the beads, thus preventing the ability to measure dextran diffusion from the alginate. The absence of dextran uptake indicated that coating the beads with PLL prevents transport molecules greater than 70 kDa **(Figure 3.2d, 3.2f)**. In general, diffusion of the dextran out of the the alginate beads with a higher percentage of alginate (2.5%) took a longer time than in the beads with a lower percentage of alginate (1.5%) for both alginate compositions **(Figure 3.2e, 3.2g)**. In addition, the beads composed of 1.5% High M alginate also exhibited slower diffusion than beads composed of 1.5% High G alginate **(Figure 3.2h)**, consistent with reports that though High G alginate is capable of greater crosslinking, it is also more porous overall [169]. No difference in diffusion was observed between the two alginate species at the higher concentration (2.5%) **(Figure 3.2i)**,

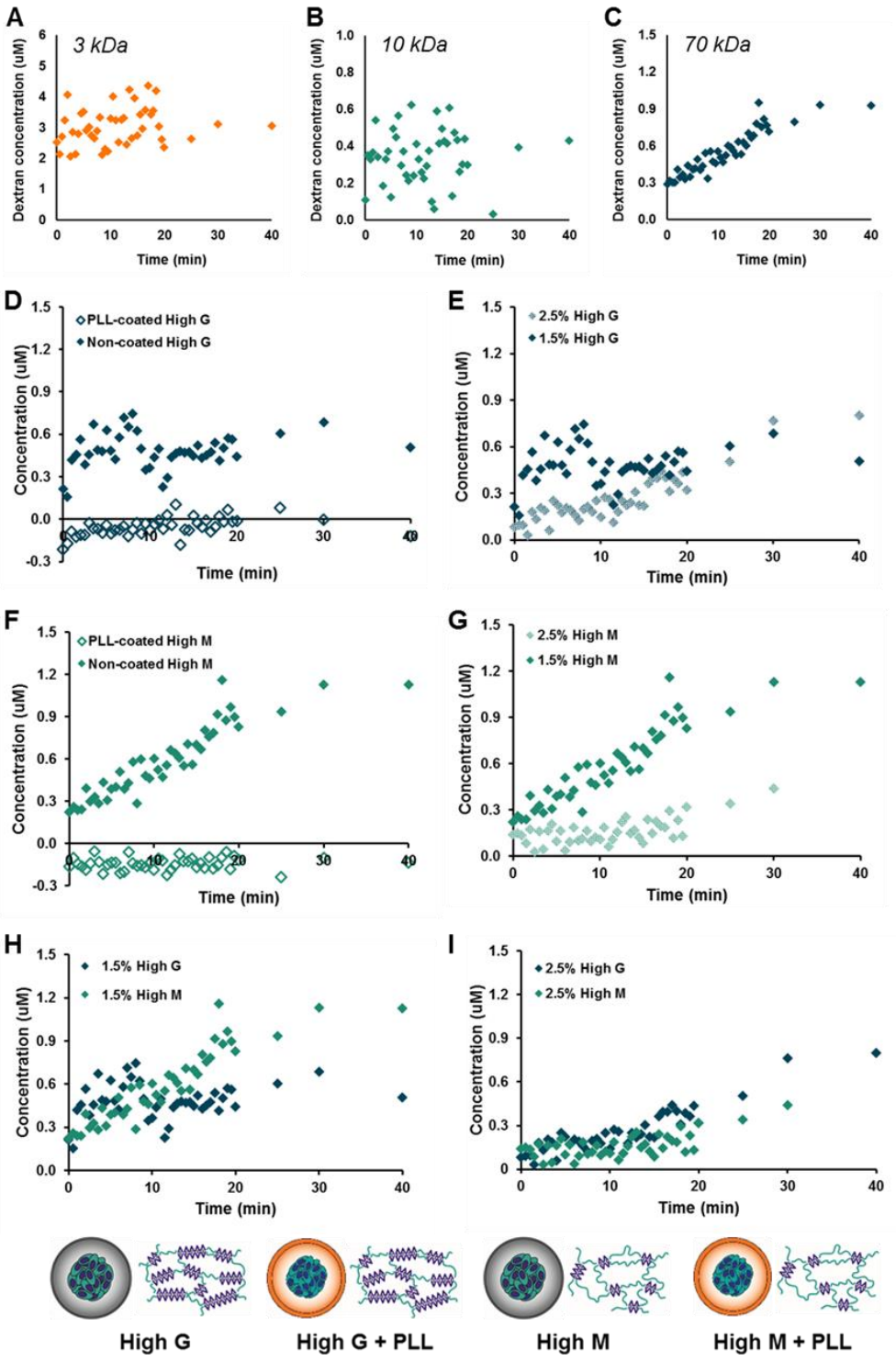

Figure 3.2. Mass transport in alginate beads. Dextran molecules of 3kDa **(A)** and 10 kDa **(B)** diffused freely through non-coated High M beads, while 70 kDa dextran **(C)** diffused more slowly. The 70 kDa dextran was used to assess a number of capsule properties **(D-I)**, with the PLL coating prohibiting diffusion **(D,F)**, the increased alginate concentration slowing diffusion **(E,G)**, and the High G alginate appearing more permeable than the High M alginate only when at the lower concentration **(H-I)**.

though there was less overall dextran released implying that less may have been originally loaded into the beads.

The bulk mechanical properties of each bead type were determined by parallel plate compression testing in which stress-strain curves were obtained for individual beads **(Figure 3.3a)**. The Young's modulus, estimated using Hertzian theory, ranged from 4-18 kPa and was consistently greater in the PLL-coated beads, likely due to the increased mechanical stability provided by the external polyelectrolyte layer, though the liquefaction of the alginate core did not result in a change of overall mechanical stiffness **(Figure 3.3b, 3.3d)**, which may indicate that poor liquefaction was achieved or that the presence of the coating dominates the mechanical profile. To determine whether the mechanical properties or stability changed with time in culture, alginate beads composed of High G or High M alginate with or without a thin PLL coating were kept in culture conditions (in media at 37°C in a humidified incubator) for up to two weeks. The uncoated High G alginate was significantly stiffer than the uncoated High M alginate at days 1 ($p = 0.011$) and 7 ($p < 0.001$) following formation **(Figure 3.3d)**, consistent with previous literature reports that alginate containing a higher proportion of guluronic acid residues enhances the mechanical strength of the hydrogels [48]. The modulus remained constant over the course of the culture period for each composition tested, indicating that the beads were physically stable for at least two weeks when cultured dynamically without enclosed cells in standard culture media **(Figure 3.3d)**. The average bead diameter (~734 μm) was relatively uniform for all of the bead compositions examined over the 14 day culture period **(Figure 3.3c)**.

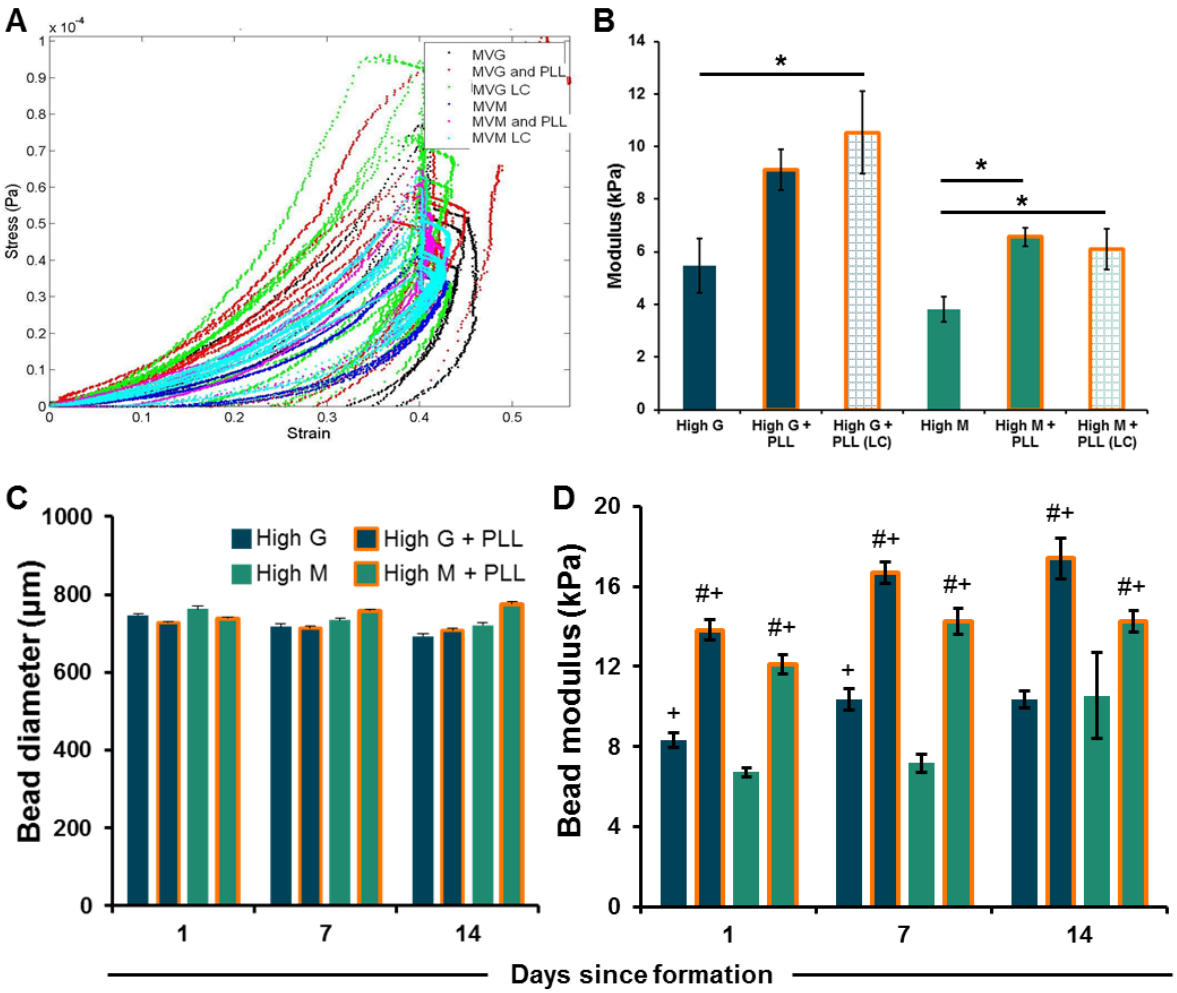

Figure 3.3. Mechanical properties of alginate beads. Stress-strain curves were recorded during parallel plate compression testing **(A)** of alginate beads immediately following formation **(B)**, and the derived elastic moduli of the PLL-coated beads were found to be significantly stiffer than the non-coated beads, though a decrease was not observed with those beads with a liquid core (LC). The mechanical stability was assessed over time in culture, during which there were no substantial changes in capsule size **(C)**. The High G alginate was initially stiffer than the High M alginate, with the PLL-coated beads exhibiting additional increases in elastic modulus **(D).** Significant ($p < 0.05$) increases are denoted between specific groups (*), over High G (#), and over High M (+).

3.3.2 Encapsulation of single embryonic stem cells

ESCs were encapsulated as single cells in High G alginate at a density of 5 x 10^6 cells/mL alginate and were cultured for seven days in uncoated or PLL-coated alginate with the center liquefied through chelation with sodium citrate **(Figure 3.4a)**. While the majority of cells appeared viable directly after encapsulation, a decrease in cell viability was observed in cells within the uncoated alginate beads over time **(Figure 3.4b-c)**. The observed cell death is likely a result of insufficient cell-cell contacts due to the solid matrix, as the majority of cells remained as single cells and did not appear to increase in number over time. In contrast, the cells cultured in the PLL-coated liquid core beads began to form small aggregates as early as three days post-encapsulation **(Figure 3.4l),** though some capsule breakage was also observed **(Figure 3.4j-k)**. In some cases, several smaller aggregates were established within a single beads, and in other instances, a single large aggregate was formed. By day 7 of culture, some of the large aggregates were observed to be bursting out of the capsule due to their large size **(Figure 3.4m)**. The formation of these aggregates led to a substantial improvement in cell viability **(Figure 3.4d-e)**. Though the culture of ESCs in liquid core beads promoted aggregate formation and cell survival, the size of aggregates was not uniform or well-controlled. In addition, the thicker PLL coating required for liquid core formation did not facilitate retrieval of the cells for further application or analysis due to difficulties enzymatically degrading the PLL. Thus, future encapsulation studies relied entirely on pre-formed ESC aggregates.

3.3.3 Encapsulation of embryonic stem cell aggregates

Embryonic stem cell spheroids were encapsulated in alginate with a high (High G) or low (High M) ratio of guluronic acid to mannuronic acid. Additionally, a portion of the

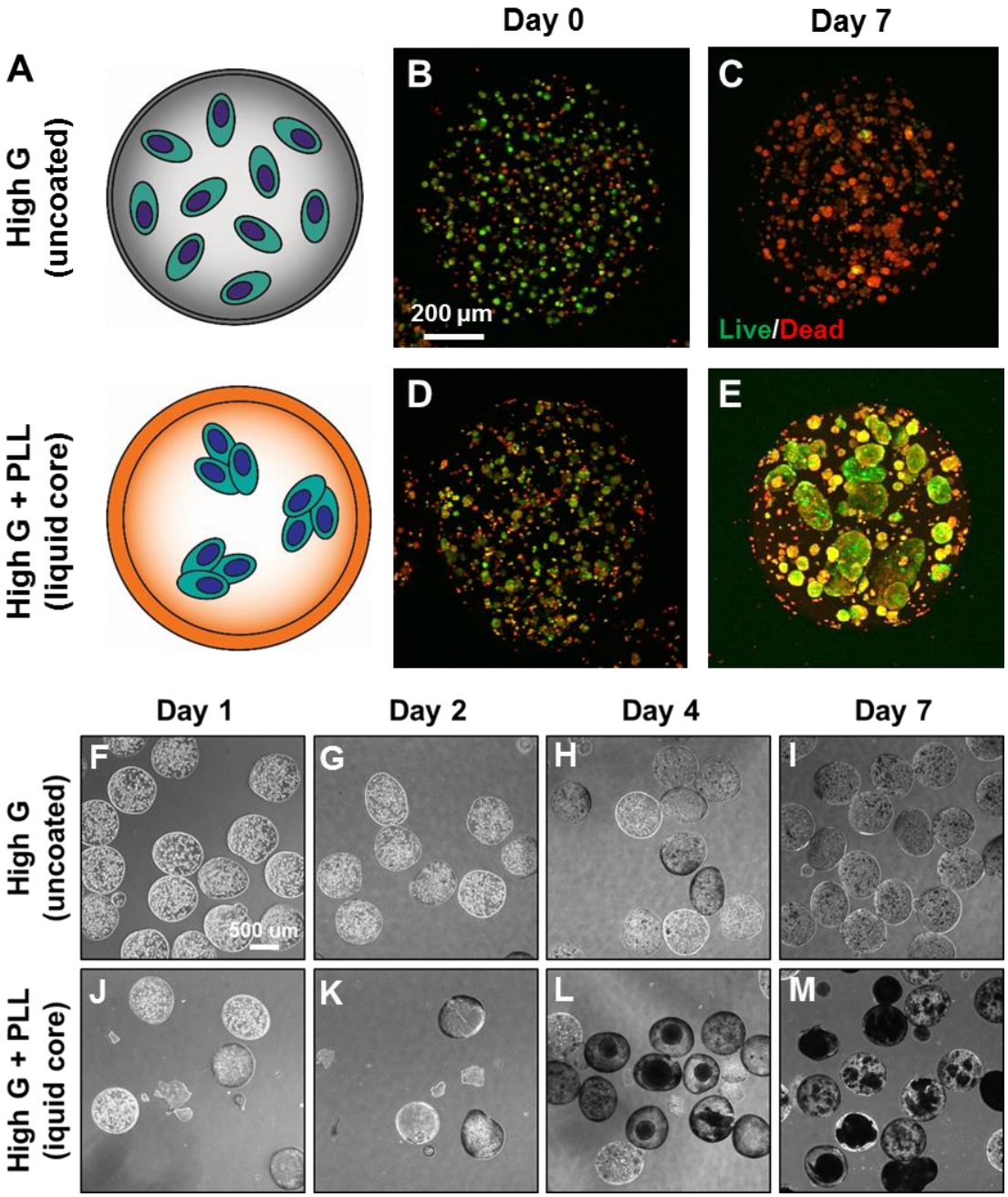

Figure 3.4. Encapsulation of single, dissociated ESCs. Single cells encapsulated in uncoated High G alginate **(A)** exhibited high initial cell viability **(B)** but were primarily non-viable by day 7 of culture **(C)**. Single cells encapsulated in PLL-coated High G alginate with the center liquefied **(A,D)** displayed higher cell viability after 7 days **(E)**. Phase images of the two conditioned over the 7 day culture period **(F-M)** demonstrate the formation of aggregates in the liquid core group and the relative lack of cell growth in the uncoated group.

beads were coated with poly-L-lysine (PLL), creating High G + PLL and High M + PLL beads in addition to uncoated beads **(Figure 3.5)**. The seeding density of spheroids in alginate gave rise to a small number (<15%) of empty beads, with the majority of beads (>71%) containing one to three spheroids, consistent with the expected Poisson distribution assuming an average rate of two aggregates per capsule **(Figure 3.5k)**. Although the beads appeared similar after one week, unencapsulated spheroids **(Figure 3.5a, 3.5f)** and aggregates within each bead type **(Figure 3.5b-e, 3.5g-j)** exhibited distinct morphologies depending on the type of alginate used. All of the encapsulated spheroids appeared smaller than unencapsulated spheroids, with those in High G and High G + PLL remaining spherical **(Figure 3.5b-c, 3.5g-h)**, whereas those in High M and High M + PLL appeared more ovoid **(Figure 3.5j)**.

Aggregate escape from the alginate beads was observed as early as four days post-encapsulation for aggregates within the High M alginate **(Figure 3.5l)**. After 14 days in culture, aggregate escape was more frequent, with many of the initially encapsulated aggregates no longer residing within the alginate beads **(Figure 3.5g, 3.5i)**. In general, the High G alginate contained the aggregates more effectively than the High M alginate, with the addition of the PLL coating improving retention. The High G + PLL formulation maintained all spheroids within beads **(Figure 3.5h)**, while the uncoated High M only retained ~4% of the aggregates within beads after 14 days of culture.

Cell viability was assessed following 14 days in culture for each of the encapsulation conditions for both encapsulated and escaped aggregates due to the incidence of spheroid escape. Viable cells were more prevalent when the aggregates were not contained within the beads **(Figure 3.6a)**, with non-viable cells present more frequently in

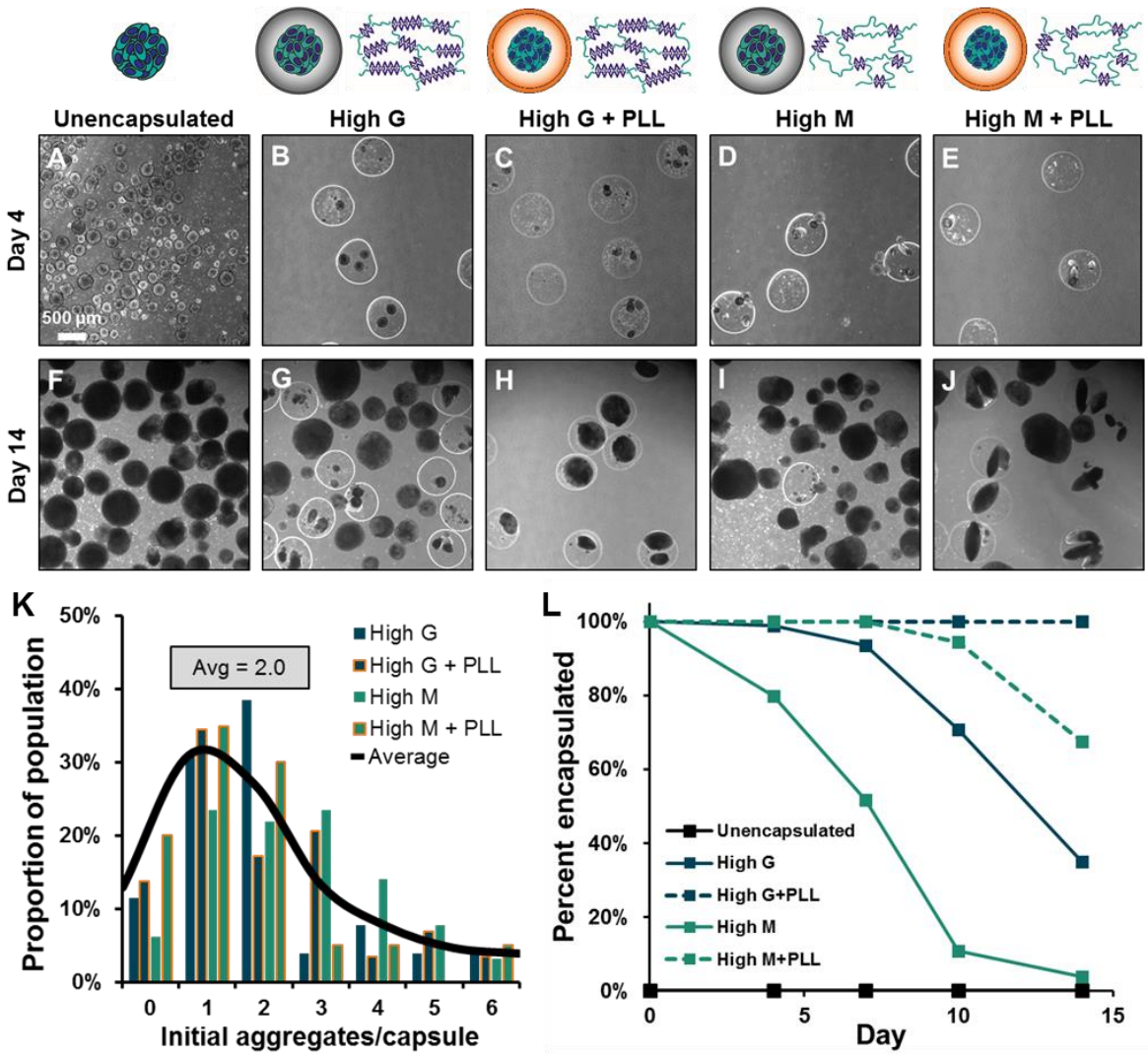

Figure 3.5. Encapsulation and escape of ESC aggregates. Pre-formed ESC aggregates were encapsulated and cultured for 14 days in four different alginate configurations in parallel with unencapsulated aggregates (**A-J)**. Initially, there was a distribution of aggregates per bead, with an overall average of two aggregates per bead **(K)**, though the aggregates began to escape from the capsules as early as four days in culture **(L)**. The High G+PLL condition was the only alginate bead configuration in which no aggregates escaped in the full 14 days of culture.

the encapsulated aggregates. The non-viable cells tended to be localized to the more rounded aggregates, with more viable cells present in the elongated region of aggregates when present. In addition, more viable cells were observed in the beads coated with PLL than in the non-coated beads.

The proliferation rates of the ESCs cultured in different configurations **(Figure 3.6b)** diverged, with the unencapsulated spheroids having the highest initial net growth rate (0.38 day^{-1} versus 0.12 day^{-1} for High G, 0.32 day^{-1} for High G + PLL, 0.24 day^{-1} for High M, and 0.22 day^{-1} for High M + PLL). After 14 days of culture, the number of cells in the unencapsulated aggregates was significantly greater than in the High G ($p = 0.016$), High G + PLL ($p < 0.001$), and High M + PLL ($p = 0.035$) conditions. Cell growth appeared most stunted in the cells within the stiffer High G and High G + PLL beads, though the beads coated with PLL exhibited overall similar growth trends to each other after day 4. A marked increase in cell number was observed after the majority of encapsulated aggregates escaped from the beads (day 7 for High M and day 10 for High G), indicating that the cells proliferated more robustly when not encapsulated. Cell growth plateaued at a cell density of ~1.8×10^6 cells/mL, likely due to the volumetric capacity of the culture system and exhaustion of nutrients from the culture media.

The elongated morphology that was observed in some groups prompted further examination into the morphological differences observed based on encapsulation conditions. At day 4, the ESC aggregates were generally small and fairly round **(Figure 3.7a-c)**, although some elongated protrusions were observed in the High M and High M + PLL groups **(Figure 3.7d-e)**. The aggregates were densely packed without any morphogenic structures, suggesting that a primarily undifferentiated phenotype persisted.

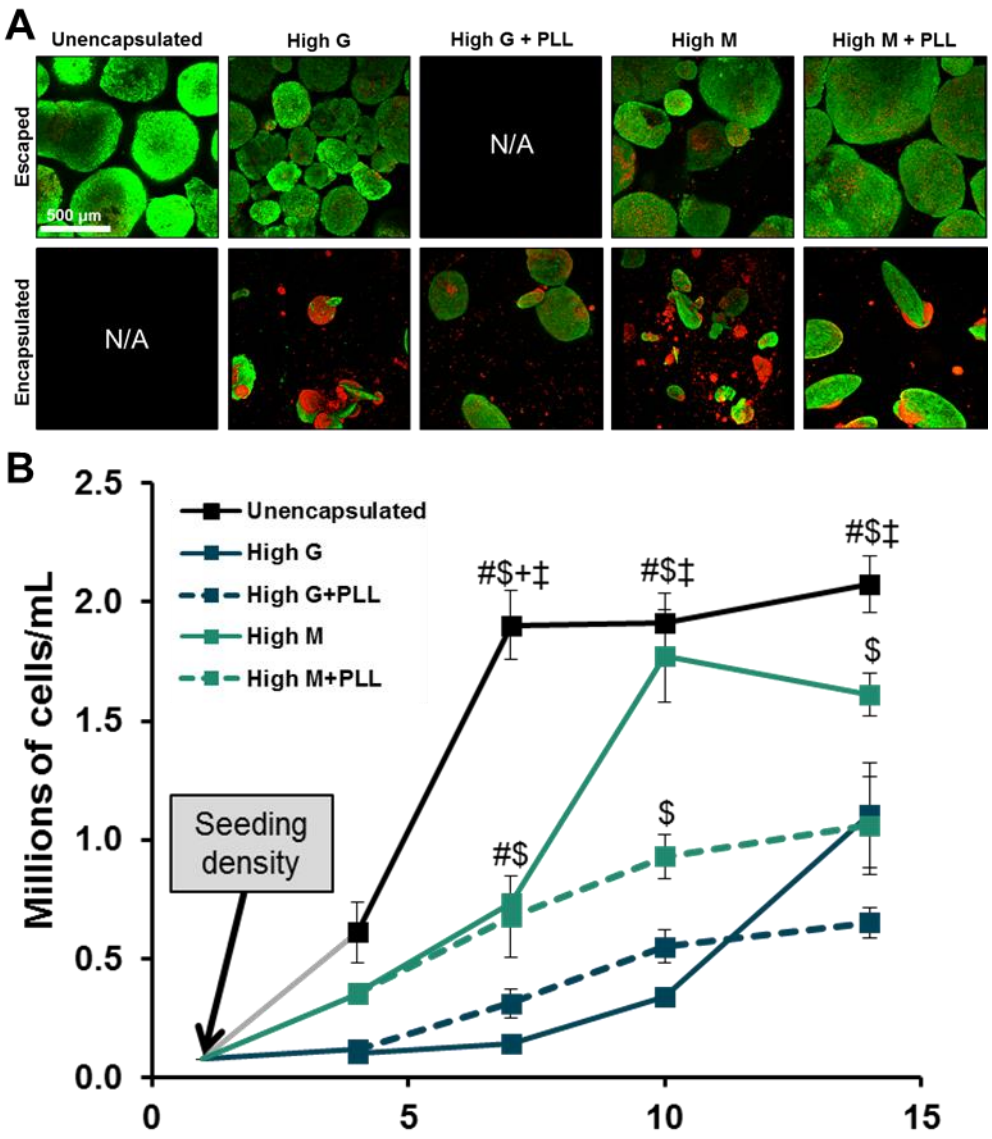

Figure 3.6. Cell viability and proliferation within alginate beads. Viability was assessed following 14 days in culture for each of the encapsulation conditions using a LIVE/DEAD assay, and projection images were obtained via confocal microscopy **(A)**. Due to the incidence of spheroid escape, both escaped and encapsulated aggregates were examined (when present). Viable cells, indicated in green, were more frequently observed when the aggregates were not within the beads, with non-viable cells, indicated in red, present at a higher frequency in the encapsulated aggregates. Cell viability appeared to be better maintained in the beads coated with PLL when compared to the non-coated counterparts. The proliferation rates for the ESCs cultured in the different configurations diverged **(B)**, with the cell density in the unencapsulated condition significantly higher than the cell density in the High G, High G + PLL, and High M + PLL conditions. Scale bar = 500 µm. Significant ($p < 0.05$) increases over unencapsulated (*), High G (#), High G + PLL ($), High M (+), and High M + PLL (‡) are denoted.

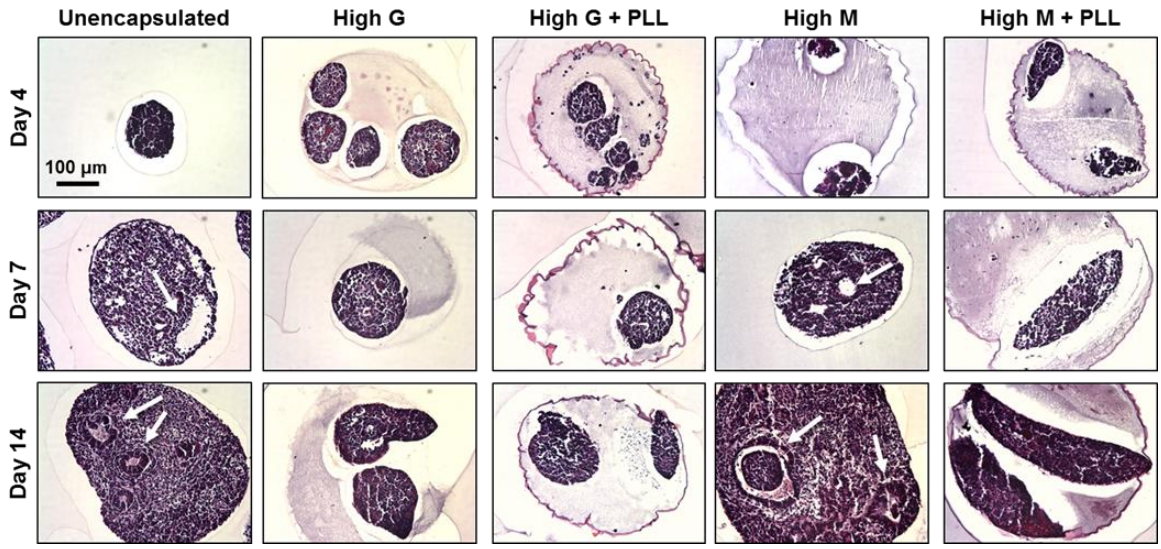

Figure 3.7. Histological analysis of aggregate morphology. Hematoxylin and eosin (H&E) staining of encapsulated and unencapsulated spheroids were examined at days 4, 7, and 14 of differentiation. At day 4, the aggregates were generally small, densely packed, and fairly circular **(A-C)**, though some elongated protrusions were observed in the High M and High M + PLL groups **(D-E)**. By day 7 of differentiation, some cavitation was observed in the unencapsulated **(F)** and High M **(I)** conditions. The aggregates in the High G **(G)** and High G + PLL **(H)** alginates appeared relatively spherical, whereas more elongated aggregates were observed in the High M + PLL **(J)** condition. By day 14, more organized structures were formed in the unencapsulated **(K)** and High M **(N)** groups, including epithelial arrangement, small neural rosettes, and continued cavitation, while elongated protrusions began to appear in the High G and High G + PLL groups **(L-M)** and continued to exist in the High M + PLL group **(O)**. White arrows indicate distinct morphological organization. Scale bar = 100 µm.

By day 7 of differentiation, some cavitation was observed in the unencapsulated **(Figure 3.7f)** and High M **(Figure 3.7i)** conditions (which by day 7 contained only half of the spheroids within beads), suggesting that differentiation was progressing more rapidly in the unencapsulated condition and the High M alginate beads. While the aggregates in the High G **(Figure 3.7g)** and High G + PLL (Figure 4H) alginate beads still appeared relatively round, more distinguished extension of the ovoid geometry occurred in the High M + PLL **(Figure 3.7j)** condition. After two weeks in culture, more differentiated structures were formed in the unencapsulated **(Figure 3.7k)** and High M **(Figure 3.7n)** groups, including epithelial layer arrangement, small neural rosettes, and cavitation. The unencapsulated and High M conditioned aggregates appeared larger, consistent with the cell proliferation data **(Figure 3.7b)** previously described. In contrast, aggregates encapsulated in the High G **(Figure 3.7l)** and High G + PLL **(Figure 3.7m)** beads continued to exhibit a smaller cross-sectional area, though more multicellular protrusions were observed than at earlier time points. The significantly elongated morphology in the High M + PLL condition at day 14 **(Figure 3.7o)** was present at similar levels to the High M + PLL at day 7 and at greater frequency than any of the other experimental groups.

3.3.4 Impact of encapsulation parameters on ESC aggregate phenotype

To determine what, if any, impact encapsulation in alginate with varying compositions had on stem cell differentiation, gene and protein expression were examined over the course of two weeks. Relative to the undifferentiated ESC starting population, most conditions exhibited decreased gene expression of the pluripotency markers *Oct4* **(Figure 3.8a)** and *Nanog* **(Figure 3.8b)** over time. However, different temporal trajectories were observed, with the cells encapsulated in the High G and High G + PLL beads

exhibiting significantly higher *Oct4* levels at day 7 compared to cells in unencapsulated ($p < 0.001$ and $p < 0.001$, respectively), High M ($p < 0.001$ and $p < 0.001$), and High M + PLL ($p < 0.001$ and $p = 0.006$,) conditions. Furthermore, the cells within the High M and High M + PLL had expressed higher levels of *Oct4* when compared to the unencapsulated spheroids ($p < 0.001$ and $p < 0.001$, respectively), signifying that residence within the alginate beads, even temporarily, may delay or impede differentiation. By day 14, cells in the High G and High G + PLL beads continued to express higher levels of *Oct4* compared to the unencapsulated, High M, and High M + PLL conditions. A similar trend was observed in the expression of *Nanog*, with cells in the High G alginate exhibiting higher levels compared to unencapsulated cells at day 4 and aggregates in the High G and High G + PLL conditions expressing higher levels than the unencapsulated aggregates at day 7. After 14 days, the cells in the High G + PLL beads maintained significantly increased expression over the unencapsulated and High M groups. The steady *Nanog* levels observed in the High G + PLL group, as opposed to the decrease observed in all other groups, was noteworthy since High G + PLL was the only condition to retain 100% of the spheroids over the entire two week period of culture.

Genes representative of the three germ lineages were also examined to determine if encapsulation conditions could impact differentiated phenotype(s), since culture as aggregates can lead to spontaneous differentiation as embryoid bodies (EBs). *Pax6*, an early ectodermal marker, was elevated in the unencapsulated, High M, and High M + PLL conditions compared to the High G and High G + PLL conditions at day 7 **(Figure 3.8c)** and increased in all groups by day 14, with the High G + PLL and High M + PLL groups having significantly higher levels than the High M and unencapsulated groups.

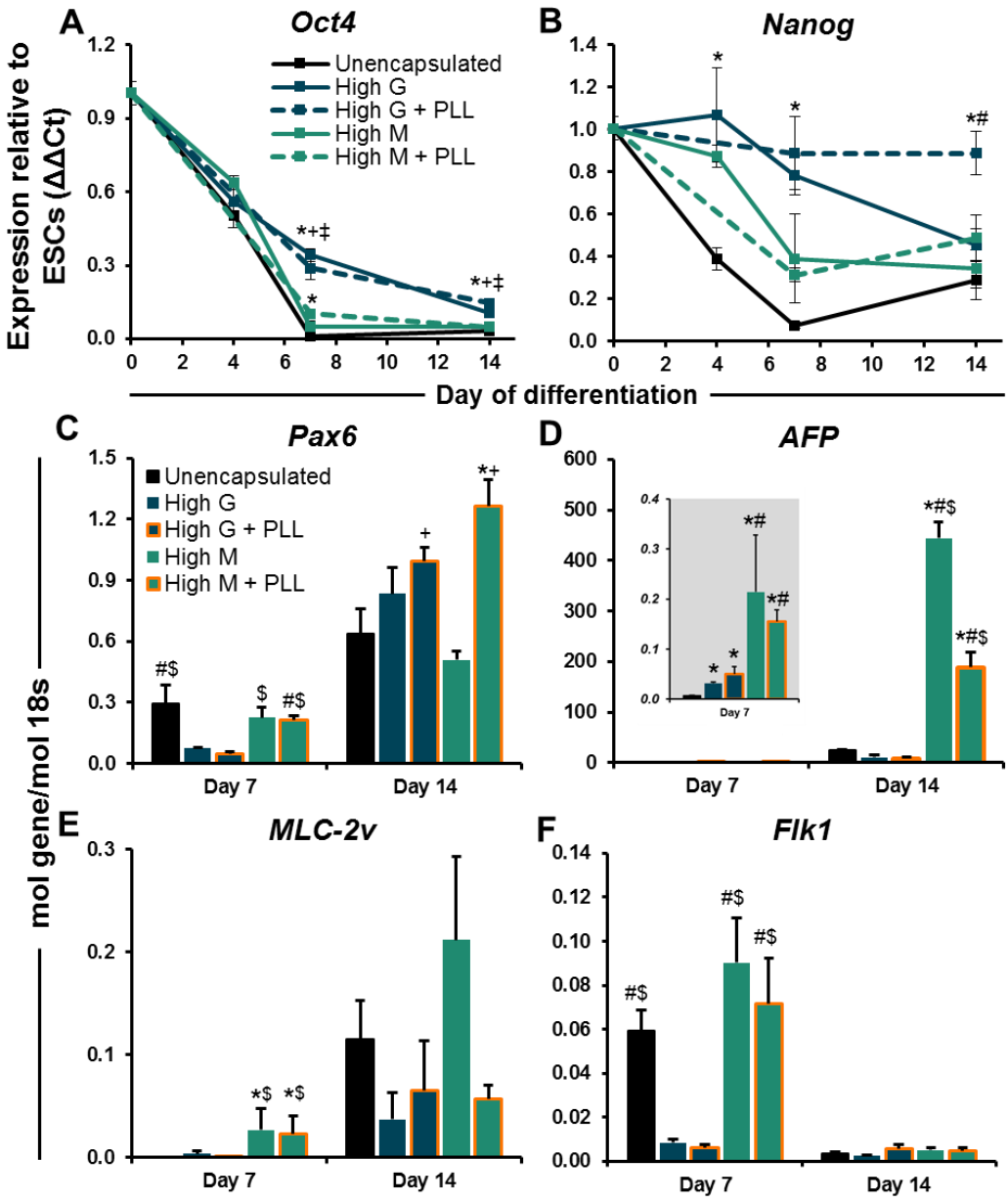

Figure 3.8. Gene expression analysis of encapsulated aggregates. Relative to the undifferentiated ESC starting population, most conditions exhibited decreased gene expression of the pluripotency markers *Oct4* **(A)** and *Nanog* **(B)** over time, however different temporal trajectories were observed, with encapsulated cells, particularly those in the High G and High G + PLL groups, maintaining *Oct4* and *Nanog* expression longer than the unencapsulated aggregates. *Pax6* was elevated in the unencapsulated, High M, and High M + PLL conditions over the High G and High G + PLL conditions at day 7 **(C)** and increased in all groups by day 14, with the High G + PLL and High M + PLL expressing *Pax6* at higher levels than the High M and unencapsulated groups. Expression of alpha-fetoprotein (*AFP*) was increased in the High M and High M + PLL groups **(D)**, with significantly higher expression compared to other groups observed both at day 7 and 14 of differentiation. Expression of *MLC-2v* was elevated in High M and High M + PLL conditions at day 7 **(E)**. *Flk1* was more highly expressed in the unencapsulated, High M, and High M + PLL conditions at day 7 **(F)**. Significant ($p < 0.05$) increases over unencapsulated (*), High G (#), High G + PLL ($), High M (+), and High M + PLL (‡) are denoted.

Investigation of alpha-fetoprotein (*AFP*) expression, an endodermal marker, revealed dramatic increases in the High M and High M + PLL groups **(Figure 3.8d)**, with significantly higher expression compared to all other groups observed both at day 7 and 14 of differentiation.

Spontaneous contractile beating was observed in approximately half of the unencapsulated aggregates and approximately one-third of the High M aggregates at days 10 and 14, motivating further examination into mesodermal cardiac differentiation. Expression of *MLC-2v*, an isoform of myosin light chain-2, was elevated in High M and High M + PLL conditions at day 7 **(Figure 3.8e)**. Furthermore, increased *MLC-2v* expression was observed in the unencapsulated and High M groups at day 14, consistent with the visually observed beating activity. In addition, expression of *Flk1*, which encodes for VEGF receptor-2 and is a common marker of primitive mesoderm differentiation, was increased in the unencapsulated, High M, and High M + PLL conditions at day 7 **(Figure 3.8f)**, though only transient expression was observed, as levels were decreased in all groups by day 14 compared to day 7.

To determine spatial patterns of phenotype expression within encapsulated aggregates, whole mount staining of unencapsulated and encapsulated aggregates was performed at day 10 of differentiation **(Figure 3.9a)**. While the cell viability dyes were easily able to penetrate the PLL barrier **(Figure 3.9b)**, antibodies were unable to diffuse into the PLL-coated beads **(Figure 3.9c)**. The ESCs within the non-coated High G beads exhibited higher expression of the pluripotent transcription factor OCT4 and carbohydrate surface marker stage-specific embryonic antigen 1 (SSEA-1), consistent with the gene

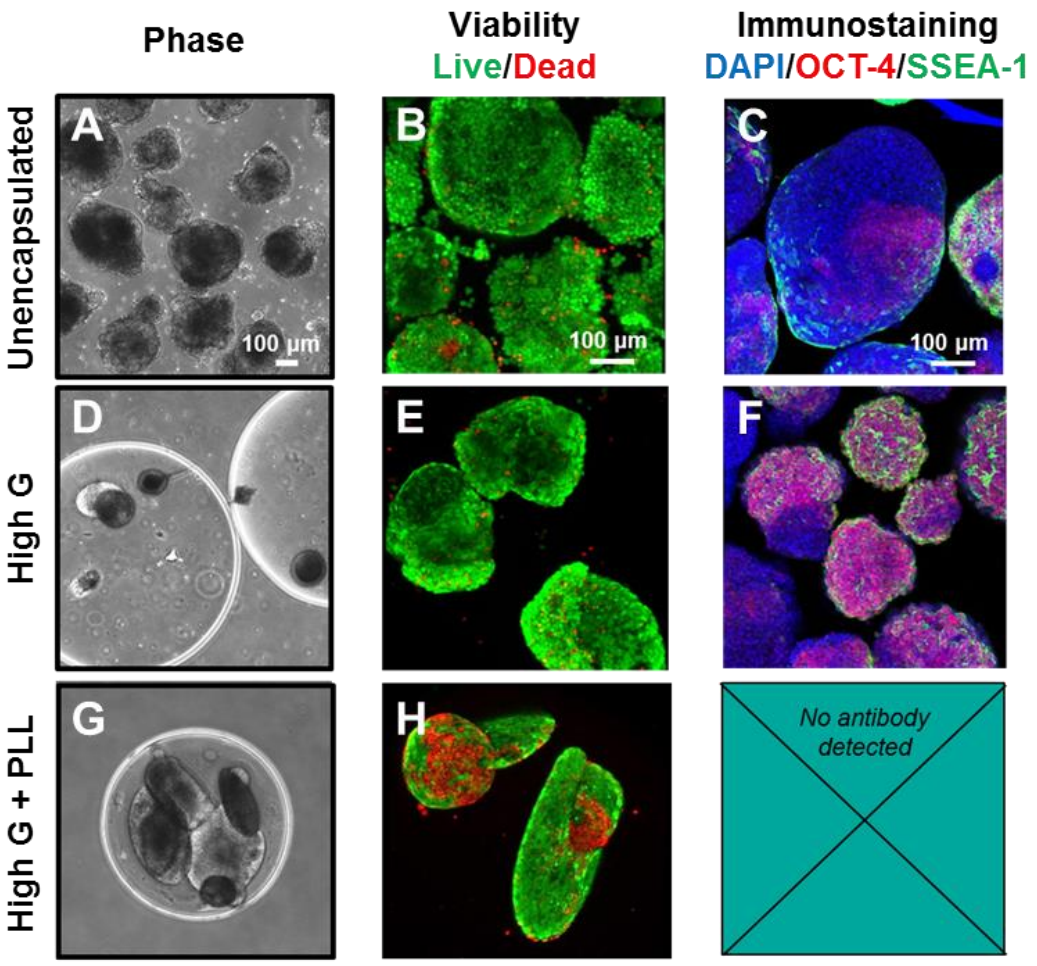

Figure 3.9. Whole mount immunostaining of encapsulated aggregates. Unencapsulated aggregates and aggregates encapsulated in uncoated and PLL-coated High G alginate were imaged after 10 days of culture. Phase contrast images indicate that less cell growth is observed in cells within the uncoated alginate **(D)** in comparison to unencapsulated **(A)** and PLL-coated alginate **(G)** and that cell viability was maintained in all conditions **(B,E,H)**. Whole mount immunostaining for the pluripotency markers OCT-4 and SSEA-1 indicates higher expression in the cells encapsulated in uncoated High G alginate **(F)** in comparison to unencapsulated cells **(C)**. The antibody was unable to penetrate the PLL barrier in the PLL-coated beads. Scale bar = 100 µm.

expression data indicating that encapsulation in High G alginate delayed differentiation in comparison to unencapsulated aggregates.

To assess protein expression for all groups (including the PLL-coated conditions), the aggregates were sectioned and immunostained for OCT-4, AFP, and alpha smooth muscle actin (α-SMA). Similar to what was observed in the gene expression and whole mount staining data, the relative intensity of OCT-4 expression in the encapsulated groups **(Figure 3.10b-e)** was elevated compared to the unencapsulated group **(Figure 3.10a)** at day 7. AFP was expressed most frequently in cells from the High M condition **(Figure 3.10i)** at day 14, with little to no expression detected in the other groups **(Figure 3.10g-h, 3.10j-k)**. In the High M conditions, AFP was commonly observed throughout the aggregates or in central localized regions surrounded by an epithelial layer, as displayed in Figure 6I. Expression of α-SMA was observed frequently at localized regions near the aggregate exterior in the unencapsulated **(Figure 3.10k)** and High M **(Figure 3.10n)** groups at day 14, the same conditions in which spontaneous beating was observed. More diffuse expression of α-SMA was observed in the High G **(Figure 3.10l)**, High G + PLL **(Figure 3.10m)**, and High M + PLL groups **(Figure 3.10o)**, none of which exhibited spontaneous beating in culture.

To determine whether encapsulation in High G or High M alginate impacted the secretion of growth factors produced by ESCs, conditioned media from unencapsulated and encapsulated ESC aggregates after 72 hours of culture between day 4 and day 7 of differentiation was assessed for the concentration of vascular endothelial growth factor (VEGF) **(Figure 3.11a)** and bone morphogenetic protein-4 (BMP-4) **(Figure 3.11b)**. There was no significant difference observed between media collected from unencapsulated

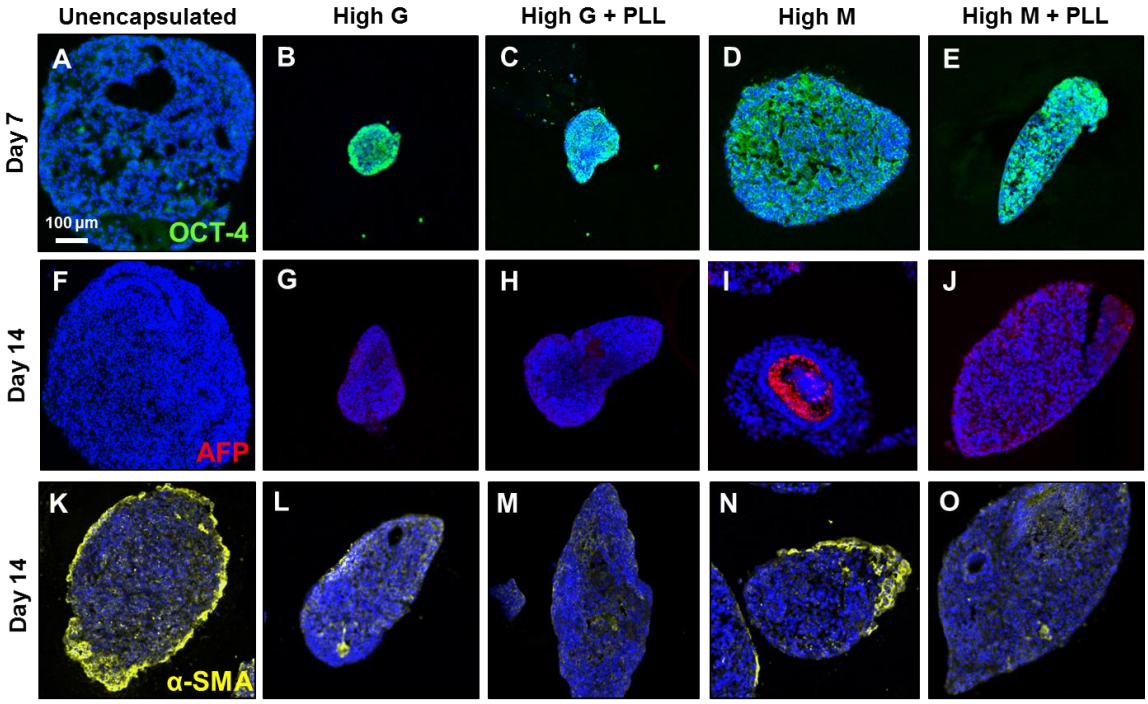

Figure 3.10. Cryosection immunostaining analysis. Frozen sections from each group were stained for OCT-4, AFP, and alpha smooth muscle actin (α-SMA) and counterstained for cell nuclei. The extent of OCT-4 expression was higher in the encapsulated groups **(B-E)** compared to the unencapsulated group **(A)** at day 7. AFP was observed frequently in the High M condition **(I)** at day 14, with little to no expression detected in the other groups **(G-H, J-K)**. Expression of α-SMAwas observed at localized regions in the unencapsulated **(K)** and High M **(N)** groups at day 14. More diffuse expression of α-SMA of a lower relative intensity was observed in the High G **(L)**, High G + PLL **(M)**, and High M + PLL groups **(O)**. Scale bar = 100 µm.

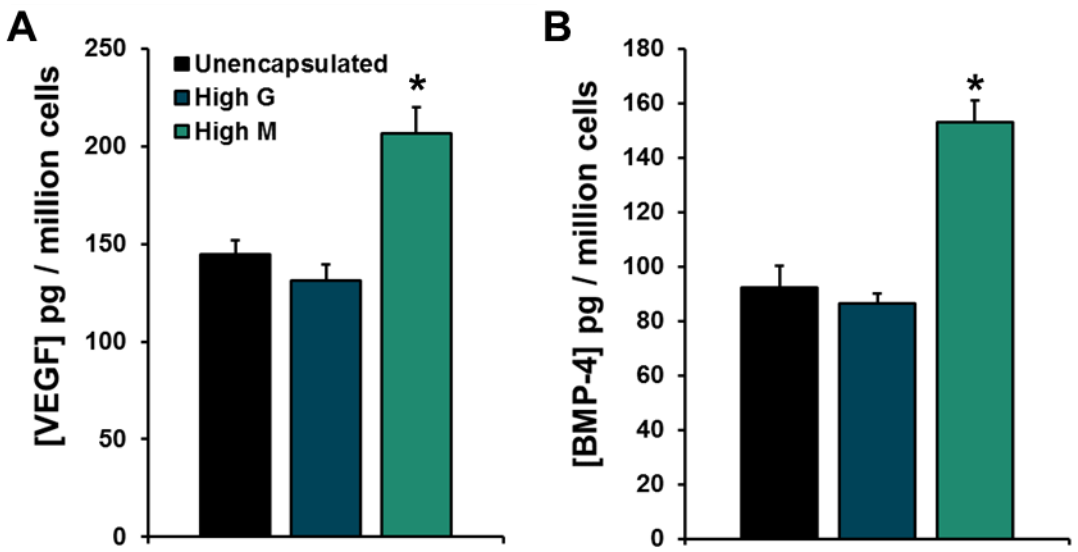

Figure 3.11. Growth factor concentrations in conditioned media. Spent media that was conditioned between days 4 and 7 of differentiation was collected and analyzed using ELISAs for the growth factors vascular endothelial growth factor (VEGF) **(A)** and bone morphogenetic protein-4 (BMP-4) **(B)**. No differences were observed between unencapsulated cells or cells encapsulated in High G alginate, though culture in High M alginate led to a significant increase in concentration. * = $p < 0.05$ from all other groups.

aggregates and aggregates cultured in High G alginate, however a significant increase in concentration for both growth factors was observed in media collected from aggregates cultured in High M alginate (for VEGF, $p = 0.021$ and $p = 0.009$ for unencapsulated and High G, respectively; for BMP-4, $p = 0.004$ and $p = 0.003$ for unencapsulated and High G, respectively).

3.4 Discussion

The findings of this study indicate that the composition of alginate beads can have a dramatic impact on the expansion and phenotype of microencapsulated ESCs. Examination of four different bead compositions (High G, High G + PLL, High M, and High M + PLL) yielded divergent phenotypes of the enclosed ESC aggregates. The addition of a PLL coating to alginate beads dramatically reduced the rate of cell escape

from the microbeads, completely preventing escape in the case of the High G + PLL condition. Encapsulation generally retarded cell growth while also inhibiting the loss of pluripotency, particularly for cells cultured in the stiffer High G alginate than cells in the more flexible High M alginate. These results demonstrate that encapsulation material properties and format impact pluripotent stem cell expansion and differentiation.

Though there have been several reports of encapsulating single ESCs in alginate beads [66,67], very low cell viability was observed when using single, dissociated cells in this study, likely a result of the lack of cell-cell and cell-ECM contacts. Native alginate does not contain adhesive moieties necessary for cell attachment, thus it is unsurprising that cells lacking these cues did not survive. Previous studies have overcome the issue of cell attachment through the incorporation of adhesive cues into the alginate material, either by mixing it with a second polymer such as collagen [69,170] or by modifying the alginate polymer with the addition of adhesive peptides like arginine-glycine-aspartic acid (RGD) [171]. Another approach to improve cell survival has been to permit cell aggregation within the beads through liquefaction of the center, though this method leads to uncontrolled formation kinetics and less regulated aggregate size. While some success was observed using the PLL-coated liquid core beads to form aggregates, the number and dimensions of the aggregates were quite variable **(3.4e, 3.4l-m)**. In addition, the thick PLL coating required for subsequent liquefaction was not compatible with later retrieval of the encapsulated cells for analysis, particularly because the positively charged PLL molecule can interfere with RNA extraction methods. Due to these complications, the remainder of the studies employed pre-formed aggregates rather than single cell suspensions.

To define the physical microenvironment experienced by the encapsulated ESCs, the mass transport and mechanical characteristics of the alginate beads were evaluated. Coating the beads with PLL prevented the diffusion of 70 kDa dextran molecules into and/or out of the beads, indicating that the molecular weight cut-off was below 70 kDa **(Figure 3.2d, 3.2f)**. This finding is consistent with later observations that antibody molecules were unable to penetrate the capsule barrier **(Figure 3.9)** in addition to previous reports indicating that immune molecules are unable to penetrate PLL-coated alginate beads [172]. While 3 kDa and 10 kDa dextran molecules did not appeared to be at all hindered in their transport, the 70 kDa dextran took approximately 20 minutes to achieve a steady state concentration in the High M alginate, though the transport appeared more instantaneous in the more porous High G alginate **(Figure 3.2h)**. Increasing the concentration of alginate from 1.5% by weight to 2.5% also impeded diffusion, as it appeared that the incubation time was insufficient to allow full transport of the 70 kDa dextran molecules **(Figure 3.2e, 3.2g)**. The secretion of ESC-produced proteins (VEGF and BMP-4 are 38 kDa and 47 kDa, respectively) did not appear to be impeded by the non-PLL-coated alginate beads given sufficient time for diffusion **(Figure 3.11)**.

The elastic modulus for the different bead composition was also determined, and the values of the different alginate beads (4-18 kPa) were similar to previously reported literature values [74,77,170,173,174]. PLL-coated alginate beads were stiffer than the non-coated beads **(Figure 3.3b, 3.3d)**, consistent with the increased stability exhibited following polycation addition. The elastic modulus of PLL-coated beads did not decrease following liquefaction of the core **(Figure 3.3b)**, indicating that the bulk elastic modulus is primarily based on exterior strength and may not accurately reflect the mechanical forces

encapsulated cells experience locally within beads. Uncoated High G alginate was significantly stiffer (~1.3-fold) compared to the High M alginate, indicating that the cells within the High G beads may experience a more constrained microenvironment than those in the High M beads. No significant decrease in modulus within the same group was observed over two weeks of culture, which was unexpected based on previous reports that bead stability decreases with time [156,158,175] and the data presented here regarding aggregate escape from the beads **(Figure 3.5l)**.

The difference between the constant elastic modulus over time and the increasing frequency of aggregate escape may be due to the discrepancy between a bulk mechanical measure like the Young's modulus and the incidence of local fissures in the material that can create pathways for cell escape. The formation and propagation of local cracks in the beads is further supported by the correlation between the extended, ovoid morphology and the frequency of escape **(Figure 3.5)**, indicating that the aggregates appear to grow and expand along the primary axis of weakness prior to escape. Although some previous reports of elongated, "lens-like" morphology of microencapsulated cells have been described [151,170], no clear explanation for this phenomenon has been offered. The correlation between cell growth and cell escape is likely related to differences in gel mechanics, however it is unclear whether stiffer alginate materials impede cell growth (and therefore the expansion of aggregates out of the bead) directly, or whether less stress is exerted on the stiffer alginate due to less net cell growth, leading to prolonged bead stability. It is also possible that local gradients in calcium due to cellular calcium use may contribute to the generation of local weak points in the alginate. In general, greater cell numbers and higher cell viability were observed in the conditions with more elongated aggregates, indicating

that in cases where elongation was not observed, cell growth may have been physically impeded. Increased initial cell growth rates **(Figure 3.6b)** and higher cell viability **(Figure 3.6a)** were observed in the PLL-coated capsules, which is consistent with previous studies that directly compared PLL-coated and uncoated alginate capsules [156,170]. While the direct mechanism behind the differences observed in PLL-coated and non-coated beads is unknown, it is possible that the increased barrier to diffusion in the PLL-coated beads [170] could result in "trapping" of autocrine growth factors within the bead, leading to increased cell proliferation and viability. While others have found that encapsulation within alginate can slow cell proliferation [155,173,176], it is not universally observed, indicating that the diverse alginate compositions reported in the literature have yielded varying conclusions regarding the impact of microencapsulation on cell growth.

In addition to proliferative and morphologic changes, differences in phenotype were observed for cells from the different encapsulation conditions, implying that the bead configuration can impact the differentiation trajectory of the entrapped cells. Generally, the longer that cells were entrapped within the beads without escape, the more prolonged the expression of pluripotency markers was observed. The High M group, which had the highest incidence of aggregate escape, exhibited pluripotency marker expression similar to the unencapsulated aggregates, whereas the cells in the High G + PLL group, which contained the aggregates for the entire 14 days of culture, had the highest expression of both *Oct4* and *Nanog* at day 14. In the High G + PLL group, *Nanog* expression remained relatively unchanged from undifferentiated ESC levels even as *Oct4* expression decreased, indicating that regulation of *Nanog* may be occurring separately from the other pluripotent transcription factors [177–179]. Persistent OCT-4 signal in encapsulated ESC aggregates

was also observed via immunostaining **(Figure 3.9f, 3.10b-e)**. The correlation between lower cell growth and high expression of the pluripotency markers appears somewhat counterintuitive given that undifferentiated cells are commonly believed to proliferate at a faster rate. However, recent work has demonstrated that inhibiting cell division of hESCs led to increased NANOG levels [180], implying that a similar mechanism of action may be responsible for the high *Oct4* and *Nanog* levels observed in the groups which grew more slowly than others. Previous reports have indicated that microencapsulation can be used to prevent or delay differentiation of both single ESCs [67,69] and ESC aggregates [70], which is interesting given that aggregation of ESCs is often deemed to be an important initiating step in many differentiation protocols and indicates that differentiation within alginate hydrogels alters the kinetics and trajectory of differentiation. Therefore, when directed differentiation within alginate is desired, the presence of additional cues, either soluble or co-entrapped within the material matrix, may be critical for efficient ESC differentiation.

Along with changes in the loss of pluripotency, modulation of differentiation lineage commitment was also observed depending on the bead configuration, which is not commonly reported. The most striking difference was the increased propensity of cells within High M beads to differentiate toward an endodermal lineage, evidenced by alpha-fetoprotein (AFP) gene **(Figure 3.8d)** and protein **(Figure 3.10i)** expression. In some cases, the AFP+ cells were localized to regions surrounded by an epithelial-looking layer, similar to structures observed via histology **(Figure 3.7N)**. Interestingly, even though 96% of the aggregates in the High M condition escaped the bead prematurely and therefore were actually unencapsulated at day 14 of differentiation, dramatic differences in AFP were

observed between the High M group and the unencapsulated group, indicating that the earlier period of encapsulation may have primed or directed the differentiation of the entrapped cells toward an endodermal fate. In addition, cells encapsulated in High M alginate produced more VEGF and BMP-4 **(Figure 3.11)**, which has been correlated with increased mesendoderm differentiation [181]. The other major phenotypic distinction observed was the high frequency of spontaneous contractile beating in the unencapsulated and High M cultures, and the complete lack of beating in the other conditions, though it is possible that entrapment within the alginate limited the detection of beating in other groups. *MLC-2v* levels were elevated in the unencapsulated, High M, and High M + PLL conditions **(Figure 3.8e)**, and staining for alpha smooth muscle actin (α-SMA) exhibited strong localized expression in the unencapsulated and High M groups **(Fig 3.10k, 3.10n)**. There are several hypotheses for the increased incidence of cardiac differentiation which may not be directly related to encapsulation parameters. First, culture of EBs under rotary orbital suspension has been previously implicated in inducing cardiomyogenic differentiation [182], and the unencapsulated condition was directly exposed to the hydrodynamic forces throughout the culture period. Due to the early escape of cells from the beads **(Figure 3.5l)**, the High M group was also exposed to hydrodynamic forces for a more prolonged duration than the other encapsulated conditions that were shielded within the beads for a longer time period. A second hypothesis is based on the recent finding that high lactate culture environments lead to preferential survival of cardiomyocytes [183]. Since the unencapsulated and High M conditions consistently yielded higher cell densities than the other conditions **(Figure 3.6b)**, there were possibly higher levels of lactate present in the culture media. Finally, while effort was put forth to control for initial aggregate size, the

aggregates in the unencapsulated and High M groups resulted in larger diameter EBs. Previous work investigating the impact of aggregate size on differentiation has observed that larger aggregates have a greater tendency to undergo cardiac differentiation [184–186]. Overall, these results suggest that sustained encapsulation impedes cardiomyogenic differentiation, which along with sustained expression of pluripotency markers, signifies that encapsulation is a capable platform for maintenance and/or expansion of ESCs in a less differentiated state.

3.5 Conclusions

Overall, this study establishes the significant impacts of alginate bead composition on the expansion and phenotype of encapsulated pluripotent stem cells. Alginate beads with a high ratio of guluronic acid residues maintain a less differentiated phenotype and addition of a PLL coating to the High G alginate prevents cell escape from the bead while maintaining cell viability. Additionally, employing alginate with a high ratio of mannuronic to guluronic acid residues induced differentiation toward an endodermal lineage. Future work with human pluripotent stem cells (hPSCs) may provide further insight into the impact of encapsulation parameters on hPSC behavior and determine whether alginate microencapsulation is a feasible expansion and/or differentiation platform for hPSC bioprocessing or collection of cell secreted factors. Overall, the findings of this study suggest that selecting different alginate compositions for PSC expansion or differentiation provides a facile approach to control stem cell fate, as distinct phenotypes may be yielded by different material compositions and hydrogel properties.

CHAPTER 4

DESIGN OF A PACKED BED PERFUSION BIOREACTOR FOR STEM CELL CULTURE AND TROPHIC FACTOR PRODUCTION

4.1 Introduction

Classical bioprocessing approaches revolve around using cells to generate valuable products. In standard bacterial fermentation, microorganisms are exploited to produce molecules ranging from simple chemicals, such as ethanol or acetic acid, to enzymes, including lactase and catalase [187]. Advances in the scalable culture of mammalian cells and in recombinant DNA technology led to approval of the first mammalian-derived protein therapeutic, human tissue plasminogen activator, in 1986. By 2010, 28 different monoclonal antibody therapeutics had been approved by the United States Food and Drug Administration, primarily for applications in immune disorders and cancer [188], and approximately 60-70% of these proteins were produced in mammalian systems [189], likely due to unique ability of mammalian cells to perform post-translational modifications. Despite the robust history of producing cell-secreted proteins, often primarily from engineering of simple cell types, there has been limited research applying bioprocessing principles to harness more complex cell types and the generation of composite protein mixtures.

Since stem cells have emerged on the scientific scene, most of the direct applications have initially focused on exploiting the differentiation capacity of stem cells for the replacement of damaged tissues. However, the results of initial *in vivo* transplantation studies indicated that many of the observed functional improvements were

due to the transient paracrine actions of the transplanted stem cells, rather than the stem cells permanently engrafting and replacing the damaged cellular material [190,191]. Thus, research on the identity and potency of paracrine factors secreted by stem cells has become an increased area of focus in the regenerative medicine field. The majority of research to date has focused on mesenchymal stem/stromal cells (MSCs), as MSCs have been found to secrete significant quantities of pro-angiogenic, anti-inflammatory, and anti-apoptotic molecules [192,193]. Thus far, the secretory properties of pluripotent stem cells, including embryonic stem cells (ESCs), have been largely neglected despite records of improvement in embryonic cardiac phenotype [30] and reduced myocardial dysfunction post-ischemia [31] due to the presence of ESC paracrine factors. ESCs are thus an underexplored cell population with a unique and potent secretome due to their mitogenic and morphogenic roles during the early stages of development. Because many of the morphogens and growth factors produced by ESCs may be in low individual abundance, engineering a system to increase the yield of cell-derived factors may enhance the relative potency.

Despite the substantial knowledge base in bioprocess design for obtaining cell-secreted products, essentially all of the published literature regarding stem cell bioprocessing has focused on bioreactor design for cell cultivation rather than for protein production, consistent with the initial emphasis on cell therapy applications. There are numerous challenges in designing systems in which the cells themselves are the product, including the need for more intense process validation and characterization of the cell product, which necessitates the development of complex monitoring and control systems [136]. In order to facilitate expansion of stem cells to achieve the anticipated high numbers required for cell therapies and to remain consistent with standard bioprocessing systems,

suspension culture platforms, at least in the macroscale, have been the dominant paradigm. Because most stem cells, with the exception of hematopoietic stem cells, are adherent in nature, culturing stem cells in a single cell suspension is not typically successful [194]. Therefore, the cells are commonly cultured as aggregates, on the surface of microcarriers, within bulk hydrogel constructs, or in hydrogel microcapsules. Stirred suspension systems, usually in the form of bench-scale spinner flasks, are the most common format due to their scalability and ease of integration with monitoring systems [195].

Encapsulation of stem cells within hydrogel microbeads or microcapsules can be employed to provide a defined environment for adherent stem cell populations while enabling culture in large scale bioreactor systems [143]. Culture within hydrogels can also protect the enclosed cells from experiencing shear forces inherent to stirred bioreactor systems, which is particularly important in the case of stem cells due to their phenotypic sensitivity to hydrodynamic forces [196]. Spinner flask culture of microencapsulated human ESCs (hESCs) found that while encapsulation of single hESCs led to poor viability, encapsulation of hESC aggregates and hESCs on microcarriers allowed for maintenance of viability and pluripotency for up to two weeks in suspension culture [70]. In addition to stirred tank bioreactors, other reactor configurations have been investigated, including the high aspect ratio vessel (HARV), a rotary microgravity reactor that operates under the laminar flow regime to lessen the impact of mechanical forces. A HARV reactor has been used with murine ESC-containing alginate microcapsules to create mineralized constructs for bone tissue engineering [74].

Perfusion bioreactors are often used to enhance the yield of cell number through continuous provision of nutrients and removal of cell waste products while also providing

a relatively homogeneous soluble environment when compared to unmixed static cultures [197]. Perfusion culture of stem cells was first reported in the early 1990s as a method to expand bone marrow stem and progenitor cell populations [198] and has since been applied to the culture of pluripotent stem cells [72,199–201]. The published perfusion bioreactor systems for ESCs have been restricted to stirred suspension, HARV, and hollow fiber platforms; however using a packed bed reactor configuration offers the additional advantage of a high local cell density. Only a handful of studies have implemented packed bed perfusion bioreactor systems with encapsulated stem cells. A fixed bed reactor in which CellBeads, a commercially available product consisting of human MSC aggregates in alginate microcapsules, were packed and perfused with culture medium was able to maintain viability and induce adipogenic differentiation [75]. A similar system of alginate beads containing human MSCs was assembled into a tube and perfused with media as a method of direct assembly of a tissue-engineered construct [76,77]. Thus far, there have been no reports of culturing microencapsulated ESCs within a packed bed system for either expansion or collection of ESC-produced factors, despite the ease in which the protein-rich perfusate could be easily collected and/or delivered downstream.

In order to take advantage of the robust knowledge in bioprocessing and apply it to the novel application of harnessing pluripotent stem cells for their unique protein secretion, a first generation bioreactor platform for microencapsulated ESCs was designed and validated. Specifically, cell viability, proliferation, and growth factor secretion were compared between static and perfusion culture. Additionally, the impact of perfusion flow rate and multiple passes through the system were assessed to determine whether the efficiency of growth factor production could be modulated through adjusting engineering

design parameters. Overall, the results of this study demonstrate the design and validation of a uniquely engineered system capable of culturing ESCs and concentrating ESC secreted factors with applications for delivery to downstream paracrine-factor mediated processes.

4.2 Materials and methods

4.2.1 Bioreactor construction

The packed bed perfusion bioreactors were assembled using the following materials (all purchased from McMaster-Carr): high-temperature soft silicone rubber tubing, 1/4" ID, 3/8" OD in semi clear white and cut into 1.5" lengths; high-temperature silicone rubber tubing, 1/16" ID, 1/8" OD in semi-clear white and cut into 5" lengths; polyester mesh discs, 72 x 72 mesh, 0.0091" opening, cut into circles with 1/4" diameter; lightweight quick-turn tube couplings with barbed plugs for 1/4" tube ID; lightweight quick-turn tube couplings with barbed sockets for 1/16" tube ID; and 4" nylon cable ties. The mesh was inserted between the end of the 1/4" barbed plug and the top 3/8" of a 20 µL pipette tip (Rainin), removed using a razor blade, and affixed using lab tape (VWR). The 1.5" of 1/4" ID silicone tubing was pushed over the ends of the two barbed plugs to form a bed volume of approximately 0.5 mL, with several cable ties securing the connection to prevent leaks. The 1/16" quick-turn barbed socket couplings were fitted on either side of the 1/4" barbed plug and attached to 5" length 1/16" silicone tubing. The other end of the 1/16" silicone tubing was fitted to an additional 1/16" quick-turn barbed socket couplings and secured to syringes (BD). All bioreactor parts were sterilized individually via autoclave and assembled in a sterile manner in a biosafety cabinet.

4.2.2 Embryonic stem cell culture

Murine ESCs (D3 cell line) were cultured on tissue culture treated polystyrene dishes (Corning) adsorbed with 0.1% gelatin (EmbryoMax). Undifferentiated ESC culture media consisted of Dulbecco's modified Eagle's medium (DMEM) (Mediatech) supplemented with 15% fetal bovine serum (Hyclone), 100 U/mL penicillin, 100 μg/mL streptomycin, and 0.25 μg/mL amphotericin (Mediatech), 2 mM L-glutamine (Mediatech), 1x MEM non-essential amino acid solution (Mediatech), 0.1 mM 2-mercaptoethanol (Fisher Scientific), and 10^3 U/mL of leukemia inhibitory factor (LIF) (ESGRO). Cultures were replenished with fresh media every other day and passaged prior to reaching 70% confluence.

4.2.3 ESC aggregate formation

A single cell suspension of undifferentiated ESCs was obtained through dissociation of monolayer cultures with 0.05% trypsin-EDTA (Mediatech). Defined, serum-free KO N2B27 media (*note*: formulation is slightly different than what was used in Chapter 3) was used for all aggregate cultures and consisted of Knock-Out (KO) DMEM (Life Technologies) supplemented with N2 (Gibco), B27 (Gibco), 100 U/mL penicillin, 100 μg/mL streptomycin, and 0.25 μg/mL amphotericin (Mediatech), 2 mM L-glutamine (Mediatech), 1x MEM non-essential amino acid solution (Mediatech), and 0.1 mM 2-mercaptoethanol (Fisher Scientific). Aggregation of ESCs was achieved by centrifugation (200 rcf) of ESCs into 400 μm square polydimethylsiloxane (PDMS) micro-wells (Aggrewell™, Stem Cell Technologies) as previously reported [19,152]. The cell seeding density yielded approximately 500 cells per individual well. The ESCs were incubated in the wells for approximately 24 hours in serum-free KO N2B27 culture media to allow for aggregate formation.

4.2.4 Cell microencapsulation

Ultrapure medium viscosity MVG alginate (Pronova), which contains greater than 60% G residues (High G), was prepared at 1.5 wt% in calcium-free DMEM (Gibco) and autoclaved for sterilization no more than one day before use. An electrostatic bead generator (Nisco) was utilized for encapsulation. Pre-formed ESC aggregates were resuspended in alginate at a density of 12,000 aggregates per mL of alginate, and the cell-containing alginate solution was extruded through a 400 μm nozzle using a syringe pump at a flow rate of 6 mL/hour and a voltage of 10 kV to drop the beads into a stirred hardening bath of 100 mM calcium chloride (EMD). The beads were washed three times with serum-free media prior to downstream culture.

4.2.5 Static and perfusion culture of encapsulated aggregates

Static cultures of encapsulated ESC aggregates were cultured in sterile 100 x 15 mm bacteriological grade polystyrene Petri dishes (BD) at a typical seeding density of 3 x 10^6 cells in 10 mL of KO N2B27 medium, unless otherwise noted. For perfusion cultures, encapsulated ESC aggregates were added into the silicone packed bed during bioreactor assembly at a typical seeding of 3 x 10^6 cells, unless otherwise noted. The reactor was perfused with KO N2B27 medium using a syringe pump (Cole-Palmer) at a typical rate of 150 μL/hr, unless otherwise noted, and the perfusate was collected into an output syringe (BD). Most experiments were performed for a duration of three days, unless otherwise noted.

4.2.6 Cell viability staining and imaging

Cell viability was assessed using a LIVE/DEAD kit (Molecular Probes Inc., Eugene, OR). Samples were incubated in PBS containing 0.1 μM calcein AM and 8 μM

ethidium homodimer-1 at 4°C for 1 hour. The samples were washed with PBS, transferred to a glass-bottomed 24-well plate, and immediately imaged using a Zeiss LSM 700-405 confocal microscope or a Zeiss Axio Observer inverted fluorescence microscope.

4.2.7 Cell number quantification

Encapsulated aggregates were released from beads through 5 minute incubation with 55 mM sodium citrate (Sigma), as previously described [73]. The cells were centrifuged at 200 rcf for 5 minutes and rinsed 3x with PBS. Cells from all conditions were pelleted at 375 rcf for 4 minutes followed by supernatant removal and storage at -20°C. A CyQUANT Cell Proliferation Assay Kit (Molecular Probes Inc., Eugene, OR) was used to determine cell number, with a standard curve created using undifferentiated ESCs that were counted using a hemocytometer. The fluorescence (480 nm excitation, 520 nm emission) was read using a Synergy H4 plate reader (Biotek) or an i3 plate reader (Molecular Devices).

4.2.8 Conditioned media analysis

Spent media was collected from encapsulated ESC aggregates cultured under static or perfusion conditions. The conditioned media was centrifuged at 3000 rcf for 5 minutes to remove cellular debris, and the supernatant was transferred to a new 15 mL conical tube for storage at -20°C. Enzyme-linked immunosorbent assay (ELISA) kits were used to quantify the amount of VEGF, (DuoSet, R&D), BMP-4 (DuoSet, R&D), and IGFBP-2 (PicoKine, Boster Bio) present in the conditioned media. Concisely, capture antibody was adsorbed onto 96 well MaxiSorp Immunoplates (Nunc), blocked with 1% BSA in PBS, incubated with standards and samples, and bound with detection antibody. The concentration of protein was determined using a colorimetric reaction of peroxidase and

tetramethylbenxidine and a plate reader to measure the absorbance at 450 nm. The absorbance values for the conditioned media samples were compared to a standard curve to determine the protein concentration.

4.2.9 Quantitative real time PCR

Encapsulated aggregates were released from beads through 5 minute incubation with 55 mM sodium citrate (Sigma), as previously described [73]. The cells were centrifuged at 200 rcf for 5 minutes and rinsed 3x with PBS. RNA was extracted from the aggregates with the RNeasy Mini kit (Qiagen Inc, Valencia, CA). The RNA (300 ng/sample) was converted to complementary DNA using the iScript cDNA synthesis kit (Bio-Rad, Hercules, CA) and analyzed using real time PCR (MyIQ cycler, Bio-Rad). Forward and reverse primers for *18s*, *Oct4*, *Vegf*, and *Hif-1α* were designed with Beacon Designer software (sequences and conditions are given in **Table 4.1**) and purchased from Invitrogen. Gene expression were calculated with respect to undifferentiated ESC expression levels as previously described [168].

Table 4.1. Primer sequences for quantitative real-time PCR analysis

Gene	Forward sequence	Reverse sequence	Melt temperature (°C)
18s	CTCTAGTGATCCCTGAGAAGTTCC	ACTCGCTCCACCTCATCCTC	60.0
Oct4	CCGTGTGAGGTGGAGTCTGGAG	GCGATGTGAGTGATCTGCTGTAGG	60.0
Vegf	TGCACCCACGACAGAAGG	GCACACAGGACGGCTTGA	60.0
Hif-1α	GAGGTGGATATGTCTGGGTTG	AGGGAGAAAATCAAGTCGTGC	60.0

4.2.10 Statistics

All experiments were performed with replicate samples from independent conditions. The data is represented as the mean of the independent replicates, and the error bars represent the standard error of the mean. Before performing statistical analysis, data were normalized using a Box–Cox power transformation to normalize data variance. One-way ANOVAs were calculated between different conditions as appropriate, followed by post hoc Tukey analysis to determine significant differences ($p < 0.05$). All statistical analysis was performed using MatLab and SYSTAT software.

4.3 Results

4.3.1 Bioreactor design and construction

An initial observation regarding ESC secretion kinetics was made in the context of unencapsulated ESC aggregates cultured on a rotary orbital shaker. While the concentration of the growth factor bone morphogenetic protein-4 (BMP-4) initially rose and subsequently leveled off within a 48 hour culture period, the introduction of fresh media into the system at 24 hours led to continued BMP-4 secretion **(Figure 4.1)**. Within the 24 hour time period between the first and second day of culture, the ESC aggregates cultured in fresh media generated sufficient protein to lead to a 51 pg/mL increase in BMP-4 concentration, in contrast to the 39 pg/mL increase in BMP-4 concentration observed in the cultures which did not receive a media exchange. The results of this study indicated that depletion of external growth factors may influence cell secretion dynamics, perhaps through negative feedback inhibition mechanisms. Thus, a culture platform capable of

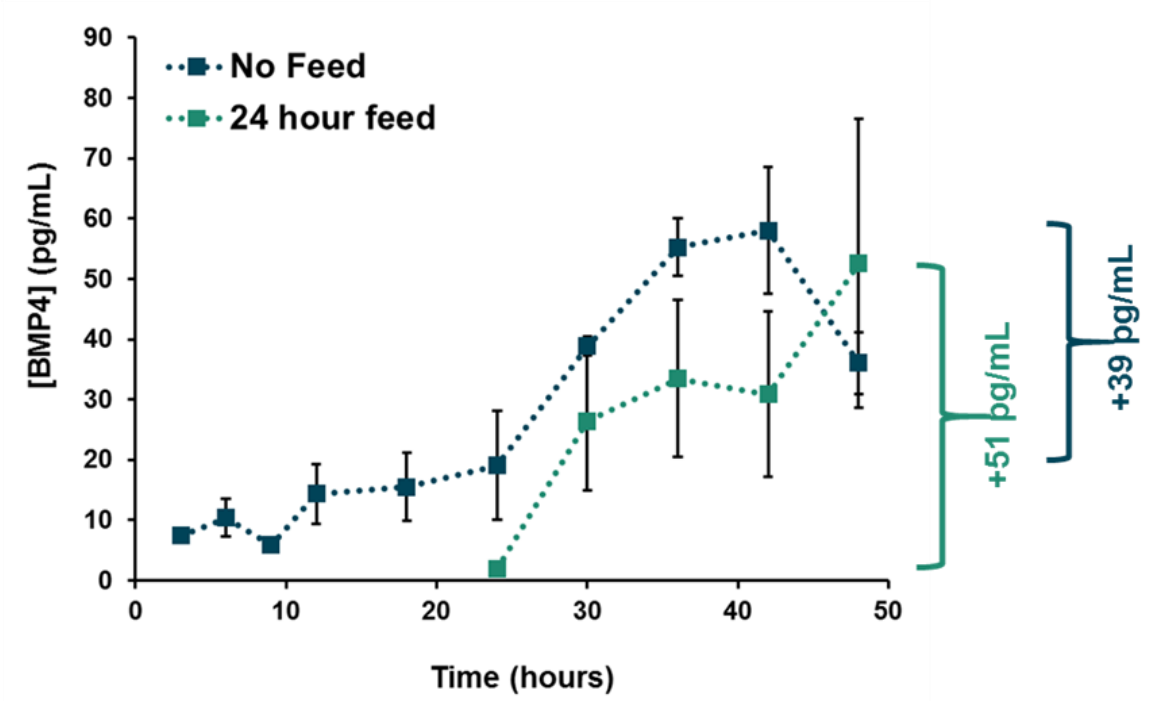

Figure 4.1. Media replacement enhances production of ESC secreted growth factor. Analysis of conditioned media collected from unencapsulated ESC aggregates cultured in rotary suspension for bone morphogenetic protein-4 (BMP-4) concentration indicates that performing a media exchange can enhance the yield of BMP-4.

constant depletion of cell-secreted products may be able to enhance overall ESC trophic factor production.

In order to maximize the concentration of ESC secreted factors, a high density culture platform with integrated media perfusion was designed. Three-dimensional culture generally enables higher cell densities than two-dimensional monolayer cultures, thus ESCs were aggregated into multicellular spheroids. ESC spheroids were maintained within alginate microbeads to ensure sufficient separation between aggregates, as multiple aggregates often agglomerate into large cell masses, leading to uncontrolled oxygen and nutrient gradients,. A classic packed bed reactor design was thus chosen to enable high density packing of the ESC aggregates and continuous media perfusion.

Several important design parameters were considered, including that the reactor be (1) fully sterilizable via autoclaving or similar method, (2) gas permeable to ensure sufficient oxygen transport, (3) closed such that there are no leaks to minimize contamination, and (4) have an adjustable bed volume such that the number of encapsulated aggregates could be altered as needed. The design consists of medical grade silicone tubing (1/4" ID) fitted on either side with barbed Luer locks and polyester mesh with a 0.0091" opening **(Figure 4.2)**. Gas permeable silicon tubing was used both for the packed bed itself as well as for the tubing used for media delivery to ensure adequate oxygen delivery to the cells. For most studies, a bed volume of approximately 0.5 cm^3 (height = ½", width = ¼") was employed. Assuming a void fraction of 0.39 (poured random packing for spheres), an average bead diameter of 600 μm, and an average of two aggregates per bead, the approximate capacity is 3600 beads per 0.5 cm^3 of bed volume (approximately 7.2 x 10^6 cells/mL).

Using a syringe pump, an initial flow rate of 150 μL/hr was delivered, as this is comparable to the exchange rate that is performed in typical batch culture (exchanging 10 mL of media every 72 hours). To establish whether this flow rate should be sufficient for removal of cell-secreted products, the dimensionless Peclet number for the system was determined. The Peclet number (*Pe*) describes the ratio of advective transport to diffusive transport by combining the Reynolds (*Re*) and Schmidt (*Sc*) numbers for a packed bed configuration:

$$Pe = \frac{advective\ transport\ rate}{diffusive\ transport\ rate} = Re_L Sc = \left(\frac{\rho v L}{\mu}\right)\left(\frac{\mu}{\rho D}\right) = \frac{vL}{D}$$

where ρ is the fluid density, v is the superficial velocity, L is the characteristic length (diameter), μ is the fluid viscosity, and D is the diffusion coefficient of the species of

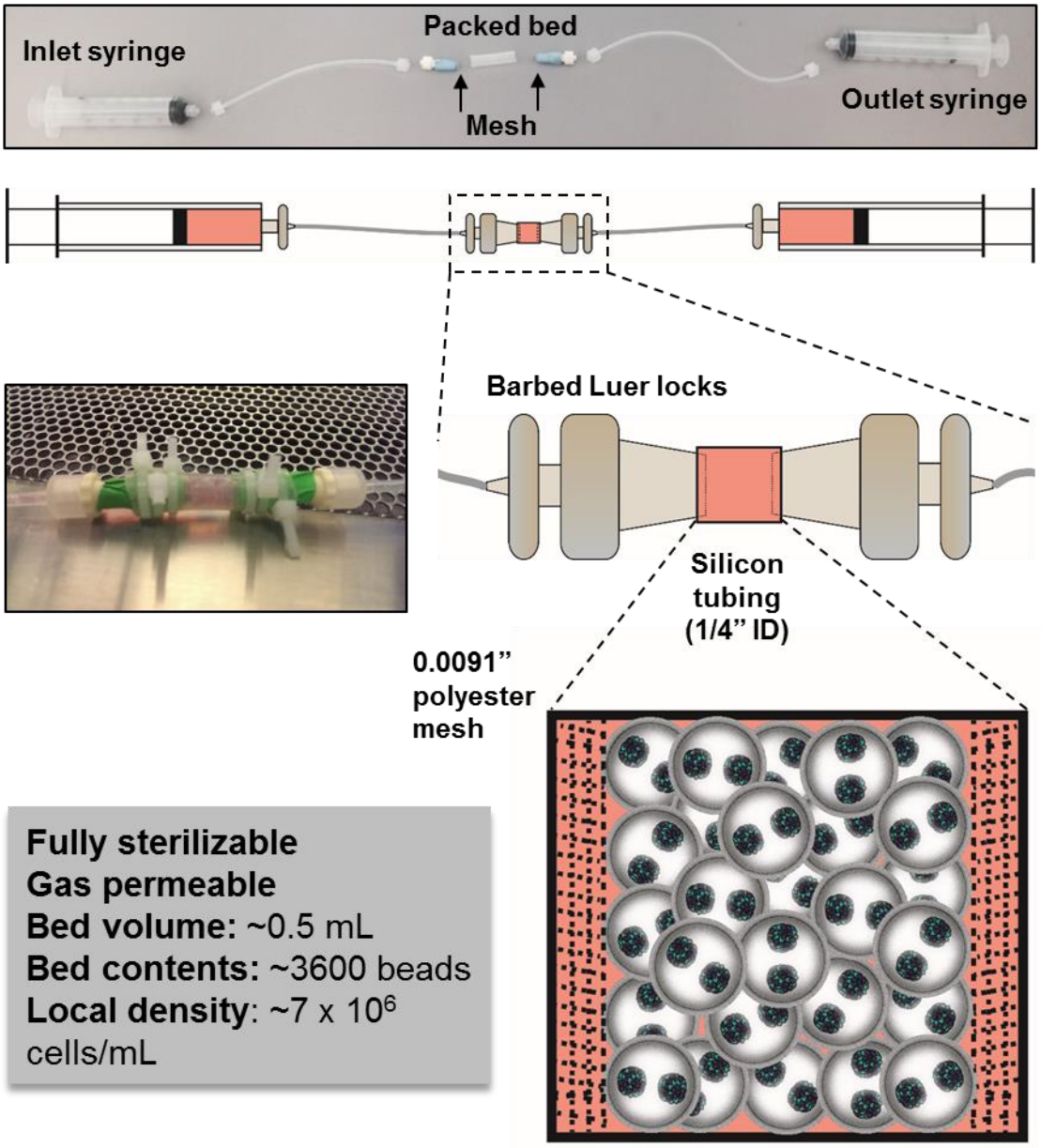

Figure 4.2. Design of a packed bed perfusion bioreactor for culture of encapsulated ESC aggregates. Silicone tubing with a 1/4" inner diameter (ID) was fitted on either end with a polyester mesh to contain alginate microbeads within the bed volume. The silicone tubing is gas permeable to enable oxygen transport, and all components of the bioreactor are sterilizable via autoclave. The bed volume can be modified by altering the length of the 1/4" silicone tubing, with a typical volume of 0.5 mL containing approximately 3600 beads (average diameter of 600 μm) and 3.5 x 10^6 cells.

interest in the fluid medium. Given the approximation of the system parameters ($v \approx 1.3 \times 10^{-4}$ cm/s, $L \approx 0.64$ cm, and D for proteins $\approx 5 \times 10^{-7}$ cm^2/s), a Peclet number of ~168 was obtained, indicating that the flow rate used should be sufficient to remove cell-secreted proteins. Several assumptions are required in this estimation, including that (1) there is no electrostatic force between the negatively-charged alginate and proteins which would influence transport, (2) the diffusive transport is dominated by transport through the media and not the alginate, (3) production of the proteins is relatively constant and not affected by flow, and (4) that the ESCs are consuming (i.e. receptors on the cells binding to the ligand) a low proportion of the protein.

4.3.2 Cell function and secretion within bioreactor

To assess whether culture of encapsulated ESC aggregates within the packed bed reactor affected basic cell function, the viability, growth, and differentiation of cells cultured under perfusion were compared to encapsulated ESC aggregates cultured in static suspension. After 24 hours of culture, similar degrees of cell viability were observed in aggregates cultured in static and perfusion conditions **(Figure 4.3a-b)**. To determine if the position within the bioreactor (i.e. near the entrance or exit) affects cell viability, cell-containing alginate beads were extracted from approximately the front 10% and back 10% of the reactor. Similar levels of viability after 72 hours of culture were observed regardless of position **(Figure 4.3c-d)**, implying that adequate transport of nutrients are provided throughout the length of the system. The aggregate morphology **(Figure 4.3e-j)** and cell growth curves **(Figure 4.3k)** were comparable between the encapsulated cells in static and perfusion conditions. Similar downregulation of the pluripotency marker *Oct4* after 72 hours was observed in cells from both settings **(Figure 4.3l)**, indicating that culture in the

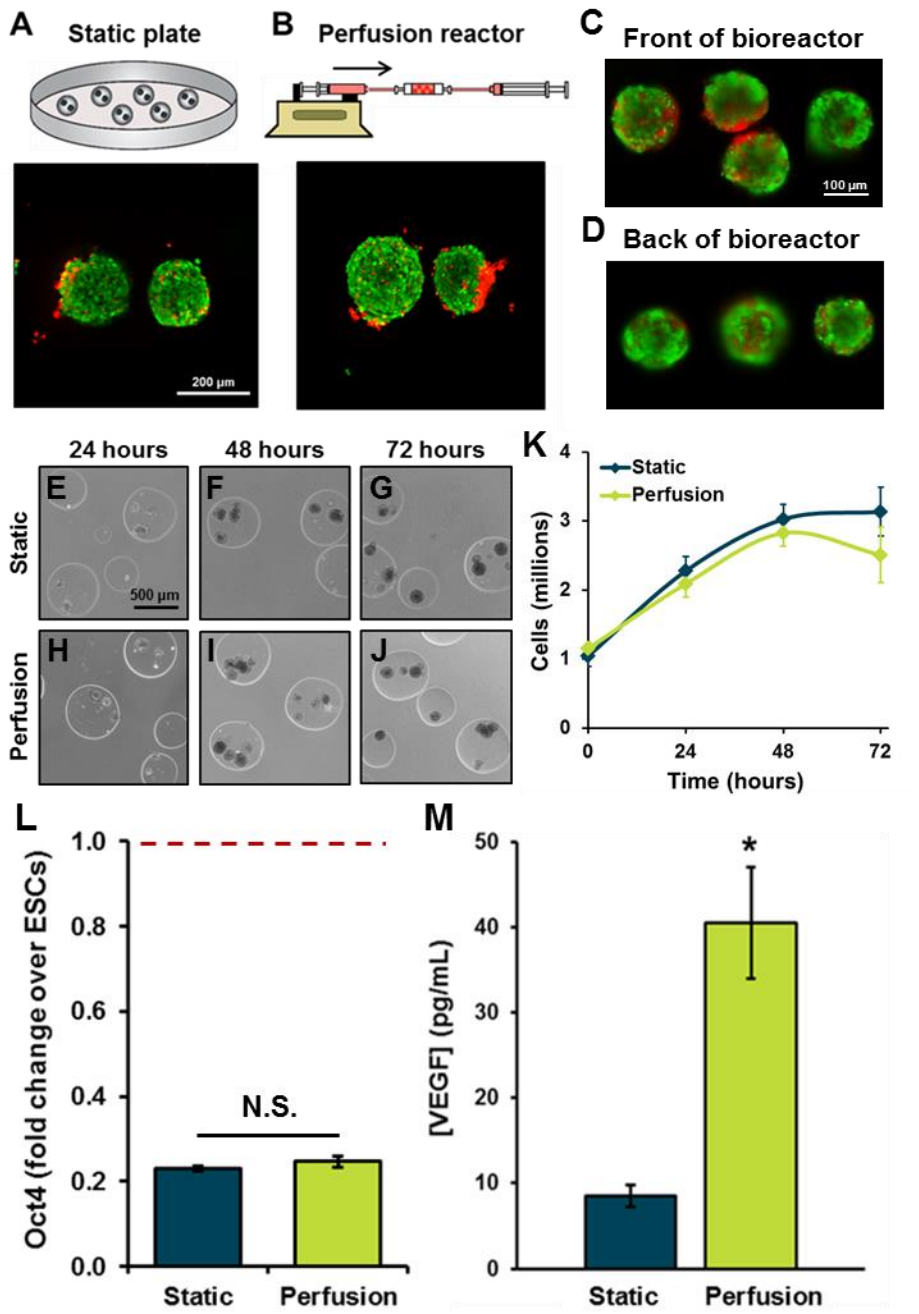

Figure 4.3. Influence of perfusion culture on ESC viability, proliferation, differentiation, and secretion. ESCs cultured in a static petri dish or within the perfusion bioreactor (flow rate 150 µL/hr) exhibited similar viability after 24 hours **(A-B)** (scale bar = 200 µm), and no differences in viability were observed after 72 hours of culture between ESCs cultured at the front and back of the bioreactor **(C-D)** (scale bar = 100 µm). Similar morphology **(E-J)** (scale bar = 500 µm) and cell growth curves **(K)** were observed in static and perfusion cultures throughout the course of culture. The loss of the pluripotency marker Oct4 was unchanged in static and perfusion cultures relative to undifferentiated ESCs (red dotted line) **(L)**. Higher concentrations of vascular endothelial growth factor (VEGF) were observed in the perfusate than in the conditioned media collected from static cultures. Significant ($p < 0.05$) differences (*) are denoted.

packed bed bioreactor did not significantly influence the transition from the pluripotent state. Analysis of the perfusate at the outlet of the bioreactor revealed that the concentration of ESC-produced vascular endothelial growth factor (VEGF) was significantly increased (4.9-fold increase) in comparison to the conditioned medium collected from the static cultures **(Figure 4.3m)**, despite the analogous overall cell densities.

It is possible that the increased VEGF production is a byproduct of the culture platform, perhaps due to limitations in oxygen transport; therefore a static bioreactor that lacked convective transport was examined. Transport of nutrients within the static bioreactor was driven entirely by diffusion from the media-containing syringes at either end of the reactor **(Figure 4.4a)**. Reduced cell viability after 72 hours was observed in the static bioreactor **(Figure 4.4c)** in comparison to both the static plate **(Figure 4.4b)** and the perfused bioreactor **(Figure 4.4d)**, and significantly fewer cells were observed in the static bioreactor **(Figure 4.4e)**. The medium conditioned by the perfusion reactor once again contained the highest concentrations of VEGF **(Figure 4.4f)**, and very little VEGF was observed in the medium conditioned in the static reactor. At the gene expression level, there were no significant differences between the groups in expression of hypoxia-inducible factor-1α (HIF-1α) or VEGF **(Figure 4.4g-h)**, indicating that the increased production of VEGF was likely being regulated at the protein level. The results of this study indicate that the increased VEGF concentration observed was likely not a secondary effect of culture within the bioreactor, as the results were not recapitulated in an identically configured static bioreactor.

To determine if the growth factor concentration could be increased by recycling the previously conditioned medium back through the reactor, a double pass scheme was

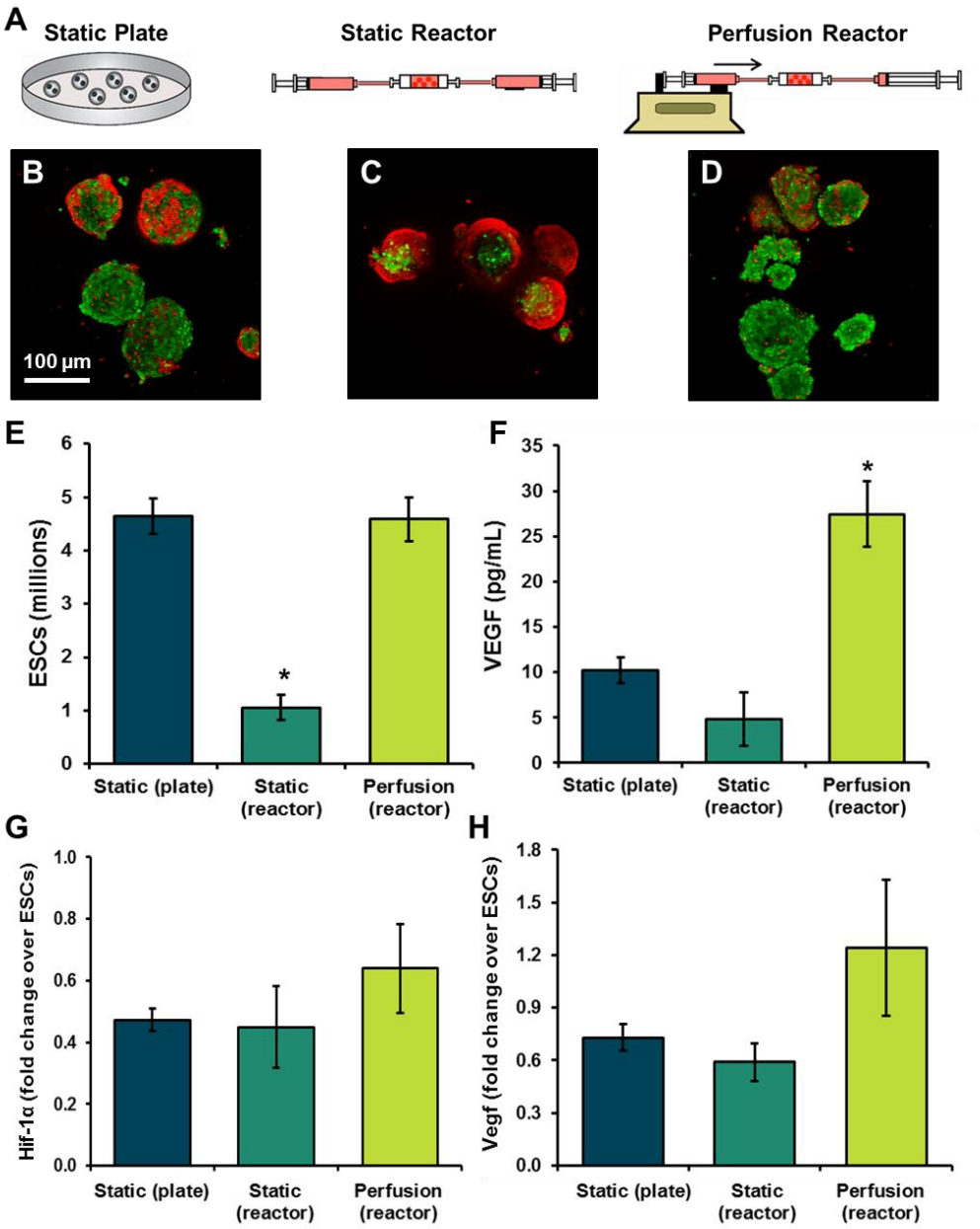

Figure 4.4. Lack of hypoxic response observed due to bioreactor culture. ESCs were cultured in a static petri dish, in a static bioreactor, or within a bioreactor subject to a flow rate of 150 µL/hr **(A)**. Lower cell viability was observed in cells cultured in the static bioreactor **(C)** in comparison with the static plate **(B)** and perfusion reactor for 72 hours **(D)** (scale bar = 100 µm), with lower cell numbers observed in the static reactor **(E)**. The media conditioned by the perfusion reactor contained higher concentrations of VEGF **(F)**, though no differences in gene expression of hypoxia-inducible factor-1α or VEGF were observed between the groups. Significant ($p < 0.05$) differences (*) from all other conditions are denoted.

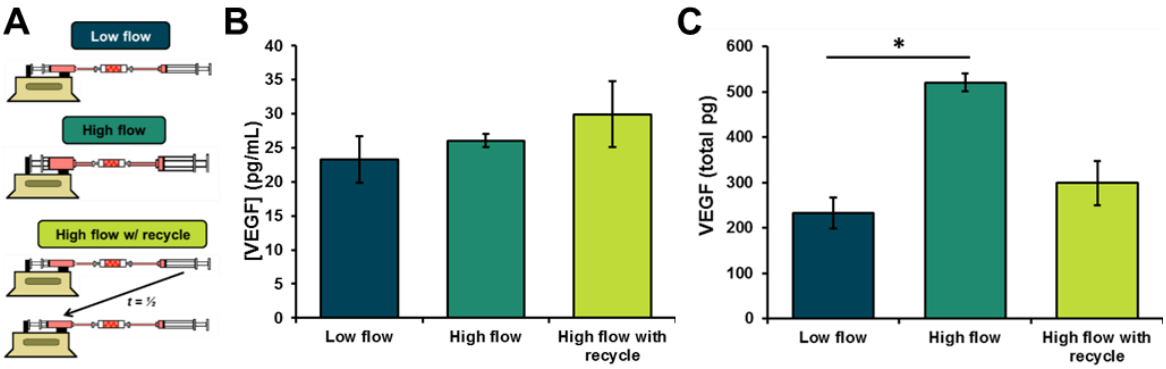

Figure 4.5. Influence of recycled perfusion on growth factor yield. Encapsulated ESCs were perfused for 72 hours at a low flow rate (150 µL/hr), a high flow rate (300 µL/hr), or a high flow rate (300 µL/hr) with the media conditioned for the first 36 hours recycled through the reactor for the second 36 hours **(A)**, as described in **Table 4.2**. Similar concentrations of vascular endothelial growth factor (VEGF) were observed in the conditioned media from all conditions **(B)**, but higher overall quantities of VEGF were yielded in the high flow rate condition **(C)**. Significant ($p < 0.05$) differences (*) are denoted.

compared to a single pass configuration **(Figure 4.5a)**. In order to maintain the same overall cell density, the flow rate through the reactor was doubled from 150 µL/hr to 300 µL/hr; therefore, an additional condition of a single pass approach with the higher flow rate of 300 µL/hr was also included to account for any differences based on flow rate **(Table 4.2)**. The concentration of VEGF was similar for all conditions **(Figure 4.5b)**, indicating that recycling the once-conditioned medium through the packed bed of ESCs a second time did not lead to increased growth factor concentration. However, because the single-pass, high flow rate condition circulated double the total volume of media through the reactor, the total amount of VEGF produced by the cells was also approximately doubled in comparison to the other conditions **(Figure 4.5c)**.

Table 4.2. Flow rates and total volumes delivered for double-pass experiment

Condition	Flow rate	Total volume
Low flow	150 µL/hr	10 mL
High flow	300 µL/hr	20 mL
High flow with recycle	300 µL/hr	10 mL

Based on this observation, the effect of flow rate on ESC secretion dynamics was evaluated at a greater range of flow rates/dilution rates **(Table 4.3)** and for two different growth factor species: VEGF and insulin-like growth factor binding protein-2 (IGFBP-2), identified as protein produced by ESCs in high levels **(Figure 5.3, 5.7)**. Images of encapsulated ESC aggregates cultured under perfusion for 72 hours at 75 µL/hr, 150 µL/hr, 300 µL/hr, and 600 µL/hr appeared similar in morphology **(Figure 4.6a-d)**, though "escape" of aggregates seemed to be more prevalent in the 600 µL/hr condition which may indicate that the alginate beads were under more mechanical stress at the higher flow rate that led to reduced integrity of the alginate beads. Approximately 3 x 10^6 cells were seeded into each bioreactor, though analysis of cell number following 72 hours of perfusion culture indicated that there were differences in cell expansion **(Figure 4.6e)**. The cells cultured under the lowest flow rate (75 µL/hr) were present in significantly lower numbers in comparison to the higher flow rate conditions (300 µL/hr and 600 µL/hr), conceivably due to a lack of sufficient nutrients and/or greater accumulation of cell byproducts. As expected based on the experimental design, greater overall cell densities were observed at the lower flow rates **(Figure 4.6e)**.

Table 4.3. Experimental conditions for multiple flow rate experiment

Flow rate (µL/hr)	Bed volume exchange (hr)	Dilution rate (hr^{-1})	Starting cell density (cells/mL)	Cells seeded in reactor
75	6.7	0.15	600,000	3 x 10^6
150	3.3	0.3	300,000	3 x 10^6
300	1.7	0.6	150,000	3 x 10^6
600	0.8	1.2	75,000	3 x 10^6

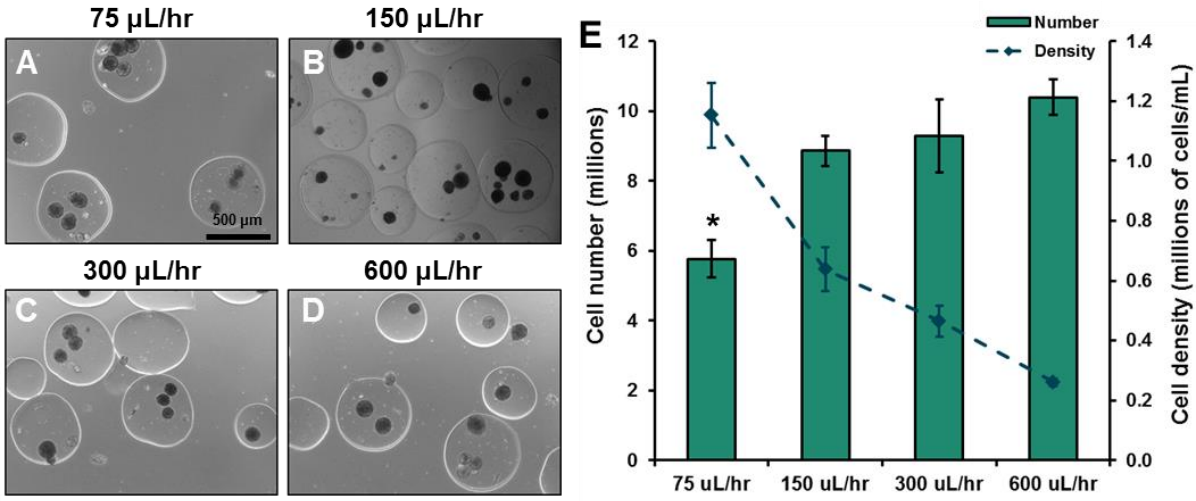

Figure 4.6. Growth of encapsulated ESCs under different perfusion flow rates. Encapsulated ESCs were perfused at four different flow rates for 72 hours: 75 µL/hr **(A)**, 150 µL/hr **(B)**, 300 µL/hr **(C)**, and 600 µL/hr **(D)**. Because different total volumes are being perfused through the system, the cell density decreases with increasing flow rate **(E)**. An equivalent number of cells were seeded into each bioreactor, but a lower number of cells were observed in the low 75 µL/hr flow rate condition following 72 hours of culture **(E)**. A significant ($p < 0.05$) difference (*) from the 300 µL/hr and 600 µL/hr conditions is denoted.

Perfusate from the reactors was collected every 24 hours and analyzed for VEGF and IGFBP-2 content, both as a concentration and as an absolute amount based on the volume of media that had been conditioned. In general, higher protein concentrations were observed at the lower flow rates **(Figure 4.7a-b)**, consistent with the higher cell densities in these conditions. However, intermediate flow rates led to higher absolute quantities at most time points **(Figure 4.6c-d)** since higher volumes of media were being conditioned. At the higher flow rate conditions (≥150 µL/hr), the concentration and absolute quantity of VEGF and IGFBP-2 was relatively constant over time, while the concentration and quantity appeared to increase over time in the 75 µL/hr flow rate condition. By calculating the overall concentration and quantity of the proteins after 72 hours of perfusion, the productivity of each bioreactor flow rate was determined for each protein. Similar to previous results **(Figure 4.5c)**, a flow rate of 300 µL/hr led to the highest amount of VEGF

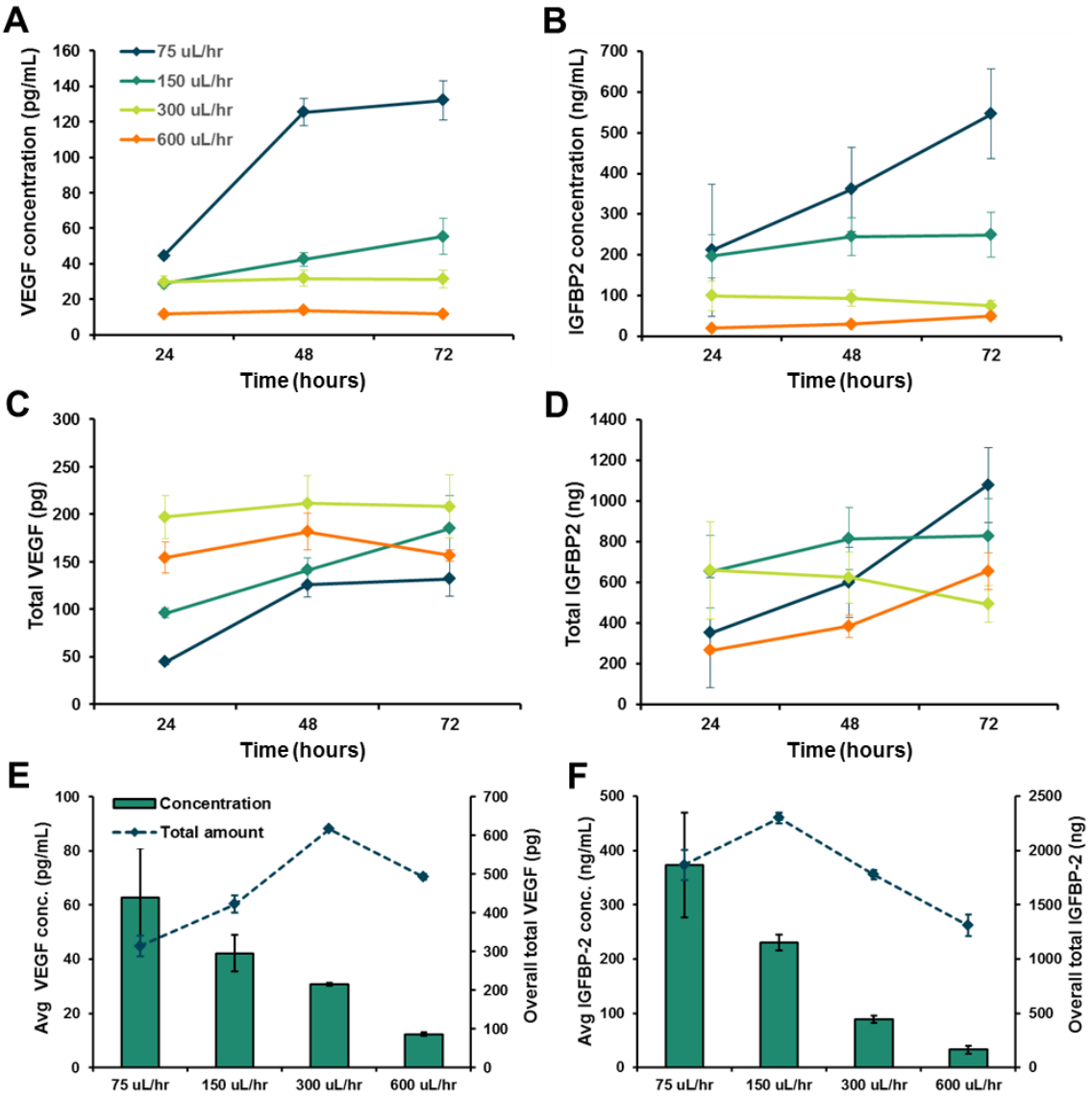

Figure 4.7. Influence of perfusion flow rate on ESC secreted growth factor concentration and yield. Encapsulated ESCs were perfused at four different flow rates for 72 hours: 75 µL/hr, 150 µL/hr, 300 µL/hr, and 600 µL/hr. For the higher flow rates, the concentration **(A-B)** and local quantity **(C-D)** of vascular endothelial growth factor (VEGF) and insulin-like growth factor binding protein-2 (IGFBP-2) were fairly constant over time. Compiling the temporal data into an overall concentration and amount for the full 72 hours, a higher concentration of VEGF **(E)** and IGFBP-2 **(F)** were observed with lower flow rates. The highest yield of VEGF was obtained at a flow rate of 300 µL/hr **(E)**, while the highest yield of IGFBP-2 was obtained at a flow rate of 150 µL/hr **(F)**.

produced by the ESCs **(Figure 4.7e)**, while a flow rate of 150 μL/hr yielded the highest amount of IGFBP-2 **(Figure 4.7f)**.

4.4 Discussion

The design and validation of a novel packed bed perfusion bioreactor for encapsulated ESC culture is a novel approach to harness and deliver stem cell secreted products. In this work, a bioreactor was constructed using silicone tubing in combination with a polyester mesh and luer connections to create a defined environment in which culture media can be continuously conditioned by encapsulated ESCs. Cell viability and proliferation were not affected over the 72 hour culture period, in comparison to static controls at comparable overall cell to media densities, yet an increased yield of ESC-produced growth factor was observed in the perfused conditioned medium **(Figures 4.3, 4.4)**.

To understand the mechanism behind the increased concentration, several factors were interrogated in parallel. The amount of protein present in a system at a given time is dependent on several parameters but can be estimated using simple mass balances in which protein accumulation (*dP/dt*) is the sum of protein entering the system (+), protein being generated by cells (+), protein being consumed, either through cellular uptake or protein degradation (–), and protein leaving the system (–). In a static system, there is no protein entering or leaving the system over the period of culture, while protein is continuously leaving the system under a perfusion conditions. Because similar cell growth was observed in static and perfusion systems **(Figure 4.3k, 4.4e)**, the consumption term can be assumed to be equivalent in both conditions given that the consumption rate is directly related to cell number.

Based on early studies with static cultures, it was observed that cells provided with fresh, unconditioned media secreted more growth factor than cells that did not experience a media change **(Figure 4.1)**. In addition, the recycling of conditioned media back through the bioreactor for a second pass did not lead to further concentration of the conditioned media **(Figure 4.5)**. There are several possible explanations for these observations, including that the addition of fresh media provided more energy or material for the transcriptional and translational processes required for protein production. Alternatively, there may some form of negative feedback inhibition in which the cells slowed their production of growth factor in response to the high extracellular growth factor concentrations, either due to the accumulation of protein locally in the static condition or the re-perfusion of previously conditioned media. Examining a case in which no negative feedback inhibition is present, the amount of product present (as well as the concentration of product, assuming constant volume) would rise linearly over time, while the rate of secretion (first derivative of the amount of product) would be constant with time **(Figure 4.8a)**. However, under the effects of feedback inhibition, the rate of product secretion would slow over time, thus the concentration and amount would cease to increase linearly and ultimately level off, similar to what was observed experimentally **(Figure 4.1)**. By introducing an exchange of volume into the system, the exogenous concentration of product could be modulated to diminish or even negate the effect of negative feedback inhibition. At steady state, the average concentration of a cell-secreted product in a continually perfused system could be maintained at a semi-constant level, assuming that the rate of dilution with fresh media largely prevents feedback inhibition **(Figure 4.8b)**. While the concentration and amount of product are directly correlated in a system with

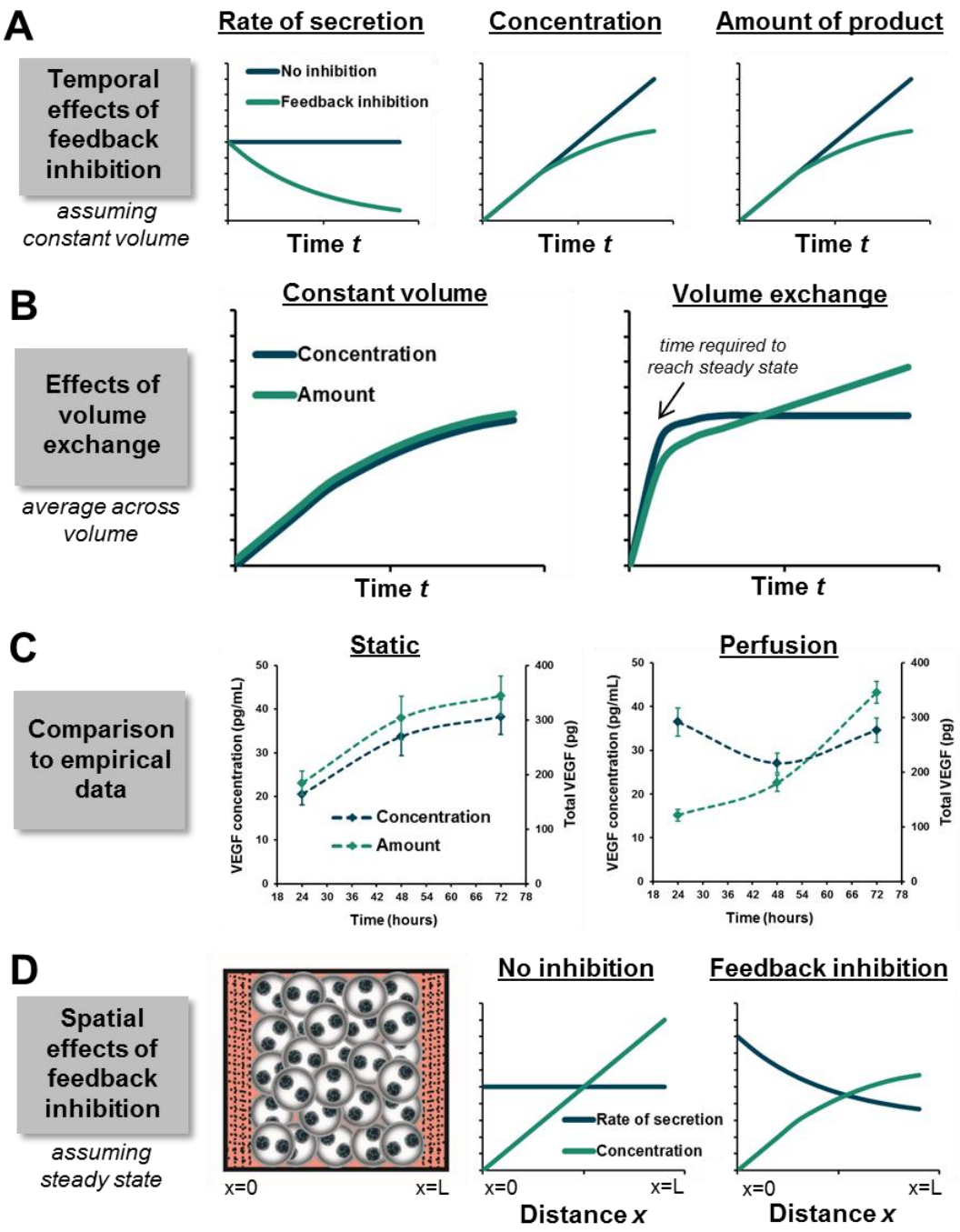

Figure 4.8. Theoretical and experimental trends of growth factor production. Expected dynamics for growth factor secretion, concentration, and overall amount in the absence or presence of feedback inhibition, assuming a constant volume **(A)**. Expected dynamics for growth factor concentration and total amount in the presence of volume exchange, assuming an average spatial value **(B)**, aligns with experimental data for static and perfusion culture **(C)**. Expected spatial gradient in a perfusion reactor in the presence of feedback inhibition, assuming steady state has been achieved **(D)**.

fixed volume, the total amount of product yielded in a system with dynamic volume would instead be correlated with the integral of the concentration and would thus increase over time **(Figure 4.8b)**. Comparing the theoretical relationships of product concentration, product amount, media volume, and time with experimental results, very similar trends are observed for the theoretical fixed, constant volume condition and the static experimental condition, as well as for the theoretical dynamic volume exchange condition with the experimental perfusion system **(Figure 4.8c)**. The concentration and absolute amount of VEGF in the static condition increased over time but appeared to level off by 72 hours of culture. In contrast, the concentration of VEGF was relatively constant over time in the perfusion bioreactor (consistent with the results for flow rates ≥150 μL/hr in **Figure 4.7a-b**), thus the total VEGF yielded increased with time.

Assuming that negative feedback inhibition is present in the system also implies that spatial differences likely exist within the packed bed bioreactor configuration. In the absence of inhibition, the rate of secretion would be constant across the length of the bed, leading to an increase in concentration across the *x* dimension (starting at zero concentration and ending at the final concentration of the perfusate) **(Figure 4.8d)**. However, in the presence of negative feedback inhibition, the rate of secretion would be highest at the packed bed entrance and would decrease with increasing concentration along the *x* direction, still fixed by the boundary conditions of zero concentration at the entrance and the final perfusate concentration at the exit. By altering the geometry of the packed bed bioreactor (i.e. increasing the ratio of the diameter to the length), the gradient along the length of the reactor could theoretically be reduced. In addition to spatial variance along the length of the bioreactor, other spatial heterogeneities may exist depending on the

packing of the alginate beads in the reactor. In general, if the perfused structure is not homogeneous, only partial perfusion is achieved since the fluid flow will likely follow the path of least resistance and flow unevenly through specific channels within the packed bed, which could lead to local heterogeneities in cell secretion and product concentration [202]. To experimentally determine if spatial heterogeneities exist, cells from different regions of the bioreactor could be collected for downstream analysis (gene and protein expression); alternatively, the entire bioreactor could be fixed in place through snap freezing and embedding within a filler medium to enable histological sectioning.

Quantitative modeling of product formation is possible for defined systems in which certain parameters are known. For example, microbial growth to produce simple products, such as ethanol, can be predicted using mass balance calculations based on the specific rate of product formation product (q_p), which can in turn be dependent on the product yield coefficient ($Y_{P/S}$) [187]. Products can also be described as growth-associated, non-growth associated, or mixed-growth-associated, depending if the product is produced concurrent with cell growth or once the cells have achieved a stationary growth phase. Extension of simple models to mammalian cell systems has proven to be challenging, and several attempts to model cell growth, metabolism, and antibody production from hybridoma and chinse hamster ovary (CHO) cells have had to employ complex unstructured kinetic models or logistic equations [203,204]. In general, the production of antibodies in mammalian cells appears to be non-growth associated, though the mechanism is dependent on the culture platform and feeding strategy [204–206]. However, describing the production of a recombinant protein, which has been optimized to be a high efficiency expression system, is a distinct process from endogenous protein production, and thus it is

difficult to correlate published results to the production of multiple growth factors from stem cell populations.

In general, the secretion of protein products from cells is a highly regulated process involving the folding and assembly of proteins in the endoplasmic reticulum followed by glycosylation and packaging within lipid vesicles in the Golgi apparatus. Through the process of exocytosis, the vesicle containing the proteins can be transported through the plasma membrane and into the extracellular environment [207]. While most cell-secreted proteins follow this classical pathway, others, including fibroblast growth factors 1 and 2 (FGF-1 and FGF-2), undergo unconventional secretory processes [208–210] in which processing by the Golgi is altered or entirely absent. Additionally, cell secretion can be broken down into constitutive secretion and regulated secretion mechanisms, particularly for cell types with primary endocrine functions [211]. With constitutive secretion, the protein is constantly secreted regardless of specific external signals. In contrast, cells with regulated secretion processes accumulate secretory vesicles intracellularly and only release them when triggered by the appropriate signal, termed the secretagogue. For example, epithelial cells lining the gastrointestinal system secrete acid in response to the secretagogue hormone gastrin [212]. Feedback mechanisms are known to exist for many protein hormones, including growth hormone (GH), as well as growth factors like insulin-like growth factor-2 (IGF-2) [213,214]. In some cases, high concentrations of the protein itself repress gene expression and protein production, such as with IGF-2 which is appears to be mediated by the type I IGF receptor. While the mechanism of self-regulation of gene expression has not been observed for VEGF, several endogenous proteins which are induced by VEGF expression act as feedback inhibitors of angiogenesis [215–217], and it

is possible that their co-expression with VEGF may in turn reduce the quantity of VEGF produced.

Based on the flow rate used (and the equivalent dilution rate), different efficiencies of protein production were achieved **(Figure 4.7)**. The highest quantity of VEGF was produced at a flow rate of 300 µL/hr (dilution rate of 0.6) **(Figure 4.7e)**, while the most IGFBP-2 was produced at a flow rate of 150 µL/hr (dilution rate of 0.3) **(Figure 4.7f)**. The difference in peak efficiency between the two proteins could be explained by a variety of hypotheses, including that IGFBP-2, which is produced in much higher quantities (10^3-10^4 higher concentrations than VEGF), is less sensitive to the feedback inhibition mechanisms which might come into play at the lower flow rates. At the higher flow rates, it is also possible that the removal of autocrine factors from the cells influences their capacity for the production of certain growth factors, as it has been observed that removal of autocrine factors from ESC populations affects differentiation and tissue specification [218].

The bioreactor system designed in this study is similar to several commercial products, most of which have been designed for tissue engineering applications. Kiyatec produces 3DKUBE™, a three-dimensional cell culture chamber with a volume of 250 µL that has an optional co-culture configuration through addition of a permeable membrane between the two chambers. On a slightly larger scale, 3D Biotek manufactures three dimensional perfusion bioreactor systems that can be fitted with multiple scaffold discs composed of polystyrene, polycaprolactone, or tri-calcium phosphate. Instron offers OsteoGen™, a more advanced perfusion stimulation bioreactor system that can be coupled with pulsatile flow simulator. All of types of these perfusion systems currently involve the use of large scaffolds to maintain the cells in place, which is more relevant for the tissue

engineering of large constructs. However, they could be modified to include filters at the entrance and exit to restrict microcapsules within the system, thereby enabling the study of perfused ESC aggregates in a different geometric configuration. Similar changes in dimension could also be achieved with the system designed herein by altering the length and diameter of the tubing used for the packed bed.

4.5 Conclusions

Overall, the results of this study demonstrate the utility of a novel perfused packed bed bioreactor for the culture of encapsulated embryonic stem cells and for increasing the production of stem cell secreted growth factors. While the precise mechanism for the increased concentration is unknown, it may stem from stimulation of secretion due to the continuous removal of exogenous growth factor. Recycling previously conditioned medium through the reactor did not lead to increases in growth factor concentration, though higher yields of growth factor could be obtained by determining the flow rate which balances high cell secretion with low dilution. Taken together, the bioreactor designed in this study will enable several applications, including the continuous delivery of growth factor-enriched perfusate to downstream cell and tissue populations.

CHAPTER 5

GLOBAL ANALYSIS OF EMBRYONIC STEM CELL SECRETED FACTORS

5.1 Introduction

Pluripotent embryonic stem cells (ESCs) are isolated from the inner cell mass of the pre-implantation blastocyst [1,3] and thus simulate mammalian early embryonic development [219]. During embryogenesis, the *in vivo* equivalents of pluripotent stem cells act as an autonomous source of morphogenic signals that stimulate histogenesis of neighboring cells through paracrine actions, as well as differentiation of the ESCs themselves through autocrine signals. Through their secretion of growth factors, cytokines, chemokines, and mitogens, ESCs create a microenvironment that stimulates the morphogenic events leading to subsequent tissue and organ formation [219,220]. Despite their significant paracrine actions, the emphasis of most research in stem cell pluripotency and differentiation has been on defining phenotypic markers and signaling pathways rather than on coincident expression and/or secretion of morphogenic growth factors.

Because of the role of pluripotent stem cells in developmental processes, it is anticipated that ESCs may be exceptionally unique in their expression and secretion of morphogenic proteins. There are several classes of proteins, such as the fibroblast growth factor (FGF), bone morphogenetic protein (BMP), insulin-like growth factor (IGF), and Wnt families, which play important roles in developmental processes in addition to acting as key regulators of multipotent stem cells and somatic cell populations. The FGF family includes 18 proteins that can be broken down into six sub-families, five of which act as

paracrine factors that dictate patterning and morphogenesis during embryonic development as well as act as mitogenic and cytoprotective agents in mature cellular systems [221]. Members of the FGF family have also been implicated as key regulators of both pluripotent and multipotent stem cell populations and generally stimulate cell proliferation and self-renewal while inhibiting cellular senescence [222]. The BMP family is actually a subgroup representing approximately 1/3 of the members of the larger transforming growth factor-β (TGF-β) superfamily of growth factors, and under the umbrella of the BMP family are several other signaling growth factors, including growth differentiation factors (GDFs). Though the primary focus of BMPs has been their role in the musculoskeletal system, a much larger range of functions has been established including most processes relating to epithelial-to-mesenchymal and mesenchymal-to-epithelial transitions [223]. The IGF family contains fewer members than the FGF and BMP families, consisting only of two IGFs and six IGF-binding proteins (IGFBPs). The IGFBPs have much higher affinities for the IGFs than the IGF receptors do and thus play crucial roles in controlling IGF activity [224]. During embryonic development, members of the IGF family are involved in critical functions during morphogenesis through the control of apoptosis in order to sculpt and pattern specific regions [225]. Interestingly, the role of IGFs appears to shift over the lifespan of an animal, as the proteins have primarily mitogenic roles during development and early in life but are actually observed to augment the aging process later in life [226,227]. The Wnt family consists of highly conserved small secreted signaling proteins which influence cell proliferation and fate specification through canonical (through Frizzled receptors and β-catenin translocation to the nucleus) and non-canonical (not acting through β-catenin) pathways [228]. In addition to key roles during development, members

of the Wnt family are key signaling molecules involved in the maintenance and self-renewal of multipotent stem cell populations, including hematopoietic stem cells [229].

Despite the evidence of ESC trophic factors and their paracrine actions, little work has been performed to characterize specifically what stem cells produce. A challenge in determining the secretome is that secretion is likely dependent on a number of environmental factors, such as the type of media or supplements used, the culture format, the presence of differentiation stimuli, and the stage of differentiation. Proteomic mass spectrometry has been used to identify a number of secreted molecules present during undifferentiated culture, including growth factors (e.g. BMPs, FGFs, VEGF, TGF-β) and signaling molecules involved in the GSK3β/Wnt/β-catenin, Jak/Stat, Notch/Delta, and MAPK/ERK pathways [230–232]. However, mass spectrometry studies are constrained due to technical limitations (e.g. presence of contaminants, high background concentration of carrier proteins such as albumin, low concentrations of species of interest), and thus gene expression analysis has also been performed. Large scale microarray analysis [233,234] in addition to more targeted gene expression screens [235,236] have been used to discriminate gene expression profiles between undifferentiated and differentiating pluripotent stem cells as well as to determine differentially regulated genes based on embryoid body (EB) size. However, a focused analysis of secreted morphogens would provide insight into the unique profiles of expression that pluripotent stem cells possess in comparison to other cell types.

Various pre-conditioning approaches have been found to alter the secretion profile of stem cells by providing more defined and regulated microenvironments. Reducing the oxygen tension of the culture to hypoxic levels (<5%), which more closely resembles the

physiologic microenvironment, increases expression of hypoxia-inducible factors [237–239], which in turn can lead to increased expression of various cytokines and growth factors, including VEGF, IGF-2, and TGF-α [240,241]. Additionally, mesoderm differentiation of ESCs, the lineage that further differentiates into components of the bone marrow compartment (e.g. hematopoietic progenitors, stromal cells, and osteoblasts), may lead to secretion of hemogenic-specific factors. Directed mesoderm differentiation can be induced through the addition of specific proteins (e.g. BMP-4, VEGF, FGF-2, activin A) [146,242,243] or small molecules (e.g. CHIR99021, a GSK3 inhibitor) [244], during early stages of differentiation. From previous findings (Chapter 3), it has also been observed that varying the alginate composition can induce changes in cell phenotype and the secretion of specific growth factors [245]. The type of culture platform employed, such as culture under static or perfusion conditions, may also influence the expression of specific proteins [246].

In order to harness the unique paracrine activities of pluripotent stem cells for applications in stimulating adult stem cell populations, further characterization of their expression of secreted morphogens is essential. Thus, the objective of this study was to perform a global analysis of pluripotent stem cell secreted factors in response to exposure to distinct environmental conditions. Specifically, manipulating the oxygen tension, alginate composition, culture platform, and induction of mesoderm differentiation provide additional engineering approaches to specify and control the secretion of pluripotent stem cell-derived trophic factors. A combination of proteomic and gene expression approaches were employed to assess the influence of these environmental parameters as well as to

distinguish the expression profiles of undifferentiated embryonic stem cells from other cell types and from differentiating stem cell populations.

5.2 Materials and methods

5.2.1 Embryonic stem cell culture

Murine ESCs (D3 cell line) were cultured on tissue culture treated polystyrene dishes (Corning) adsorbed with 0.1% gelatin (EmbryoMax). Undifferentiated ESC culture media consisted of Dulbecco's modified Eagle's medium (DMEM) (Mediatech) supplemented with 15% fetal bovine serum (Hyclone), 100 U/mL penicillin, 100 µg/mL streptomycin, and 0.25 µg/mL amphotericin (Mediatech), 2 mM L-glutamine (Mediatech), 1x MEM non-essential amino acid solution (Mediatech), 0.1 mM 2-mercaptoethanol (Fisher Scientific), and 10^3 U/mL of leukemia inhibitory factor (LIF) (ESGRO). Cultures were replenished with fresh media every other day and passaged prior to reaching 70% confluence.

5.2.2 ESC aggregate formation

A single cell suspension of undifferentiated ESCs was obtained by dissociation of monolayer cultures with 0.05% trypsin-EDTA (Mediatech). Defined, serum-free KO N2B27 media (*note*: formulation is slightly different than what was used in Chapter 3) was used for all aggregate cultures and consisted of Knock-Out (KO) DMEM (Life Technologies) supplemented with N2 (Gibco), B27 (Gibco), 100 U/mL penicillin, 100 µg/mL streptomycin, and 0.25 µg/mL amphotericin (Mediatech), 2 mM L-glutamine (Mediatech), 1x MEM non-essential amino acid solution (Mediatech), and 0.1 mM 2-mercaptoethanol (Fisher Scientific). Aggregation of ESCs was achieved by centrifugation

(200 rcf) of ESCs into 400 μm square polydimethylsiloxane (PDMS) micro-wells (Aggrewell™, Stem Cell Technologies) as previously reported [19,152]. The cell seeding density yielded approximately 500 cells per individual well. The ESCs were incubated in the wells for approximately 24 hours in serum-free KO N2B27 culture media to allow for aggregate formation.

5.2.3 Cell microencapsulation

Two different medium viscosity alginates were used: ultrapure MVG (Pronova) which contains greater than 60% G residues (High G) and ultrapure MVM (Pronova) which contains greater than 50% M residues (High M). Alginate solutions were prepared at 1.5 wt% in calcium-free DMEM (Gibco) and autoclaved for sterilization no more than one day before use. An electrostatic bead generator (Nisco) was utilized for encapsulation. Pre-formed ESC aggregates were resuspended in alginate at a density of 12,000 aggregates per mL of alginate, and the cell-containing alginate solution was extruded through a 400 μm nozzle using a syringe pump at a flow rate of 6 mL/hour and a voltage of 10 kV to drop the beads into a stirred hardening bath of 100 mM calcium chloride (EMD). The beads were washed three times with serum-free media prior to downstream culture. A thin PLL-coating was used to prevent aggregate escape for the seven day factorial experiment examining the influence of oxygen tension, alginate type, and mesoderm-induction. The beads were coated with 0.05% PLL (MW 15,000-30,000; Sigma) for 2 minutes prior to three additional media rinses.

5.2.4 Microencapsulated cell culture and differentiation

Microencapsulated ESC aggregates were generally cultured statically in sterile 100 x 15 mm bacteriological grade polystyrene Petri dishes (BD) in 10 mL serum-free KO

N2B27 media (see 5.2.2) at an initial cell density of 3 x 10^5 cells/mL media. A 90% media exchange was performed every three days. For the factorial experiment examining the influence of oxygen tension, alginate type, and mesoderm-induction, the encapsulated aggregates were cultured statically in 6 well plates in 3 mL culture media at a seeding density of 1.5x10^5 cells/mL media. To induce mesodermal differentiation, recombinant human bone morphogenetic protein-4 (BMP-4; R&D) was supplemented at 10 ng/mL at each media exchange. Cells were cultured in humidified incubators under either normoxic (21% oxygen, 5% carbon dioxide) or hypoxic (3% oxygen, 5% carbon dioxide) conditions. Cells cultured under perfusion were placed in a custom packed bed perfusion reactor (3 x 10^6 cells/reactor) and received serum-free KO N2B27 media at a rate of 150 µL/hr (see Chapter 4).

5.2.5 Mesenchymal stem cell and mouse embryonic fibroblast culture

Murine bone marrow-derived mesenchymal stem cells (MSCs, isolated from C57Bl/6J mice) were obtained from the Texas A&M College of Medicine Institute for Regenerative Medicine The cryopreserved MSCs were thawed and plated onto a 15-cm tissue culture dish in 20 mL MSC complete expansion medium (CEM) which consists of Iscove's Modified Dulbecco's Medium; Invitrogen/GIBCO) supplemented with 10% fetal bovine serum (FBS; Hyclone, Logan, UT), 10% horse serum (Hyclone), 2 mM L-glutamine (Invitrogen/GIBCO), 100U/mL penicillin, 100 µg/mL streptomycin and 0.25 µg/mL amphotericin B (Invitrogen/ GIBCO). Following overnight incubation at 37°C, adherent MSCs were washed with phosphate-buffered saline (PBS, Invitrogen/GIBCO) and detached from the tissue culture plate using 0.25% trypsin and 1 mM EDTA (Invitrogen/GIBCO). Cells were plated onto 15-cm tissue culture dishes, at a density of 50

cells/cm^2 in 20 mL CEM per dish. Cells were fed every 3–4 days with 20 mL of fresh CEM and maintained until they reached ~70% confluence, at which point cells were once again trypsinized, counted and either re-plated or collected for downstream quantitative real time PCR analysis. Mouse embryonic fibroblasts (mEFs) were isolated from day 14.5 embryos using digestion with 0.25% trypsin/EDTA. The equivalent of one embryo was plated per 15-cm tissue culture dish in 30 mL of mEF complete media which consists high glucose DMEM (Gibco) supplemented with 10% fetal bovine serum (Hyclone), 1% penicillin/streptomycin (Mediatech), 2 mM l-glutamine (Mediatech), and 1x MEM non-essential amino acid solution (Mediatech). The isolated cells were cultured for 3-4 days until they reached 90% confluence before freezing at 2 x 10^7 million cells/mL. To collect the mEFs for PCR, a vial of approximately 1 x 10^6 cells was thawed into a 10 cm tissue culture dish in 10 mL of mEF complete media, and the cells were collected after 2 days of culture.

5.2.6 Cell number quantification

Encapsulated aggregates were released from beads through 5 minute incubation with 55 mM sodium citrate (Sigma) for all beads, as previously described [73]. The cells were centrifuged at 200 rcf for 5 minutes and rinsed 3x with PBS. Cells from all conditions were pelleted at 375 rcf for 4 minutes followed by supernatant removal and storage at -20°C. A CyQUANT Cell Proliferation Assay Kit (Molecular Probes Inc., Eugene, OR) was used to determine cell number, with a standard curve created using undifferentiated ESCs that were counted using a hemocytometer. The fluorescence (480 nm excitation, 520 nm emission) was read using a Synergy H4 plate reader (Biotek).

5.2.7 Quantitative real time PCR

Encapsulated aggregates were released from beads through 10 minute incubation with TrypLE™ (Invitrogen) to remove the PLL coating, trituration, and 5 minute incubation with 55 mM sodium citrate (Sigma) to break down the alginate. The cells were centrifuged at 200 rcf and rinsed 3x with PBS to remove residual PLL. RNA was extracted from the aggregates with the RNeasy Mini kit (Qiagen Inc, Valencia, CA). The RNA (300 ng/sample) was converted to complementary DNA using the iScript cDNA synthesis kit (Bio-Rad, Hercules, CA) and analyzed using real time PCR (MyIQ cycler, Bio-Rad). Forward and reverse primers for *18s*, *Oct4*, *Nanog*, *Vegf*, *Igf1*, *Igf2*, *Fgf2*, *Bmp4*, and *Gdf11* were designed with NCBI's Primer-BLAST (sequences and conditions are given in **Table 5.1**) and purchased from Invitrogen. Gene expression were calculated with respect to undifferentiated ESC expression levels as previously described [168].

Table 5.1. Primer sequences for quantitative real time PCR

Gene	Forward sequence	Reverse sequence	Melt temperature (°C)
18s	CTCTAGTGATCCCTGAGAAGTTCC	ACTCGCTCCACCTCATCCTC	60.0
Oct4	CCGTGTGAGGTGGAGTCTGGAG	GCGATGTGAGTGATCTGCTGTAGG	60.0
Vegf	TGCACCCACGACAGAAGG	GCACACAGGACGGCTTGA	60.0
Igf1	TCCGCCAGGTTGCCTCTAG	GGAAGCAGGTGGATGGTCAG	60.0
Igf2	AGCTGACCTCATTTCCCGAT	AATGTGCGACGGGACAGAAC	60.0
Fgf2	AGCGACCCACACGTCAAACTAC	CAGCCGTCCATCTTCCTTCATA	60.0
Bmp4	GAGCCATTCCGTAGTGCCAT	ACGACCATCAGCATTCGGTT	60.0

5.2.8 Cytokine array analysis of conditioned media

Spent media was collected from encapsulated ESC aggregates after 72 hours of culture. The conditioned media was centrifuged at 3000 rcf for 5 minutes to remove cellular debris, and the supernatant was transferred to a new 15 mL conical tube for storage at -20°C. The presence of 96 cytokines in ESC conditioned media was assessed using two

Table 5.2. Protein species present on cytokine antibody arrays (Abcam)

62-target array				34-target array	
Axl	IGFBP-6	Leptin R	SDF-1a	bFGF	MDC
BLC	IL-10	LIX	sTNF RI	DPPIV/CD26	MMP-2
CD30 L	IL-12 p40/p70	L-Selectin	sTNF RII	Dtk	MMP-3
CD30 T	IL-12 p70	Lymphotactin	TARC	E-Selectin	Osteopontin
CD40	IL-13	MCP1	TCA-3	Fcy RIIB	Osteoprotegrin
CRG-2	IL-17	MCP-5	TECK	Flt-3 Ligand	pro-MMP 9
CTACK	IL-1a	M-CSF	TIMP-1	GITR	Resistin
CXCL16	IL-1b	MIG	TNFa	HGF R	Shh-N
Eotaxin	IL-2	MIP-1 gamma	TPO	ICAM-1	Thymus CK-1
Eotaxin 2	IL-3	MIP-1a	VCAM-1	IGF-1	TIMP-2
Fas Ligand	IL-3 Rb	MIP-2	VEGF A	IGF-2	TRANCE
Fractalkine	IL-4	MIP-3a		IGFBP-2	TROY
GCSF	IL-5	MIP-3b		IL-15	TSLP
GM-CSF	IL-6	PF-4		IL-17B R	VEGF D
IFN gamma	IL-9	P-Selectin		IL-7	VEGF R1
IGFBP-3	KC	RANTES		I-TAC	VEGF R2
IGFBP-5	Leptin	SCF		Lungkine	VEGF R3

commercially-available cytokine arrays (Mouse Cytokine Antibody Array – 62 targets and Mouse Cytokine Antibody Array – 34 targets; Abcam) (species listed in **Table 5.2**). Briefly, the provided membranes were blocked with Blocking Buffer for 30 minutes at room temperature, followed by overnight incubation with undiluted conditioned media at 4ºC. The next day, the membranes were washed in 25 mL of Wash Buffer I for 30 minutes under gentle agitation. Three subsequent washes with 2 mL of Wash Buffer I (5 min each) were performed, followed by two washes with 2 mL of Wash Buffer II (5 min each). Biotin-Conjugated Anti-Cytokines were added to the membranes and incubated at 4ºC overnight. The three washes with Wash Buffer I and two washes with Wash Buffer II were repeated before application of a solution of HRP-Conjugated Streptavidin (2 mL per membrane), which was incubated with the membranes overnight at 4ºC. The wash step were repeated, and the membranes were then transferred to clean plastic sheets and covered with 500 µL

of detection buffer. After 2 minutes of incubation, a second plastic sheet was placed on top of the membrane to sandwich it in plastic, and the array was immediately imaged using a Li-Cor Odyssey Fc imager equipped with a CCD camera. The arrays were quantified using ImageJ (http://imagej.nih.gov/ij/) by (1) converting the image to 8 bit, (2) inverting it so that it has a black background, (3) subtracting the background, (4) enabling the "integrated density" measurement, (5) drawing a circle around the largest dot and measuring the integrated density, and (6) moving the drawn circle to each dot and measuring the integrated density. The intensity of each species was averaged between two dots and reported as an intensity relative to the average intensity of the six positive control dots on each membrane.

5.2.9 Fluidigm custom PCR array

Encapsulated aggregates were released from beads through 5 minute incubation with 55 mM sodium citrate (Sigma). RNA was extracted from the aggregates with the RNeasy Plus Mini kit (Qiagen Inc, Valencia, CA). The RNA (840 ng/sample) was converted to complementary DNA using the iScript cDNA synthesis kit (Bio-Rad, Hercules, CA). Forward and reverse primers for 96 genes were designed with NCBI's Primer-BLAST (identities and sequences are given in **Table 5.3a-b**) and were pooled into a single tube (1 µL of each 100 µM primer stock such that the final concentration of each primer is 500 nM). The cDNA (1 µL) was combined with the pooled primers and PreAmp Master Mix (Fluidigm) (4 µL, 5 µL total volume) prior to pre-amplification (2 minute hold at 95ºC, 15 cycles of 15 sec at 95ºC and 4 min at 60ºC) using a SimpliAmp thermal cycler (Life Technologies). Exonuclease treatment was then performed to remove unincorporated primers by adding Exonuclease I and Exonuclease I Reaction Buffer (New England

Table 5.3a. Genes and primer sequences for Fluidigm array (18s – Hgf)

Gene name	Abbrev.	Forward	Reverse
18S ribosomal RNA	18s	CTCTAGTGATCCCTGAGAAGTTCC	ACTCGCTCCACCTCATCCTC
Angiopoietin 1	Angpt1	GAATGGGGGAGGTTGGACAG	CTGTGAGTAGGCTCGGTTCC
Angiopoietin 2	Angpt2	TCGCTGGTGAAGAGTCCAAC	CACATGCGTCAAACCACCAG
Angiopoietin-like protein 2	Angptl2	CAGGAGAGAAGAGGCTTTCAGT	AGTGTAGGTGCACTTGTCGG
Angiopoietin-like protein 3	Angptl3	GCACCAAGAACTACTCCCCC	CATGGACTGCCTGATTGGGT
Bone morphogenetic protein 10	Bmp10	AACGCCAAGGGGAACTACTG	GGGTAGTTACACACACCCCG
Bone morphogenetic protein 2	Bmp2	TAGAAAAGCTCTCGCCACCC	AGCCCCCTGGAAGGGATTAT
Bone morphogenetic protein 3	Bmp3	GAAGAAGGCAAGGCGAAAGC	TGGATGGTGGCGTGATTTGA
Bone morphogenetic protein 4	Bmp4	GAGCCATTCCGTAGTGCCAT	ACGACCATCAGCATTCGGTT
Bone morphogenetic protein 5	Bmp5	GCCTGCTGGAGGTGGAATTA	GATTTGTCCGGCAGCCTAGT
Bone morphogenetic protein 6	Bmp6	TGACACGCAGACACATCTCC	CTAAAACTACTCCGGGCGGG
Bone morphogenetic protein 7	Bmp7	CAGGGCTTCTCCTACCCCTA	TCAAACCGGAACTCCCGATG
Bone morphogenetic protein 8a	Bmp8a	CGTCAGCTTCCGTGACCTT	AGGTGCACCAGAGACTGCAA
Bone morphogenetic protein 8b	Bmp8b	GGAGCGCAGTCGTCTTAGAG	AGGCCCAGTAGCCATAGGAG
Chemokine (C-C motif) ligand 11 (Eotaxin 1)	Ccl11	CCACCCACTCTGCTCCCTAT	GGTGAAGGAAGTGACCGTGA
Chemokine (C-C motif) ligand 12 (MCP-5)	Ccl12	AGAGACACTGGTTCCTGACTCC	TCCGGACGTGAATCTTCTGC
Chemokine (C-C motif) ligand 2 (MCP-1)	Ccl2	CAGTTAACGCCCCACTCACC	GACCCATTCCTTCTTGGGGT
Chemokine (C-C motif) ligand 27a (CTACK)	Ccl27a	CCTTCAGGAACCGTTCGGAG	GGCTTGTTGGAGACATCGGA
Chemokine (C-X-C motif) ligand 1 (KC)	Cxcl1	GCCTCTAACCAGTTCCAGCA	TTGAGGTGAATCCCAGCCAT
Chemokine (C-X-C motif) ligand 11 (I-TAC)	Cxcl11	TGGAACATGCAGCCACGTAT	CCACAGAAGGTAGCGTGGAG
Chemokine (C-X-C motif) ligand 12 (SDF-1)	Cxcl12	CCTTCAGATTGTTGCACGGC	TTGCATCTCCCACGGATGTC
Chemokine (C-X-C motif) ligand 2 (MIP-2a)	Cxcl2	TCTCAAGGGCGGTCAAAAAGT	GTACGATCCAGGCTTCCCG
Colony stimulating factor 1 (macrophage)	Csf1	TGTACCCTAAAGCCACCCCT	TATGCGAAGGGGAAGCTCAC
Colony stimulating factor 2 (granulocyte-macrophage)	Csf2	GCCAGGAGATTCCACAACTCA	GGTGCTGAGAGGCTGTAGAC
Colony stimulating factor 3 (granulocyte)	Csf3	CTTCCGGGGGACAAGACATC	CCAGTCAATTCCGGGGCTAA
Epidermal growth factor	Egf	CTGTTGTTGGAGGGAGCGAT	CGTGATTCCACTGGGTTCCA
Fibroblast growth factor 1	Fgf1	CGGTTGTGTACGAAGTCCCA	CATCAGGGGATACACCCAGC
Fibroblast growth factor 10	Fgf10	CAGATCCGTACCCAGAGGGA	ACTGAAACTCTCGGCACTGG
Fibroblast growth factor 11	Fgf11	TGTCGCTTTAAGGAGTGCGT	AGAGAAGGCTCCCGGTACAT
Fibroblast growth factor 13	Fgf13	TCCCGGGTCAAACTCTTTGG	AGACCCACAGGGATGAGGTT
Fibroblast growth factor 14	Fgf14	CTTGATCCGTCAGAAACGGC	TGGTCACTATGCCCTTGAGC
Fibroblast growth factor 15	Fgf15	GACTGCGAGGAGGACCAAAA	CAGCCCGTATATCTTGCCGT
Fibroblast growth factor 17	Fgf17	GTTGGTGCGGGTCAGGAATA	CTCGCTCTCTTGGGCTACTG
Fibroblast growth factor 18	Fgf18	GATGTATTCAGCGCCCTCCG	AGCTGCTTCCGACTCACATC
Fibroblast growth factor 2	Fgf2	GGCTGCTGGCTTCTAAGTGT	TCTGTCCAGGTCCCGTTTTG
Fibroblast growth factor 22	Fgf22	TTTTTCCTGCGTGTGGACCT	TAGACCCGCGACCCATAGAG
Fibroblast growth factor 3	Fgf3	GACGGCTGTATGCTTCGGAT	TTCACCGACACGTACCAAGG
Fibroblast growth factor 4	Fgf4	CACGAGGGACAGTCTTCTGG	TGAGGGCCATGAACATACCG
Fibroblast growth factor 5	Fgf5	CCCACGAAGCCAGTGTGTTA	TGGCACTTGCATGGAGTTTT
Fibroblast growth factor 6	Fgf6	GGCTCTCGTCTTCTTAGGCG	ACCAAATAGCCGCTTTCCCA
Fibroblast growth factor 7	Fgf7	CGTGGCAGTTGGAATTGTGG	AGGCAACGAACATTTCCCCT
Fibroblast growth factor 8	Fgf8	AACCCAGCTGACACTCTCGG	CTGTAGAGCTGGTAGGTCCG
Fibroblast growth factor 9	Fgf9	CTCTCCGGTTTGCATCAGGT	CACTGCTTGGGGACATTTGC
Growth differentiation factor 10	Gdf10	GAGCCAATCCCGATACCTCG	GGCTGAGTAACGGTGGTGAA
Growth differentiation factor 11	Gdf11	CTGCCCCAAGCCTGTTTTTC	TTACTTTGCCCCATCCTCGG
Growth differentiation factor 5	Gdf5	CAGAGACTACCCCCTCCACA	GCCCACTCAGAGTCTGTTCC
Growth hormone	GH	TGGACAGATCACTGCTTGGC	GTAGGCACGCTCGAACTCTT
Hepatocyte growth factor	Hgf	AGTCAGCACCATCAAGGCAA	ACCAGGACGATTTGGGATGG

Table 5.3b. Genes and primer sequences for Fluidigm array (Igf1 – Wisp1)

Gene name	Abbrev.	Forward	Reverse
Insulin-like growth factor 1	Igf1	ATGTTCCCCCAGCTGTTTCC	GGCAGGGATAATGAGGCGAA
Insulin-like growth factor 2	Igf2	AGCTGACCTCATTTCCCGAT	AATGTGCGACGGGACAGAAC
Insulin-like growth factor binding protein 1	IGFBP-1	TCGTGACCACTGAGCAACTG	ACGCCAATCTGGAAGGACAG
Insulin-like growth factor binding protein 2	IGFBP-2	AGAAAGAAGGCAAGGAGGCG	AAGAGCAGCAGCAAGAGCAA
Insulin-like growth factor binding protein 3	IGFBP-3	CTCACTGCCCTCACTCTGC	GGAGGCGCGCACTGG
Insulin-like growth factor binding protein 4	IGFBP-4	GTGGTGAACATTGAACGCCC	GCAAGGCATTGTCGGATGAC
Insulin-like growth factor binding protein 5	IGFBP-5	CACGGTTGGAAACAAGGCTG	ATGTTTGAGTCGGGCAGAGG
Insulin-like growth factor binding protein 6	IGFBP-6	GGTCTACAGCCCTAAGTGCG	CCGGTCTCTGTGGTTTGTGT
Interleukin 10	IL-10	TAAGGCTGGCCACACTTGAG	GTTTTCAGGGATGAAGCGGC
Interleukin 11	Il-11	GCTGCTCACACTCACAAACC	CCAGGGGCAACGACTCTATC
Interleukin 1a	IL-1a	AGGGAGTCAACTCATTGGCG	AGATGGTCAATGGCAGAACTGT
Interleukin 4	IL-4	CCATATCCACGGATGCGACA	AAGCACCTTGGAAGCCCTAC
Kit ligand (stem cell factor)	Kit-L	CTTGCTACCCGTGACCTTGT	TCAGCACTCAGACGTTTCCC
Left right determination factor 1	Lefty1	AATGGGCAATCCCTGTGTGT	GTGCTTCGCATACAGTGCAG
Leukemia inhibitory factor	Lif	CGAGACCACGGCTCCAGTAT	GGTGGCATTTACAGGGGTGA
Myostatin	Mstn	AATCCTCAGTAAGCTGCGCC	TGCCATCCGCTTGCATTAGA
Nerve growth factor	Ngf	CGCATCGAGTGACTTTGGAG	ACGACCACAGGCCAAAACTC
Nodal	Nodal	GCCGACATCATTTGCCAGAC	CCCTCACAGCGATAGGCATT
Osteopontin	Opn	AGCAAGAAACTCTTCCAAGCAA	GTGAGATTCGTCAGATTCATCCG
Placental growth factor	Pgf	ATCCTTTCACATCGCTCCGA	ACAATCACCATGCTCGTCCC
Platelet derived growth factor, alpha	Pdgfa	GTACTGAATTTCGCCGCCAC	CGGATGCTGTGGATCTGACT
Platelet derived growth factor, B polypeptide	Pdgfb	CTCAAGCTCGGGTGACCATT	CATCGAGACAGACGGACGAG
Secreted frizzled-related protein 1	Sfrp1	TAAAATCGCTGCCTGCCTGA	ATACCTCTGGGCACTTGGGA
Sonic hedgehog	Shh	GTGATCCTTGCTTCCTCGCT	TGTCGGGGTTGTAATTGGGG
Transforming growth factor alpha	Tgfa	ATGGTGACGTTGGTCCCTTC	CCTTTGGCCTTGGGAGAGAG
Transforming growth factor, beta 1	Tgfb1	AGGGCTACCATGCCAACTTC	CCACGTAGTAGACGATGGGC
Transforming growth factor, beta 2	Tgfb2	AGTTCAGGGTCTTCCGCTTG	CGTCGAAGGAGAGCCATTCA
Transforming growth factor, beta 3	Tgfb3	GATCACCACAACCCACACCT	AGGTTCGTGGACCCATTTCC
TYRO3 protein tyrosine kinase 3	Tyro3/Dtk	GAGTCTTCCTATCCTGCCGC	GCCAGTGAGACGTCCCATAC
Vascular endothelial growth factor A	Vegfa	GGAGTCTGTGCTCTGGGATT	AGAACCAACCTCCTCAAACCG
Vascular endothelial growth factor B	Vegfb	ATCATCCATCCCACTCCAGC	CACCTACAGGTGTCTGGGTT
Vascular endothelial growth factor C	Vegfc	AGAAGTATGCCGCTGTGTCC	TCCTCTCCCGCAGTAATCCA
Wnt family, member 2	Wnt2	GTTTGCCCGTGCCTTTGTAG	GTACAGGAGCCACTCACACC
Wnt family, member 1	Wnt1	CAACAGTAGTGGCCGATGGT	GGGTTCTGTCGGATCAGTCG
Wnt family, member 10A	Wnt10A	TGAACACCCGGCCATACTTC	CATGTTCTCCATCACCGCCT
Wnt family, member 11	Wnt11	CCCAATCTGCCCCCAAATCT	TCACATACAGGGAAACGGGC
Wnt family, member 16	Wnt16	ACTGGATGTGGTTGGGCATC	TGGCGACCATACAGTTCCAC
Wnt family, member 2B	Wnt2B	CCCCCACATCCACTATTCCG	TAGGATGTTTGCCACCTCGG
Wnt family, member 3	Wnt3	ACTTTTGTGAGCCCAACCCA	TTCTCCGTCCTCGTGTTGTG
Wnt family, member 3A	Wnt3A	TGGCTCCTCTCGGATACCTC	ACAGAGAATGGGCTGAGTGC
Wnt family, member 4	Wnt4	CGTGCGAGAAACTCAAAGGC	TCCGGAACTGGTATTGGCAC
Wnt family, member 5A	Wnt5a	GCCCAGAAGCCCATTGGAATA	GAGAGGCTGTGCACCTATGA
Wnt family, member 5B	Wnt5B	CTGCTGACTGACGCCAACT	CCTGATACAACTGACACAGCTTT
Wnt family, member 6	Wnt6	TACCAAGGCATGACGGAGTG	AGACGCCTGACAACTAAGCC
Wnt family, member 7A	Wnt7A	CACAGTTCCGAGAGCTAGGC	GGTAGGACAGGGGCTTCTTG
Wnt family, member 7B	Wnt7B	CTGAGCGTGGTCCTACCG	ATGACAATGCTCCGAGCTTCA
Wnt family, member 9A	Wnt9A	GGAAAGGACCGGCTATGTGT	GCCTCTGTATACTGCCACCC
WNT1 inducible signaling pathway protein 1	Wisp1	TGATGACGCAAGGAGACCAC	CCGGGCATTGACGTTAGAGA

BioLabs) to each sample, digesting for 30 min at 37ºC, and inactivating for 15 min at 80ºC. The final product at this stage was diluted 5-fold with TE Buffer (Teknova). The samples were then combined with 2X SsoFast EvaGreen Supermix with Low ROX (Bio-Rad) and 20X DNA Binding Dye Sample Loading Reagent (Fluidigm) (2.5 µL EvaGreen Supermix and 0.25 µL DNA Binding Dye per 2.25 µL sample) and vortexed thoroughly. The assay mix was prepared by combining the forward and reverse primer for each gene (0.25 µL total primer volume) with 2.5 µL Assay Loading Reagent (Fludigm) and 1X DNA Suspension Buffer (Teknova) and vortexed thoroughly. A 96.96 Dynamic Array IFC (Fluidigm) was primed with control line fluid (Fluidigm) and loaded with 5 µL of each sample and assay mixture. A BioMark HD system was used to run the chip, and BioMark HD Data Collection Software and Fluidigm Real-Time PCR Analysis Software were used to run and analyze the chip. For heat map analysis, gene expression values were calculated with respect to undifferentiated ESC expression levels, and the data was hierarchically clustered and plotted using Genesis software (Institute for Genomics and Bioinformatics, Graz University of Technology).

5.2.10 Ingenuity Pathway Analysis (IPA)

Ingenuity Pathway Analysis (IPA, QIAGEN, Redwood City, www.qiagen.com/ ingenuity) software was used to analyze biological functions and signaling networks associated with proteins and genes expressed by pluripotent stem cells. For the cytokine array data, the presence of detected proteins in specific pathways was determined using IPA's database of biological processes. To compare the gene expression profile of undifferentiated ESCs to mEF and MSC gene expression profiles, genes were filtered using a minimum 10-fold change threshold between the two cell types to create a list of focus

genes. Those focus genes were then compared to the reference gene set for functional categories, and a right-tailed Fisher Exact Test was used to determine significance by identifying over-representation of the focus genes in the specific process. In addition, the Benjamini-Hochberg (B-H) multiple testing correction method was applied to account for false-positives. The top 10 functions for ESCs vs. mEFs and ESCs vs. MSCs are reported in **Table 5.4-5.5**, with each function having a significance of $p < 10^{-7}$ and a list of the relevant focus genes for each functional pathway recorded.

5.2.11 Statistics

All experiments were performed with replicate samples from independent conditions, with the exception of the cytokine arrays which were performed with pooled samples on a single array. Data is generally represented as the mean of the independent replicates, and the error bars represent the standard error of the mean. Before performing statistical analysis, data were normalized using a Box–Cox power transformation to normalize data variance. A three-way ANOVA was calculated in MatLab to determine the influence of alginate composition, external oxygen tension, and the presence of mesoderm stimuli, followed by post hoc Tukey analysis to determine significant differences ($p < 0.05$). Volcano plots describing differences in gene expression profile between time points of differentiation and cells cultured under static and perfusion were calculated through paired t-tests between the delta Ct values calculated for each gene and normalized to the housekeeping gene *18s*.

5.3 Results

5.3.1 Influence of microenvironment on ESC growth factor gene expression

To determine the how specific environmental parameters can promote the expression of growth factors, encapsulated ESC aggregates cultured statically were studied in a three factor, two level (2^3 factorial design, 8 total conditions) experiment. The three factors were (1) alginate composition (Level 1: High G alginate, Level 2: High M alginate; both had thin PLL coatings to maintain the aggregates within the beads for 7 days), (2) external oxygen tension (Level 1: normoxia – 21% O_2, Level 2: hypoxia – 3% O_2), and (3) presence of the mesoderm stimulating protein bone morphogenetic protein-4 (BMP-4) (Level 1: no BMP-4 added, Level 2: 10 ng/mL BMP-4 added) **(Figure 5.1a)**. The morphology of the encapsulated aggregates over time **(Figure 5.1b-q)** was consistent with previous findings, with aggregates cultured in the High G alginate maintaining a spherical structure while aggregates cultured in the High M alginate became elongated over time [245]. No drastic changes in morphology were observed in response to oxygen level or the presence of BMP-4, though some of the BMP-4 treated groups appeared to have distinct light and dark regions **(Figure 5.1m, 5.1q)**, which can be a sign of morphogenesis and differentiation [247,248].

Analysis of gene expression for a pluripotency marker and a number of growth factors after seven days indicated that the environmental parameters were capable of modulating ESC cell state. Expression of the pluripotency marker *Oct4* was decreased in comparison to undifferentiated ESCs in all groups, as expected after seven days of differentiation **(Figure 5.2a)**. However, culture with BMP-4, particularly under hypoxic conditions, promoted increased *Oct4* expression in the High M alginate only. Two growth factors which have been identified as sensitive to oxygen level, *Vegf* and *Igf2*, exhibited differential responses to the environmental conditions. The expression of *Vegf* was

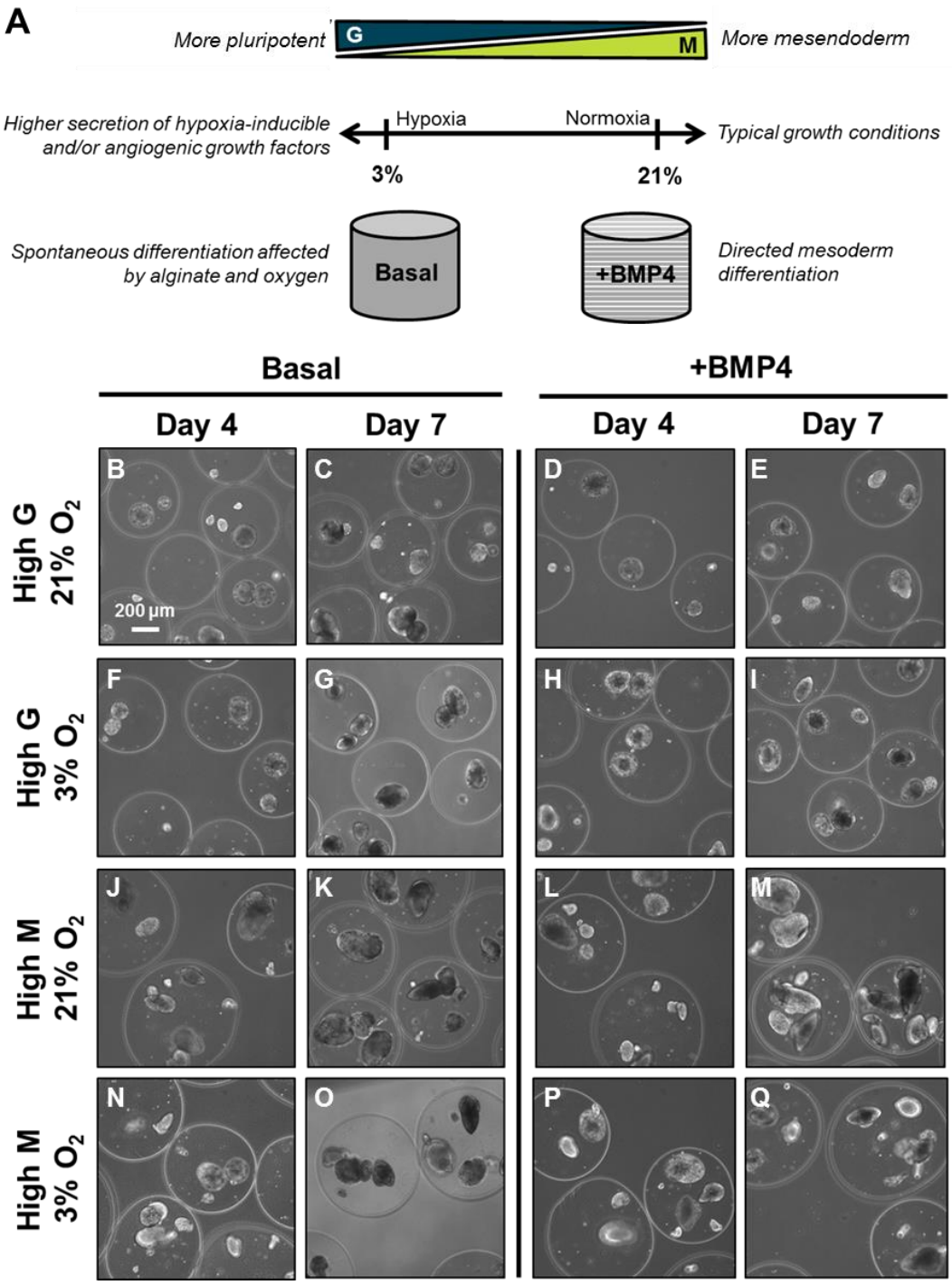

Figure 5.1. Factorial experiment of environmental parameters. ESCs were encapsulated in either High G alginate or High M alginate and cultured in either hypoxic or normoxic oxygen concentrations with or without the presence of the mesoderm-stimulating protein BMP-4 **(A)**. Phase images of each condition at day 4 and day 7 of differentiation exhibit morphological differences, including elongation of the aggregates and the presence of contrasting dark/light morphogenic regions **(B-Q)**. Scale bar = 200 µm.

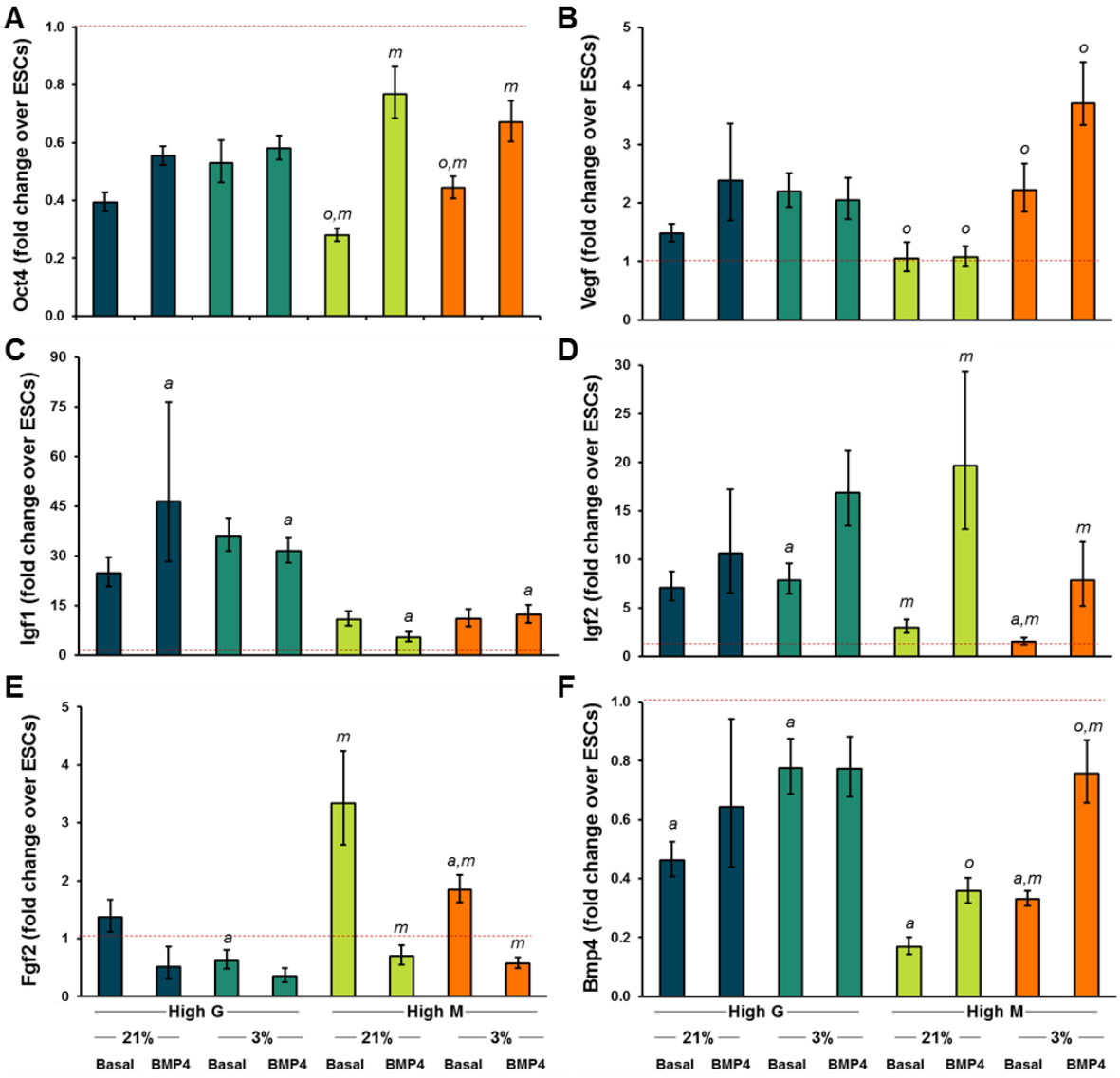

Figure 5.2. Growth factor gene expression profiles resulting from environmental conditioning. Gene expression results at day 7 of differentiation for the pluripotency marker Oct4 **(A)** and growth factors Vegf **(B)**, Igf1 **(C)**, Igf2 **(D)**, Fgf2 **(E)**, and Bmp4 **(F)** are displayed relative to the expression level of undifferentiated ESCs (denoted by the red dashed line). Significant differences ($p < 0.05$) between paired alginate composition are denoted by an *a*; significant differences between paired oxygen concentrations are denoted by an *o*; and significant differences between paired media conditions, namely the presence or absence of BMP-4, are denoted by an *m*.

increased in response to low oxygen, but this response was only observed in the High M alginate **(Figure 5.2b)**. Conversely, the expression of *Igf2* was not affected by oxygen level but was expressed more highly when cultured in High G alginate or in the presence of BMP-4 **(Figure 5.2d)**. The growth factor *Igf1* was affected only by alginate composition and was significantly more highly expressed in the High G + BMP-4 groups than in the High M + BMP-4 groups **(Figure 5.2c)**. In contrast, *Fgf2* was expressed more highly by cells cultured in High M alginate in the absence of BMP-4 **(Figure 5.2e)**. Finally, the expression of *Bmp4* was influenced by all three environmental parameters and was generally increased in High G alginate, in low oxygen conditions, and the presence of external BMP-4 **(Figure 5.2f)**. The results of this study indicate that the growth factor expression of ESCs is not exclusively regulated by a single environmental parameter (or combination of environmental parameters) but that the defined culture conditions play a significant role in controlling expression patterns.

5.3.2 Global analysis of ESC secreted factors using cytokine arrays

To assess the presence of cytokines and growth factors at a more comprehensive level, commercially-available antibody arrays were used to determine if certain secreted factors were present in the ESC conditioned media. The two arrays used were capable of assessing the presence of 96 unique proteins (identified in **Table 5.2)**. Perfusate collected from ESC aggregates encapsulated in High G alginate and perfused at 150 µL/hr for 4 days (day 1-5 of differentiation; pooled from 6 different reactors) was analyzed using both arrays and subsequently quantified to obtain relative abundance. Of the 96 species, 59 were present above the threshold of 10% of the intensity of the positive control spot **(Figure 5.3)**. The species in highest abundance (semi-quantitative only) were insulin-like growth

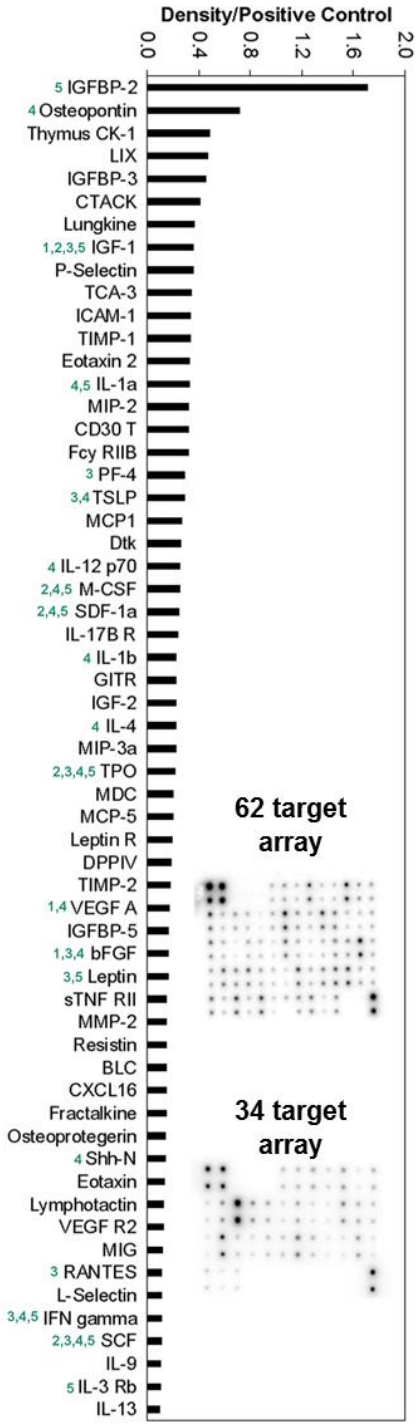

Figure 5.3. Relative intensity of protein species present in ESC conditioned medium. Commercial antibody arrays were used to determine the presence of 96 proteins in conditioned media collected from perfused ESCs between days 1-5 of differentiation. Ingenuity Pathway Analysis (IPA) was used to categorize the proteins into the following categories: (1) Increase proliferation of mesenchymal cells; (2) Affect developmental processes of bone marrow cells; (3) Decrease cell death of hematopoietic progenitors; (4) Increase proliferation of hematopoietic progenitor cells; and (5) Increase the quantity of hematopoietic cells.

factor binding protein-2 (IGFBP-2), osteopontin, thymus CK-1 (CXCL7), LIX (CXCL5), and insulin-like growth factor binding protein-3 (IGFBP-3). Many of the detected proteins play roles in processes related to the bone marrow physiology. Using Ingenuity Pathway Analysis (IPA), the presence of detected proteins in five functional categories was explored. IGF-1, VEGF-A, and bFGF are documented as "increasing proliferation of mesenchymal cells;" IGF-1, M-CSF, SDF-1α, TPO, and SCF "affect developmental processes of bone marrow cells;" IGF-1, PF-4, TSLP, TPO, bFGF, Leptin, RANTES, and SCF "decrease cell death of hematopoietic progenitors;" Osteopontin, IL-1α, TSLP, IL-12p70, M-CSF, SDF-1α, IL-1β, IL-4, TPO, VEGF-A, bFGF, SHH-N, and SCF "increase proliferation of hematopoietic progenitor cells;" and IGFBP-2, IGF-1, IL-1α, M-CSF, SDF-1α, TPO, Leptin, SCF, and IL-3 Rb "increase the quantity of hematopoietic cells."

To determine how the global secretion profiles change with differentiation stage and culture under perfusion, ESCs were cultured in either basal or mesoderm-promoting conditions and under static or perfusion culture **(Figure 5.4)**. Smaller alginate beads composed of High G alginate were used for the early stage of differentiation **(Figure 5.4b-c)**, while larger alginate beads of High M alginate **(Figure 5.4e)** were used for the later stage, mesoderm-primed cultures so that the larger aggregates **(Figure 5.4d)** would not be subjected to shear stress during the encapsulation process and due to previous findings that culture in High M alginate promotes mesoderm differentiation [245].

A global increase in protein concentration was observed in the conditioned media collected from the day 4-7 "mesoderm-primed" cultures in comparison to the day 1-4 "early differentiating" cultures **(Figure 5.5a-b)**. This is likely due to the increase in cell number **(Figure 5.5c)** owing to the extended period of time for cell proliferation. Though

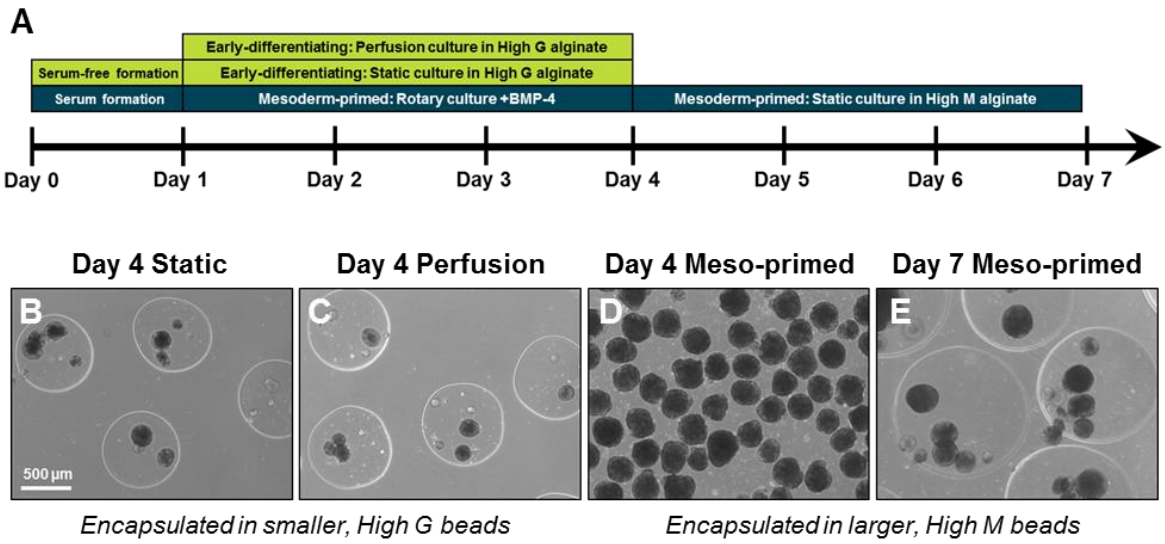

Figure 5.4. Comparison of ESC differentiation stage and culture platform. A timeline **(A)** of ESC culture and encapsulation indicating the two stages of differentiation (early-differentiating cells cultured in High G alginate from day 1-4 and mesoderm-primed cells cultured unencapsulated in the presence of BMP-4 from day 1-4 and subsequently encapsulated in High M alginate and cultured for three additional days in the absence of BMP-4). ESC aggregates cultured in static **(B)** and perfusion **(C)** culture exhibit similar morphology, while unencapsulated ESC aggregates primed with BMP-4 **(D)** are larger after three days of culture. The larger aggregates were encapsulated in larger alginate beads composed of High M alginate **(E)** and did not appear to increase in size in the subsequent three days in culture.

there was a general increase in concentration of all proteins, some species were increased more or less relative to the average increase **(Figure 5.5d)**. Proteins involved in mesoderm-related processes, including SDF-1α, VEGF-A, and MMP-2, had a greater relative increase than would be expected based on cell number alone, while species involved in more early stage development and general mitogenesis, such as IGF-1, IGF-2, and several of the IGFBPs, exhibited a lower relative increase than would be expected based on cell number.

Comparing the static and perfusion culture platforms **(Figure 5.6a-b)**, the perfusate collected from the packed bed reactor contained higher concentrations of all but two detected protein species, with an overall average increase of 1.6-fold over static **(Figure 5.6d)**. This increase was observed despite the lower cell number observed in the perfusion

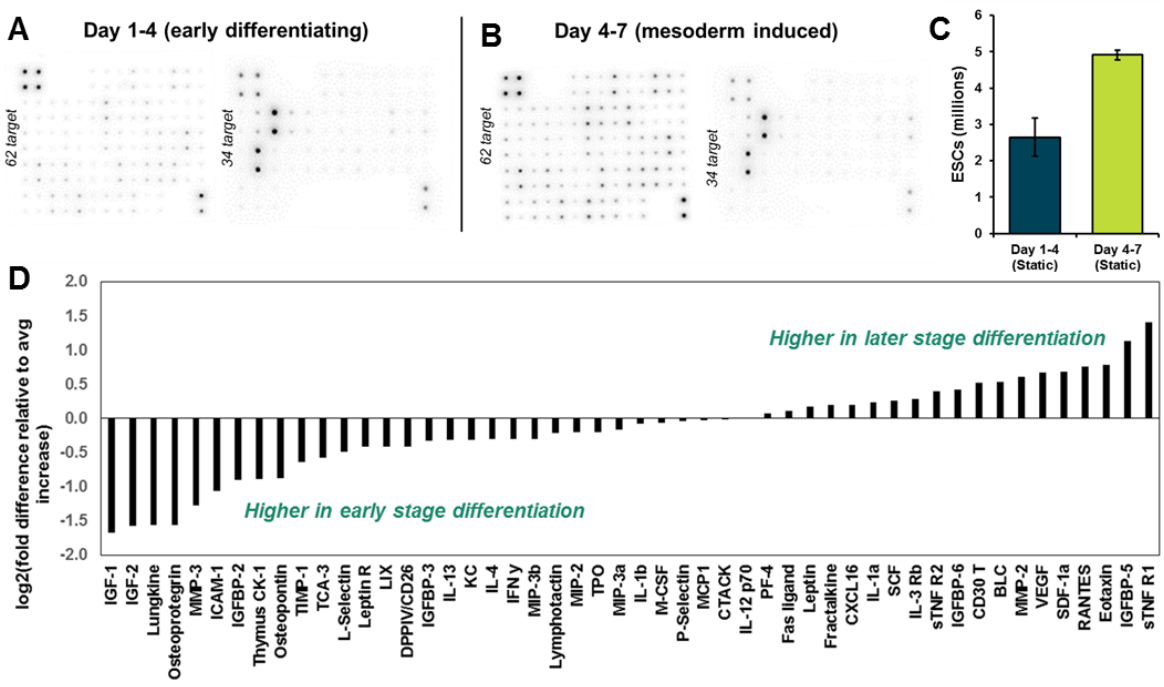

Figure 5.5. Secreted profiles of early differentiating and mesoderm induced ESCs. Antibody arrays were used to analyze the contents of ESC conditioned media collected from cells in an early stage of differentiation **(A)** and at a late, more directed stage of differentiation **(B)**. More cells were present in the mesoderm-induced, later stage differentiation **(C)**, which may be partially responsible for the general increase in intensity observed. The intensity of each detected protein was normalized to the overall average increase to attempt to account for the influence of cell number, and certain species were found to be present at higher or lower concentrations relative to that average increase **(D)**.

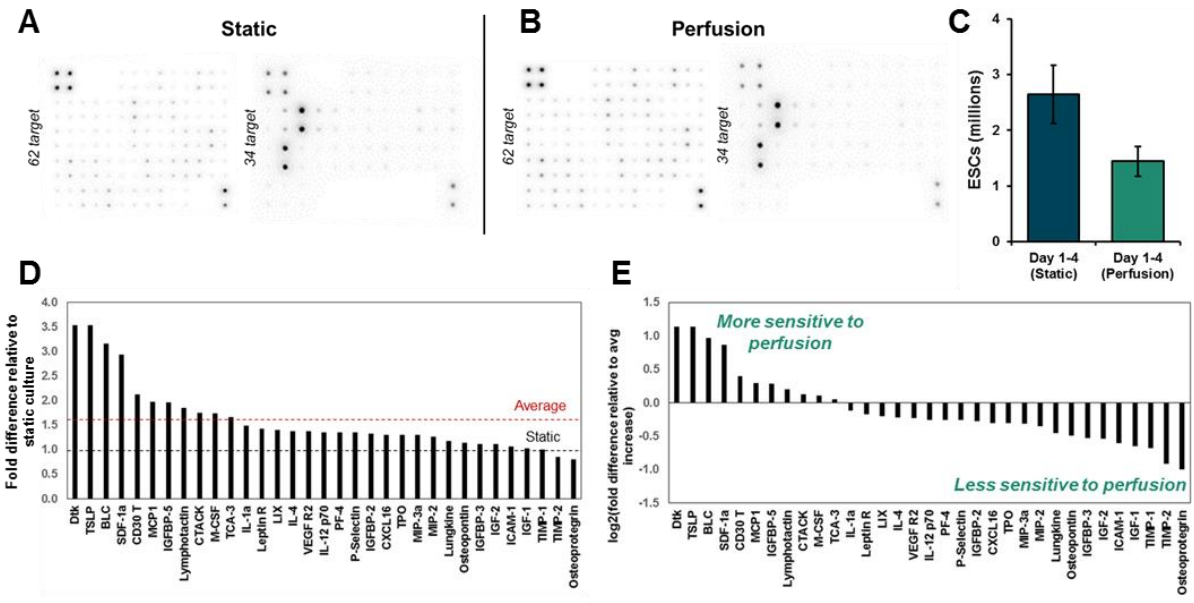

Figure 5.6. Secreted profiles of ESCs cultured under static and perfusion conditions. Antibody arrays were used to analyze the contents of ESC conditioned media collected from cells in an early stage of differentiation cultured either statically **(A)** or in a custom perfusion bioreactor at a flowrate of 150 µL/hr **(B)**. A global increase in intensity was observed in the conditioned media derived from the perfusion reactor **(D)**, despite the lower number of cells present in this condition **(C)**. The intensity of each detected protein was normalized to the overall average increase to attempt to determine if certain species were more or less sensitive to perfusion culture, and certain species were found to be present at higher or lower concentrations relative to that average increase **(E)**.

conditions **(Figure 5.6c)**, likely due to uneven initial seeding within the reactor. Though a global increase in growth factor and cytokine concentration was observed when the ESCs were cultured under perfusion, certain species were upregulated to a greater extent than others **(Figure 5.6e)**, indicating that the secretion of specific proteins may regulated to a greater extent by changes in culture condition, such as the observations observed with VEGF and IGFBP-2 in Chapter 4.

5.3.3 Comprehensive analysis of ESC morphogen expression

The limited number of cytokines and lack of developmental morphogens of interest present on commercially available arrays prompted a complementary approach to examine the proteins expressed by ESCs; thus, a custom 96 gene expression array was designed

using the Fluidigm platform. To determine what unique morphogens, growth factors, and cytokines are expressed by ESCs in comparison to other common supportive cell populations, the gene expression profiles of mouse embryonic fibroblasts (mEFs) **(Figure 5.7a)** and mouse bone marrow mesenchymal stem cells (MSCs) **(Figure 5.7b)** were directly compared to undifferentiated mouse ESCs. There were drastic increases (>1000-fold) in the expression of certain genes uniquely observed in ESCs in comparison to both mEFs and moMSCs, including *Fgf3*, *Fgf4*, *Fgf15*, *Fgf 17*, *Nodal*, and *Igfbp2*. Using IPA, the top related functions and diseases for each cell type were determined, based on genes with a 10-fold or greater difference **(Table 5.4 and 5.5)**. The genes differentially expressed by ESCs were primarily related to morphogenic events and processes, while the stromal mEFs and MSCs expressed genes associated with more general cell functions, such as migration and proliferation. The unique expression profile of ESCs in comparison to these two common support cell types indicates that they are a unique cell source for morphogenic proteins.

To evaluate the influence of differentiation stage and culture platform on gene expression in addition to protein expression, ESCs were cultured in either basal or mesoderm-promoting conditions and under static or perfusion culture as previously described **(Figure 5.4)**. Gene expression values were normalized to undifferentiated ESCs (collected at day 0 of the experiment), organized via two-dimensional hierarchical clustering, and displayed as a heatmap, with red indicating increased expression over undifferentiated ESCs and blue signifying decreased expression compared with undifferentiated ESCs. When comparing differentiation stages, the day 4 "early differentiating" samples clustered separately from the day 7 "mesoderm-primed" samples.

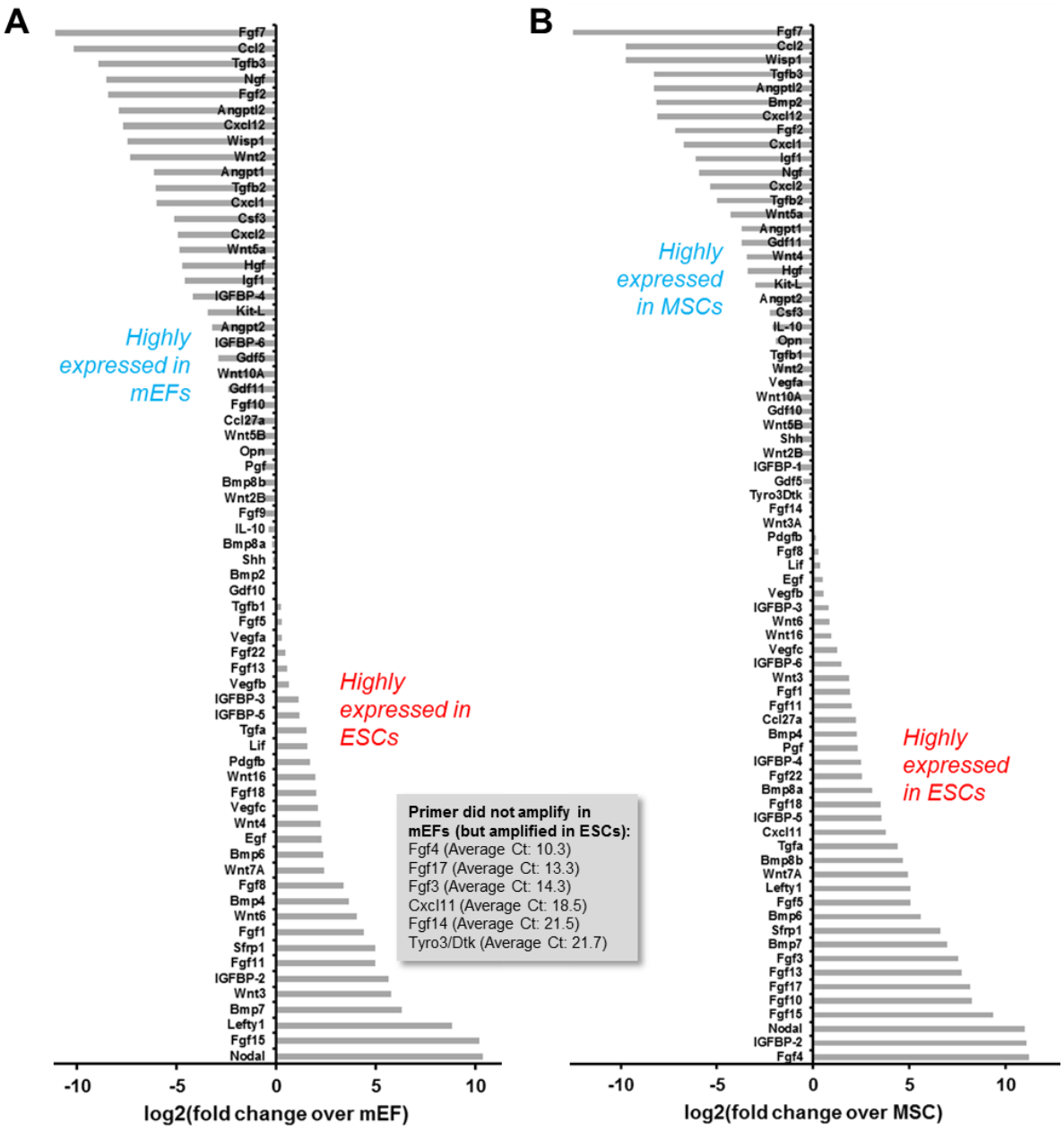

Figure 5.7. Gene expression profiles of ESCs in comparison to mouse embryonic fibroblasts (mEFs) and mesenchymal stem cells (MSCs). A custom PCR array was designed and analyzed using the Fluidigm platform, and the expression profile of undifferentiated ESCs was compared to that of mEFs **(A)** and MSCs **(B)**. Several of primers which were found to be highly expressed by ESCs in comparison to MSCs did not amplify in the mEF cell population, making direct comparison impossible.

Table 5.4. Top related functions and diseases for mEFs vs. ESCs

mEF functions	
Function	**Genes**
Development of cardiovascular system	ANGPT1,ANGPTL2,Ccl2,CSF3,CXCL12,CXCL2,CXCL3,FGF2,HGF,IGF1,IGFBP4,KITLG,TGFB2,WNT2,WNT5A
Migration of cells	ANGPT1,ANGPTL2,Ccl2,CSF3,CXCL12,CXCL2,CXCL3,FGF2,FGF7,HGF,IGF1,IGFBP4,KITLG,NGF,WISP1,WNT5A
Proliferation of cells	ANGPT1,Ccl2,CSF3,CXCL12,CXCL2,CXCL3,FGF2,FGF7,HGF,IGF1,IGFBP4,KITLG,NGF,TGFB2,TGFB3,WISP1,WNT2,WNT5A
Metastasis	ANGPTL2,Ccl2,CSF3,CXCL12,CXCL2,CXCL3,FGF2,HGF,IGF1,WISP1,WNT5A
Angiogenesis	ANGPT1,ANGPTL2,Ccl2,CSF3,CXCL12,CXCL2,FGF2,HGF,IGF1,IGFBP4,KITLG,TGFB2
Vasculogenesis	ANGPT1,Ccl2,CSF3,CXCL12,CXCL2,FGF2,HGF,IGF1,IGFBP4,KITLG,TGFB2
Necrosis	ANGPT1,Ccl2,CSF3,CXCL12,CXCL3,FGF2,HGF,IGF1,IGFBP4,KITLG,NGF,TGFB2,TGFB3,WISP1,WNT5A
Lymphangiogenesis	ANGPT1,ANGPTL2,CXCL12,FGF2,HGF,IGF1
Cancer	ANGPT1,ANGPTL2,Ccl2,CSF3,CXCL12,CXCL2,CXCL3,FGF2,HGF,IGF1,KITLG,WISP1,WNT5A
Proliferation of tumor cell lines	CSF3,CXCL12,FGF2,HGF,IGF1,IGFBP4,KITLG,TGFB2,WISP1
ESC functions	
Function	**Genes**
Development of body trunk	BMP4,BMP7,FGF1,FGF19,FGF8,IGFBP2,LEFTY1,NODAL,SFRP1,WNT6
Specification of body axis	BMP4,FGF8,LEFTY1,NODAL,WNT3
Specification of rostrocaudal axis	BMP4,LEFTY1,NODAL,WNT3
Morphogenesis of embryo	BMP4,BMP7,FGF8,NODAL,WNT3,WNT6
Formation of mesoderm	BMP4,BMP7,NODAL,WNT3
Morphogenesis of embryonic tissue	BMP4,BMP7,FGF8,NODAL,WNT6
Formation of embryonic tissue	BMP4,BMP7,FGF8,NODAL,SFRP1,WNT3
Development of abdomen	BMP4,BMP7,FGF8,IGFBP2,NODAL,SFRP1,WNT6
Morphology of primitive node	BMP4,FGF8,WNT3
Cardiogenesis	BMP4,BMP7,FGF19,FGF8,LEFTY1,NODAL

Table 5.5. Top related functions and diseases for MSCs vs. ESCs

MSC functions	
Function	**Genes**
Migration of cells	ANGPT1,ANGPTL2,BMP2,Ccl2,CXCL12,CXCL2,CXCL3,FGF2,FGF7,HGF,IGF1,NGF,WISP1,WNT4,WNT5A
Development of cardiovascular system	ANGPT1,ANGPTL2,BMP2,Ccl2,CXCL12,CXCL2,CXCL3,FGF2,HGF,IGF1,TGFB2,WNT4,WNT5A
Metastasis	ANGPTL2,Ccl2,CXCL12,CXCL2,CXCL3,FGF2,HGF,IGF1,WISP1,WNT5A
Quantity of neurons	BMP2,CXCL12,FGF2,FGF7,GDF11,IGF1,NGF,TGFB2,WNT4,WNT5A
Development of body trunk	ANGPT1,BMP2,CXCL12,CXCL3,FGF2,FGF7,GDF11,HGF,IGF1,TGFB2,TGFB3,WNT4,WNT5A
Proliferation of cells	ANGPT1,BMP2,Ccl2,CXCL12,CXCL2,CXCL3,FGF2,FGF7,GDF11,HGF,IGF1,NGF,TGFB2,TGFB3,WISP1,WNT5A
Lymphangiogenesis	ANGPT1,ANGPTL2,CXCL12,FGF2,HGF,IGF1
Morphogenesis of embryonic tissue	BMP2,FGF7,GDF11,TGFB2,TGFB3,WNT4,WNT5A
Organismal death	ANGPT1,BMP2,Ccl2,CXCL12,CXCL2,CXCL3,FGF2,FGF7,GDF11,HGF,IGF1,NGF,TGFB2,TGFB3,WNT4,WNT5A
Differentiation of stromal cell lines	BMP2,CXCL12,IGF1,WNT5A
ESC functions	
Function	**Genes**
Proliferation of cells	BMP6,BMP7,Bmp8b,FGF10,FGF17,FGF18,FGF19,FGF3,FGF4,IGFBP2,IGFBP5,LEFTY1,NODAL,SFRP1,TGFA,WNT7A
Development of genitourinary system	BMP6,BMP7,Bmp8b,FGF10,FGF3,IGFBP2,IGFBP5,NODAL,SFRP1,TGFA,WNT7A
Development of reproductive system	BMP6,BMP7,Bmp8b,FGF10,FGF3,IGFBP5,NODAL,SFRP1,TGFA,WNT7A
Development of body trunk	BMP6,BMP7,FGF10,FGF18,FGF19,FGF3,IGFBP2,LEFTY1,NODAL,SFRP1,WNT7A
Development of body axis	BMP6,BMP7,FGF10,FGF13,FGF3,FGF4,LEFTY1,NODAL,SFRP1,TGFA,WNT7A
Morphogenesis of gastrointestinal tract	BMP7,Bmp8b,FGF10,FGF4,NODAL,WNT7A
Cell movement	BMP6,Cxcl11,FGF10,FGF19,FGF3,IGFBP5,LEFTY1,NODAL,SFRP1,TGFA,WNT7A
Morphogenesis of embryo	BMP7,Bmp8b,FGF10,FGF4,NODAL,WNT7A
Differentiation of cells	BMP6,BMP7,Bmp8b,FGF10,FGF18,FGF4,FGF5,IGFBP5,NODAL,SFRP1,TGFA,WNT7A
Midline	BMP7,FGF10,FGF19,LEFTY1,NODAL,TGFA

Looking broadly, 17% of the molecules (13 genes) were consistently downregulated when compared to day 0, while ~27% (20 genes) were consistently upregulated in comparison to day 0 **(Figure 5.8a)**. The remaining ~53% of the genes were either relatively unchanged from day 0 (~13%, 10 genes) or differentially expressed between days 4 and 7 (~40%, 30 genes). To visualize the differences in expression between day 4 and day 7 of differentiation, volcano plots were constructed in which the $\log_2$ fold difference relative to day 4 was plotted with the corresponding p-value describing the statistical significance of the difference in gene expression **(Figure 5.8b)**. In comparison to the 1000+ fold changes observed when comparing different cell types, modest changes in gene expression (<10-fold) were observed between the two stages of differentiation **(Figure 5.8c)**. In general, genes involved in developmental processes, including several members of the fibroblast growth factor (FGF) family as well as leukemia inhibitory factor (LIF), Nodal, and Lefty1, were more highly expressed in the early stage of differentiation, while genes involved in slightly later developmental and cell processes, such as other members of the transforming growth factor-β and bone morphogenetic protein (TGF-β/BMP) family, were expressed more highly in the later stage, mesoderm-primed cells.

Culture of the early differentiating ESCs under static or perfusion conditions also led to subtle changes in gene expression, with cells from the two culture platforms clustering separately from one another. Relative to the undifferentiated cells collected at day 0, ~16% of the molecules (11 genes) were consistently downregulated when compared to day 0, while ~42% (28 genes) were consistently upregulated when compared to undifferentiated cells **(Figure 5.9a)**. Approximately 34% of the molecules (23 genes) were differentially regulated between static and perfusion culture, though the differences were

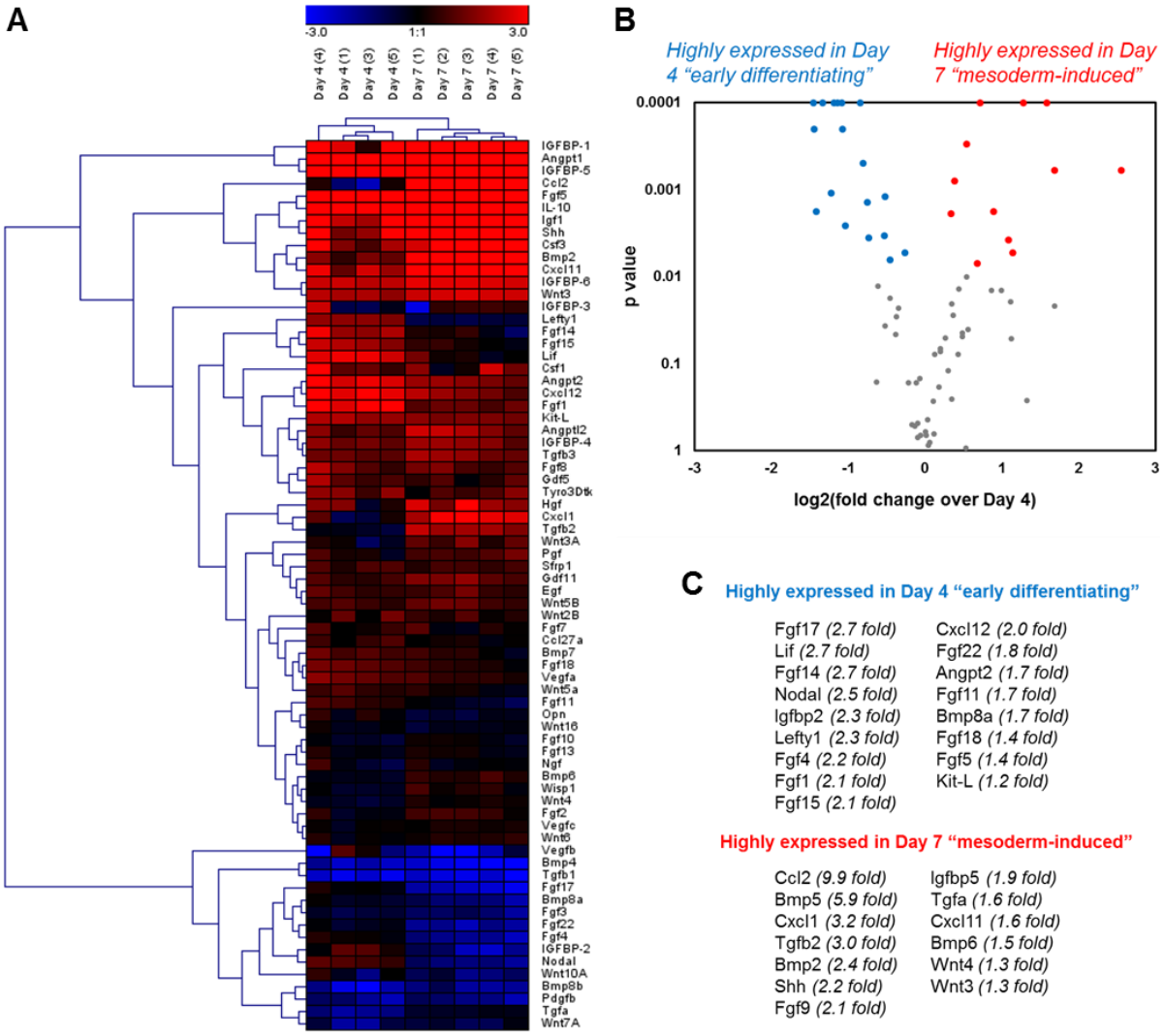

Figure 5.8. Gene expression profiles of ESCs at different stages of differentiation. Using the PCR array designed and analyzed using the Fluidigm platform, the expression profile of early-differentiating ESCs collected at day 4 can be compared to mesoderm-induced ESCs collected at day 7. A heatmap organized via two-dimensional hierarchical clustering using Genesis software with red indicating increased expression over undifferentiated ESCs and blue signifying decreased expression compared with undifferentiated ESCs **(A)**. A volcano plot indicating the log2 fold difference relative to day 4 is plotted with the corresponding p-value describing the statistical significance of the difference in gene expression **(B)**, and the highlighted genes were are statistically significant ($p < 0.01$) are listed along with the fold change **(C)**.

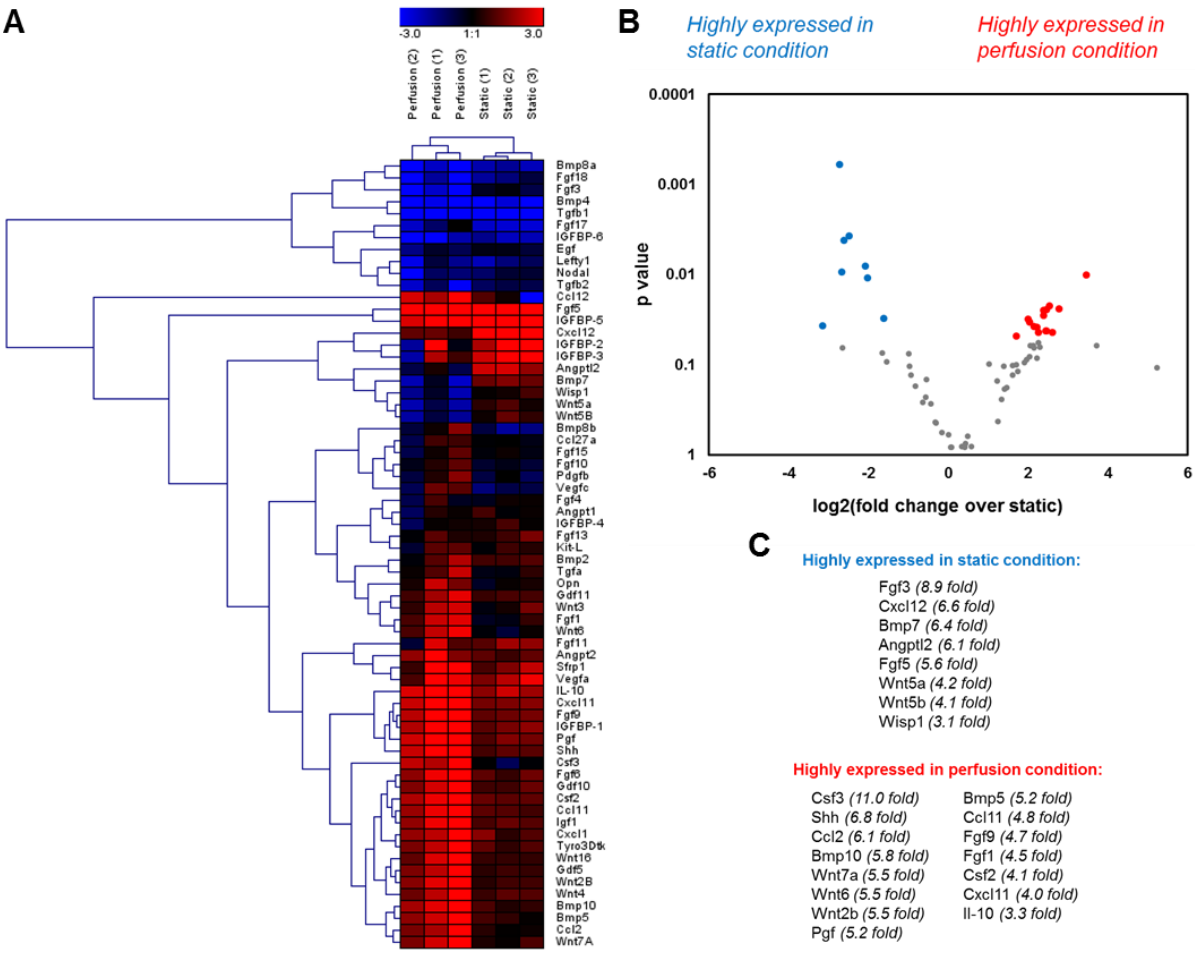

Figure 5.9. Gene expression profiles of ESCs cultured under static and perfusion conditions. Using the PCR array designed and analyzed using the Fluidigm platform, the expression profile of early-differentiating ESCs collected at day 4 cultured under either static or perfusion conditions can be compared. A heatmap organized via two-dimensional hierarchical clustering using Genesis software with red indicating increased expression over undifferentiated ESCs and blue signifying decreased expression compared with undifferentiated ESCs **(A)**. A volcano plot indicating the log2 fold difference relative to static culture is plotted with the corresponding p-value describing the statistical significance of the difference in gene expression **(B)**, and the highlighted genes were are statistically significant ($p < 0.05$) are listed along with the fold change **(C)**.

once again subtle in comparison to those observed between cell types **(Figure 5.9b-c)**. A striking difference at the global level was the general increase in gene expression observed in cells cultured under perfusion, with an overall average fold-increase of 3.3 ± 0.6 across all genes (median increase of 2.5-fold change), suggesting that the culture under perfusion may be affecting protein expression at the level of transcriptional regulation.

5.4 Discussion

The results of this study identify a profile of unique morphogens, cytokines, and growth factors that are expressed by pluripotent stem cells and that can be modulated by various parameters, including environmental conditions, bioreactor platform, or differentiation stage of the cells. Through a combination of proteomic and gene expression analysis, a total of 170 different species (96 via cytokine arrays, 95 via gene expression, 21 via both protein and gene expression) were examined in order to identify molecules of particular interest and to attain a global perspective on the dynamics of expression. Overall, the results of this study demonstrate that pluripotent stem cells are unique in their expression profiles of morphogens, cytokines, and growth factors in comparison with other cell populations frequently used for their paracrine activity and that the expression profile can be modulated by altering the environmental and culture parameters.

To determine if modulating the external environment of encapsulated ESCs led to changes in the expression of growth factors, cells were cultured in combinations of normoxic (21%) and hypoxic (3%) oxygen levels, with or without the mesoderm-stimulating molecule BMP-4, and in alginate with a high (High G) or low (High M) percentage of guluronic acid residues **(Figure 5.1)**. Intriguingly, cells cultured within the High G alginate had similar gene expression profiles regardless of oxygen tension or the

presence of BMP-4, with no significant differences in expression observed for any of the six genes evaluated **(Figure 5.2)**. This finding may indicate that signals provided through culture in the stiff High G alginate essentially override the other external signals, signifying that culture in High G alginate may provide a defined culture environment that is less susceptible to variation in environmental parameters. In contrast, cells cultured in the High M alginate had varied gene expression depending on all environmental cues, though most individual genes were only affected by 1-2 of the parameters. Increased expression of *Vegf* with culture in low-oxygen conditions **(Figure 5.2b)** is consistent with its established role as a hypoxia-induced growth factor [240], though increased expression of *Igf2* was not observed **(Figure 5.2d)**, indicating that some of the other culture parameters may have predominated the response. Indeed, the addition of BMP-4 to the culture media led to significant increases in *Igf2* **(Figure 5.2d)** and *Bmp4* **(Figure 5.2f)** expression, which is consistent with previous reports [248], and a significant decrease in *Fgf2* expression **(Figure 5.2e)**. Culture within High M alginate led to decreased expression of three growth factors (*Igf1*, *Igf2*, and *Bmp4*) and increased expression of *Fgf2*, though the differences between alginate compositions were typically observed in tandem with one to two other culture parameter combinations and not all four of the possible combinations, indicating that the influence of other environmental parameters were often the dominant signal.

A wider screen of proteins present in the ESC conditioned media was performed using commercially available antibody arrays for 96 species, mostly consisting of cytokines and chemokines in addition to some growth factors. For an initial screen, perfusate collected from ESCs encapsulated in High G alginate and cultured under perfusion was found to contain many species which are implicated in the regulation of bone

marrow populations **(Figure 5.3)**. Though some indication of relative abundance can be drawn from the intensity of each dot blot on the array, it is important to note that they provide semi-quantitative results, and thus a higher intensity of one protein does not necessarily indicate that it is present in higher abundance than a protein of lower intensity, particularly because detection of different proteins via antibody methods should ideally be optimized for each species and thus is a general caveat for all protein arrays at present [249]. Therefore, greater quantitative information is gained when comparing the same protein species across multiple samples obtained from different conditions. Consequently, the profile of proteins present in ESC conditioned media was compared between stages of ESC differentiation and the type of culture platform (static vs. perfusion) employed **(Figure 5.4)**.

A global increase in protein expression was observed in the day 7 mesoderm-induced condition in comparison to the day 4 early differentiating condition, likely due to the increase in cell number; however, several proteins of interest were identified as markedly upregulated with differentiation, including proteins involved in mesoderm-related processes such as SDF-1α, VEGF-A, and MMP-2, while others were relatively decreased in the day 7 condition, including proteins involved in early stage development and general mitogenesis, such as IGF-1, IGF-2, and several of the IGFBPs **(Figure 5.5)**. A similar signature of molecules was found at the gene expression level through designing and analyzing results from a custom 96-gene Fluidigm PCR array **(Figure 5.8)**. Similar to previously published results with differentiating mouse embryonic stem cells, comparable declines (*Fgf17*, *Nodal*, *Lefty1*, *Fgf4*, *Fgf1*, *Fgf15*, *Fgf22*, *Bmp8a*, and *Fgf18*) and increases (*Bmp5*, *Tgf-β2*, *Bmp2*, *Tgf-α*) of specific molecules over time of differentiation were

observed [236]. Reported differences in the secretome of undifferentiated human embryonic stem cells (hESCs) in comparison to hESCs which had been spontaneously differentiated for 6-8 days exhibited some similarities (*Fgf15/19*, *Igfbp2*, *Fgf4*) and some disparities (*Bmp6*) from the work presented here, which is likely attributed to differences in species or in the differentiation protocol used [250]. The shift in secretion and gene expression profile with differentiation stage indicates that secretion is dynamically regulated during ESC differentiation, as would be expected with the cells undergoing morphogenic and phenotypic changes, and that modulation of the differentiation state can be used to control the relative abundance of certain secreted proteins. For example, the secretion of IGF-2 and VEGF are reported to increase with the differentiation of ESCs as embryoid bodies [181].

Subjecting encapsulated ESC aggregates to perfusion culture led to a global increase of almost every protein detected by the antibody arrays when compared to static cultures **(Figure 5.6)**, in spite of the observation that fewer cells were present in the perfusion reactors than were present in the static plates **(Figure 5.6c)**. There are several potential explanations to elucidate the observed increase in protein concentration. At the cellular level, gene expression or the rate of packaging and secreting proteins out of the cell may be increased, either due to changes in cell phenotype, cell proliferation (depending if the proteins secreted are growth-associated or are produced independent of cell growth), or the absence/presence of feedback inhibition. The gene expression data obtained with the Fluidigm PCR array also reflects a global increase in expression for cells cultured under perfusion **(Figure 5.9)**, suggesting that the culture platform may be affecting protein expression at the level of transcriptional regulation. Though several molecules were more

highly expressed in static culture, perfusion culture led to an overall average fold-increase of 3.3 ± 0.6 across all genes (median of 2.5 fold-increase) and an average fold-increase of 4.7 ± 0.8 the subset of genes increased with perfusion culture (median of 4.0 fold-increase).

In order to establish the unique proteins expressed by ESCs in comparison to other cell types frequently employed for their paracrine actions, the expression profiles of undifferentiated ESCs were compared to mouse embryonic fibroblasts (mEFs) and mesenchymal stem cells (MSCs). Mouse embryonic fibroblasts were examined because they are traditionally used as feeder layers for embryonic stem cell culture due to their secretion of factors and extracellular matrix which maintain the pluripotent state. In addition, MSCs have been investigated for a number of clinical applications based on their paracrine secretion of pro-angiogenic and immunomodulatory cytokines [191,192]. Several protein species identified were uniquely expressed in high levels by ESCs, including insulin-like growth factor binding protein-2 (*Igfbp2*) and several members of the fibroblast growth factor family (particularly *Fgf3*, *Fgf4*, *Fgf15*, and *Fgf 17*) **(Figure 5.7, Tables 5.4-5.5)**. The protein IGFBP-2, which is generally expressed during development, is involved in modulating the activity of the IGFs and also acts independently through multiple receptors to regulate cell survival, proliferation, movement, and differentiation of many different cell types [251]. In the context of the bone marrow microenvironment, IGFBP-2 has been previously used in the *ex vivo* expansion of mouse and human hematopoietic stem cells (HSCs) in combination with angiopoietin-like proteins (Angptls) [252,253]. *In vivo*, IGFBP-2 is reported to act independently of IGF receptors and promote HSC repopulation in a non-cell autonomous manner, indicating that cells of the bone marrow niche, particularly stromal cell populations, provide the IGFBP-2 required for HSC

function [251]. The high expression level of FGF-4 was anticipated given its key developmental role as the first member of the FGF family to be expressed, though its function is not solely limited to embryogenesis [222,254]. In fact, FGF4 also play key roles in regulating bone marrow function through promoting the *ex vivo* expansion of bone marrow mesenchymal stem cells [255–257]. The distinct ability of pluripotent stem cells to produce key proteins, like IGFBP-2 and FGF-4, indicates that ESCs may be a novel source of important paracrine factors to promote exogenous cell function.

Though a large number of proteins were examined in this study with the use of antibody and gene expression arrays, a larger-scale proteomics approach would offer additional insight through recognition of unknown species of interest. Typical shotgun-based proteomics using mass spectrometry offer a number of advantages, including the lack of bias inherent with target-based approaches. However, mass spectrometry suffers from a number of technical shortcomings, including extensive sample preparation which can lead to degradation of certain classes of proteins, a limited ability for quantitation, a difficulty identifying proteins present in low abundance, and significant rates of false positive and false negatives during protein identification [249,258,259]. Even with advancement in technologies to identify and quantify individual proteins in complex mixtures, effort will still be required to standardize upstream culture protocols and sample preparation such that studies across different platforms can be directly compared [191]. Ultimately, employing unbiased proteomic approaches may reveal additional unique species produced by pluripotent stem cells and be useful to inform potential downstream applications.

5.5 Conclusions

Overall, the results of this study demonstrate that pluripotent stem cells feature expression profiles of morphogens, cytokines, and growth factors that are distinctive from other cell populations frequently used for their paracrine activity. The expression profile changes with differentiation stage of the ESCs, with proteins involved in early developmental process and general mitogenesis expressed more highly in early stages of differentiation, whereas proteins involved in tissue specification and cell migration were expressed at higher levels at later stages of differentiation. Additionally, by exercising control over the cell microenvironment through the type of alginate used for encapsulation, exposure to different oxygen tensions or to mesoderm-promoting BMP-4, and culture of the cells under perfusion, diverging expression profiles can be attained both at the single species and the global level. Specifically, culture in alginate with a higher ratio of guluronic acid appears to override the effects of stimuli provided by oxygen level or the presence of BMP-4. In addition, culture of the encapsulated cells in a perfusion bioreactor globally increases both gene expression and secreted protein concentration. Taken as a whole, this study provides new characterization of the morphogenic species expressed by pluripotent stem cells and how the expression profile of ESCs can be regulated via systematic control over culture parameters.

CHAPTER 6

INFLUENCE OF STEM CELL-DERIVED MORPHOGENS ON ADULT STEM AND PROGENITOR CELL POPULATIONS

6.1 Introduction

The concept of a stem cell "niche" was first introduced in the late 1970s [78] to describe an anatomical location which provides signals to resident stem cells to regulate their potency as well as their functional properties [79–81]. The signals that constitute the niche come in the form of secreted molecules, extracellular matrix interactions, and cell-cell interactions, and the recreation of the native stem cell niche has been an active approach in tissue engineering as a means to control cell behavior [260]. While the "niche" of the *in vivo* equivalent of embryonic stem cells is transient, multipotent and unipotent adult stem cell populations, including those which replenish the blood, skin, intestinal epithelium, muscle, and nervous system [79–81], are well established and are maintained throughout life. Each niche typically contains a resident stem cell population, progenitor cells derived from the stem cells, and supporting cells that produce signals required for the resident stem cell to remain quiescent, self-renew, or differentiate, as is appropriate.

Hematopoietic stem cells (HSCs) give rise to all blood and immune cells and are responsible for continually replenishing these cell populations for functions ranging from oxygen transport throughout the body to adaptive immune responses. Though the mature cells derived from HSCs through the process of hematopoiesis are found throughout circulation in the body, adult HSCs reside primarily in the bone marrow cavity. The bone marrow niche exists as a semi-solid matrix consisting of various collagens, proteoglycans,

glycosaminoglycans, and calcium minerals to house the resident HSCs [10,11,84,85]. Many other cell types also reside within the bone marrow niche, including mesenchymal stem/stromal cells (MSCs), endothelial progenitor cells, osteoblasts, reticular cells, adipocytes, and nerve cells. High levels of regulatory cytokines (e.g. SDF-1, SCF, interleukins, TPO) are present within the niche in addition to ligands of the Notch and Wnt signaling pathways [82,84,87–89]. Because the bone marrow niche is a vital regulator of HSC function, aberrant function of cells within the niche can lead to abnormal HSC behavior (e.g. deficient differentiation toward one or all hematopoietic cell types), as has been observed in the case of aging [261] and certain pathological disorders [262–264]. For example, a mutation in the gene encoding stem cell factor (SCF; also known as Kit-ligand) that results in a lack of membrane-bound SCF but maintains soluble SCF secretion leads to mice that are incapable of sustaining HSC populations [265–267], indicating that even the manner in which signals are physically presented can be vitally important to the resulting stem cell behavior.

In contrast to the billions of blood and immune cells produced every day from HSCs, muscle satellite cells tend to remain relatively quiescent until called upon to respond to an injury. When skeletal muscle is damaged, a well-orchestrated process occurs in which the wounded muscle fibers undergo necrosis, stimulating an inflammatory response, and resident satellite stem cells are activated to proliferate and differentiate into a large number of myoblast cells [91]. The myoblasts subsequently differentiate and undergo fusion to form the mature muscle fibers necessary to replenish the injured tissue [268]. When Pax7+ satellite cells are ablated from mice, skeletal muscle is no longer able to regenerate following injury [269–271], and transplantation of single myofibers with their associated

satellite cells are able to regenerate damaged tissue following transplantation into radiation-ablated muscles [268]. Similar to HSCs and other adult stem cell populations, satellite cells do not act autonomously and require support from their niche in the form of structural and biochemical signals. Many soluble cues, including Wnts, FGFs, IGFs, HGF, EGFs, SDF-1α, and Notch ligand, are exchanged between satellite cells and the surrounding myofibers, interstitial cells, and endothelial cells, and the identities and concentrations of the paracrine factors are responsible for maintaining quiescence, prompting self-renewal, and instigating differentiation [92–97]. The processes regulating satellite cell behavior can become dysregulated when aspects of the niche are altered, as is observed with the increased sarcopenia and decreased regenerative capacity in aged organisms when the paracrine factors secreted by cells of the interstitium, vasculature, and immune system are altered [272].

While the self-renewal capacities of adult stem cell populations *in vivo* are well-documented, similar success has not been achieved in attempts to expand the cell populations *ex vivo*. Despite decades of research, a striking contradiction persists in hematopoietic stem cell biology in that a single HSC transplanted *in vivo* can expand exponentially and eventually repopulate an entire animal, whereas HSCs cultured *ex vivo* exhibit extremely limited expansion potential and rapidly lose the capacity for self-renewal. The current standard for maintenance of HSCs *ex vivo* relies upon a cytokine cocktail consisting of three to four factors, often some combination of stem cell factor (SCF), Flt3 ligand (Flt3L), interleukin-11 (IL-11), and thrombopoietin (TPO). However, most attempts at expansion have had limited success [116–118], as HSCs must be expanded quickly or risk losing their proliferative and blood lineage potential. Due to

insufficient and unreliable HSC expansion with traditional cytokines (SCF, TPO, interleukins, Flt3), new emphasis is being placed on the use of developmental factors, such as Wnt proteins, Notch ligand, bone morphogenetic proteins (BMPs), and fibroblast growth factors (FGFs) as potential mediators of expansion [117,120,127,128]. Similar challenges with *ex vivo* expansion are observed with primary muscle populations, with a decreased capacity for re-engraftment and regeneration observed in satellite cell-derived myoblasts following expansion *ex vivo* [129–132]. Current strategies to expand mouse myoblasts cultured *in vitro* include the presentation of Notch-ligand [133] and the use of hydrogel culture substrates with a low elastic modulus that better mimics the native physiological environment [134], while recent advances in expanding human muscle stem cells have been achieved through inhibition of p38 MAPK [135]. Though the development of novel approaches has improved the expansion of multipotent stem cell populations, there is still significant room for improvement in order to achieve the cell numbers required for therapeutic transplantation.

Due to the limitations of current methodologies to expand adult stem cell populations while maintaining their functional capacity, an increasing emphasis is being placed on the use of developmental factors, such as Wnt proteins, Notch ligand, bone morphogenetic proteins (BMPs), and fibroblast growth factors (FGFs) [117,120,127,128]. Thus, exposing bone marrow and muscle cell populations to developmentally-relevant factors durin *ex vivo* culture could improve the expansion efficiency and function of these cells upon transplantation. Cells of the early embryo, the *in vivo* analog of ESCs, provide morphogenic signals during embryogenesis that stimulate histogenesis of neighboring cells through paracrine actions and also stimulate their own differentiation through autocrine

signals. By secreting growth factors, cytokines, and mitogens, ESCs create a potent microenvironment that stimulates morphogenic events leading to tissue and organ formation [219,220]. When cultured in vitro, ESCs secrete a similar array of morphogenic factors—including Wnts, bone morphogenetic proteins (BMPs), fibroblast growth factors (FGFs), and vascular endothelial growth factor (VEGF)—that stimulate the proliferation and differentiation of several cell types, as profiled in Chapter 5 [32,181]. Injection of ESCs into embryos with multiple cardiac defects has improved the embryonic cardiac phenotype, a finding attributed to secretion of insulin-like growth factor 1 (IGF-1) and Wnt5a [30]. ESC transplantation has also reduced myocardial dysfunction in a rat model of surgically induced global ischemia, presumably by increasing the secretion of VEGF and interleukin-10 [31]. Additionally, ESC co-culture has been used to expand cardiomyocytes, corneal epithelial cells, and fibroblasts *in vitro* [32–34,181,273], in all cases improving cell proliferation and function. Conditioned medium from ESCs increases the proliferation of aged satellite cells and myoblasts while inhibiting differentiation [35,250,274], and also increases the survival of hematopoietic progenitors [36]. Aside from stem cell–derived factors, systemic molecules originating from younger mice improve function in aged mice connected via parabiosis, including enhanced wound healing [37,38], improvement in muscle satellite cell function [39–41], rejuvenation of neural cells and cognitive function [42–45], and reversal of cardiac hypertrophy [46]. Therefore, the paracrine actions of trophic factors derived from pluripotent cells may provide analogous signals that enable adult stem cells to regain a more "youthful" proliferative or regenerative capability.

In order to establish the impact of ESC secreted factors on adult stem cell populations *ex vivo*, three different cell populations were studied in both co-culture and

conditioned media configurations. Cultures of bone marrow-derived mesenchymal stem cells (MSCs) were examined in addition to more heterogeneous primary cells isolated from murine bone marrow and skeletal muscle. In addition to assessing the mitogenic effects of pluripotent cell-derived factors on cell proliferation, the differentiation capacity of the adult stem and progenitor cell populations was also evaluated to discern the consequence on cell function following exposure to the unique soluble milieu. Conditioned media collected from ESCs at different stages of differentiation and ESCs cultured under different environmental settings were also directly compared to determine the impact of a shifting composition of paracrine factors. Overall, this study revealed the impact of the unique developmental morphogens produced by pluripotent stem cells on maintaining and expanding adult stem cell populations.

6.2 Materials and methods

6.2.1 Embryonic stem cell culture

Murine ESCs (D3 cell line) were cultured on tissue culture treated polystyrene dishes (Corning) adsorbed with 0.1% gelatin (EmbryoMax). Undifferentiated ESC culture media consisted of Dulbecco's modified Eagle's medium (DMEM) (Mediatech) supplemented with 15% fetal bovine serum (Hyclone), 100 U/mL penicillin, 100 μg/mL streptomycin, and 0.25 μg/mL amphotericin (Mediatech), 2 mM L-glutamine (Mediatech), 1x MEM non-essential amino acid solution (Mediatech), 0.1 mM 2-mercaptoethanol (Fisher Scientific), and 10^3 U/mL of leukemia inhibitory factor (LIF) (ESGRO). Cultures were replenished with fresh media every other day and passaged prior to reaching 70% confluence.

6.2.2 ESC aggregate formation

A single cell suspension of undifferentiated ESCs was obtained through dissociation of monolayer cultures with 0.05% trypsin-EDTA (Mediatech). Defined, serum-free KO N2B27 media (*note*: formulation is slightly different than what was used in Chapter 3) was used for all aggregate cultures and consisted of Knock-Out (KO) DMEM (Life Technologies) supplemented with N2 (Gibco), B27 (Gibco), 100 U/mL penicillin, 100 μg/mL streptomycin, and 0.25 μg/mL amphotericin (Mediatech), 2 mM L-glutamine (Mediatech), 1x MEM non-essential amino acid solution (Mediatech), and 0.1 mM 2-mercaptoethanol (Fisher Scientific). Aggregation of ESCs was achieved by centrifugation (200 rcf) of ESCs into 400 μm square polydimethylsiloxane (PDMS) micro-wells (Aggrewell^{TM}, Stem Cell Technologies) as previously reported [19,152]. The cell seeding density yielded approximately 500 cells per individual well. The ESCs were incubated in the wells for approximately 24 hours in serum-free KO N2B27 culture media to allow for aggregate formation.

6.2.3 Cell microencapsulation

Two different medium viscosity alginates were used: ultrapure MVG (Pronova) which contains greater than 60% G residues (High G) and ultrapure MVM (Pronova) which contains greater than 50% M residues (High M). Alginate solutions were prepared at 1.5 wt% in calcium-free DMEM (Gibco) and autoclaved for sterilization no more than one day before use. An electrostatic bead generator (Nisco) was utilized for encapsulation. Pre-formed ESC aggregates were resuspended in alginate at a density of 12,000 aggregates per mL of alginate, and the cell-containing alginate solution was extruded through a 400 μm nozzle using a syringe pump at a flow rate of 6 mL/hour and a voltage of 10 kV to drop the

beads into a stirred hardening bath of 100 mM calcium chloride (EMD). The beads were washed three times with serum-free media prior to downstream culture. A thin PLL-coating was used to prevent aggregate escape for the collection of conditioned media over seven days. The beads were coated with 0.05% PLL (MW 15,000-30,000; Sigma) for 2 minutes prior to three additional media rinses.

6.2.4 Microencapsulated cell culture and differentiation

Microencapsulated ESC aggregates were generally cultured statically in sterile 100 x 15 mm bacteriological grade polystyrene Petri dishes (BD) in 10 mL serum-free KO N2B27 media (see 6.2.2) at an initial cell density of 3 x 10^5 cells/mL media. A 90% media exchange was performed every three days. Cells were cultured in humidified incubators under either normoxic (21% oxygen, 5% carbon dioxide) or hypoxic (3% oxygen, 5% carbon dioxide) conditions. Cells cultured under perfusion were placed in a custom packed bed perfusion reactor (3 x 10^6 cells/reactor) and received serum-free KO N2B27 media at a rate of 150 µL/hr (see Chapter 4).

6.2.5 Mesenchymal stem cell culture

Murine bone marrow-derived mesenchymal stem cells (MSCs, isolated from C57Bl/6J mice) were obtained from the Texas A&M College of Medicine Institute for Regenerative Medicine The cryopreserved MSCs were thawed and plated onto a 15-cm tissue culture dish in 20 mL MSC complete expansion medium (CEM) which consists of Iscove's Modified Dulbecco's Medium; Invitrogen/GIBCO) supplemented with 10% fetal bovine serum (FBS; Hyclone, Logan, UT), 10% horse serum (Hyclone), 2 mM L-glutamine (Invitrogen/GIBCO), 100U/mL penicillin, 100 µg/mL streptomycin and 0.25 µg/mL amphotericin B (Invitrogen/ GIBCO). Following overnight incubation at 37°C,

adherent MSCs were washed with phosphate-buffered saline (PBS, Invitrogen/GIBCO) and detached from the tissue culture plate using 0.25% trypsin and 1 mM EDTA (Invitrogen/GIBCO). Cells were plated onto 15-cm tissue culture dishes, at a density of 50 cells/cm^2 in 20 mL CEM per dish. Cells were fed every 3–4 days with 20 mL of fresh CEM and maintained until they reached ~70% confluence. For co-culture studies with ESCs, 1900 MSCs (density of 500 cells/cm^3) were seeded into the bottom of tissue cultured treated 12 well plates (Corning) with 190,000 or 57,000 encapsulated ESCs (ratio of 100:1 and 30:1 ESC:MSC) placed in the upper portion of a transwell insert, and the media consisted of KO N2B27. For the conditioned media studies, 475 MSCs (density of 500 cells/cm^3) were seeded into the bottom of a 48 well plate (Corning) and cultured with 800 µL of growth media, 600 µL KO N2B27 with 200 µL growth media, or 600 µL ESC conditioned media with 200 µL growth media.

6.2.6 Murine bone marrow isolation and culture

Bone marrow (BM) was harvested from 8-12 week male mice (C57BL/6J or male C57BL/6 with eGFP constitutively expressed under the beta-actin promotor from Jackson Labs) by clipping the epiphysis of the femur and tibia followed by centrifugation at 1,000 rcf for 5 minutes. BM cells were resuspended in sterile PBS with 3% FBS at ~5 x 10^7 per mL. Lineage cocktail antibodies (BD Pharmingen #558074, CD3e, CD11b, B220, TER-119, Ly6G, Ly6C) were added to the resuspended BM, and cells were incubated on ice, protected from light for 30 minutes. Samples were washed with PBS, centrifuged at 500 rcf for 5 minutes at 4°C, and then resuspended in 3% FBS/PBS and sorted on a BD FACS ARIA II. Lineage negative (Lin-) cells were collected by FACS with gates established based on an unstained control BM sample. Lin- cells were seeded into tissue cultured

treated 24 well plates at a density of 50,000 cells/well in 1 mL of medium. The standard medium used for culture was MyeloCult (Stem Cell Technologies M5300), which contains a proprietary blend of Minimum Essential Media Alpha (αMEM) base media, horse serum, fetal bovine serum, 2-mercaptoethanol, and other supplements. The use of unconditioned KO N2B27 medium, ESC conditioned media, endothelial growth medium (EGM), and endothelial cell conditioned media were assessed, and co-cultures with encapsulated ESCs were performed using transwell inserts containing 300,000 ESCs. The cells were incubated in humidified incubators maintained at 33°C and 5% CO_2.

6.2.7 Endothelial cell culture

As a paracrine factor-secreting control cell population, murine yolk sac-derived endothelial cells (C166, ATCC CRL-2581) were cultured on tissue-cultured polystyrene dishes. The endothelial growth medium (EGM) was prepared by mixing 475 mL of Endothelial Basal Medium (cAP-03, Angioproteomie) and 25ml of Endothelial Growth supplement (cAP-04, Angioproteomie), which contains 5% fetal bovine serum, recombinant growth factors, and 1x penicillin and streptomycin. Endothelial cell cultures were replenished with fresh media every 2-3 days

6.2.8 Murine skeletal muscle isolation and culture

Muscle tissue was isolated from the hind limbs of 16-20 week male C57Bl/6J mice (Jackson Labs) and minced into ~1 mm pieces in PBS using scalpels. The minced tissue obtained from four limbs was placed in a 50 mL conical tube and incubated with 10 mL of 1.5 U/ml collagenase II (Life Technologies) and 2.5 U/ml dispase II (Stem Cell Technologies) in 2.5 mM $CaCl_2$ (Sigma) for 30 minutes on a shaker at 37°C, with trituration every 10 minutes. After 30 minutes of incubation, the slurry was diluted with

PBS not containing calcium and magnesium (Corning), and the supernatant was removed, centrifuged at 400 rcf for 5 minutes, and resuspended in PBS. A further 10 mL of the collagenase/dispase solution was added to the remaining slurry, and the 30 minute incubation was repeated. The resulting cell pellet from the supernatant of the second digestion was combined with the first and filtered through 100 µm and 70 µm cell strainers (BD) to remove any remaining large tissue pieces, following by centrifugation and resuspension of the pellet in growth media. The growth media consisted of Hams F10 basal media (Life Technologies) with 20% mL FBS (Hyclone), 100 U/mL penicillin (VWR), 100 µg/mL streptomycin (VWR), and 2.5 ng/mL basic fibroblast growth factor (Promega). The cell suspension was pre-plated on uncoated 100 mm tissue culture treated polystyrene dishes (Corning) for 30-60 minutes to preferentially adhere the fibroblast fraction, then the supernatant was subsequently transferred to tissue culture treated polystyrene dishes adsorbed with 0.1% gelatin (EmbryoMax) and cultured in growth media. A media exchange was performed two days post-isolation, and the cells were passaged approximately every four days afterward. When exposed to the different growth media, cells were seeded into 24 well plates adsorbed with 0.1% gelatin (EmbryoMax) and cultured in 1 mL growth media, 0.75 mL KO N2B27 with 0.25 mL growth media, or 0.75 mL ESC conditioned media (collected from day 1-4 of differentiation under perfusion conditions) with 0.25 mL growth media.

6.2.9 Cell number quantification

For the MSCs, the collected cells were centrifuged at 200 rcf for 5 minutes, rinsed 3x with PBS, and pelleted at 375 rcf for 4 minutes followed by supernatant removal and storage at -20°C. A CyQUANT Cell Proliferation Assay Kit (Molecular Probes Inc.,

Eugene, OR) was used to determine cell number, with a standard curve created using MSCs that were counted using a hemocytometer. The fluorescence (480 nm excitation, 520 nm emission) was read using a Synergy H4 plate reader (Biotek). For the bone marrow cultures derived from eGFP mice, the Cytation3 Cell Imaging Multi-Mode plate reader (BioTek) was used to determine the number of GFP+ cells one day post-seeding. Assessment of cell number at day 4 of culture was performed using a known concentration of AccuCheck counting beads (Invitrogen) during flow cytometry analysis (see section 6.2.12). For the primary muscle cultures, cell number was determined using image analysis (see section 6.2.15).

6.2.10 Quantitative real time PCR

Encapsulated aggregates were released from beads through 10 minute incubation with TrypLE^{TM} (Invitrogen), trituration, and 5 minute incubation with 55 mM sodium citrate (Sigma). The cells were centrifuged at 200 rcf and rinsed 3x with PBS to remove residual PLL. RNA was extracted from the aggregates with the RNeasy Mini kit (Qiagen Inc, Valencia, CA). The RNA (300 ng/sample) was converted to complementary DNA using the iScript cDNA synthesis kit (Bio-Rad, Hercules, CA) and analyzed using real time PCR (MyIQ cycler, Bio-Rad). Forward and reverse primers for *18s*, *Oct4*, *Nanog*, *Vegf*, *Igf1*, *Igf2*, *Fgf2*, *Bmp4*, and *Gdf11* were designed with NCBI's Primer-BLAST (sequences and conditions are given in **Table 6.1**) and purchased from Invitrogen. Gene expression were calculated with respect to undifferentiated ESC expression levels as previously described [168].

Table 6.1. Primer sequences for quantitative real time PCR

Gene	Forward sequence	Reverse sequence	Melt temperature (°C)
18s	CTCTAGTGATCCCTGAGAAGTTCC	ACTCGCTCCACCTCATCCTC	60.0
Nanog	GAAATCCCTTCCCTCGCCATC	CTCAGTAGCAG CCCTTGTAAGC	60.0
Oct4	CCGTGTGAGGTGGAGTCTGGAG	GCGATGTGAGTGATCTGCTGTAGG	60.0
Vegf	TGCACCCACGACAGAAGG	GCACACAGGACGGCTTGA	60.0
Igf1	TCCGCCAGGTTGCCTCTAG	GGAAGCAGGTGGATGGTCAG	60.0
Igf2	AGCTGACCTCATTTCCCGAT	AATGTGCGACGGGACAGAAC	60.0
Fgf2	AGCGACCCACACGTCAAACTAC	CAGCCGTCCATCTTCCTTCATA	60.0
Bmp4	GAGCCATTCCGTAGTGCCAT	ACGACCATCAGCATTCGGTT	60.0
Gdf11	GCACCCCTACCAAGATGTCC	CCACAACTTAGGAGCAGCCA	60.0

6.2.11 Conditioned media analysis

Spent media was collected from the co-cultures of MSCs and ESCs. The conditioned media was centrifuged at 3000 rcf for 5 minutes to remove cellular debris, and the supernatant was transferred to a new 15 mL conical tube for storage at -20°C. Enzyme-linked immunosorbent assay (ELISA) kits was used to quantify the amount of FGF-2 (Quantikine, R&D) and VEGF (DuoSet, R&D) present in the conditioned media. Concisely, capture antibody was adsorbed onto 96 well MaxiSorp Immunoplates (Nunc), blocked with 1% BSA in PBS, incubated with standards and samples, and bound with detection antibody. The concentration of protein was determined using a colorimetric reaction of peroxidase and tetramethylbenxidine and a plate reader to measure the absorbance at 450 nm. The absorbance values for the conditioned media samples were compared to a standard curve to determine the protein concentration.

6.2.12 Flow cytometry analysis of surface marker expression

Analysis of surface marker expression was performed by collecting the contents of each culture well via trypsinization, centrifugation (5 min at 200 rcf) and resuspension in

3% FBS/PBS. The cells were fixed with 4% paraformaldehyde for 20 minutes and resuspended in 3% FBS/PBS. Counting beads (AccuCheck counting beads; Invitrogen) and pre-conjugated antibodies (PerCP/Cy5.5 anti-mouse CD45, APC/Cy7 anti-mouse/human CD11b, PE anti-mouse/human CD45R/B220, PE/Cy7 anti-mouse CD3ε, FITC anti-mouse Ly-6G; all from BioLegend) were added, and cells were incubated on ice, protected from light for 30 minutes. Samples were washed with PBS, centrifuged at 500 rcf for 5 minutes at 4°C, and then resuspended in 3% FBS/PBS prior to analysis on a BD LSR II Flow Cytometer.

6.2.13 Analysis of cell proliferation using CFSE

Lineage negative cells were labeled with CFSE after sorting (prior to seeding with various media types) using the CellTrace CFSE Cell Proliferation Kit for flow cytometry (Molecular Probes). The CellTrace stock solution was mixed with DMSO immediately prior to use at a concentration of 5 mM. For staining, 2 µL of stock solution was added to cells in 1 mL PBS (10 µM final concentration). Cells were incubated for 20 minutes at 37°C in a cell culture incubator for 20 minutes. Cells were transferred to 5 mL Iscove's Modified Dulbecco's Medium (IMDM) with 2% FBS, incubated an additional 5 minutes, and pelleted by centrifugation (300 rcf for 5 min). Cells were resuspended in MyeloCult media and seeded in a 24 well plate at a density of 50,000 cells/well. The plate was centrifuged to bring cells to bottom of the plate and the media was removed and replaced with the appropriate test media. During flow cytometry analysis, the mean CFSE fluorescence intensity for each group was determined.

6.2.14 Colony-forming unit assays and quantitation

After 4 days of culture with each media type, cells from each condition were trypsinized, centrifuged (300 rcf for 5 min), and resuspended in IMDM with 2% FBS. MethoCult (Stem Cell Technologies) was added to each cell solution at a 1:10 ratio (IMDM:MethoCult) and mixed well. The MethoCult/cell mixture was drawn up into a sterile syringe fitted with a 16 gauge blunt-end needle (BD) and dispensed into two 35 mm dishes. A third 35 mm dish was filled with PBS, and the three dishes were placed in a larger 100 mm dish to create a humidified environment. The cells were incubated at 37°C in 5% CO_2 with ≥ 95% humidity for 12 days and then imaged for analysis using a Zeiss LSM710 confocal microscope outfitted with an automated stage. The number of colonies present in each dish was manually counted from the obtained tiled images.

6.2.15 Immunostaining and fluorescent imaging

Primary muscle cultures which had been exposed to ESC conditioned media (or growth media and KO N2B27 controls) were rinsed with PBS, fixed in 4% paraformaldehyde for 15 minutes with rotation at room temperature, and rinsed 3x with PBS. The fixed cells were blocked and permeabilized for 60 minutes at room temperature in PBS containing 5% normal donkey serum (Jackson) and 0.3% Triton X-100 (Sigma). The cells were then incubated with a primary antibody against desmin (ThermoFisher, RB-9014-1p; rabbit polyclonal; 1:200) diluted in a solution of PBS with 1% BSA (Millipore) and 0.3% Triton X-100 (Sigma) for 60 minutes at room temperature. The cells were washed 3x with PBS and incubated with secondary antibody (Life Technologies; 1:1000 Alexa Fluor 555 donkey anti-rabbit) and Hoechst (Life Technologies; 1:10,000) for 90 minutes at room temperature prior to 3x washes in PBS and imaging on a Zeiss Axio Observer equipped with a Hamamatsu camera. Image analysis was performed using ImageJ software

(http://imagej.nih.gov/ij/). To discern the nuclei, images from the Hoechst channel were converted to 8-bit, thresholded, and inverted, followed by analysis of the number of particles 10-500 pixels^2. To count the desmin-positive cells, images from the red channel were converted to 8-bit, thresholded, and inverted, followed by analysis of the number of particles of 50-1000 pixels^2 with a circularity >0.7 for the "rounded" cells and particles of 200-2000 pixels^2 with a circularity <0.7 for the "elongated" cells.

6.2.16 Statistics

All experiments were performed with replicate samples from independent conditions, with the exception of some of the flow cytometry analysis of the bone marrow populations due to limited cell number. The data is represented as the mean of the independent replicates, and the error bars represent the standard error of the mean. Before performing statistical analysis, data were normalized using a Box–Cox power transformation to normalize data variance. One–way ANOVAs were calculated between different conditions as appropriate, followed by post hoc Tukey analysis to determine significant differences ($p < 0.05$). All statistical analysis was performed using MatLab and SYSTAT software.

6.3 Results

6.3.1 Influence of ESC secreted factors on mesenchymal stem cell populations

To assess whether soluble factors from ESCs affect mesenchymal stem cell (MSC) function, encapsulated ESC aggregates were co-cultured with murine MSCs. The encapsulated ESCs were placed in the upper level of a transwell insert at a 30:1 or 100:1 ESC to MSC ratio in serum-free KO N2B27 media such that the culture environment was

intentionally dominated by ESC secreted factors. MSC morphology and growth were evaluated over 7 days and compared to cells cultured in traditional serum-containing MSC growth media, to serum-free KO N2B27 media, and to serum-free KO N2B27 media containing empty alginate beads. The MSCs co-cultured with the ESCs took on an altered morphology **(Figure 6.1j-o),** similar to what was observed with MSCs cultured in the KO N2B27 **(Figure 6.1d-i),** in which they appeared much smaller than MSCs in traditional growth media **(Figure 6.1a-c)**. However, many more MSCs were observed when cultured in the presence of ESC secreted factors than in the KO N2B27 alone, which was corroborated through quantification of cell number at the end of 7 days **(Figure 6.1p)**. In contrast to KO N2B27 alone, MSCs cultured in the presence of ESCs at either ratio had a 3.9-fold higher final cell number, indicating that soluble factors from the ESCs had a mitogenic effect on the MSCs. To determine if the ESCs were secreting fibroblast growth factor-2 (FGF-2), a known mitogen used for MSC expansion, analysis of the spent media was performed. However, FGF-2 was not detected (lower limit of detection of 15.6 pg/mL) in any condition, including ESCs cultured in the absence of MSCs **(Figure 6.1q)**. Given that FGF-2 is present in fetal bovine serum (FBS) at a concentration of approximately 37 pg/mL (~3.7 pg/mL in 10% FBS containing media), it is possible that sufficient FGF-2 to induce a response is present but is below the detection limit of the assay.

A limitation of a co-culture format in this case is the two-way communication between the ESCs and the MSCs in which the MSCs may be feeding back on the ESCs and thus influencing ESC differentiation and subsequent secretion profile. Therefore, the influence of ESC conditioned media on MSC growth was also assessed so that the ESC phenotype could be tightly and independently controlled. The conditioned media approach

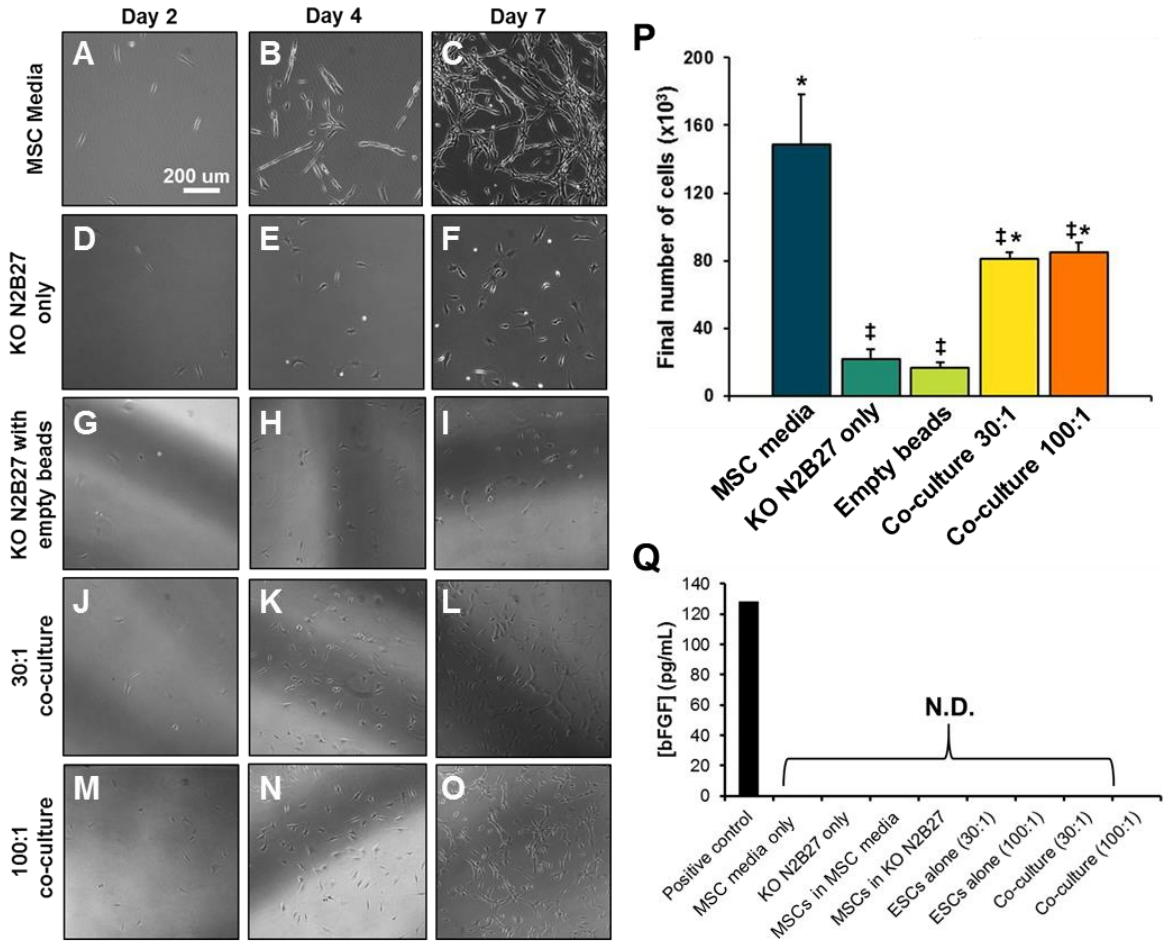

Figure 6.1. Mesenchymal stem cell co-culture with encapsulated ESCs. Mesenchymal stem cells (MSCs) were cultured in serum-containing MSC media **(A-C)**, in serum-free KO N2B27 **(D-F)**, in serum-free KO N2B27 with cell-free alginate beads **(G-I)**, and in serum-free KO N2B27 with encapsulated embryonic stem cells (ESCs) at either a 30:1 ESC:MSC **(J-L)** or a 100:1 ESC:MSC ratio **(M-O)**. Quantification of the final MSC number after 7 days of culture indicates that the highest growth was observed in the control MSC media but that co-culture with the ESCs led to MSC growth in comparison with the KO N2B27 alone **(P)**. No bFGF was observed in the culture media to explain the mitogenic effect **(Q)**. Scale bar = 200 μm. Significant ($p < 0.05$) differences from KO N2B27 only (*) and MSC media (‡) are denoted. N=3 for control groups, N=9 for ESC co-culture groups.

allows the ESCs to be cultured in distinct environmental conditions from the MSCs, including settings that may be advantageous for ESC secretion but may not be ideal for MSC culture. Therefore, conditioned media was collected from ESC aggregates encapsulated in either High G or High M alginate and cultured under normoxic (21% oxygen) or hypoxic (3% oxygen) conditions during early stage differentiation (days 1-4 post-encapsulation) or during later stage differentiation (days 4-7 post-encapsulation). The MSCs were cultured for 7 days in the presence of 75% conditioned media collected from ESCs in the described conditions and 25% serum-containing MSC growth media, and the final cell number was compared to MSCs cultured in 100% MSC growth media or serum-free KO N2B27 (75% with 25% MSC growth media). Conditioned media (CM) collected from ESCs cultured within High M alginate and under normoxic oxygen conditions led to a significant increase in MSC number in comparison with MSC growth media (1.6-fold increase for CM collected between day 1-4 of differentiation and 1.9-fold increase for CM collected between day 4-7 of differentiation) **(Figure 6.2a)**. Additionally, a significant increase in MSC number in comparison to KO N2B27 controls was observed when the MSCs were exposed to CM collected from ESCs cultured in High G alginate under normoxic conditions, and the final MSC cell number was comparable to what was obtained using growth media. In contrast, culture of the MSCs in conditioned media collected from ESCs under hypoxic conditions did not increase MSC cell number in comparison to KO N2B27 alone.

To determine if particular ESC phenotypes enhanced MSC growth, the final MSC cell number was correlated to gene and protein expression data of the ESCs from which the conditioned media had been collected (specifically, the ESCs and ESC CM collected

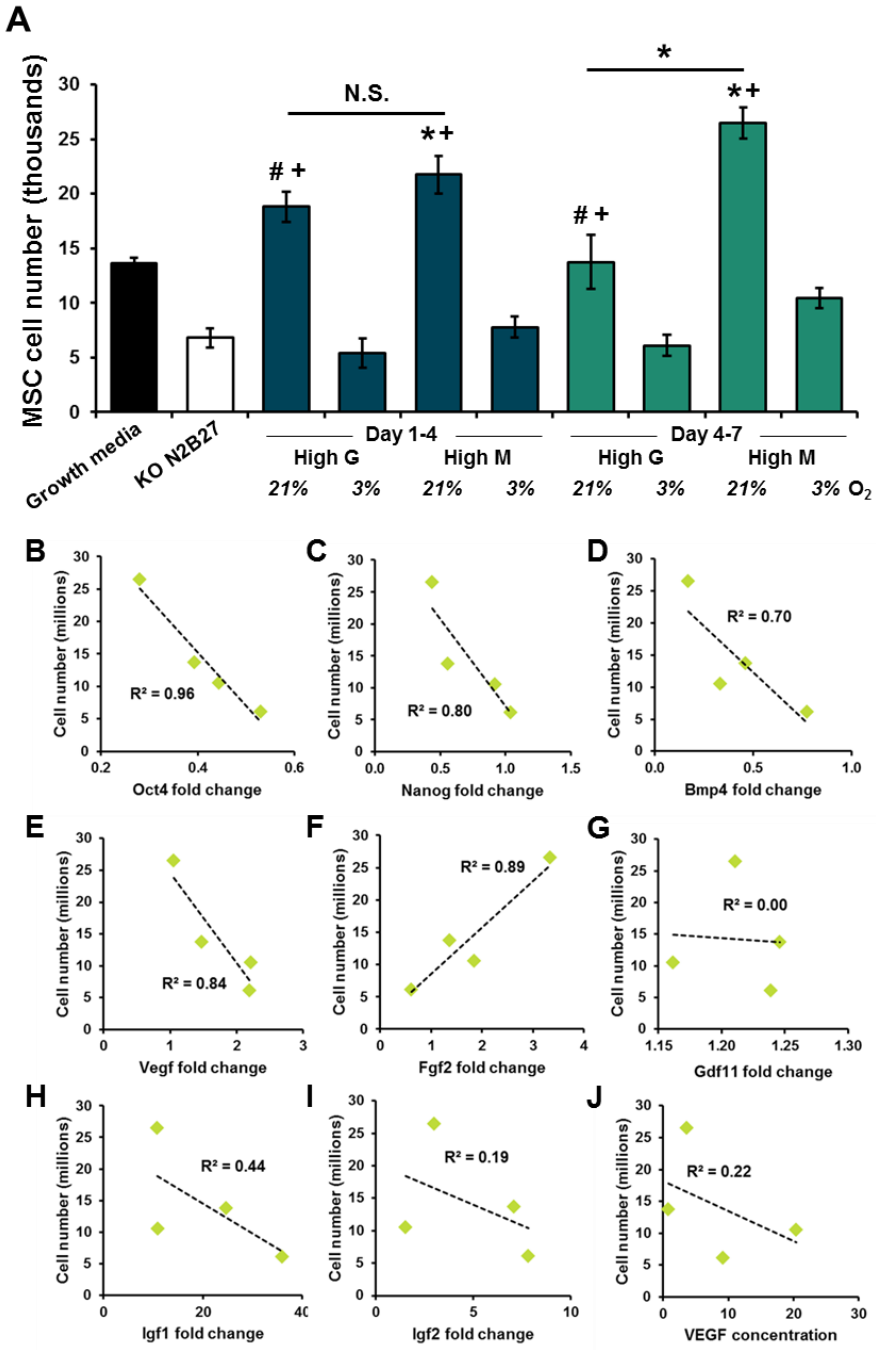

Figure 6.2. Variable ESC conditioned media effects on MSC growth. ESCs were cultured in either High G or High M alginate and in either normoxic (21% O_2) or hypoxic (3% O_2) conditions, and the conditioned media was collected at day 4 or day 7 of culture. Conditioned media collected from ESCs cultured under normoxic conditions led to improved MSC growth in comparison to media collected under hypoxic conditions **(A)**. The corresponding ESC gene expression from the cells when conditioned media was collected at day 7 was correlated to MSC growth **(B-J)** to determine what correlations exist between ESC cell state and MSC growth. Significant ($p < 0.05$) increases over growth media (*) and KO N2B27 (+), as well as a lack of significant difference ($p > 0.05$) from growth media (#) are denoted. R^2 signifies the Pearson correlation. N=6 for control groups, N=3 for ESC conditioned media groups.

at day 7 of differentiation). Increased MSC number was negatively correlated with pluripotency marker expression of the ESCs **(Figure 6.2b-c)**, indicating that ESCs in a more differentiated state may secrete factors that better promote MSC growth. Additionally, expression of the growth factors BMP-4 **(Figure 6.2d)** and VEGF **(Figure 6.2e)** were negatively correlated with MSC number, while expression of the growth factor FGF-2 was positively correlated **(Figure 6.2f)**. The gene expression of several other growth factors, including GDF-11 **(Figure 6.2g)**, IGF-1 **(Figure 6.2h)**, and IGF-2 **(Figure 6.2i)**, in addition to the concentration of VEGF present in the conditioned medium **(Figure 6.2j)**, were not found to be correlated with MSC growth.

6.3.2 Effect of pluripotent cell-derived factors on bone marrow populations

To investigate the effect of ESC-derived factors on a heterogeneous mixture of primary stem and progenitor cells, whole bone marrow was isolated from mice and sorted to obtain the Lineage-negative (Lin-negative) fraction, excluding cells with mature lineage markers. Conditioned media and co-culture approaches to expose the bone marrow populations to ESC-derived factors were explored in parallel. To determine whether factors secreted during specific stages of differentiation had differential effects or whether the timing of and duration between media exchanges created differences, several experimental groups were initially explored **(Figure 6.3)**. Prior to the isolation of bone marrow, conditioned media was collected from encapsulated ESCs at several stages: (1) at day 2 following 48 hours of conditioning, (2) at day 4 following 48 of conditioning, and (3) at day 4 following 96 hours of conditioning. Groups (1) and (2) were additionally pooled together to create (4) a pooled group in order to better mimic one of the co-culture configurations. To mimic the culture regime utilized when collecting the conditioned

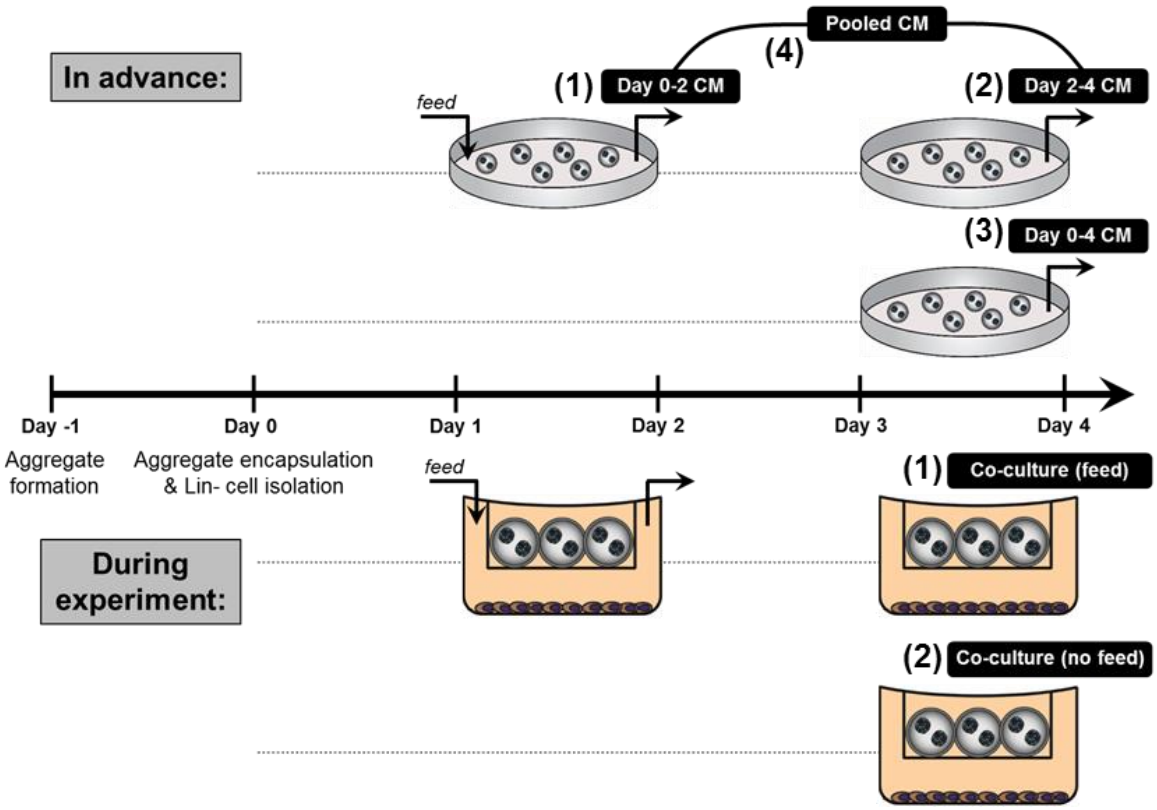

Figure 6.3. Scheme and experimental groups for exposure of hematopoietic progenitors to ESC secreted factors. Prior to the isolation of bone marrow, conditioned media was collected from encapsulated ESCs at several stages: (1) at day 2 following 48 hours of conditioning, (2) at day 4 following 48 of conditioning, and (3) at day 4 following 96 hours of conditioning. Groups (1) and (2) were additionally pooled together to create (4) a pooled group. To mimic the culture regime utilized when collecting the conditioned media, two different co-culture schemes were employed, (1) with a media exchange after 48 hours and (2) with no media exchange in the 96 hours of culture. An equivalent density of encapsulated ESCs was used in the co-cultures and in the collection of the conditioned media.

media, two different co-culture schemes were employed, (1) with a media exchange after 48 hours and (2) with no media exchange in the 96 hours of culture. An equivalent density of encapsulated ESCs was used in the co-cultures and in the collection of the conditioned media. As an additional control for the depletion of nutrients and presence of waste products in conditioned media, medium conditioned by endothelial cells and the endothelial cell base medium were also utilized.

Given the mitogenic response of MSCs to pluripotent cell-derived factors, the total number of cells present in the various methods of ESC factor delivery was investigated for the isolated bone marrow populations. After 24 hours of culture, the number of cells present was assessed using an imaging plate reader to determine the number of fluorescent cells (in this case, the whole bone marrow was isolated from eGFP mice). Significantly more cells were observed in the groups exposed to endothelial cell conditioned medium (1.8-fold) and the ESC conditioned media obtained between days 0-2 (2.5-fold) and days 2-4 (2.1-fold) when compared to the MyeloCult control, a commercially-available serum-containing media for hematopoietic progenitors **(Figure 6.4a)**. Additionally, all of the ESC conditioned media groups, with the exception of the medium collected after 4 days with no feed, led to significantly greater bone marrow cell numbers than the basal KO N2B27. The final number of cells after 4 days of exposure was evaluated using flow cytometry with counting beads, and the greatest number of cells were again observed in the ESC conditioned medium collected after 2 days of culture **(Figure 6.4b)**. There was no increase in bone marrow cell number observed in the co-culture conditions in comparison to KO N2B27 alone, indicating that the co-culture configuration was insufficient to support the bone marrow populations in the way that the conditioned media appears to be.

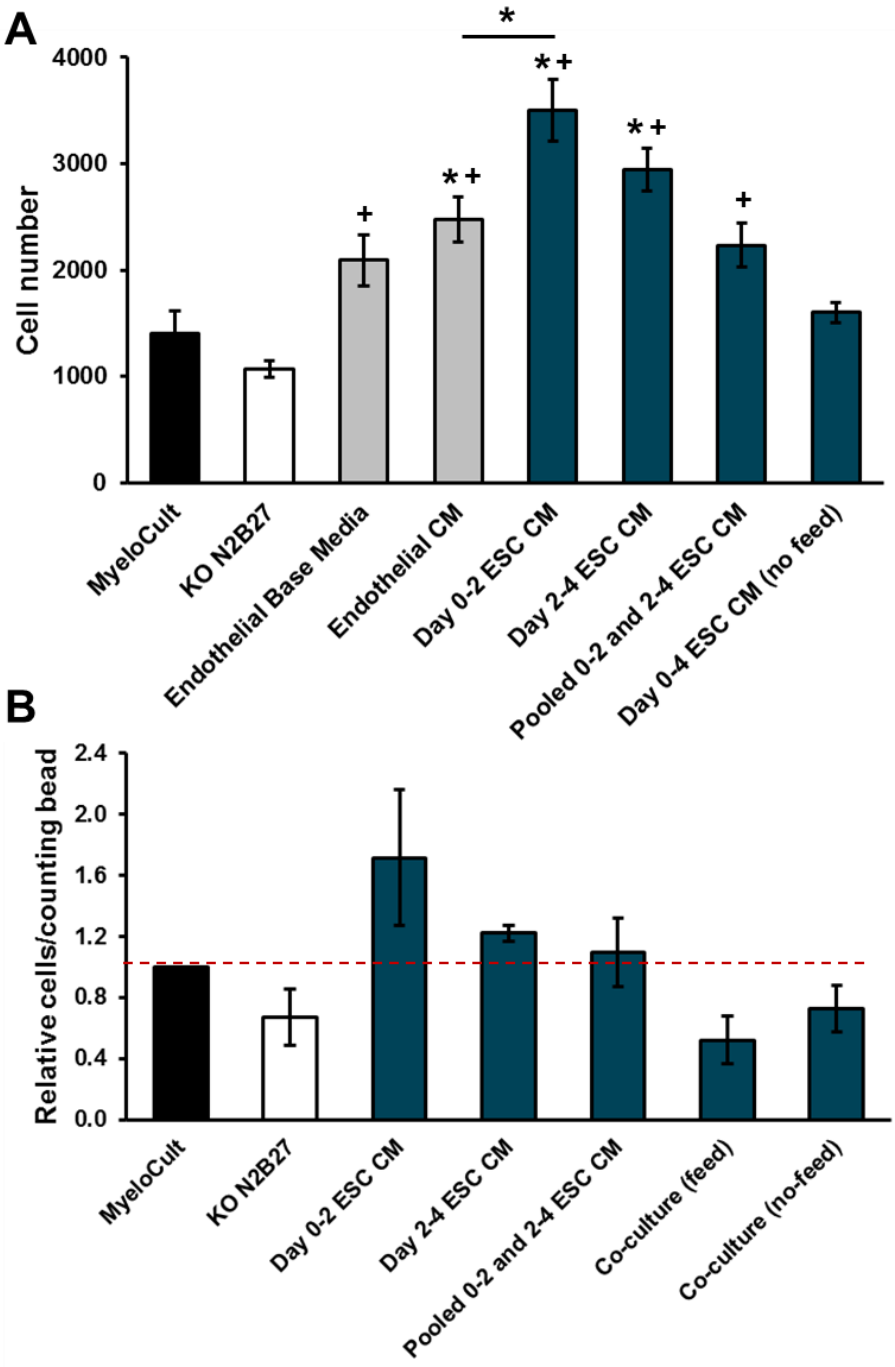

Figure 6.4. Mitogenic effects of ESC secreted factors on hematopoietic progenitor populations. The number of cells one day after seeding was quantified using an imaging plate reader **(A)** and after four days of culture using flow cytometry **(B)**. The cell number was normalized to the number of counting beads present and to the MyeloCult control media (dashed line). Significant ($p < 0.05$) increases over growth media (*) and KO N2B27 (+) as well as between groups (*) are denoted. N=4 for day 1 cell counts and N=2-3 for day 4 cell counts.

Analysis of the phenotypic composition of the cultures following exposure to the different soluble conditions was assessed via flow cytometry analysis of cell surface markers. Myeloid cell populations (CD45+CD11b+) were most highly present in the MyeloCult media and in the Day 0-2 ESC conditioned media, with lower numbers of myeloid cells present in the KO N2B27, co-cultures, and later stage-derived ESC conditioned media **(Figure 6.5a)**. In contrast, more lymphoid cells (CD45+CD11b-) were observed in all types of the ESC conditioned media than in the MyeloCult media **(Figure 6.5b)**, though hematopoietic progenitors in co-culture with the ESCs were once again at similar numbers of lymphoid cells as the KO N2B27 group. Regarding more specific myeloid lineages, monocyte/macrophages (CD45+CD11b+Ly6G-) accounted for ~50% of the total cell population in all groups **(Figure 6.5c)**, excluding the KO N2B27 condition. Neutrophil populations (CD45+CD11b+Ly6G+), on the other hand, were exclusively supported by MyeloCult media and were observed in very low numbers by all other groups **(Figure 6.5d)**, indicating that the signals necessary for neutrophil differentiation and/or survival were not provided by ESCs.

More functional assessments of the isolated bone marrow populations were performed to determine the extent of cell proliferation and differentiation capacity. To analyze cell proliferation, cells were stained with carboxyfluorescein succinimidyl ester (CFSE), with the loss of fluorescence intensity indicating that cell division has occurred [275]. A higher intensity was observed in the KO N2B27 group, while all other groups had similar intensities, indicating that cell proliferation was occurring at a lower rate in the KO N2B27 and at a uniformly higher rate among the other groups **(Figure 6.6a)**. Colony forming unit (CFU) assays were performed by isolating a fixed number of cells after the 4

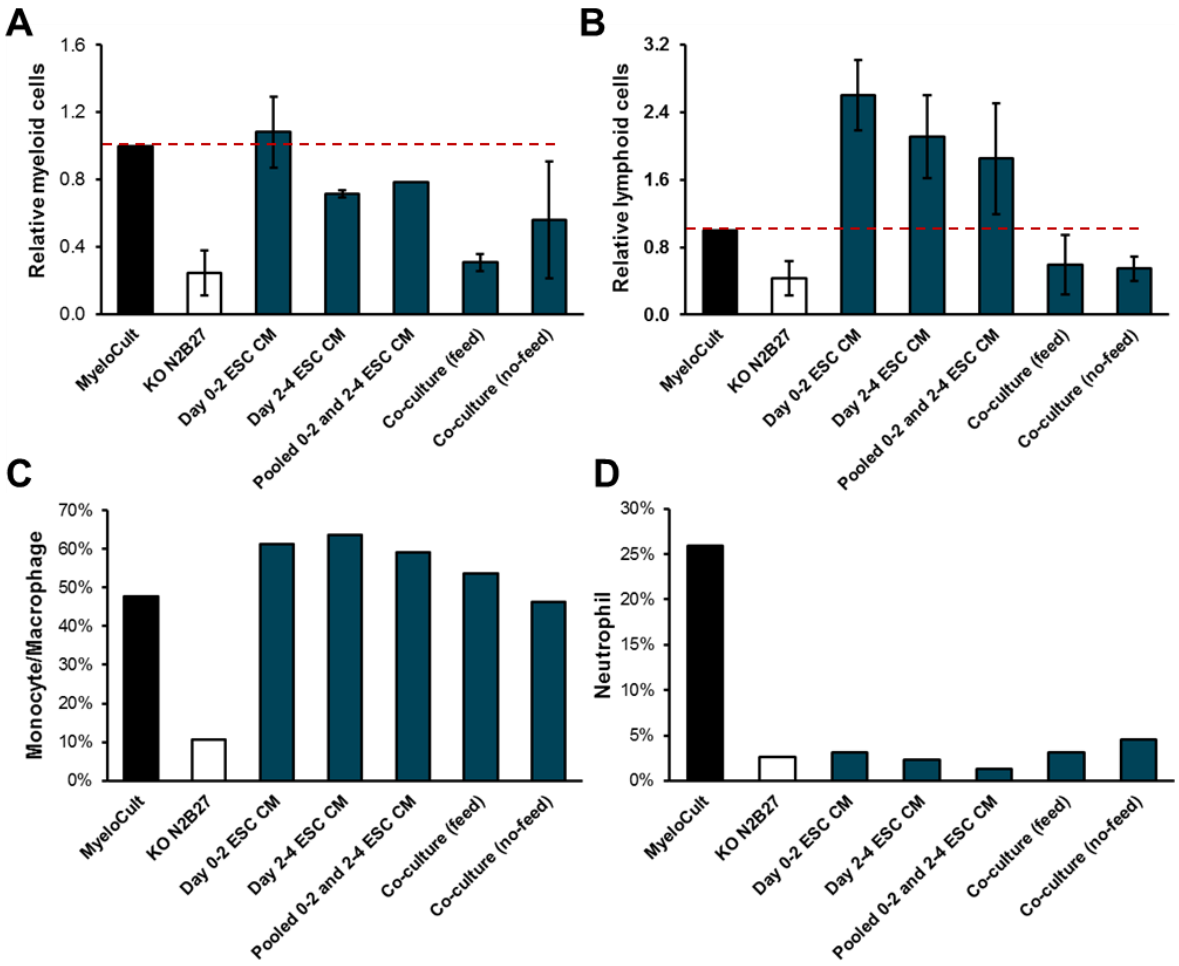

Figure 6.5. Phenotypic analysis of hematopoietic progenitors following exposure to ESC secreted factors. Flow cytometry was used to determine the composition of the cultures after 4 days. A similar number of myeloid cells (CD45+CD11b+) were present in the MyeloCult and ESC secreted factor groups **(A)**, while increased lymphoid cells (CD45+CD11b-) were observed in the cultures exposed to ESC conditioned media **(B)** but not in ESC co-cultures. Monocyte populations (CD45+CD11b+Ly6G-) were supported by all media compositions excluding the KO N2B27 **(C)**, while ESC-secreted factors were unable to support neutrophil populations (CD45+CD11b+Ly6G+) **(D)**. N=2 for myeloid and lymphoid analysis, N=1 for monocyte/macrophage and neutrophil analysis.

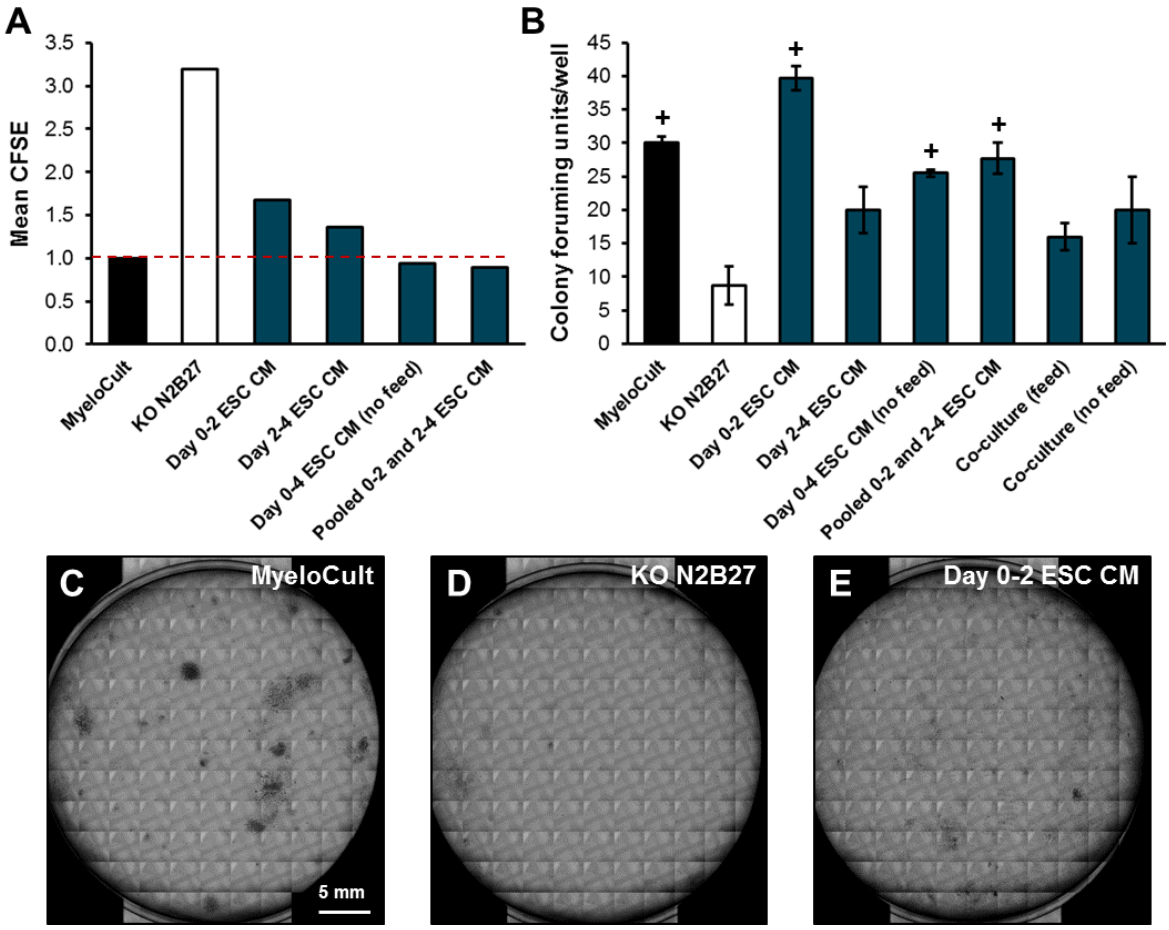

Figure 6.6. Functional analysis of hematopoietic progenitor proliferation and colony forming ability. Staining with carboxyfluorescein succinimidyl ester (CFSE) enabled analysis of cell proliferation **(A)**, with cells in all media compositions except the KO N2B27 proliferating at a rate similar to the MyeloCult control. After four days of exposure to the different culture configurations, the cells were plated for analysis of colony forming units (CFUs). Increased numbers of colonies were observed in the MyeloCult and some configurations of the ESC conditioned media in **(B-E)**. Significant ($p < 0.05$) increases over KO N2B27 (+) are denoted. N=1 for CFSE assay, N=3 for CFU assay.

days of exposure to the different soluble conditions and subsequent culture in methylcellulose for 12 days. Significantly more colonies were observed in the MyeloCult and ESC conditioned media groups (with the exception of the day 2-4 ESC conditioned medium) than in the KO N2B27 **(Figure 6.6b)**. The colonies present in the MyeloCult conditions appeared more dark and dense **(Figure 6.6c)**, while the colonies in the ESC conditioned media groups were smaller and more sparse **(Figure 6.6e)**, and very few colonies were observed in the KO N2B27 condition **(Figure 6.6d)**.

6.3.3 Impact of ESC derived factors on skeletal muscle populations

To investigate if the mitogenic effects of the ESC conditioned media translated to a different cell population, primary muscle cells were isolated from mouse hind limbs and exposed to ESC conditioned medium collected from encapsulated ESCs cultured within the packed bed perfusion reactor at days 1-4 of differentiation. Due to the heterogeneous population obtained with the primary cell isolation, a large number of fibroblasts were also present in the culture, similar to the composition in the *in vivo* environment. Following four days of culture in either 100% growth media, 75% KO N2B27/25% growth media, or 75% ESC conditioned medium/25% growth media, the cells were stained with an antibody against desmin, a muscle-specific intermediate filament, to identify the myocytes present **(Figure 6.7)**. While the majority of the cells in the culture were fibroblasts, desmin-positive cells were observed in all conditions. Smaller, myoblast-like cells were observed in the growth media condition **(Figure 6.7a, 6.7d)**, while more differentiated myocytes were observed in the KO N2B27 and ESC conditioned medium **(Figure 6.7b-c, 6.7e-f)**, including several with multiple nuclei indicating cell fusion.

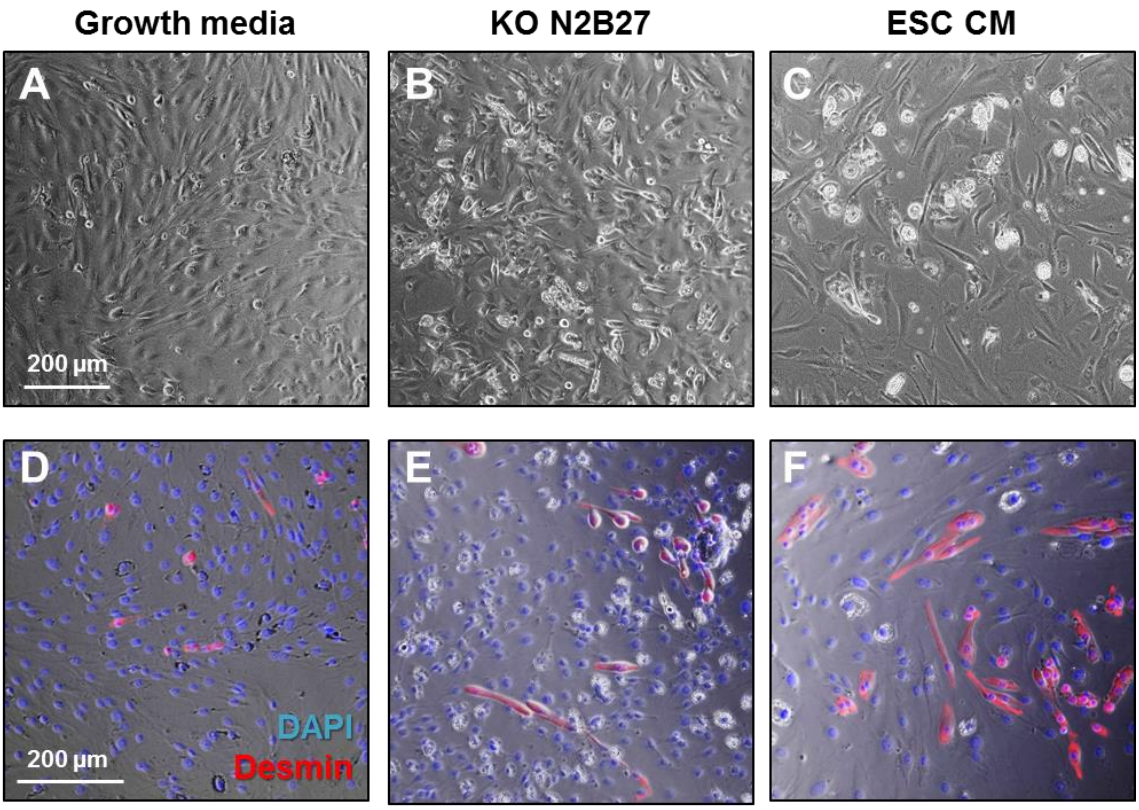

Figure 6.7. Exposure of skeletal myocytes to ESC conditioned medium. Mouse myocytes were isolated and cultured in serum-containing growth medium **(A,D)**, 75% serum-free KO N2B27 with 25% growth medium **(B,E)**, or 75% ESC conditioned medium (CM) with 25% growth medium **(C,F)**. Greater number of desmin-negative fibroblasts were observed in cells cultured in the growth medium and KO N2B27 in comparison to the ESC CM, which appeared to be enriched for desmin-positive myocytes. Scale bars = 200 µm.

The proportion of desmin-positive cells relative to total nuclei was determined by performing image analysis of a series of fluorescent images **(Figure 6.8)**. The total number of nuclei, visualized in **Figure 6.8a-c** and quantified in **Figure 6.8g**, indicates that fewer total cells were present in the culture after four days of exposure to the ESC conditioned medium. In contrast, the total number of desmin-positive cells was similar in all groups **(Figure 6.8d-f, 6.8h)**, demonstrating that there were a higher proportion of myocytes present in the ESC conditioned media than in the growth media and KO N2B27 controls **(Figure 6.8i)**. Though similar numbers of myocytes were observed in all three groups, the morphology of the myocytes varied between them, with smaller, more myoblast-like cells predominating the culture in growth media and large elongated myocytes and early myotubes present in higher abundance in the wells exposed to KO N2B27 and ESC conditioned medium **(Figure 6.8j)**. The difference in cell morphology was quantified by determining the percentage of desmin-positive cells with a small area (50-1000 pixels^2) and high circularity (>0.7), which represent a more myoblast-like morphology, from the desmin-positive cells with a larger area (200-2000 pixels^2) and low circularity (<0.7), which represent a more differentiated morphology. The differentiation of myoblasts into committed myocytes and myotubes is correlated with reduced serum concentrations, thus presence of differentiation is not surprising given that the serum concentration is reduced from 20% in the growth media to 5% in the KO N2B27 and ESC conditioned medium. However, it is interesting to note that there was a significant decrease in the presence of the elongated myocytes **(Figure 6.8j)** when cells were cultured in ESC conditioned medium (48% ± 3.3%) in comparison to KO N2B27 (57% ± 3.0%), indicating that factors

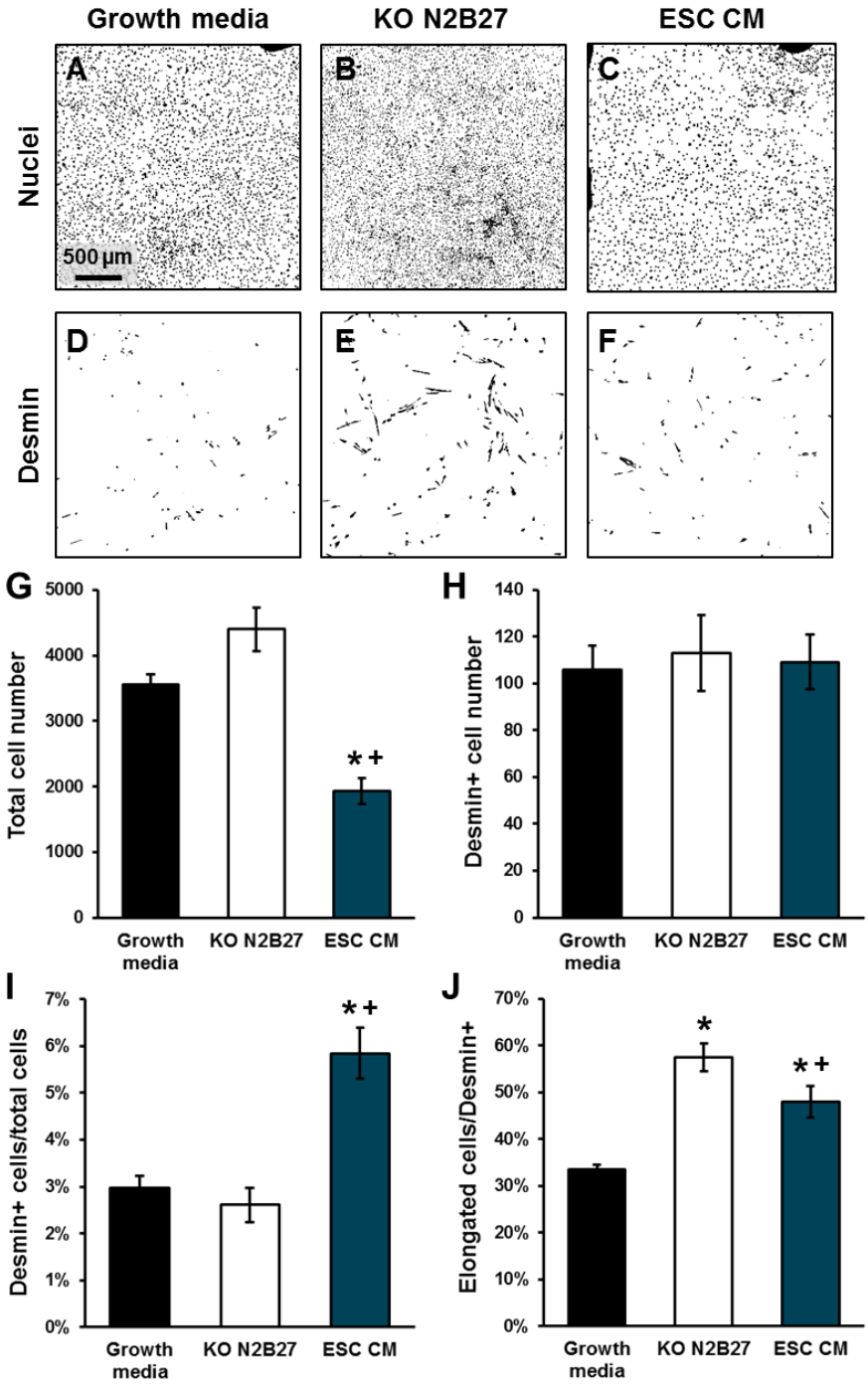

Figure 6.8. Analysis of skeletal myocyte number and morphology. Fluorescence images were analyzed to determine the total cell number, determined from the number of DAPI-stained nuclei **(A-C, G)** in addition to the number of desmin-positive myocytes **(D-F, H)**. Though similar numbers of myocytes were observed in all three conditions, fewer fibroblasts were present in the ESC conditioned medium (CM), leading to an overall enrichment of myocytes. A greater percentage of the desmin-positive cells in the KO N2B27 and ESC CM groups appeared elongated, indicating differentiation **(J)**, though the degree of elongation was reduced in the ESC CM compared with the KO N2B27. Significant ($p < 0.05$) increases from the growth media (*) and the KO N2B27 (+) are denoted. N=9 fields for the image analysis.

secreted by the ESCs may partially restore the effects of some of the growth factors found in serum.

6.4 Discussion

The results of this study suggest that embryonic stem cells (ESCs) produce signals that stimulate a mitogenic response in multiple adult stem and progenitor cell populations, including mesenchymal stem cells, hematopoietic progenitors, and myocytes. In addition to changes in cell growth, the differentiation capacity of several cell types was also altered in response to ESC secreted factors. The differentiation stage and microenvironment under which the ESCs are cultured prior to collection of the conditioned media also alters the downstream cell response, likely due to differences in the secreted milieu based on the stage of differentiation and the environmental cues provided to the ESCs (Chapter 5).

Exposure of homogeneous populations of bone marrow-derived mesenchymal stem cells (MSCs) to ESC secreted factors, either through co-culture **(Figure 6.1)** or conditioned media **(Figure 6.2)** approaches, led to increases in cell number in comparison to MSCs cultured in the basal serum-free media. Although the fold increase in MSC number was reduced in the serum-free co-culture compared with the standard serum-containing growth medium (1.8-fold higher cell number in comparison to serum-free co-culture) **(Figure 6.1p)**, a more favorable small, spindle-shaped MSC morphology was observed with exposure to pluripotent factors **(Figure 6.1j-o)**. While greater expansion of MSCs was observed in response to ESC conditioned media **(Figure 6.2a)**, the reduced MSC expansion in the co-culture conditions may be due to the ESCs consuming many of the required nutrients and leaving fewer available for MSC consumption, as there were 30-fold or 100-fold more total cells seeded into the wells in comparison with the MSC growth media

condition. The change in MSC growth observed between co-culture and conditioned media may also be due to the media composition, of which 25% consisted of unconditioned MSC growth media, and the MSCs were thus in a less nutrient-depleted environment. An additional hypothesis is that co-culture with the MSCs may have altered the ESC secretion profile or kinetics, leading to differences in the paracrine factors produced which may not have been as favorable for MSC growth. A previous study using human ESC-conditioned media to expand Wharton's jelly-derived MSCs also reported increased MSC growth in comparison with FBS-containing growth media [273], though the ESC medium used had been collected from ESCs cultured on fibroblast feeder cells and supplemented with fibroblast growth factor, making it difficult to establish which of the specific components was responsible for the enhanced MSC growth.

Depending on the settings under which the ESC conditioned media was collected, differential MSC growth responses were observed. One striking difference in MSC growth was observed in media conditioned by ESCs cultured under hypoxic (3% oxygen) conditions, which yielded no improvement in MSC number when compared to the serum-free media alone, unlike the media conditioned by ESCs cultured under normoxic (21% oxygen) conditions that promoted MSC growth **(Figure 6.2a)**. Culture of ESCs under hypoxia has been observed to increase the production of certain hypoxia-induced growth factors, including vascular endothelial growth factor (VEGF) and insulin-like growth factor-2 (IGF-2), as well as prevent or delay ESC differentiation [238–240,276]. However, the reduction in oxygen may have also limited ESC growth, leading to fewer cells producing relevant growth factors. The presence of hypoxia-inducible factor-1α (HIF-1α) in the conditioned media may have activated growth-restricting signaling pathways in the

MSCs, though culture of MSCs in hypoxic conditions has been previously observed to have negligible or even positive impact on MSC growth, likely due to the low oxygen tension of the native bone marrow compartment [277,278]. To examine the correlation of MSC growth with ESC phenotype, gene expression values for two pluripotency markers and six growth factors, in addition to the concentration of VEGF in the conditioned media, were compared to MSC number. Many of the negatively-correlated relationships **(Figure 6.2b-c, 6.2e, 6.2j)** were associated with the response to the hypoxia-derived conditioned media, as higher expression of the pluripotency markers *Oct4* and *Nanog* and the growth factor *Vegf* were observed when the ESCs were cultured under low oxygen. The only positively-correlated growth factor was fibroblast growth factor-2 (*Fgf2*), which is a well-known mitogen used to promote MSC growth [255,256]. Interestingly, protein levels of FGF-2 are generally upregulated by low oxygen conditions through interaction with HIF-1α, though a decrease in gene expression is observed as the protein concentration rises [279].

Moving from the homogeneous population of MSCs to a mixed population of primary hematopoietic progenitor cells, similar mitogenic effects were observed in response to exposure to ESC conditioned media **(Figure 6.4)**. The highest cell numbers were observed in cells cultured in ESC conditioned media obtained from early-stage ESCs (day 0-2 post-encapsulation), in comparison to MyeloCult, a commercially-available medium used to expand hematopoietic progenitors, to the serum-free KO N2B27 used as a base media for ESC culture, and to media conditioned by C166 endothelial cells, which are specifically recommended to support proliferation of multipotential hematopoietic stem and progenitor cells [280]. However, the mitogenic effect was attenuated in conditioned

media obtained from later stage ESCs (day 2-4 post-encapsulation), and no increase in growth was observed with ESC co-culture in comparison to basal KO N2B27. The decrease in potency with ESC differentiation stage may be due to changes in the secretome, such as lower concentrations of specific mitogens or higher concentrations of specific inhibitors. The difference could also be the consequence of metabolic differences, as lower concentrations of nutrients and higher concentrations of wastes would be present at the later stages of ESC culture due to the greater number of cells present.

When the data describing overall cell number **(Figure 6.4)** is combined with the results of the CFSE cell proliferation assay **(Figure 6.6a)**, it appears that the hematopoietic progenitors are actually proliferating at a similar rate across all conditions, with the exception of cells in the KO N2B27 basal medium which are proliferating at a slower rate. Thus, the overall differences in cell number are likely due to contrasts in differentiation to downstream hematopoietic progenitors rather than in proliferation. This hypothesis is supported by the composition and number of lineage-specific cells identified through surface marker expression. While the number of myeloid cells (CD45+CD11b+) treated with ESC conditioned media (day 0-2) was similar relative to the number of myeloid cells in MyeloCult **(Figure 6.5a)**, there were many more lymphoid cells (CD45+CD11b-) in the ESC conditioned media groups **(Figure 6.5b)**, which is likely accounting for the increase in overall cell number **(Figure 6.4b)**. An interesting observation from the analysis of lineage composition is that while the ESC-produced factors were able to support the differentiation toward monocyte and macrophage phenotypes (CD45+CD11b+Ly6G-) to a similar extent as the MyeloCult medium **(Figure 6.5c)**, the presence of ESC secreted factors was not sufficient for differentiation toward or survival of neutrophil populations

(CD45+CD11b+Ly6G+) **(Figure 6.5d)**. Alternatively, the ESCs may be producing cues that are inhibitory to neutrophil populations. It is likely that the specific cytokines and growth factors necessary for support of neutrophils, such as granulocyte-colony stimulating factor (G-CSF), stem cell factor (SCF), and interleukin-5 (IL-5), were not produced in high enough levels by the ESCs in comparison to the serum concentration present in the MyeloCult, while monocyte-colony stimulating factor (M-CSF), which is required for the differentiation of monocytes, may have been present in sufficient quantities [281,282]. Indeed, examining at the cytokine array analysis of ESC conditioned media in Chapter 5, M-CSF was detected in the conditioned media while G-CSF was not **(Figure 5.3)**. While many of the parameters assessed (cell number, colony formation, number of lymphoid cells) were varied based on the manner of delivery, it is of interest that the proportion of monocytes and neutrophils present did not appear to be dependent on the specific method of delivering the ESC secreted factors, as similar percentages were observed in all conditioned media and co-culture groups **(Figure 6.5c-d)**.

In general, co-culture of the hematopoietic progenitors with the encapsulated ESCs did not lead to the robust increases in cell number **(Figure 6.4)** or colony-forming units **(Figure 6.6b)** observed in specific ESC conditioned media groups. The decrease in potency in the co-culture is consistent with the previous results with MSCs in which conditioned media generally led to a greater increase in cell number, though the co-cultures with the MSCs still enhanced cell growth in comparison to the KO N2B27 **(Figure 6.1p)**. In contrast, the ESC-hematopoietic progenitor co-cultures generally yielded similar results to the KO N2B27 alone, indicating that there was little impact of the ESCs over the base effect of the media. The one exception is in the proportion of monocytes **(Figure 6.5c)**, in

which case co-culture with the ESCs appeared sufficient to promote differentiation toward or survival of monocyte populations. It is possible that subjecting the ESCs to co-culture with the hematopoietic progenitors led to changes in the ESC secretion profile or secretion kinetics, or potentially even to ES cell death, which in turn reduced their capacity to support the bone marrow populations. An additional theory is that the diminishing mitogenic effect observed in the conditioned media collected from ESCs at later stages (day 2-4) was exaggerated in the co-culture conditions, as those cells were present for the entire four day duration **(Figure 6.3)**.

Transitioning from the bone marrow compartment to the muscle niche, the influence of ESC conditioned media on primary myocytes was assessed to determine whether the mitogenic effects might translate to another tissue-specific stem and progenitor cell population. In addition, existing literature describes the ability of pluripotent cell-derived factors to "rejuvenate" muscle populations *in vitro*, with conditioned media from undifferentiated human ESCs promoting proliferation of young and old myoblasts, while conditioned media from human ESCs differentiated down the neural lineage promoted myocyte differentiation and inhibited proliferation [35,274]. Primary myocytes were isolated from the hind limbs of mice, and though preferential adhesion steps were performed to reduce the number of fibroblasts present in the culture, the composition of the culture was still dominated by fibroblasts (~95% fibroblast). While the heterogeneous culture makes it challenging to examine the impact of ESC secreted factors on myocytes alone, the mixed culture better recapitulates the *in vivo* muscle niche in which fibroblasts play an important supportive role [270], as it has been reported that removing fibroblasts from the satellite cell niche promotes premature satellite cell differentiation and an

exhaustion of the stem cell pool. Following four days of exposure to a standard FBS-containing growth medium, to the basal serum-free KO N2B27 (75%, 25% growth medium), or to the ESC conditioned medium (75% with KO N2B27 base medium, 25% growth medium), the cultures in the ESC conditioned medium appeared to be enriched for desmin-positive myocytes **(Figure 6.7)**, and the myocytes present in the both the KO N2B27 and ESC conditioned medium groups tended to be more elongated and multinucleated, hallmark signs of myogenic differentiation. Image analysis of the mixed cultures confirmed that a greater percentage of desmin-positive cells were present when cultured in the ESC conditioned medium **(Figure 6.8i)**, although this was due to a decrease in the fibroblast number rather than to an increase in the myocyte number **(Figure 6.8g-h)**. While conditioned media from ESCs has previously been observed to promote fibroblast proliferation [181], the more proliferative fibroblasts may require nutrients present in the media in higher abundance than the myocytes, and therefore the myocytes preferentially survived.

Through the image analysis, it was determined that fewer myocytes exhibited the elongated, differentiated morphology when cultured in the ESC conditioned medium (48%) in comparison to the KO N2B27 (57%), though the least differentiation was observed in the growth media (34%) **(Figure 6.8j)**. Some differentiation is expected in both low-serum groups, as serum deprivation inhibits proliferation and promotes differentiation and myotube formation [283], and the FGF-2 concentration was also reduced to one-quarter of the concentration found in the growth medium. However, the decreased extent of differentiation when the cells were cultured with exposure to ESC conditioned medium indicates that the paracrine factors produced by the ESCs may be

capable of compensating for the lack of growth factor-rich serum. Fetal bovine serum contains a multitude of undefined growth factors, some of which seem to be responsible for maintaining myocytes in a proliferative state. Fibroblast growth factor-2 is the most commonly attributed factor for maintenance of muscle stem and progenitor cells [284], hence its inclusion as a supplemental growth factor in many media compositions, but other growth factors, including FGF-1, have also been implicated [285,286]. Conversely, insulin-like growth factors (IGFs) have been found to promote both the proliferation and the differentiation of myoblasts [287,288]. As both FGFs and IGFs have been found to be expressed/produced by ESCs (Chapter 5), competing roles of the different growth factors are possible.

For all three cell populations examined in this study, further functional assessment would clarify the specific effects of the ESC-derived factors. In cases where greater cell numbers were observed, it is unclear if the overall increase in cell number was due to an increase in cell proliferation or an increase in cell survival. A previous study found that exposure of bone marrow-derived hematopoietic progenitors to ESC conditioned medium increased the number of granulocyte-monocyte colony forming units likely by increasing cell survival, as the number of cells undergoing apoptosis was reduced with culture in ESC conditioned medium [36]. For the skeletal muscle cells, it will be important to determine if the cells exposed to the ESC secreted factors retain the ability to engraft *in vivo*, as it has been determined that *ex vivo* expansion of mouse satellite cells for only three days led to a 10-fold decrease in the efficiency of engraftment [129], a reduction that has also been observed between freshly isolated and *ex vivo* cultured canine muscle progenitor cells [133]. Similar engraftment studies could also be performed with the hematopoietic

progenitors, as *ex vivo* expansion of hematopoietic stem cells generally results in decreased engraftment efficiency and repopulation activity [117].

6.5 Conclusions

Overall, the results of this study suggest that ESCs are a potent source of mitogens and growth factors capable of stimulating the growth of multiple stem and progenitor cell types. Populations of bone marrow-derived mesenchymal stem cells exhibited increased growth in response to ESC co-culture or exposure to ESC conditioned media. Furthermore, the application of ESC conditioned media to a heterogeneous population of hematopoietic progenitors led to increased proliferation and colony-forming ability, though the mitogenic effect decreased with more differentiated ESCs and was not recapitulated with a co-culture configuration. Exposure to ESC-secreted factors generally supported both lymphoid and myeloid differentiation, with the exception of neutrophils. When applied to skeletal myocytes, the growth factors present in the ESC conditioned medium enriched for myocytes over fibroblasts while reducing the differentiation of the myocytes to multinucleated myotubes. Taken together, the results demonstrate the potent mitogenic role of pluripotent stem cell-derived factors across multiple adult stem cell niches.

CHAPTER 7

FUTURE CONSIDERATIONS

Taken together, the data presented in this dissertation establish pluripotent stem cells as a unique source of potent growth factors and cytokines which can be regulated and concentrated using engineering design parameters to stimulate the proliferation and differentiation of adult stem and progenitor cell populations. As with most avenues of research, many of the findings motivate additional investigation which may lead to further advances in the realms of material and bioreactor design as well as identification of unique molecules produced by pluripotent stem cells and their subsequent influence on adult stem cell populations.

The development of an alginate microencapsulation-based platform for ESC culture described herein was not the first instance of such an approach [66,69,70,149]; however, it was the first report of the phenotypic influences of the alginate material employed (Chapter 3). Correlations were established between the composition of alginate used and the phenotype of the enclosed ESCs, with mechanically stiffer alginate fostering a pluripotent state and a mechanically softer alginate priming the ESCs for mesendodermal differentiation. A wide body of work has examined the influence of mechanical stiffness on stem cell differentiation and phenotype, with the majority of these studies conducted by culturing cells in 2D on different hydrogel substrates [289]. Mechanotransductive pathways that cause the observed phenotypic changes are not yet completely understood, though recent work indicates that the transcriptional coactivators YAP (Yes-associated protein) and TAZ (transcriptional coactivator with PDZ-binding motif), both part of the

Hippo pathway, may be key regulators that can sense cytoskeletal tension [290]. There are significant challenges in deciphering the specific role(s) of matrix mechanics on cell fate, including the difficulty in separating changes in mechanical stiffness from inherently linked changes in hydrogel porosity and solute permeability. The mechanical assessment performed in Chapter 3 was also a bulk measure and did not represent local interactions, which may better relate to the subsequent stem cell behavior.

Microencapsulation of ESCs within alginate beads facilitated the creation of a high density perfusion bioreactor that enabled increased production of ESC-secreted products (Chapter 4). The increased concentration achieved with perfusion in addition to the dependence of protein production on flow rate prompted the hypothesis that a negative feedback mechanism may be involved. In order to further investigate the validity of this hypothesis, exogenous protein could be added to the culture media to act as a prospective negative feedback regulator. Using standard techniques to determine the concentration of proteins in the culture media (such as ELISAs), it would be impossible to distinguish the exogenously added protein from endogenously secreted protein. However, changes could be examined at the gene expression level if the feedback is affecting protein expression at the level of transcriptional regulation. Alternatively, assuming the protein is being secreted through classical secretion pathways, an inhibitor of protein transport (such as GolgiPlug™) may enable intracellular buildup of the protein for subsequent analysis of the cell lysate rather than the media supernatant.

In the initial development and validation of the bioreactor platform, only two protein species (VEGF and IGFBP-2) known to be produced by ESCs were examined as indicators of protein production and concentration. Additional characterization in Chapter

5 using antibody arrays indicated that protein expression was globally increased with perfusion culture. However, a more global indicator of cell secretion would enable stronger claims regarding the ability of the perfusion bioreactor to increase cell secretion at a comprehensive level. The genetic engineering of ESCs to express secreted alkaline phosphatase (SEAP) or *Gaussia* luciferase may be enable those secreted factors to act as a surrogate for the general processes of protein synthesis and secretion [291,292]. While the global investigation of ESC secreted protein expression in Chapter 5 demonstrated profiles of morphogens, cytokines, and growth factors that are distinctive from other cell populations, there are likely additional unique species produced by pluripotent stem cells. A larger-scale proteomics approach using mass spectrometry would offer additional insight through recognition of unknown species of interest. In addition, non-biased genetic approaches such as RNA sequencing (RNA-seq) may be useful to identify mRNAs and proteins differentially regulated in specific culture configurations, whether it be the stage of ESC differentiation, the presences of perfusion flow, or another environmental stimuli.

The application of pluripotent stem cell-derived factors to stem and progenitor cell populations in Chapter 6 demonstrated their mitogenic effect as well as their ability to modulate differentiation, as was observed with hematopoietic progenitor and myoblast populations. In the initial studies described in this dissertation, the ESC conditioned media was provided as a bolus; however, integration of the downstream cell culture directly with the perfusion reactor upstream could be employed to enable continuous delivery such that the ESC paracrine factors would not be depleted through cellular uptake or degradation. A fed batch culture such as this has already been reported to be favorable for HSC culture due to the dilution of inhibitory feedback signals [246]. Depending on the length of the

culture period, the ESCs in the upstream reactor may need to be replaced with fresh "cartridges" of encapsulated ESCs to maintain the ESCs at the proper differentiation state. To determine whether the observed effects are reversible or sustained, the adult stem and progenitor populations could be reverted back to standard culture conditions following a set period of exposure to ESC secreted factors. Given the development of a robust *in vitro* platform, further examination of the functionality of adult stem cell populations post-transplantation, such as the ability for homing, engraftment, differentiation, and re-population, should be performed.

In contrast to the approaches discussed above in which the pluripotent cell-derived factors are used to expand and/or rejuvenate adult stem cell populations prior to their re-transplantation, the effect of delivering ESC-derived factors directly *in vivo* could also be explored. For example, a radioprotection assay could be performed to determine whether pluripotent cell-derived factors exhibit radioprotective properties on sublethally irradiated bone marrow. Exposure to ionizing radiation induces DNA damage in the bone marrow, leading to anemia, hemorrhage, and infection due to low numbers of circulating blood cells caused by the inability of bone marrow progenitors to effectively repopulate the hematopoietic system [30,31]. The search for radioprotective agents, molecules which reduce the lethality of radiation following a medical procedure or accidental exposure, has focused primarily on synthetic thiol compounds, antioxidants, and cytokines, either delivered individually or in combination [32,33]. However, approaches that more holistically regenerate the hematopoietic compartment by improving HSC function may have reduced toxicity and therefore diminish undesired side effects common to current therapies [34]. Therefore, positive outcomes of a radioprotection assay in which ESC

secreted factors are injected subcutaneously prior to or concurrent with radiation may be more broadly interpreted as evidence that pluripotent cell-derived factors can interact with bone marrow populations in an *in vivo* setting.

The results of this dissertation provide a basis for future exploration of a number of unique opportunities in the realm of regenerative medicine. The application of pluripotent stem cell-derived factors specifically to aged cell populations may be useful as a "rejuvenative" treatment to reverse the age-related dysfunction present in stem cell niches. The translation of the packed bed perfusion bioreactor system into a re-conception as an extracorporeal device would enable investigation of pluripotent cell-derived factors in a continuous *in vivo* context. In addition, enhanced material design approaches may be used for better upstream control of the encapsulated ESCs and their secreted proteins. Finally, additional characterization of other forms of secreted products, specifically the contents and role of ESC-derived exosomes and microvesicles, may provide additional information regarding the mechanisms of ESC stimulation and inhibition of other cell populations.

7.1 Application of pluripotent cell-derived factors to aged cell populations

One of the hallmarks of aging is a reduced capacity for regeneration which can be attributed to diminished function of adult stem cell populations [293]. At this point, it is unclear the extent to which the reduced function of aged stem cells is intrinsically linked to replicative or chronological age, or is instead associated with extrinsic changes in the surrounding environment [294]. There are many components that might be altered in an aged stem cell niche, including the soluble paracrine factors secreted by neighboring cells, the constitution of the surrounding extracellular matrix, or the direct contacts with specific

membrane-bound proteins and lipids. In a whole organism view, aging is not occurring only in the immediate niche but also at the scale of entire tissues and organ systems; thus, changes in the composition of systemic factors also plays a role and may be interacting with the transformations experienced at all physiological levels. Therefore, the decline in ability of aged stem cell populations to maintain deteriorating tissues seems to reflect inadequate support from the surrounding aged environment.

The extent to which a given multipotent stem cell population is affected by aging may be directly linked to its role in maintaining its derived tissue population. For example, hematopoietic stem cells (HSCs) are responsible for constantly replenishing the blood and immune systems and are thus defined as having both high cellular turnover and high regenerative potential [294]. In contrast, satellite cells (SCs) of the skeletal muscle are able to rapidly respond to injury in order to regenerate damaged muscle but are preserved in a quiescent state for the majority of time. On the opposite end of the spectrum are neural stem cells (NSCs), which are capable of limited neurogenesis but generally exhibit both low cellular turnover and low regenerative potential [295]. Based on the distinct functionalities of these multipotent populations throughout life, different responses to and impacts of aging can be anticipated.

Aging of HSCs is typically manifested by anemia, impairment of adaptive immune function due to a reduced lymphoid differentiation, and expansion of myeloid cells and HSCs in the bone marrow [261,296–301]. The decline in functionality was initially thought to reflect intrinsic changes to the HSCs themselves; however, recent studies suggest that signals from the aged bone marrow microenvironment are at least partially responsible [295,302–304]. For example, the increased local concentration of the inflammatory

cytokine Rantes/CCL5 promotes a bias toward myeloid differentiation [305], and the decreased plasma concentration of SDF-1/CXCL12 has been implicated in the increased turnover of HSCs [306]. When aged HSCs are cultured *in vitro*, there is no apparent difference in cell proliferation or colony-formation [307], and aged HSCs are still able to reconstitute all lineages when transplanted to a young donor [308–310]. However, decreased capacities for homing and engraftment are observed with aged HSCs [307], though some deficiencies can be reversed through exposure to an appropriate microenvironment [311].

The primary indication of aging in skeletal muscle is the decreased ability to regenerate following injury, with recovery taking longer and the regenerated muscle fibers exhibiting smaller diameters with an increased presence of fibrosis [40,312]. When cultured *in vitro*, aged satellite cells also display an increased propensity to differentiate toward adipocyte [313] or fibroblast phenotypes instead of to a myoblast phenotype [103]. The increased conversion from a myogenic to a fibrogenic lineage has been attributed to activation of canonical Wnt signaling, which may stem from an increased presence of Frizzled-binding proteins found in the aged serum [103]. Additionally, the niches of aged satellite cell populations with limited self-renewal capacity contain elevated levels of fibroblast growth factor-2 (FGF-2). In aged satellite cells which have retained the capability for self-renewal, the FGF-inhibitor Sprouty1 is expressed at high levels, with exogenous inhibition of FGF signaling also found to prevent the exhaustion of satellite cells [314].

In contrast to the unchanging quantity of hematopoietic stem cells and satellite cells, the raw numbers of neural stem cells decline with age, which is likely responsible for

the difference in physiological function [315–317]. In aged rodents, decreases in olfactory and cognitive function are observed, likely linked to the decreased numbers of NSCs in both the subventricular zone and the hippocampus, respectively [318–320]. When cultured *in vitro* as neurospheres, aged NSCs also demonstrate a decreased capacity for self-renewal [317]. The paracrine secretion of Wnt3 by astrocytes is essential for NSCs to retain their capacity for neurogenesis, and a reduced number of Wnt3-secreting astrocytes and a lower overall concentration of Wnt3 in the brain are observed with aging [321]. Overall, changes in the extrinsic environments lead to decreased functionality of all three stem cell populations, though the way in which the dysfunctionality manifests itself differs.

To counteract the unsupportive environment found in aged tissues, several approaches have been investigated to rejuvenate stem cell populations. There are several bodies of work that suggest that factors or materials from "younger" sources are capable of improving cell function. Parabiosis, a century-old technique that involves the union of the circulatory systems of two animals [322,323], has reemerged as a powerful technique to interrogate the influence of young and aged systemic milieus on cell and tissue function [324]. Systemic molecules present in younger mice improve function in aged mice connected via heterochronic parabiosis, including enhanced wound healing [37,38], improvement in muscle satellite cell function [39–41], rejuvenation of neural cells and cognitive function [42–45], and reversal of cardiac hypertrophy [46]. An additional approach to rejuvenate cell populations has been to expose them to extracellular matrix (ECM) components derived from younger cells. The decreased capacity for self-renewal and osteogenic differentiation observed in MSCs derived from older (18 month) mice was reversed by culturing the MSCs *ex vivo* on ECM produced by young (3 month) femoral

marrow cells [325], and the culture of adult MSCs on ECM produced by fetal MSCs promoted increased proliferation in comparison to ECM produced by adult MSCs [326].

Similar to several previous approaches to rejuvenation, the paracrine actions of trophic factors derived from pluripotent cells may provide analogous signals that enable dysfunctional adult stem cells to regain a more "youthful" proliferative or regenerative capability. In preliminary studies with conditioned media obtained from undifferentiated human embryonic stem cells, promotion of proliferation was observed in myoblasts isolated from aged mice [35,250,274]. In an additional report, media conditioned by induced pluripotent stem cells prevented stress-induced senescence of rat cardiomyocyte-derived H9C2 cells [327], which may translate to an aged system. In a slightly more eccentric vein, a recently clinical study in South Korea injected conditioned media obtained from hESC-derived endothelial progenitor cells into one side of the face using microneedle rollers, while the other side was injected with saline [328]. After 10 weeks of biweekly treatment, significant improvements in the presence of pigmentation and wrinkles were observed in the side of the face given the stem cell-derived growth factors.

There are several specific ESC-produced factors identified in Chapter 5 that have been implicated in aging. The serum concentration of insulin-like growth factor-1 declines with age [329]; however it has also been observed that IGF-1 signaling can potentiate the aging process, as mice with reduced IGF-1 levels in the serum exhibit reduced growth but extended lifespan [227,330–332]. IGF-1 also plays a critical role in muscle regeneration, and expression of IGF-1 in aged muscle supports skeletal muscle repair [333,334]. Insulin-like growth factor binding proteins (IGFBPs) are high affinity binders of IGF-1 and IGF-2 and act primarily to transport IGFs in the serum and to regulate IGF activity. High levels

of IGFBP-2 were found to be expressed and secreted by ESCs (Chapter 5), and IGFBP-2 is the primary IGFBP found in the mammalian brain and cerebral spinal fluid. IGFBP-2, which is also the major fetal binding protein, has a much higher affinity for IGF-2 than IGF-1 [335]. IGFBP-3 is the primary binder of IGF-1, and the decreased serum concentrations of IGFBP-3 with age may be causally linked to the decreased amounts of IGF-1 [336,337]. Though the complex interplay of IGFBPs with IGFs and the role of the system with aging are still under active investigation [330], the family of growth factors appears to play a critical role in many processes related to aging. Other proteins expressed and/or produced by ESCs that have been implicated in aging include SDF-1, which is present in lower serum concentration with age and has been associated with the increased turnover and decreased function of HSCs [306]. ESCs also express Wnt3, and decreased concentrations of Wnt3 in the brain with age have been linked to decreased neurogenic function [321]. Growth differentiation factor-11 (GDF-11) has been identified in several heterochronic parabiosis studies [41,43,46] to mediate age-related phenotypes, including cardiac hypertrophy, the decreased capacity for skeletal muscle regeneration, and reduced neurogenesis. While GDF-11 was expressed more highly by embryonic fibroblasts and mesenchymal stem cells **(Figure 5.7)**, GDF-11 was also present in ESC lysates (data not shown). Overall, the paracrine actions of trophic factors derived from pluripotent cells may provide signals to enable dysfunctional adult stem cells to regain a more "youthful" regenerative capability.

7.2 Extension to extracorporeal devices

The design of a continuously perfusable system for delivering stem cell secreted factors conjures up images of a platform which directly integrates into the circulation.

Dialysis, a common medical procedure used in patients with kidney failure, functions by exposing circulating blood to a semi-permeable membrane to facilitate diffusion of highly concentrated waste products out of the blood. A similar paradigm could be employed to deliver beneficial paracrine factors secreted by cell populations, analogous in some ways to the parabiosis studies in which an inadequate systemic composition is supplemented with beneficial factors. The development of an extracorporeal device based on the packed-bed design (Chapter 4) to deliver cell-secreted products would allow for sustained delivery and release of factors without complications of directly transplanting cells, such as immune rejection or, in the case of stem cell populations, teratoma formation.

A similar approach to this envisioned paradigm has been previously investigated for bioartificial liver-assist devices. The goal of bioartificial liver devices is to assist with the detoxification functionality of the liver for patients transitioning to a transplant or in need of temporary support [338]. Hepatocytes have been cultured within the device as single cells anchored onto microcarriers [339] and hollow fibers [340,341] or microencapsulated within hydrogel beads [342,343]. Aggregated hepatospheres have also been encapsulated in hydrogel matrices [344], and the three-dimensional spheroid culture of the hepatocytes led to a two-fold increase in metabolic activity in comparison to encapsulated single hepatocytes [345], demonstrating the advantages to using platforms which enable 3D culture. Ultrafiltration membranes are used in the bioartificial liver devices to isolate the enclosed hepatocytes from patient immune cells and molecules [338]. Several blood flow configurations through the devices have been explored. For hollow fiber reactors, the hepatocytes have been cultured within the fibers in collagen gels while the blood moves through the extracapillary space [346], or the hepatocytes have been

grown on the outer surface of the fibers while the blood flows through the hollow fibers [340]. Fluidized bed configurations consisting of microencapsulated hepatocytes have also been explored [347–349], thus there is precedent for the use of packed bed perfusion systems as successful extracorporeal devices.

7.3 Material design parameters to control and enable trophic factor delivery

In the context of this dissertation, alginate was selected as the material for encapsulation for a number of reasons, including its historical prevalence and its biocompatible and gentle cross-linking procedure. However, more advanced materials exist and/or are capable of being synthesized which may enhance the production and delivery of stem cell secreted factors. While it was determined that the composition of alginate employed could shift the phenotype of the enclosed ESCs (Chapter 3), more direct material modifications could be made to control cell fate and thus regulate the identity and quantity of secreted factors. Additionally, the way in which the encapsulation material interacts with the secreted factors could be useful for modulating the composition of molecules delivered downstream.

Modifying the material properties of microbeads and microcapsules can influence stem cell differentiation by mimicking elements of the native microenvironment and/or through specific functionalization with relevant protein molecules. For example, alginate-gelatin microcapsules with functional properties more akin to the native adipogenic microenvironment led to higher proliferation and more efficient adipogenic differentiation of entrapped adipose-derived stem cells (ADSCs) when compared to those encapsulated in alginate without gelatin [364]. Additionally, functionalizing agarose with vascular

endothelial growth factor (VEGF) yielded more efficient differentiation of microencapsulated mESCs to blood progenitors than soluble treatment with VEGF [146], and increasing collagen concentrations and/or initial cell seeding density of hMSCs encapsulated in collagen beads enhanced chondrogenesis [365]. By functionalizing the material used to encapsulated the enclosed stem cells, more direct control over the downstream composition of secreted factors could be achieved.

In addition to using material properties to control cell phenotype, the physical interactions of the material with the secreted species could be used as a sort of filtration system. The charge of the hydrogel polymer can be used to selectively bind and sequester molecules of the opposing charge, thus limiting their diffusion and delivery downstream. For example, glycosaminoglycan-based materials are negatively charged and can therefore be used to sequester positively-charged growth factors, such as bone morphogenetic protein-2 (BMP-2), fibroblast growth factor-2 (FGF-2), and vascular endothelial growth factor (VEGF) [366,367]. Alginate is also a negatively charged polymer and likely reduced the diffusion of these positively-charged proteins out of the microbeads. An additional material property which can be modulated to restrict the diffusion of certain molecules is the pore size, which has been taken advantage of in microencapsulation systems to prevent access of immune molecules to the enclosed cells. To prevent the release of large molecules from the hydrogel, increasing the cross-linking density and polymer weight percentage generally decrease the pore size, or a surface coating such as poly-L-lysine can be applied to provide a tighter diffusive barrier [368]. To allow for diffusion of large structures, such as microvesicles, several approaches have been applied to increase hydrogel pore size, including electrospinning, gas foaming, lyophilization, solvent casting with particle

leaching, and the creation of hydrophilic–hydrophobic hybrid hydrogels [369]. Increasing the pore size with these methods can also facilitate cellular processes, such as proliferation and migration.

7.4 Microvesicles as paracrine mediators

While the focus of this dissertation has been on soluble paracrine factors, there is increasing evidence regarding the role of extracellular vesicles as intercellular delivery vehicles of proteins, lipids, and nucleic acids. Though microvesicles were identified in human plasma almost 50 years ago [350], they were widely regarded as insignificant membranous debris until recently. Extracellular vesicles are comprised of many subcategories of vesicles ranging from 20 nm to 1 μm in diameter, including nanoparticles, exosomes, microparticles, microvesicles, and apoptotic blebs [351]. Exosomes, which are in the smaller range of 40-100 nm, are derived from endosomal membranes that have been expelled from the membrane of activated cells, while microvesicles (100 nm to 1 μm) are shed from the plasma membrane through a budding process [352,353]. Microvesicles enable cell-cell communication and represent a unique endogenous approach for horizontal gene transfer, as most microvesicles contain both messenger RNAs (mRNAs) and non-coding RNAs like microRNAs (miRNAs) [354].

Microvesicles are produced by most cell populations, including pluripotent and multipotent stem cells. The microvesicles derived from adult stem cell populations, including hematopoietic stem and progenitor cells, mesenchymal stem cells, and neural stem cells, have stimulated pro-regenerative responses in many contexts by increasing cell survival and proliferation while promoting vascularization [355–357]. Analyses of the contents within the microvesicles have found many species of mRNA and miRNA

(including mir126 and mir130 which have been implicated in cell survival and angiogenic mechanisms), bioactive lipids (including sphingosine-1-phosphate and ceramide-1-phosphate), and proteins (including many cytokines and growth factors like stem cell factor and vascular endothelial growth factor) [358].

With most of the focus on multipotent stem cells populations, only a handful of studies have been performed to identify the presence, contents, and functions of pluripotent cell-derived microvesicles. The first report of ESC-derived microvesicles was less than a decade ago based on the hypothesis that the robust self-renewal capacity of ESCs may induce a similar proliferative response in a population of hematopoietic progenitor cells [359]. Indeed, improved survival and increased expansion was observed with the addition of microvesicles isolated from undifferentiated ESC cultures. High concentrations of the Wnt3 protein along with mRNA for pluripotent transcription factors (Oct-4, Gata-2, Gata-4, Scl/Tal1, Nanog, Rex-1, HoxB4), cytokines (Sdf-1, Kit-L, Vegf, Cxcr4, c-Met, Lif, IL-8, Fgf-2, Epo), cell cycle and apoptosis proteins (Cyclin D1, Bcl-xl, Cyclin a2, Bcl-2), structural proteins (Wnt3, Myogenin, VE-cadherin, Cathepsin, Nestin, P-selectin, β-2 microglobulin), and proteolytic enzymes (Mmp-2, Timp-1, Timp-2). Following exposure to the ESC-derived microvesicles, expression of many of these unique genes was observed in the hematopoietic progenitor cells, indicating that the horizontal transfer of genetic information may have prompted the changes in survival and proliferation. The contents of ESC microvesicles were further characterized in a second study, and despite some similarities in the mRNA and protein content between ESCs and their shed microvesicles, certain proteins and RNAs are significantly enriched in the microvesicles [360]. The presence and identity of several miRNAs was also established, in addition to evidence of

ESC microvesicle fusing with and transferring contents to other ESCs and embryonic fibroblasts. The most recent report applied ESC-derived microvesicles to retinal progenitor Müller cells, which exhibited increased expression of genes and miRNAs related to pluripotency, proliferation, early ocular phenotypes, and retinal regeneration and decreased expression of genes and miRNAs associated with differentiation and cell cycle arrest [361]. Taken together, the results of previous studies indicate that microvesicles shed from ESCs play significant roles in regulating the phenotypes of surrounding cells and that a significant portion of their overall paracrine activity may be through extracellular vesicles rather than through the secretion of soluble factors.

Due to the large size of extracellular vesicles in comparison to individual proteins (10 to 1000-fold larger), enabling transport of the vesicles through hydrogel matrices becomes a greater challenge in material design. Typical alginate hydrogels have a pore size of 10-30 nm, significantly smaller than most microvesicles [175,362]. Specialized alginate sponges with larger pore sizes can be produced [363], though the problem of cell containment increases as the size of the microvesicle approaches the size of an individual cell. Based on the alginate hydrogels used for ESC encapsulation in this dissertation, it is unlikely that significant transport of microvesicles to the downstream perfusate of the packed bed reactor was achieved. It is interesting that a similar trend in increased proliferation of hematopoietic progenitor cells (in comparison to the results of [359]) was achieved despite the lack of microvesicles, which indicates that a significant paracrine response can be achieved based on the delivery of soluble proteins alone. The culture of cells in hydrogels with molecular weight cut-offs (MWCOs) lower than the average

diameter of microvesicles could thus act as a simple method for screening paracrine interactions.

APPENDIX A

SINGLE-CELL ANALYSIS OF EMBRYOID BODY HETEROGENEITY USING MICROFLUIDIC TRAPPING ARRAY[4]

A.1 Introduction

Pluripotent embryonic stem cells (ESCs) have many potential applications as a cell source for regenerative medicine and as a vehicle to attain new insights into embryonic development. Though ESCs are clonal and therefore are often assumed to exist as a homogenous cell population, there are subtle discrepancies in cell phenotype even in the undifferentiated state prior to the induction of differentiation [370,371]. It has been suggested that undifferentiated stem cells exist as a heterogeneous population so they can be simultaneously influenced to differentiate while also maintaining their ability for self-renewal [372]. Heterogeneity may result from the ability of a single cell type to interconvert stochastically between different pluripotent states, as it has been observed that ESCs can occupy a continuum of cell states, each with their own distinct phenotypic characteristics [373]. Examples of *in vivo* heterogeneity of pluripotent cells, such as the "salt-and-pepper" expression of transcription factors in the inner cell mass [374], imply that such diversity is not simply a product of *in vitro* culture; in fact, the diversity may confer an innate response to environmental or physiological stress [375] via cells existing in a bivalent state in which they are primed for differentiation while retaining self-renewal capacity [376]. In addition

---

[4]Modified from: Wilson JL, Suri S, Singh A, Rivet CA, Lu H, McDevitt TC. Single-cell analysis of embryoid body heterogeneity using microfluidic trapping array. Biomed Microdevices 2014; 16:79-90.

to heterogeneity of the pluripotent state of ESC populations, often some level of spontaneous differentiation exists within the undifferentiated population of cells [377]. Attempts to direct the differentiation of an initially heterogeneous population of stem cells is likely to compromise the overall yield and efficiency, as cells in different states may respond differentially to the same stimuli. Thus, in order to efficiently proceed with stem cell applications and directed differentiation methods, it is necessary to understand and account for the presence of multiple cell states within a population of stem cells.

Embryonic stem cells are often differentiated as three-dimensional multicellular aggregates referred to as "embryoid bodies" (EBs) due to their ability to spontaneous yield derivatives of the three germ lineages simultaneously [154]. EB differentiation is commonly used to model morphogenesis in addition to differentiation since analogous structures and patterns are observed within EBs that mimic the morphogenic events of early embryonic development [20,21,23,378–380]. Significant research has been conducted to examine the ability of different biochemical and environmental factors to direct EB differentiation [17,18], and EB formation remains a critical step in many differentiation protocols [154,381–386]. Differentiation of cells as three-dimensional multicellular aggregates inherently adds the complication of spatial gradients that can differentially impact cell phenotypes between the center and exterior of EBs [387]. Consequently, the size of EBs used has been found to impact the differentiation propensity [388–392]; for example, larger EBs tend to have a greater tendency toward cardiac differentiation than smaller EBs [184–186] . However, it is difficult to directly compare studies since EB formation methods and size ranges differ from study to study, thus definitive correlations between size and differentiated phenotypes have been mixed. Furthermore, aggregate size

alone does not account for all the variance in EB phenotype, as heterogeneity between EBs of the same size is often observed [17], even when all other parameters are seemingly taken into account.

One of the challenges of investigating the cellular composition of EBs is the deficiency of current analytical methods to determine the phenotype of all of the individual cells that comprise a single aggregate. Examining phenotypic properties on a single cell level provides more information than population averaging-based methods, as one can discern whether a small subpopulation is solely responsible for the change in expression or if all cells in the population are undergoing similar changes [393]. Previous research has demonstrated that ESC gene expression results differ greatly when examined at a single cell, rather than a population, level [394], further motivating the development of high throughput methods for investigating single stem cell fate. Existing methods, such as flow cytometry, provide a high-throughput means to analyze phenotypic characteristics of a cell population, but typically require cell quantities (10^{5-6}) that are much greater than the number of cells comprising a single multicellular aggregate (10^{3-4}). Confocal microscopy, another common analytical method, is a low-throughput process that has a limited capacity to image three-dimensional tissues [395–397]. Due to the high cell density of EBs [17], which do not exhibit a large degree of extracellular matrix at early stages of differentiation [236], imaging greater than 50 μm into an EB has been challenging due to optical limitations.

Analytical techniques that enable increased understanding of when and where heterogeneity is occurring in a cell population could lead to better assessments of directed differentiation techniques. Therefore, the objective of this study was to develop an

approach to analyze the individual phenotypes of cells not only from populations of EBs, but single EBs as well. To achieve this, a microfluidic cell trap device originally designed to examine calcium dynamics in Jurkat cells [398] was adapted and validated to examine expression of the pluripotent transcription factor OCT-4 in single cells from EBs of different sizes (defined by the initial number of cells per aggregate) and at different stages of differentiation. Additionally, single cells from dissociated pooled EBs or individual EBs were examined separately to discern potential differences in the value or variance of expression between the different methods of analysis. The results of this study indicate that examining single cell phenotype using a microfluidic approach can provide previously unidentified information about heterogeneity of EBs and may act as a complementary analysis method that provides more specific information regarding single stem cell fate(s) within complex multicellular aggregates.

A.2 Methods

A.2.1 Microfluidic device fabrication

Polydimethylsiloxane (PDMS) devices were fabricated via soft lithography rapid prototyping and replica molding, followed by plasma-bonding onto glass slides [398]. Briefly, negative molds were fabricated on silicon wafers using photoresist (SU8-2010, 14–16 μm, and SU8-2002, 1.5–3 μm thickness) (Microchem) and treated with tridecafluoro-1,1,2,2-tetrahydrooctyl-1-trichlorosilane vapor (United Chemical Technologies, Bristol, PA). PDMS with base polymer to crosslinker ratio of 10:1 was molded onto wafers and cured at 70°C for 2 hours. Individual devices were cut, access

holes were punched and devices were bonded in an air plasma. Devices were stored at room temperature until further use.

A.2.2 Embryonic stem cell culture

Murine ESCs (D3 cell line) were cultured on tissue culture-treated polystyrene dishes (Corning Inc., Corning, NY) adsorbed with 0.1% gelatin (Millipore, EmbryoMax). Undifferentiated ESC culture media consisted of Dulbecco's modified Eagle's medium (DMEM) (Mediatech) supplemented with 15% fetal bovine serum (Hyclone, Logan, UT), 100 U/mL penicillin, 100 μg/mL streptomycin, and 0.25 μg/mL amphotericin (Mediatech, Herndon, VA), 2 mM L-glutamine (Mediatech), 1x MEM non-essential amino acid solution (Mediatech), 0.1 mM 2- mercaptoethanol (Fisher Scientific, Fairlawn, NJ), and 10^3 U/mL of leukemia inhibitory factor (LIF) (ESGRO, Chemicon, Temecula, CA). Cultures were replenished with fresh media every other day and passaged at approximately 70% confluence.

A.2.3 Embryoid body (EB) formation and culture

A single cell suspension of undifferentiated ESCs was obtained through dissociation of monolayer cultures with 0.05% trypsin-EDTA (Mediatech). Aggregation of ESCs was achieved by centrifugation (200 rcf) of ESCs into 400 μm diameter polydimethylsiloxane (PDMS) micro-wells (Aggrewell™, Stem Cell Technologies, Vancouver, Canada), as previously reported [19,152]. The cell seeding density was varied to achieve approximately 250 or 1000 cells per individual well. The ESCs were incubated in the wells for approximately 20 hours in undifferentiated ESC culture media without LIF to allow for EB formation. The resulting EB population was transferred to suspension culture (approximately 1500 EBs in 10 mL of undifferentiated ESC culture media without

LIF) in sterile 100 x 15 mm bacteriological grade polystyrene Petri dishes (BD, Franklin Lakes, NJ) and maintained on rotary orbital shakers [166] at a frequency of approximately 65 rpm. A 90% media exchange was performed every other day following gravity-induced sedimentation of the EBs in 15 mL conical tubes. Suspension cultures were maintained for up to 10 days of differentiation.

A.2.4 Cell loading into microfluidic devices

At days 5 and 10 of differentiation, EBs were collected and dissociated into a single cell suspension by incubation in 0.25% trypsin-EDTA and trituration every 5 minutes for 20 minutes. After 10 days of differentiation, individual EBs were manually removed from the plate, imaged, and similarly dissociated using 0.25% trypsin. The resulting cell suspensions were centrifuged (200 rcf, 5 minutes) and resuspended in culture media supplemented with 3 mM EGTA for a 30 minute incubation (37°C) to inhibit intercellular adhesion and reduce clogging in the microfluidic device. A LIVE/DEAD cell assay (Invitrogen) was performed to evaluate cell viability post-loading. Prior to cell loading, the devices were perfused with a 2% solution of bovine serum albumin (Millipore). Single cells were loaded into the devices by pipetting the cell suspension into an inlet made with a 19-gauge needle. The cells were loaded into the device by gravity-driven flow. Once loaded, the device was perfused with a 4% paraformaldehyde solution (Alfa Aesar) for 10 minutes to fix cells. Cells were also collected at day 0 (prior to EB formation) and similarly loaded into the devices. Cell-laden devices were stored with PBS at 4°C until immunofluorescent staining was performed for parallel samples at the same time.

A.2.5 On-chip immunofluorescent staining

Immunofluorescent staining was performed in the devices by attaching a pipette tip containing the solution into the inlet and attaching 2.5 ft of polyethylene tubing (PE3, Scientific Commodities) to the outlet to induce gravity-driven flow. The cells were permeabilized with 0.05% Triton X and 2% donkey serum in PBS for 45 minutes at room temperature prior to overnight incubation at 4°C with the primary antibody against OCT-4 (Santa Cruz Biotechnology sc-8628; 1:100 in 2% donkey serum in PBS). The devices were perfused with PBS for 15 minutes to wash the cells prior to 1 hour incubation with the secondary antibody solution (1:200 AlexaFluor®488 donkey anti-goat in 2% donkey serum in PBS). The devices were perfused with PBS for 15 minutes to wash the cells prior to 10 minute incubation with blue whole cell stain (HCS CellMask^{TM}, Invitrogen). A final 15 minute perfusion with PBS was performed prior to imaging.

A.2.6 Cell trap imaging and image analysis

The devices were imaged using a Nikon TE 2000 inverted microscope equipped with a SPOT Flex camera (Diagnostic Instruments). Each chamber in the device was imaged on three channels (phase, Hoechst, and FITC). Image analysis was performed using ImageJ software (http://rsbweb.nih.gov/ij/). A threshold was applied to the whole cell stain image (blue channel) to determine the cell area. Subsequently, the fluorescent intensity of OCT-4 staining (green channel) was determined for individual cells and normalized to the cell area. Area and intensity values were exported to Microsoft Excel for further analysis.

A.2.7 Flow cytometry

EBs were collected and dissociated into a single cell suspension through incubation in 0.25% trypsin-EDTA and trituration every 5 minutes for 30 minutes. Cells were also collected at day 0 prior to EB formation. The cell suspension was centrifuged (200 rcf, 5

minutes) and resuspended in culture media supplemented with 3 mM EGTA for 30 minute incubation (37°C), as was performed prior to loading in the microfluidic devices. Cells were fixed in 4% paraformaldehyde, washed 3x with PBS, and stored at 4°C until staining was performed. Cells were permeabilized in 0.05% Triton X-100 in blocking buffer (1 mg/ml BSA and 0.1% Tween20 in PBS) for 30 minutes, then washed in blocking buffer for 15 minutes. Cells were incubated at room temperature with the primary antibody against OCT-4 (Santa Cruz Biotechnology sc-101462; 1μg/million cells) for 1 hour. Cells were washed with blocking buffer, then incubated with the secondary antibody (AlexaFluor®488 donkey anti-goat at 1μg/million cells) for 30 minutes at room temperature. The cells were resuspended in 300 μL blocking buffer, filtered through the 35μm cell-strainer cap of a 5 mL polystyrene round-bottom tube (BD Biosciences, San Jose, CA), and analyzed with an Accuri C6 flow cytometer for a minimum of 10,000 events. Normal goat IgG was used in place of primary antibody incubation as an isotype control, with positive gates set above 2% of the IgG isotype control population. Analysis was performed using FlowJo software (Tree Star, Inc., Ashland, OR).

A.2.8 Whole mount staining and imaging

EBs were washed in PBS, fixed for 30 minutes in 4% paraformaldehyde, and washed 3x with PBS. EBs were stored in PBS at 4°C until staining was performed. EBs were permeabilized for 30 minutes in 1.5% Triton X-100, re-fixed in 4% paraformaldehyde for 15 minutes, and blocked in wash buffer (2% donkey serum, 0.1% Tween-20 in PBS) for 3 hours. Samples were incubated in OCT-4 primary antibody (Santa Cruz Biotechnology sc-8628; 1:100) overnight at 4°C, rinsed with wash buffer (3 times, 15 min), and incubated with the secondary antibody solution (1:200 AlexaFluor®488 donkey anti-

goat in wash buffer) and Hoechst (1:100) for 4 hours at 4°C. To image, samples were re-suspended in a low volume of wash buffer and imaged with a Zeiss LSM 700-405 confocal microscope (Carl Zeiss Inc.).

A.2.9 Statistics

All population-based experiments were performed with triplicate samples from independent conditions (n=3). The data is represented as the mean of the independent replicates, and the error bars represent the standard error of the mean. Before performing statistical analysis, data were normalized using a Box–Cox power transformation to equalize variance. A two-way ANOVA was calculated between the analysis method (cell trap and flow cytometry) and experimental groups, with post hoc Tukey analysis to determine significant differences ($p < 0.05$) between the different analysis methods and experimental groups. A one-way ANOVA was calculated between the individual groups (population and single EB), with a post hoc Tukey analysis to determine significant differences ($p < 0.05$) between the groups.

A.3 Results

A.3.1 Embryonic stem cell (ESC) on-chip analysis

To assess heterogeneity in the cell populations comprising embryoid bodies (EBs), murine embryonic stem cells were aggregated within PDMS microwells at two different seeding densities to form distinct EB sizes, transferred to suspension culture, and allowed to differentiate for up to 10 days **(Figure A.1)**. After five days of differentiation, EBs of each size were dissociated into single cell suspensions, and the population from each plate was divided for cell trap and flow cytometry analysis. Intact EBs were also collected for

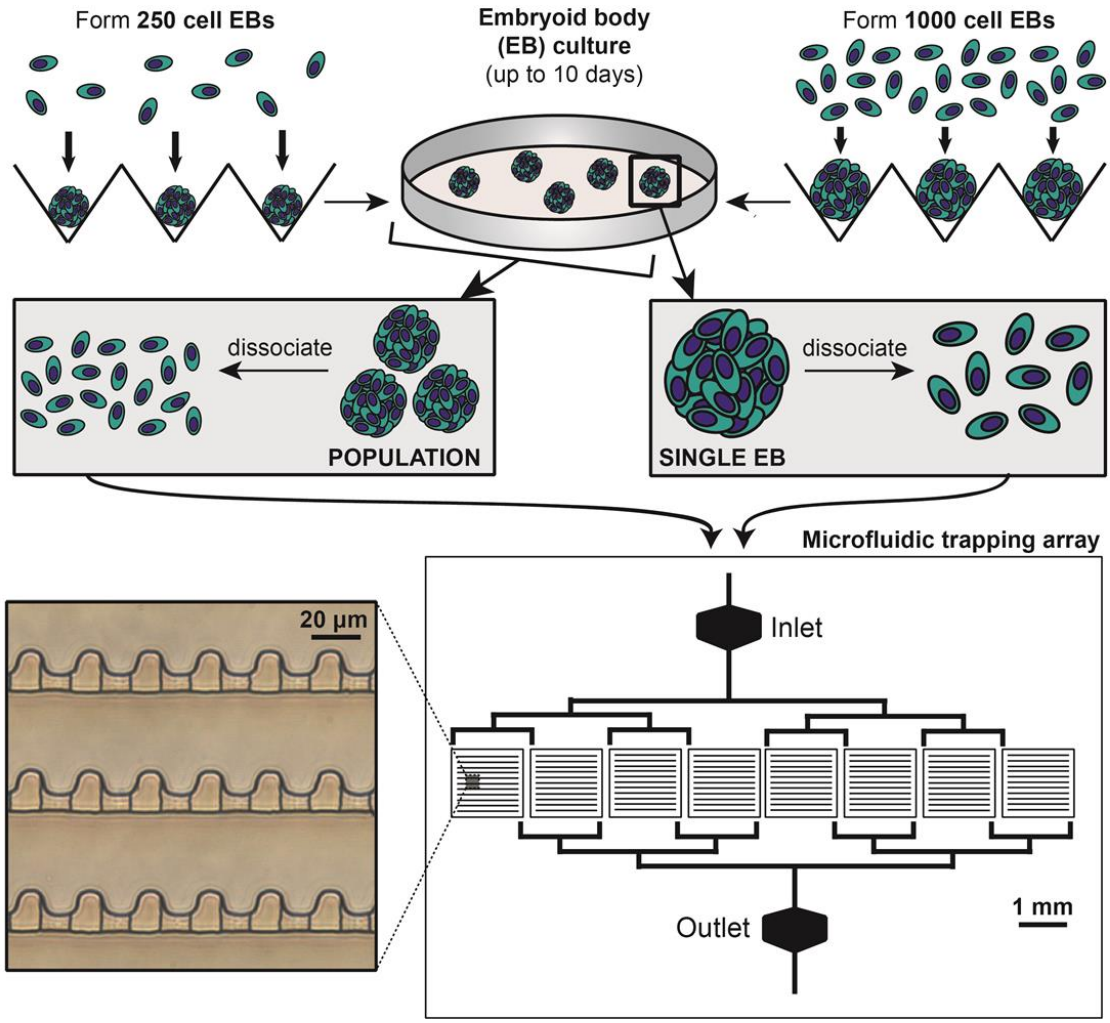

Figure. A.1. Overview of experimental approach for cell trap device. Embryoid bodies (EBs) of 250 or 1000 cells were formed via forced centrifugation in PDMS microwells and cultured for up to 10 days of differentiation. After 5 or 10 days of suspension culture, single cells were obtained from either from a dissociated population of EBs (~1500 total) or from hand-picked individual aggregates, and loaded into the microfluidic cell trapping array for immunostaining and image analysis.

whole mount immunostaining analysis. The single cell suspensions designated for cell trap analysis were loaded into the microfluidic device using gravity-driven flow as previously described [398]. Populations of EBs were similarly processed after 10 days of differentiation, and single EBs were individually removed manually from the cultures, imaged, and dissociated prior to loading into cell trap devices.

Prior to EB formation, the ESC population used to form the EBs **(Figure A.2a)** was dissociated into single cells and loaded into cell trap devices or reserved for flow cytometric analysis. After five days of EB differentiation, differences in diameter were visually observed between the EBs initially seeded at a ratio of 250 cells per EB **(Figure A.2b)** and the EBs seeded at 1000 cells per EB **(Figure A.2c)**. By day 10 of differentiation **(Figure A.2d, A.2e)**, the presence of distinct EB sizes was no longer prevalent, though minor variability in size was observed in both cultures. Single cells derived from the different populations exhibited efficient cell loading into the device **(Figure A.2f-o)**, with a low incidence of both empty traps and multiple cells per trap (<10%). The cells were stained on-chip using a whole cell stain (blue), with the intensity remaining consistent throughout all groups **(Figure A.2f-j)**. On-chip immunofluorescent staining for the pluripotent transcription factor OCT-4 was performed just prior to whole cell staining. The undifferentiated ESC population used for EB formation exhibited high intensity staining for OCT-4 at day 0 **(Figure A.2k)**, and the intensity was reduced as the cells differentiated as EBs **(Figure A.2l-o)**. After five days of differentiation, fewer cells expressed OCT-4 with an intensity as great as those observed with cells on day 0 **(Figure A.2l, A.2m)** and majority of the cells had a faint antibody signal. At day 10 of differentiation, the cells from the 250 cell EBs appeared to have a relatively uniform additional attenuation of staining

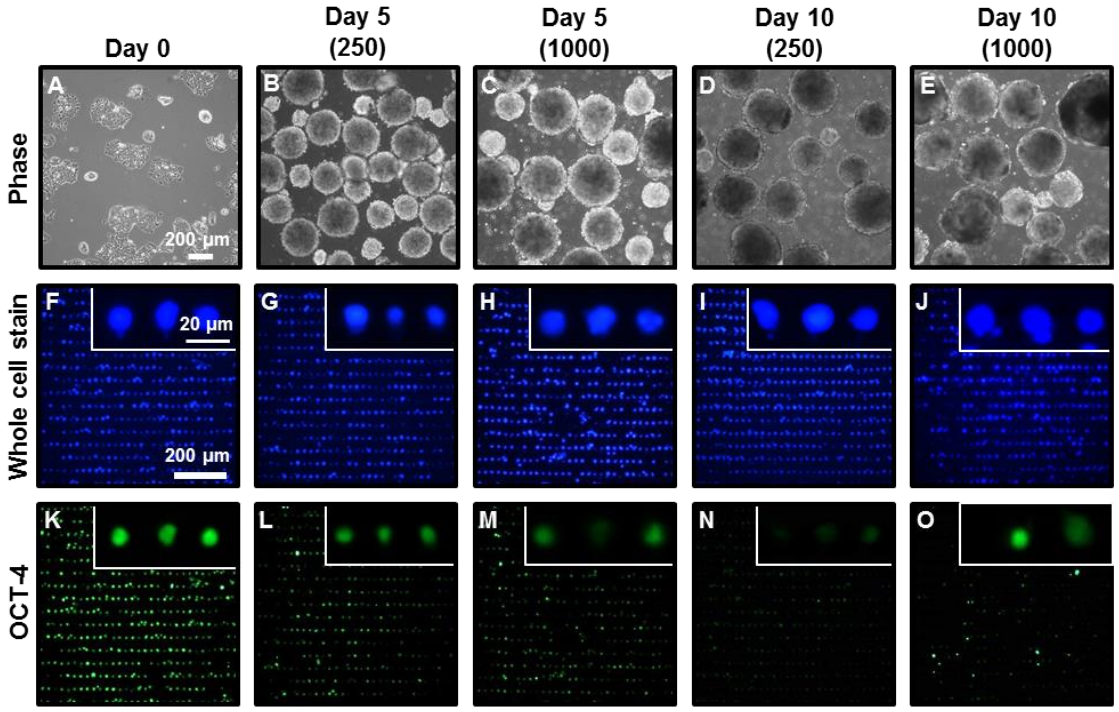

Figure A.2. Image time course and representative cell trap chamber images. Undifferentiated ESCs **(A)** were aggregated to form EBs comprised initially of 250 cells **(B,D)** or 1000 cells **(C,E)**. The dissociated EBs were loaded into the cell traps at days 5 and 10 of differentiation and stained with HCS CellMask™ **(F-J)** and an antibody against the pluripotent transcription factor OCT-4 **(K-O)**. The initial undifferentiated ESC population exhibited bright staining for OCT-4 at day 0 **(K)**, but the intensity decreased as expected as the cells differentiated as EBs **(L-O)**. Scale bar = 200 µm.

intensity **(Figure A.2n)**. In comparison, qualitative analysis of the cells from the 1000 cell EBs indicated that a sub-set of the population of cells retained high levels of OCT-4 expression, while most cells exhibited low to no expression of OCT-4 **(Figure A.2o)**.

A.3.2 Examining populations of embryoid bodies (EBs) with cell traps and flow cytometry

In order to validate the cell trap analytical method, flow cytometry analysis was performed on cells dissociated from a population of EBs. Overall, both forms of analysis detected a similar decrease in OCT-4 expression **(Figure A.3)** as the cells differentiated. Based upon cell trap analysis, the 250 cell EB population exhibited an average intensity of 38% ± 3% and 16% ± 3% at days 5 and 10, respectively and relative to the day 0 ESCs. In comparison, analysis of the 1000 cell EB population in the cell trap device displayed 44% ± 22% and 42% ± 17% of the day 0 intensity at days 5 and 10, respectively. The minor disparities between the cell trap and flow cytometry methods were not statistically significant ($p = 1.000, 0.561, 0.198, 0.974$).

A benefit of single cell analysis methods is the ability to examine the variance and heterogeneity of a cell population in addition to calculating simply population average information. Therefore, the OCT-4 intensity values were plotted as histograms in order to examine the variance of OCT-4 expression in the different groups. In general, OCT-4 expression was broadly expressed in the starting ESC population at day 0 **(Figure A.4a, A.4d)**, though several peaks were observed at higher intensities (10-20 units). While most devices exhibited a similar trend, some had a peak at a slightly lower intensity value that was not observed in the corresponding flow cytometry histogram **(Figure A.4a inset)**. After five days of differentiation, there was little variability observed in the 250 cell EB

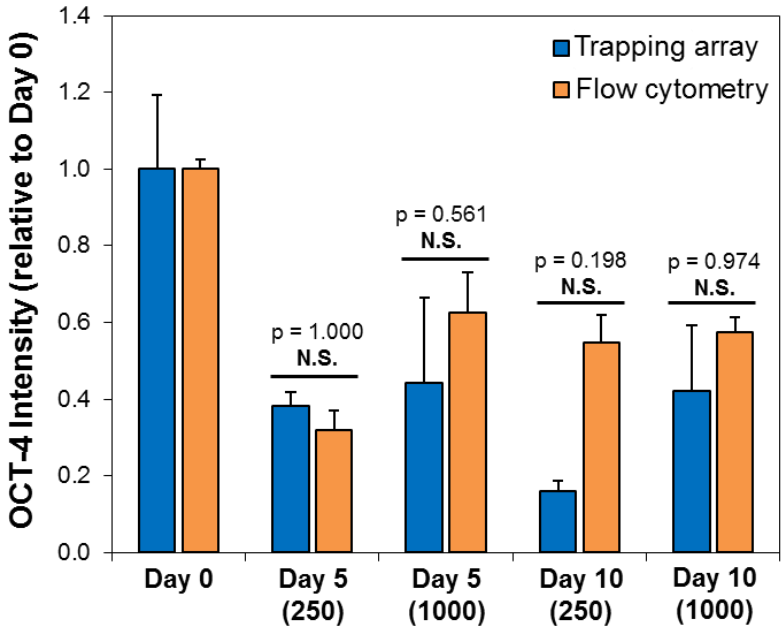

Figure A.3. Comparison of microfluidic trapping array and flow cytometry mean fluorescent intensities. The mean fluorescent intensities were calculated by averaging the intensity of individual cells within the cell trap devices or from the mean intensity values obtained by flow cytomery with a 533/30 nm filter and positive gates set at 2% of the IgG isotype control population. No statistically significant differences were found between the two analytical methods ($p < 0.05$) at any of the time points examined.

population samples **(Figure A.4b)**, whereas the 1000 cell EBs appeared to have more variability between different populations at day 5 **(Figure A.4e)**. After 10 days of differentiation, the variability of OCT-4 expression in the 250 cell EBs remained low **(Figure A.4c)**, with decreased OCT-4 expression reflected by the narrowed peak of the intensity value and leftward shift. In the 1000 cell EBs at day 10 **(Figure A.4f)**, the expression pattern was similar to that at day 5, with more cells exhibiting greater OCT-4 intensity compared to the 250 cell EBs. In general, the shapes of the histograms of the cell trap analysis were in agreement with the flow cytometry results **(Figure A.4 insets)**. For example, the flow cytometry histograms for the 1000 cell EBs at day 5 **(Figure A.4e)** also exhibited a higher degree of variability amongst individual experimental replicates.

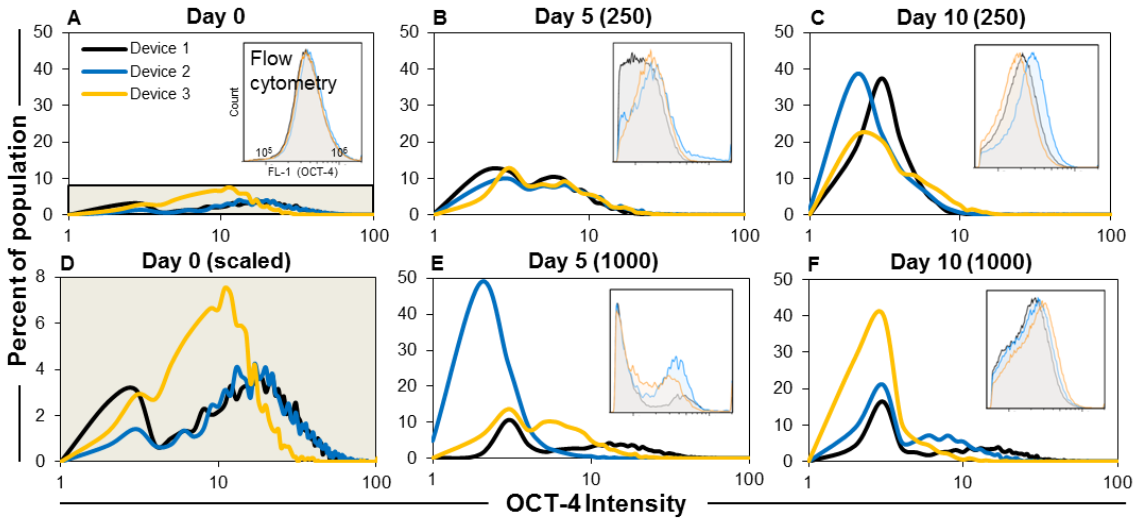

Figure A.4. Histogram analysis of OCT-4 heterogeneity. The percentage of the population with a given OCT-4 intensity (log scale) was plotted to display the value of the peak intensity as well as the width of the peak for the day 0 undifferentiated starting population **(A,D)**, the 250 cell **(B)** and 1000 cell **(E)** EBs at day 5 of differentiation, and the 250 cell **(C)** and 1000 cell **(F)** EBs at day 10 of differentiation. The histogram outputs of the corresponding flow cytometry analysis (cell count vs. OCT-4 intensity) are displayed as insets.

A.3.3 Comparing expression and heterogeneity of single EBs to population values

The microfluidic cell trap device has the unique ability to efficiently and rapidly trap cells from a single EB, thus enabling the analysis of inter-EB variability that could be masked in more common population-based methods. Confocal microscopy techniques allow for examination of the cellularity of single EBs; however, imaging is a low-throughput method that is limited by the lack of complete optical sectioning through densely packed multicellular tissues [396], restricting the information obtained for all the cells in a tissue or EB. For comparison with the single EB results from the cell trap, immunostaining for OCT-4 was performed on intact 250 cell and 1000 cell EBs at days 5 and 10 differentiation, followed by confocal imaging in which optical sections were acquired (depth of 30 μm presented in **Figure A.5**). Decreasing expression of OCT-4 was observed in both sizes between days 5 and 10 of differentiation. After five days of

differentiation, the 250 cell EBs **(Figure A.5a)** generally had similar OCT-4 expression, indicating low inter-EB variability, whereas increased variation was observed between EBs in the 1000 cell EBs at day 5 **(Figure A.5c)**. After 10 days of differentiation, spatially-constrained "pockets" of high and low OCT-4 expression were observed in both groups, though cells highly expressing OCT-4 appeared more frequently in the 1000 cell EBs **(Figure A.5d)** than in the 250 cell EBs **(Figure A.5b)**. These results clearly indicate an increased variability of OCT-4 expression within single EBs in comparison with the more uniform expression of OCT-4 by individual cells at day 5.

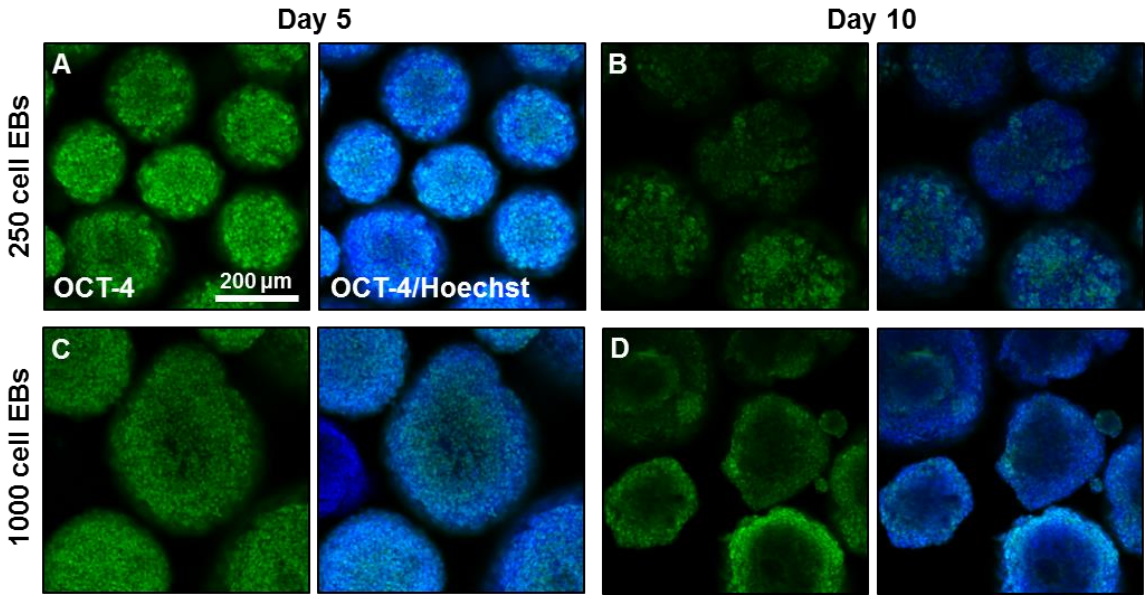

Figure A.5. Whole mount immunostaining for OCT-4 in intact EBs. EBs were collected at the same time points for which single cell expression was analyzed and stained for OCT-4 expression. Images represent optical sections at a 30 µm depth into the EB. The merged images (right panels) signify OCT-4 staining in addition to nuclear counterstaining with Hoechst. Relatively strong expression of OCT-4 was observed in both groups at day 5 **(A,C)**. After 10 days of differentiation, OCT-4 expression decreased in both groups, though it appeared cells with high expression appear more frequently higher in the 1000 cell EBs **(D)** than in the 250 cell EBs **(B)**.

The differences in the intensity and spatial variance of OCT-4 expression within EBs of different sizes over time prompted further investigation into the single cell OCT-4 expression between individual EBs as compared to a population of EBs. Thus, single EBs were manually removed and dissociated individually prior to their loading into the cell trap devices, with approximately 45% of the individual cells from a single EB successfully captured within a device. The reduced capture efficiency could be primarily attributed to the difficulty of dissociating a single EB and the subsequent transfer steps where many cells were lost. The ability to capture many cells from a single EB indicates the power of cell-trap devices despite the difficulty of working with such low cell populations.

The mean OCT-4 intensity values were compared for cells from populations and single EBs at day 10 of differentiation within the cell trap devices. Representative analyses of single EBs are presented in **Figure A.6b** (250 cells/EB) and **Figure A.6c** (1000 cells/EB). In general, the single EBs exhibited lower OCT-4 expression levels than the population-averaged value **(Figure A.6a)**, though this difference was not significant ($p = 0.939$ for 250 cell EBs; $p = 0.137$ for 1000 cell EBs). A decrease ($p < 0.05$) in OCT-4 expression relative to the day 0 ESC starting population was observed for three of the four experimental groups at day 10 of differentiation (250 cell EB population, averaged 250 cell single EBs, and averaged 1000 cell single EBs), indicating that most experimental conditions had significantly decreased pluripotent transcription factor expression by day 10 of EB culture. The 1000 cell EBs assessed at the population level did not exhibit a significant decrease in expression, which may indicate that the cells within the larger EBs may exhibit slower differentiation kinetics than the 250 cell EBs.

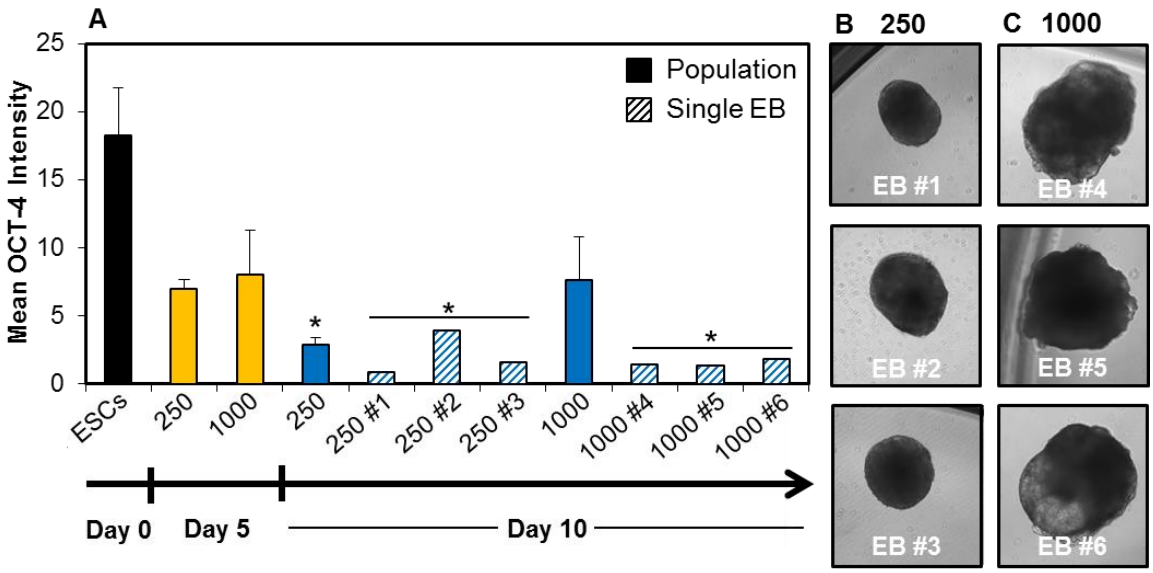

Figure A.6. Population and single EB OCT-4 expression. The mean intensity obtained from the cell trap device was assessed for each condition, including the single EBs **(A)**. The single EBs of both sizes were imaged **(B,C)** immediately prior to their dissociation and loading at day 10 of differentiation. In general, single EBs exhibited lower OCT-4 expression than the population-averaged values **(A)**, though the differences were not statistically significant ($p = 0.939$ for 250 cell EBs; $p = 0.137$ for 1000 cell EBs). * indicates significant decrease in OCT-4 intensity compared to the day 0 starting population ($p < 0.05$).

In an attempt to elucidate whether inter-EB or intra-EB heterogeneity was dominant in the different sizes, the values for each cell analyzed at day 10 of differentiation were arrayed with regard to intensity and cell size/area. Although the flow cytometry scatter plots for the population samples were similar for the two EB sizes **(Figure A.7a, A.7d)**, the cell trap population scatter plots demonstrated that the 1000 cell EB population **(Figure A.7e)** appeared more heterogeneous than the 250 cell EB population **(Figure A.7b)**. The scatter plot for the 250 cell single EBs **(Figure A.7c)** had a similar appearance to the corresponding population scatter plot **(Figure A.7b)**, suggesting that the heterogeneity of phenotypes within individual EBs was more prevalent than the overall heterogeneity between EBs of this size. In contrast, the 1000 cell single EB data exhibited less

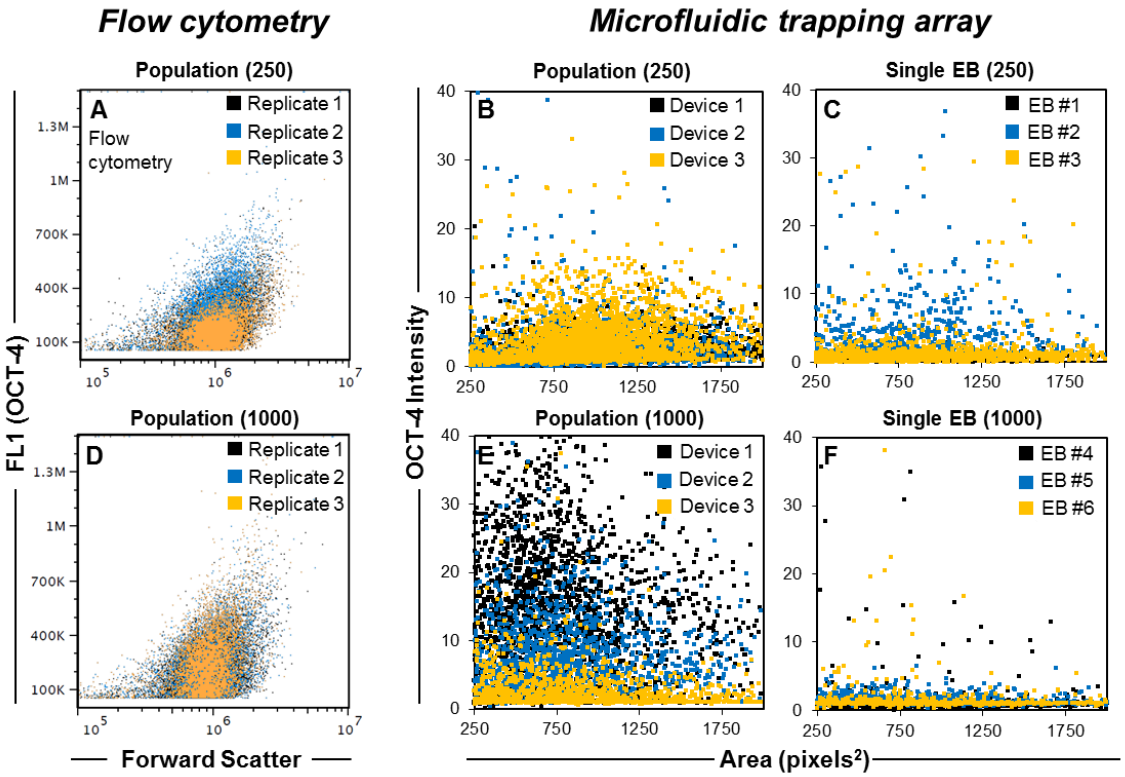

Figure A.7. Heterogeneity of OCT-4 expression in EB populations versus single EBs. Values of OCT-4 intensity vs. forward scatter (or cell size) were graphed as scatter plots for both population and single EB analysis of both sizes at day 10. Corresponding flow cytometry scatter plots for 250 cell EBs **(A)** and 1000 cell EBs **(D)** are displayed for comparison. Similar shapes are observed between the 250 cell population **(B)** and single EBs **(C)** but differential patterns are observed in the 1000 cell population **(E)** and single EBs **(F)**.

heterogeneity than the EB population analysis **(Figure A.7f)**, which indicates that inter-EB heterogeneity was more prevalent for larger EBs of this size.

A.4 Discussion

The differentiation of pluripotent stem cells as embryoid bodies (EBs) remains a common method for inducing differentiation toward many lineages, including cardiac [384,399], hematopoietic [154,385], and neural [383,400]. However, differentiation via EB methods typically gives rise to heterogeneity in the cell population, as most cells differentiate in parallel toward multiple lineages while some may remain undifferentiated. In addition to different media compositions, physical parameters, such as the size of the EBs, can contribute to phenotypic variation through the establishment of nutrient and oxygen gradients [387]. Therefore, the objective of this work was to examine EB heterogeneity on the single-cell level, which was accomplished using a microfluidic cell trap device in combination with on-chip staining and imaging. Information regarding the degree and heterogeneity of single cell OCT-4 expression was obtained for both a population of EBs and for single EBs. The results from the cell trap device were compared with flow cytometry and whole mount immunostaining to compare the overall OCT-4 expression as well as the heterogeneity of expression observed with each approach. Overall, assessing the variability of OCT-4 expression in single EBs in comparison with the variability in a population of EBs represents a novel approach for evaluating how heterogeneity is manifested in EB cultures.

Microfluidic systems are being increasingly used as instruments for sorting stem cells [401–403] and for deciphering stem cell function owing to their capacity to array cells in a high-throughput fashion, to precisely deliver solutions in well-controlled spatial and

temporal manner, and to enable real-time imaging. Several studies have examined microfluidic methods to control EB culture and differentiation on-chip [404,405], although the devices previously developed do not include any downstream analysis of the single cells within the aggregates. Other studies have described devices which enable trapping of single-cell populations [406–408] for cell pairing and real-time monitoring, some of which have examined stem cell populations. Studies with hematopoietic stem cells (HSCs) have been most often described, likely due to their non-adherent phenotype, and include investigations into the differences in proliferation and survival of normal [409] and diseased HSCs [410], as well as the percentage of HSCs in different stages of the cell cycle [411]. Other microfluidic platforms capable of performing on-chip staining and imaging similar to flow cytometry have been described for a number of cell types as a means to decrease reagent volumes and the required cell sample size [412,413], similar to advantages achieved with the device described in this paper. However, there has been a deficiency of microfluidic approaches describing the analysis of small tissue constructs, like EBs, that are difficult to evaluate using typical analytical tools owing to the high cell density and small cell numbers of individual aggregates. The ability to quantitatively examine the protein expression of the single cells that comprise individual EBs, as achieved with the hydrodynamic cell trap in this paper, could provide new information while also complementing emerging strategies offered by microfluidic-based single cell PCR systems [394,414,415] as a means to examine differential gene and protein expression patterns.

In order to substantiate the results obtained with the microfluidic cell trap, the outcomes were compared to those obtained via flow cytometry and whole mount immunostaining. Flow cytometry is perhaps the most common tool for examining single

cell phenotype, and the results from the cell trap generally agreed with those obtained with flow cytometry **(Figure A.3)**. However, some differences were observed for certain groups and time periods (i.e. **Figure A.3**, 250 cell EBs at day 10). Some divergence is to be expected due to the number of cells being sampled in each case. For flow cytometry, a minimum of 10,000 events were collected, and the contribution of non-specific binding could be removed with gates using an isotype control. In contrast, only approximately 2000 cells were examined per microfluidic device. The fact that 20% fewer cells were used for the cell traps compared to flow cytometry may account for some of the variability seen, although it is interesting to note that both analytical tools assessed only a fraction of the cells (< 0.5%) present in an experimental replicate (approximately 2 million cells total). The other method used to compare the results of the cell trap was immunostaining and whole mount imaging using confocal microscopy **(Figure A.5)**. While confocal microscopy is relatively low-throughput, it is useful in that it provides spatial information; however, the technique is technically limited due to poor optical penetration into embryoid bodies greater than 50 μm in diameter. Nevertheless, EBs imaged by confocal microscopy exhibited OCT-4 expression patterns that were consistent with the quantitative data obtained from the cell traps. For example, areas of bright and dim OCT-4 expression were observed in the 1000 cell EBs at day 10 **(Figure A.5d)**, which corresponded to the cell trap images **(Figure A.2o)** and histograms demonstrating the relative proportion of OCT-4 intensities of individual cells **(Figure A.4f)**.

While flow cytometry can be used to evaluate the phenotypic state of a population of EB-derived cells, there is no current method that can easily be used to quantify the phenotypic diversity of single EBs because of the small numbers of cells in single EBs.

Therefore, flow cytometry is unable to aid in the confirmation and deciphering of the lower OCT-4 expression detected in single EBs compared to the average population values **(Figure A.6a)**. One caveat is that the fraction of the sampled population is very small (< 1% of the EBs from a plate of 1500); therefore any observed differences may be based on the limited sampling due to the low throughput nature of the current method. When the variability in OCT-4 expression was inspected for the population and single EBs **(Figure A.7)**, similar patterns were observed in the 250 cell EB population and single EBs, indicating that the individual EBs sampled were representative of the population and/or that variability between EBs (inter-EB variability) was less significant for the 250 cell aggregates and the variance of phenotypes within a single EB (intra-EB variability) governed heterogeneity. In contrast, the divergent patterns of OCT-4 expression observed between the population of 1000 cell EBs and single EBs may indicate that the single EBs examined were not characteristic of the population, or it may signify that the variance of cell phenotypes between individual EBs (inter-EB variability) is greater for larger sized EBs.

The implications of greater inter-EB variability than intra-EB heterogeneity may be that that a culture process is impacting different aggregates in a divergent manner, which may indicate that some EBs are experiencing appreciably different environmental influences than others. On the other hand, if high intra-EB variability is present, this may imply that internal nutrient/oxygen gradients or contrasting local cell-cell interactions are the primary contributor(s) to the observed heterogeneity of cell phenotypes [387,416]. In general, the subtle differences observed in OCT-4 expression between different EB sizes are consistent with previous literature which has demonstrated that larger 1000 cell EBs

tend to exhibit a delayed temporal decrease of OCT-4 expression compared to smaller 250 cell EBs [417], as was found with all of the methods of analysis used in this study **(Figure A.2, A.4, A.5)**.

A.5 Conclusions

Overall, the development and subsequent validation of an approach to quantitatively assess information about individual EBs at a single cell resolution was established, leading to notable findings regarding the variance of OCT-4 expression within single EBs. In the future, coupling of single-cell analysis with long-term live cell imaging could provide additional information regarding the dynamics of protein expression and could lead to an improved understanding about the underlying cause of heterogeneity in stem cell populations. Nevertheless, the approach described will be beneficial in evaluating the variability encountered during stem cell differentiation and can provide more specific information regarding single stem cell fate within complex multicellular aggregates.

REFERENCES

[1] M.J. Evans, M.H. Kaufman, Establishment in culture of pluripotential cells from mouse embryos, *Nature*. 292 (1981) 154–156.

[2] G.R. Martin, Isolation of a Pluripotent Cell Line from Early Mouse Embryos Cultured in Medium Conditioned by Teratocarcinoma Stem Cells, *Proc. Natl. Acad. Sci.* 78 (1981) 7634–7638.

[3] J.A. Thomson, J. Itskovitz-Eldor, S.S. Shapiro, M.A. Waknitz, J.J. Swiergiel, V.S. Marshall, et al., Embryonic Stem Cell Lines Derived from Human Blastocysts, *Science (80-.).* 282 (1998) 1145–1147.

[4] K. Takahashi, S. Yamanaka, Induction of pluripotent stem cells from mouse embryonic and adult fibroblast cultures by defined factors., *Cell*. 126 (2006) 663–76.

[5] J. Yu, M. a Vodyanik, K. Smuga-Otto, J. Antosiewicz-Bourget, J.L. Frane, S. Tian, et al., Induced pluripotent stem cell lines derived from human somatic cells., *Science*. 318 (2007) 1917–20.

[6] M.F. Pittenger, a M. Mackay, S.C. Beck, R.K. Jaiswal, R. Douglas, J.D. Mosca, et al., Multilineage potential of adult human mesenchymal stem cells., *Science (80-.).* 284 (1999) 143–7.

[7] P.A. Zuk, M. Zhu, P. Ashjian, D.A. De Ugarte, J.I. Huang, H. Mizuno, et al., Human Adipose Tissue Is a Source of Multipotent Stem Cells, *Mol. Biol. Cell*. 13 (2002) 4279–4295.

[8] J.E. Till, E. a McCulloch, A direct measurement of the radiation sensitivity of normal mouse bone marrow cells., *Radiat. Res.* 175 (1961) 145–9.

[9] H.E. Broxmeyer, G.W. Douglas, G. Hangoc, S. Cooper, J. Bard, D. English, et al., Human umbilical cord blood as a potential source of transplantable hematopoietic stem/progenitor cells., *PNAS*. 86 (1989) 3828–32.

[10] G. Klein, The extracellular matrix of the hematopoietic microenvironment, *Experientia*. 51 (1995) 914–926.

[11] M. Hines, L. Nielsen, J. Cooper-White, The hematopoietic stem cell niche: what are we trying to replicate?, *J. Chem. Technol. Biotechnol.* 443 (2008) 421–443.

[12] C. Guguen-Guillouzo, A. Guillouzo, Modulation of functional activities in cultured rat hepatocytes, *Enzym. Induction Modul.* 3 (1983) 35–56.

[13] J.M. Lee, P. Mhawech-Fauceglia, N. Lee, L.C. Parsanian, Y.G. Lin, S.A. Gayther, et al., A three-dimensional microenvironment alters protein expression and chemosensitivity of epithelial ovarian cancer cells in vitro., *Lab. Invest.* 93 (2013) 528–42.

[14] A.C. Luca, S. Mersch, R. Deenen, S. Schmidt, I. Messner, K.-L. Schäfer, et al., Impact of the 3D microenvironment on phenotype, gene expression, and EGFR inhibition of colorectal cancer cell lines., *PLoS One*. 8 (2013) e59689.

[15] F. Ruedinger, A. Lavrentieva, C. Blume, I. Pepelanova, T. Scheper, Hydrogels for 3D mammalian cell culture: a starting guide for laboratory practice., *Appl. Microbiol. Biotechnol.* 99 (2015) 623–36.

[16] C.A. DeForest, K.S. Anseth, Advances in bioactive hydrogels to probe and direct cell fate., *Annu. Rev. Chem. Biomol. Eng.* 3 (2012) 421–44.

[17] A.M. Bratt-Leal, R.L. Carpenedo, T.C. McDevitt, Engineering the Embryoid Body Microenvironment to Direct Embryonic Stem Cell Differentiation, *Biotechnol. Prog.* 25 (2009) 43–51.

[18] H. Kurosawa, Methods for inducing embryoid body formation: in vitro differentiation system of embryonic stem cells., *J. Biosci. Bioeng.* 103 (2007) 389–98.

[19] M.D. Ungrin, C. Joshi, A. Nica, C. Bauwens, P.W. Zandstra, Reproducible, ultra high-throughput formation of multicellular organization from single cell suspension-derived human embryonic stem cell aggregates., *PLoS One*. 3 (2008) e1565.

[20] M. Eiraku, N. Takata, H. Ishibashi, M. Kawada, E. Sakakura, S. Okuda, et al., Self-organizing optic-cup morphogenesis in three-dimensional culture., *Nature*. 472 (2011) 51–6.

[21] H. Suga, T. Kadoshima, M. Minaguchi, M. Ohgushi, M. Soen, T. Nakano, et al., Self-formation of functional adenohypophysis in three-dimensional culture., *Nature*. 480 (2011) 57–62.

[22] J.R. Spence, C.N. Mayhew, S. a Rankin, M.F. Kuhar, J.E. Vallance, K. Tolle, et al., Directed differentiation of human pluripotent stem cells into intestinal tissue in vitro., *Nature*. 470 (2011) 105–9.

[23] F. Antonica, D.F. Kasprzyk, R. Opitz, M. Iacovino, X.-H. Liao, A.M. Dumitrescu, et al., Generation of functional thyroid from embryonic stem cells., *Nature*. 491 (2012) 66–71.

[24] M.A. Lancaster, M. Renner, C.-A. Martin, D. Wenzel, L.S. Bicknell, M.E. Hurles, et al., Cerebral organoids model human brain development and microcephaly, *Nature*. (2013).

[25] P. Lu, L.L. Jones, E.Y. Snyder, M.H. Tuszynski, Neural stem cells constitutively secrete neurotrophic factors and promote extensive host axonal growth after spinal cord injury, *Exp. Neurol.* 181 (2003) 115–129.

[26] L. Bai, D.P. Lennon, A.I. Caplan, A. DeChant, J. Hecker, J. Kranso, et al., Hepatocyte growth factor mediates mesenchymal stem cell–induced recovery in multiple sclerosis models, *Nat. Neurosci.* 15 (2012) 862–870.

[27] T. Kinnaird, E. Stabile, M.S. Burnett, M. Shou, C.W. Lee, S. Barr, et al., Local delivery of marrow-derived stromal cells augments collateral perfusion through paracrine mechanisms., *Circulation*. 109 (2004) 1543–9.

[28] J.-P. Lee, M. Jeyakumar, R. Gonzalez, H. Takahashi, P.-J. Lee, R.C. Baek, et al., Stem cells act through multiple mechanisms to benefit mice with neurodegenerative metabolic disease., *Nat. Med.* 13 (2007) 439–47.

[29] M. Güttinger, D. Fedele, P. Koch, V. Padrun, W.F. Pralong, O. Brüstle, et al., Suppression of kindled seizures by paracrine adenosine release from stem cell-derived brain implants., *Epilepsia*. 46 (2005) 1162–9.

[30] D. Fraidenraich, E. Stillwell, E. Romero, D. Wilkes, K. Manova, C.T. Basson, et al., Rescue of cardiac defects in id knockout embryos by injection of embryonic stem cells., *Science (80-.).* 306 (2004) 247–52.

[31] P.R. Crisostomo, A.M. Abarbanell, M. Wang, T. Lahm, Y. Wang, D.R. Meldrum, Embryonic stem cells attenuate myocardial dysfunction and inflammation after surgical global ischemia via paracrine actions., *Am. J. Physiol. Heart Circ. Physiol.* 295 (2008) H1726–35.

[32] W.A. LaFramboise, P. Petrosko, J.M. Krill-Burger, D.R. Morris, A.R. McCoy, D. Scalise, et al., Proteins secreted by embryonic stem cells activate cardiomyocytes through ligand binding pathways., *J. Proteomics*. 73 (2010) 992–1003.

[33] D.K. Singla, D.E. McDonald, Factors released from embryonic stem cells inhibit apoptosis of H9c2 cells., *Am. J. Physiol. Heart Circ. Physiol.* 293 (2007) H1590–5.

[34] J. Zhou, F. Chen, J. Xiao, C. Li, Y. Liu, Y. Ding, et al., Enhanced functional properties of corneal epithelial cells by coculture with embryonic stem cells via the integrin β1-FAK-PI3K/Akt pathway., *Int. J. Biochem. Cell Biol.* 43 (2011) 1168–77.

[35] I.M. Conboy, H. Yousef, M.J. Conboy, Embryonic anti-aging niche., *Aging (Albany. NY).* 3 (2011) 555–63.

[36] Y. Guo, B. Graham-Evans, H.E. Broxmeyer, Murine embryonic stem cells secrete cytokines/growth modulators that enhance cell survival/anti-apoptosis and stimulate colony formation of murine hematopoietic progenitor cells., *Stem Cells*. 24 (2006) 850–6.

[37] G. Pietramaggiori, S.S. Scherer, M. Alperovich, B. Chen, D.P. Orgill, A.J. Wagers, Improved cutaneous healing in diabetic mice exposed to healthy peripheral circulation., *J. Invest. Dermatol.* 129 (2009) 2265–74.

[38] G. Song, D.T. Nguyen, G. Pietramaggiori, S. Scherer, B. Chen, Q. Zhan, et al., Use of the parabiotic model in studies of cutaneous wound healing to define the participation of circulating cells., *Wound Repair Regen.* 18 (2010) 426–32.

[39] I.M. Conboy, M.J. Conboy, G.M. Smythe, T.A. Rando, Notch-mediated restoration of regenerative potential to aged muscle., *Science (80-.).* 302 (2003) 1575–7.

[40] I.M. Conboy, M.J. Conboy, A.J. Wagers, E.R. Girma, I.L. Weissman, T. a Rando, Rejuvenation of aged progenitor cells by exposure to a young systemic environment., *Nature*. 433 (2005) 760–4.

[41] M. Sinha, Y.C. Jang, J. Oh, D. Khong, E.Y. Wu, R. Manohar, et al., Restoring systemic GDF11 levels reverses age-related dysfunction in mouse skeletal muscle., *Science (80-.).* 344 (2014) 649–52.

[42] S. a Villeda, J. Luo, K.I. Mosher, B. Zou, M. Britschgi, G. Bieri, et al., The ageing systemic milieu negatively regulates neurogenesis and cognitive function., *Nature*. 477 (2011) 90–4.

[43] L. Katsimpardi, N.K. Litterman, P. a Schein, C.M. Miller, F.S. Loffredo, G.R. Wojtkiewicz, et al., Vascular and neurogenic rejuvenation of the aging mouse brain by young systemic factors., *Science (80-.).* 344 (2014) 630–4.

[44] S. a Villeda, K.E. Plambeck, J. Middeldorp, J.M. Castellano, K.I. Mosher, J. Luo, et al., Young blood reverses age-related impairments in cognitive function and synaptic plasticity in mice., *Nat. Med.* (2014) 1–8.

[45] L.K. Smith, Y. He, J.-S. Park, G. Bieri, C.E. Snethlage, K. Lin, et al., B2-Microglobulin Is a Systemic Pro-Aging Factor That Impairs Cognitive Function and Neurogenesis, *Nat. Med.* 21 (2015) 1–8.

[46] F.S. Loffredo, M.L. Steinhauser, S.M. Jay, J. Gannon, J.R. Pancoast, P. Yalamanchi, et al., Growth Differentiation Factor 11 Is a Circulating Factor that Reverses Age-Related Cardiac Hypertrophy., *Cell*. 153 (2013) 828–39.

[47] T.M.S. Chang, Semipermeable Microcapsules, *Science (80-.).* 146 (1964) 524–525.

[48] H. Uludag, P. De Vos, P.A. Tresco, Technology of mammalian cell encapsulation, *Adv. Drug Deliv. Rev.* 42 (2000) 29–64.

[49] J. Rabanel, X. Banquy, H. Zouaoui, M. Mokhtar, P. Hildgen, Progress Technology in Microencapsulation Methods for Cell Therapy, *Biotechnol. Prog.* 25 (2009) 946–963.

[50] J.T. Wilson, E.L. Chaikof, Challenges and emerging technologies in the immunoisolation of cells and tissues., *Adv. Drug Deliv. Rev.* 60 (2008) 124–45.

[51] G. Helmlinger, P.A. Netti, H.C. Lichtenbeld, R.J. Melder, R.K. Jain, Solid stress inhibits the growth of multicellular tumor spheroids, *Nat. Biotechnol.* 15 (1997) 778–783.

[52] X. Huang, X. Zhang, X. Wang, C. Wang, B. Tang, Microenvironment of alginate-based microcapsules for cell culture and tissue engineering., *J. Biosci. Bioeng.* 114 (2012) 1–8.

[53] I. Pajić-Lijaković, D. Bugarski, M. Plavšić, B. Bugarski, Influence of microenvironmental conditions on hybridoma cell growth inside the alginate-poly-l-lysine microcapsule, *Process Biochem.* 42 (2007) 167–174.

[54] A. Haug, B. Larsen, O. Smidsrod, A Study of the Constitution of Alginic Acid by Partial Acid Hydrolysis, *Acta Chem. Scand.* 20 (1966) 183–190.

[55] Y. a Mørch, I. Donati, B.L. Strand, G. Skjåk-Braek, Effect of Ca2+, Ba2+, and Sr2+ on alginate microbeads., *Biomacromolecules*. 7 (2006) 1471–80.

[56] M.D. Darrabie, W.F. Kendall, E.C. Opara, Effect of alginate composition and gelling cation on micro-bead swelling., *J. Microencapsul.* 23 (2006) 29–37.

[57] B.L. Strand, Y. a Mørch, T. Espevik, G. Skjåk-Braek, Visualization of alginate-poly-L-lysine-alginate microcapsules by confocal laser scanning microscopy., *Biotechnol. Bioeng.* 82 (2003) 386–94.

[58] F. Lim, A.M. Sun, Microencapsulated Islets as Bioartificial Endocrine Pancreas, *Science (80-.).* 210 (1980) 908–910.

[59] G.M. Vandenbossche, P. Van Oostveldt, J. Demeester, J.P. Remon, The molecular weight cut-off of microcapsules is determined by the reaction between alginate and polylysine., *Biotechnol. Bioeng.* 42 (1993) 381–6.

[60] M. De Castro, G. Orive, R.M. Hernández, a R. Gascón, J.L. Pedraz, Comparative study of microcapsules elaborated with three polycations (PLL, PDL, PLO) for cell immobilization., *J. Microencapsul.* 22 (2005) 303–15.

[61] R.G. Willaert, B.- Brüssel, Gel entrapment and micro-encapsulation: methods, applications and engineering principles, *Rev. Chem. Eng.* 12 (1996).

[62] D. Serp, E. Cantana, C. Heinzen, U. Von Stockar, I.W. Marison, Characterization of an encapsulation device for the production of monodisperse alginate beads for cell immobilization., *Biotechnol. Bioeng.* 70 (2000) 41–53.

[63] M. Whelehan, I.W. Marison, Microencapsulation using vibrating technology, *J. Microencapsul.* 28 (2011) 669–688.

[64] S. Sakai, K. Kawabata, T. Ono, H. Ijima, K. Kawakami, Preparation of mammalian cell-enclosing subsieve-sized capsules (<100 microm) in a coflowing stream., *Biotechnol. Bioeng.* 86 (2004) 168–73.

[65] S.M. Dang, S. Gerecht-Nir, J. Chen, J. Itskovitz-Eldor, P.W. Zandstra, Controlled, Scalable Embryonic Stem Cell Differentiation Culture, *Stem Cells*. 22 (2004) 275–282.

[66] T. Maguire, E. Novik, R. Schloss, M. Yarmush, Alginate-PLL Microencapsulation: Effect on the Differentiation of Embryonic Stem Cells Into Hepatocytes, *Biotechnol. Bioeng.* 93 (2005) 581–591.

[67] X. Wang, W. Wang, J. Ma, X. Guo, X. Yu, X. Ma, Proliferation and differentiation of mouse embryonic stem cells in APA microcapsule: A model for studying the interaction between stem cells and their niche., *Biotechnol. Prog.* 22 (2006) 791–800.

[68] S. Sakai, I. Hashimoto, K. Kawakami, Production of Cell-Enclosing Hollow-Core Agarose Microcapsules Via Jetting in Water-Immiscible Liquid Paraffin and Formation of Embryoid Body-Like Spherical Tissues From Mouse ES Cells Enclosed Within These Microcapsules, *Biotechnol. Bioeng.* 99 (2008) 235–243.

[69] N. Siti-Ismail, A.E. Bishop, J.M. Polak, A. Mantalaris, The benefit of human embryonic stem cell encapsulation for prolonged feeder-free maintenance., *Biomaterials*. 29 (2008) 3946–52.

[70] M. Serra, C. Correia, R. Malpique, C. Brito, J. Jensen, P. Bjorquist, et al., Microencapsulation Technology: A Powerful Tool for Integrating Expansion and Cryopreservation of Human Embryonic Stem Cells, *PLoS One*. 6 (2011) e23212.

[71] M.G. Levee, G. Lee, S. Pack, B. Palsson, Marrow Cultures: A Potential Culture System for the Clonal Outgrowth of Hematopoietic Progenitor Cells, *Biotechnol. Bioeng.* 43 (1994) 734–739.

[72] C. Bauwens, T. Yin, S. Dang, R. Peerani, P.W. Zandstra, Development of a perfusion fed bioreactor for embryonic stem cell-derived cardiomyocyte generation: oxygen-mediated enhancement of cardiomyocyte output., *Biotechnol. Bioeng.* 90 (2005) 452–61.

[73] D. Jing, A. Parikh, E.S. Tzanakakis, Cardiac cell generation from encapsulated embryonic stem cells in static and scalable culture systems, *Cell Transplant.* 19 (2010) 1397–1412.

[74] Y.-S. Hwang, J. Cho, F. Tay, J.Y.Y. Heng, R. Ho, S.G. Kazarian, et al., The use of murine embryonic stem cells, alginate encapsulation, and rotary microgravity bioreactor in bone tissue engineering., *Biomaterials*. 30 (2009) 499–507.

[75] C. Weber, S. Pohl, R. Pörtner, C. Wallrapp, M. Kassem, P. Czermak, Cultivation and Differentiation of Encapsulated hMSC-TERT in a Disposable Small-Scale Syringe-Like Fixed Bed Reactor, *Open Biomed. Eng. J.* 1 (2007) 64–70.

[76] A.B. Yeatts, J.P. Fisher, D. Ph, Tubular Perfusion System for the Long-Term Dynamic Culture of Human Mesenchymal Stem Cells, *Tissue Eng. Part C.* 17 (2011) 337–348.

[77] A.B. Yeatts, C.N. Gordon, J.P. Fisher, Formation of an Aggregated Alginate Construct in a Tubular Perfusion System., *Tissue Eng. Part C. Methods*. 17 (2011) 1171–1178.

[78] R. Schofield, The relationship between the spleen colony-forming cell and the haemopoietic stem cell, *Blood Cells*. 4 (1978) 7–25.

[79] D.L. Jones, A.J. Wagers, No place like home: anatomy and function of the stem cell niche., *Nat. Rev. Mol. Cell Biol.* 9 (2008) 11–21.

[80] D.T. Scadden, The stem-cell niche as an entity of action., *Nature*. 441 (2006) 1075–9.

[81] S.J. Morrison, A.C. Spradling, Stem cells and niches: mechanisms that promote stem cell maintenance throughout life., *Cell*. 132 (2008) 598–611.

[82] J. Zhang, C. Niu, L. Ye, H. Huang, X. He, S. Harris, et al., Identification of the haematopoietic stem cell niche and control of the niche size, *Nature*. 425 (2003) 836–841.

[83] M.J. Kiel, O.H. Yilmaz, T. Iwashita, O.H. Yilmaz, C. Terhorst, S.J. Morrison, SLAM family receptors distinguish hematopoietic stem and progenitor cells and reveal endothelial niches for stem cells., *Cell*. 121 (2005) 1109–21.

[84] G.B. Adams, D.T. Scadden, The hematopoietic stem cell in its place., *Nat. Immunol.* 7 (2006) 333–7.

[85] A. Wilson, A. Trumpp, Bone-marrow haematopoietic-stem-cell niches., *Nat. Rev. Immunol.* 6 (2006) 93–106.

[86] S.J. Morrison, D.T. Scadden, The bone marrow niche for haematopoietic stem cells, *Nature*. 505 (2014) 327–334.

[87] A. Ehninger, A. Trumpp, The bone marrow stem cell niche grows up: mesenchymal stem cells and macrophages move in., *J. Exp. Med.* 208 (2011) 421–8.

[88] L.D. Wang, A.J. Wagers, Dynamic niches in the origination and differentiation of haematopoietic stem cells., *Nat. Rev. Mol. Cell Biol.* 12 (2011) 643–55.

[89] R.A. Lawal, L.M. Calvi, The Niche as a Target for Hematopoietic Manipulation and Regeneration, *Tissue Eng. Part B.* 17 (2011) 415–422.

[90] H.K. a. Mikkola, The journey of developing hematopoietic stem cells, *Development*. 133 (2006) 3733–3744.

[91] H. Yin, F. Price, M. a Rudnicki, Satellite cells and the muscle stem cell niche., *Physiol. Rev.* 93 (2013) 23–67.

[92] A. Otto, C. Schmidt, G. Luke, S. Allen, P. Valasek, F. Muntoni, et al., Canonical Wnt signalling induces satellite-cell proliferation during adult skeletal muscle regeneration., *J. Cell Sci.* 121 (2008) 2939–2950.

[93] D. Luo, V.M. Renault, T. a. Rando, The regulation of Notch signaling in muscle stem cell activation and postnatal myogenesis, *Semin. Cell Dev. Biol.* 16 (2005) 612–622.

[94] M.Z. Ratajczak, M. Majka, M. Kucia, J. Drukala, Z. Pietrzkowski, S. Peiper, et al., Expression of functional CXCR4 by muscle satellite cells and secretion of SDF-1 by muscle-derived fibroblasts is associated with the presence of both muscle progenitors in bone marrow and hematopoietic stem/progenitor cells in muscles., *Stem Cells*. 21 (2003) 363–371.

[95] R. Tatsumi, J.E. Anderson, C.J. Nevoret, O. Halevy, R.E. Allen, HGF/SF is present in normal adult skeletal muscle and is capable of activating satellite cells., *Dev. Biol.* 194 (1998) 114–128.

[96] S. Machida, F.W. Booth, Insulin-like growth factor 1 and muscle growth: implication for satellite cell proliferation., *Proc. Nutr. Soc.* 63 (2004) 337–340.

[97] K.J. Miller, D. Thaloor, S. Matteson, G.K. Pavlath, Hepatocyte growth factor affects satellite cell activation and differentiation in regenerating skeletal muscle., *Am. J. Physiol. Cell Physiol.* 278 (2000) C174–C181.

[98] T. Sato, J.H. van Es, H.J. Snippert, D.E. Stange, R.G. Vries, M. van den Born, et al., Paneth cells constitute the niche for Lgr5 stem cells in intestinal crypts., *Nature*. 469 (2011) 415–8.

[99] D. Tan, N. Barker, Intestinal stem cells and their defining niche, in: Stem Cells Dev. Dis., 2014: pp. 77–107.

[100] E. Fuchs, Finding One's Niche in the Skin, *Cell Stem Cell*. 4 (2009) 499–502.

[101] J.C. Conover, R.Q. Notti, The neural stem cell niche., *Cell Tissue Res.* 331 (2008) 211–24.

[102] B.-Y. Ryu, K.E. Orwig, J.M. Oatley, M.R. Avarbock, R.L. Brinster, Effects of aging and niche microenvironment on spermatogonial stem cell self-renewal., *Stem Cells*. 24 (2006) 1505–1511.

[103] A.S. Brack, M.J. Conboy, S. Roy, M. Lee, C.J. Kuo, C. Keller, et al., Increased Wnt signaling during aging alters muscle stem cell fate and increases fibrosis., *Science*. 317 (2007) 807–10.

[104] M. Boyle, C. Wong, M. Rocha, D.L. Jones, Decline in Self-Renewal Factors Contributes to Aging of the Stem Cell Niche in the Drosophila Testis, *Cell Stem Cell*. 1 (2007) 470–478.

[105] D. Visnjic, Z. Kalajzic, D.W. Rowe, V. Katavic, J. Lorenzo, H.L. Aguila, Hematopoiesis is severely altered in mice with an induced osteoblast deficiency, *Blood*. 103 (2004) 3258–3264.

[106] Y. Zhu, P. Ghosh, P. Charnay, D.K. Burns, L.F. Parada, Neurofibromas in NF1: Schwann cell origin and role of tumor environment., *Science*. 296 (2002) 920–922.

[107] J.B. Sneddon, H.H. Zhen, K. Montgomery, M. van de Rijn, A.D. Tward, R. West, et al., Bone morphogenetic protein antagonist gremlin 1 is widely expressed by cancer-associated stromal cells and can promote tumor cell proliferation., *Proc. Natl. Acad. Sci. U. S. A.* 103 (2006) 14842–14847.

[108] J. Corre, K. Mahtouk, M. Attal, M. Gadelorge, a Huynh, S. Fleury-Cappellesso, et al., Bone marrow mesenchymal stem cells are abnormal in multiple myeloma, *Leukemia*. (2007) 1079–1088.

[109] J. Uitto, A.M. Christiano, W.H.I. McLean, J. a McGrath, Novel Molecular Therapies for Heritable Skin Disorders, *J. Invest. Dermatol.* 132 (2012) 820–828.

[110] F. Mavilio, G. Pellegrini, S. Ferrari, F. Di Nunzio, E. Di Iorio, A. Recchia, et al., Correction of junctional epidermolysis bullosa by transplantation of genetically modified epidermal stem cells, *Nat. Med.* 12 (2007) 1397–1402.

[111] S.W. Lane, D. a Williams, F.M. Watt, Modulating the stem cell niche for tissue regeneration, *Nat. Biotechnol.* 32 (2014) 795–803.

[112] K. Ballen, A.M. Mendizabal, C. Cutler, I. Politikos, K. Jamieson, E.J. Shpall, et al., Phase II Trial of Parathyroid Hormone after Double Umbilical Cord Blood Transplantation, *Biol. Blood Marrow Transplant.* 18 (2012) 1851–1858.

[113] M.J. Olnes, P. Scheinberg, K.R. Calvo, R. Desmond, Y. Tang, B. Dumitriu, et al., Eltrombopag and Improved Hematopoiesis in Refractory Aplastic Anemia, *N. Engl. J. Med.* 367 (2012) 11–19.

[114] S.J. Rosenfeld, J. Kimball, D. Vining, N.S. Young, Intensive immunosuppression with antithymocyte globulin and cyclosporine as treatment for severe acquired aplastic anemia., *Blood*. 85 (1995) 3058–3065.

[115] L.B. To, J.P. Levesque, K.E. Herbert, How I treat patients who mobilize hematopoietic stem cells poorly, *Blood*. 118 (2011) 4530–4540.

[116] S. Karlsson, Stem cell expansion: success and complexities, *Blood*. 104 (2004) 2210–2211.

[117] M.A. Walasek, R. van Os, G. de Haan, Hematopoietic stem cell expansion: challenges and opportunities., *Ann. N. Y. Acad. Sci.* 1266 (2012) 138–50.

[118] A. Dahlberg, C. Delaney, I.D. Bernstein, Ex vivo expansion of human hematopoietic stem and progenitor cells., *Blood*. 117 (2011) 6083–90.

[119] B. Schiedlmeier, H. Klump, E. Will, G. Arman-Kalcek, Z. Li, Z. Wang, et al., High-level ectopic HOXB4 expression confers a profound in vivo competitive growth advantage on human cord blood CD34+ cells, but impairs lymphomyeloid differentiation., *Blood*. 101 (2003) 1759–68.

[120] S. Stier, Notch1 activation increases hematopoietic stem cell self-renewal in vivo and favors lymphoid over myeloid lineage outcome, *Blood*. 99 (2002) 2369–2378.

[121] S.N. Robinson, J. Ng, T. Niu, H. Yang, J.D. McMannis, S. Karandish, et al., Superior ex vivo cord blood expansion following co-culture with bone marrow-derived mesenchymal stem cells., *Bone Marrow Transplant.* 37 (2006) 359–66.

[122] S. Kedong, F. Xiubo, L. Tianqing, H.M. Macedo, J. LiLi, F. Meiyun, et al., Simultaneous expansion and harvest of hematopoietic stem cells and mesenchymal stem cells derived from umbilical cord blood., *J. Mater. Sci. Mater. Med.* 21 (2010) 3183–93.

[123] K. Song, G. Zhao, T. Liu, L. Zhang, X. Ma, J. Liu, et al., Effective expansion of umbilical cord blood hematopoietic stem/progenitor cells by regulation of microencapsulated osteoblasts under hypoxic condition., *Biotechnol. Lett.* 31 (2009) 923–8.

[124] P.Z. Andrade, F. dos Santos, G. Almeida-Porada, C.L. da Silva, J.M.S. S Cabral, Systematic delineation of optimal cytokine concentrations to expand hematopoietic stem/progenitor cells in co-culture with mesenchymal stem cells., *Mol. Biosyst.* 6 (2010) 1207–15.

[125] M.M. Bonab, K. Alimoghaddam, F. Talebian, S.H. Ghaffari, A. Ghavamzadeh, B. Nikbin, Aging of mesenchymal stem cell in vitro., *BMC Cell Biol.* 7 (2006) 14.

[126] W. Wagner, P. Horn, M. Castoldi, A. Diehlmann, S. Bork, R. Saffrich, et al., Replicative senescence of mesenchymal stem cells: a continuous and organized process., *PLoS One*. 3 (2008) e2213.

[127] G. Bhardwaj, B. Murdoch, D. Wu, D.P. Baker, K.P. Williams, K. Chadwick, et al., Sonic hedgehog induces the proliferation of primitive human hematopoietic cells via BMP regulation., *Nat. Immunol.* 2 (2001) 172–80.

[128] T. Reya, A.W. Duncan, L. Ailles, J. Domen, D.C. Scherer, K. Willert, et al., A role for Wnt signalling in self-renewal of haematopoietic stem cells., *Nature*. 423 (2003) 409–14.

[129] D. Montarras, J. Morgan, C. Collins, F. Relaix, S. Zaffran, A. Cumano, et al., Direct isolation of satellite cells for skeletal muscle regeneration., *Science*. 309 (2005) 2064–2067.

[130] A. Sacco, R. Doyonnas, P. Kraft, S. Vitorovic, H.M. Blau, Self-renewal and expansion of single transplanted muscle stem cells., *Nature*. 456 (2008) 502–506.

[131] Z. Qu-Petersen, B. Deasy, R. Jankowski, M. Ikezawa, J. Cummins, R. Pruchnic, et al., Identification of a novel population of muscle stem cells in mice: potential for muscle regeneration., *J. Cell Biol.* 157 (2002) 851–864.

[132] E. Gussoni, G.K. Pavlath, a M. Lanctot, K.R. Sharma, R.G. Miller, L. Steinman, et al., Normal dystrophin transcripts detected in Duchenne muscular dystrophy patients after myoblast transplantation., *Nature*. 356 (1992) 435–438.

[133] M.H. Parker, C. Loretz, A.E. Tyler, W.J. Duddy, J.K. Hall, B.B. Olwin, et al., Activation of notch signaling during ex vivo expansion maintains donor muscle cell engraftment, *Stem Cells*. 30 (2012) 2212–2220.

[134] P.M. Gilbert, K.L. Havenstrite, K.E.G. Magnusson, A. Sacco, P. Kraft, N.K. Nguyen, et al., Substrate Elasticity Regulates Skeletal Muscle Stem Cell Self-Renewal in Culture, *Science (80-.).* 1902 (2010) 1078–1082.

[135] G.W. Charville, T.H. Cheung, B. Yoo, P.J. Santos, G.K. Lee, J.B. Shrager, et al., Ex Vivo Expansion and In Vivo Self-Renewal of Human Muscle Stem Cells, *Stem Cell Reports*. 5 (2015) 1–12.

[136] D.C. Kirouac, P.W. Zandstra, The systematic production of cells for cell therapies., *Cell Stem Cell*. 3 (2008) 369–81.

[137] R.P. Wolfe, T. Ahsan, Shear stress during early embryonic stem cell differentiation promotes hematopoietic and endothelial phenotypes., *Biotechnol. Bioeng.* 110 (2013) 1231–42.

[138] H.W. Leung, P.D. Cand, A. Chen, P. D, A.B.H. Choo, S. Reuveny, et al., Agitation can Induce Differentiation of Human Pluripotent Stem Cells in Microcarrier Cultures, *Pharm. Biotechnol.* 17 (2011) 1–8.

[139] T. Gareau, G.G. Lara, R.D. Shepherd, R. Krawetz, D.E. Rancourt, K.D. Rinker, et al., Shear stress influences the pluripotency of murine embryonic stem cells in stirred suspension bioreactors, *J. Tissue Eng. Regen. Med.* (2012).

[140] C.Y. Sargent, G.Y. Berguig, M.A. Kinney, L.A. Hiatt, R.L. Carpenedo, R.E. Berson, et al., Hydrodynamic modulation of embryonic stem cell differentiation by rotary orbital suspension culture., *Biotechnol. Bioeng.* 105 (2010) 611–26.

[141] D.E. Kehoe, D. Jing, L.T. Lock, E.S. Tzanakakis, Scalable Stirred-Suspension Bioreactor Culture of Human Pluripotent Stem Cells, *Tissue Eng. Part A.* 16 (2010) 405–421.

[142] M. Serra, C. Brito, C. Correia, P.M. Alves, Process engineering of human pluripotent stem cells for clinical application., *Trends Biotechnol.* 30 (2012) 350–359.

[143] J.L. Wilson, T.C. McDevitt, Stem cell microencapsulation for phenotypic control, bioprocessing, and transplantation., *Biotechnol. Bioeng.* 110 (2013) 667–682.

[144] M. Tang, W. Chen, M.D. Weir, W. Thein-Han, H.H.K. Xu, Human embryonic stem cell encapsulation in alginate microbeads in macroporous calcium phosphate cement for bone tissue engineering., *Acta Biomater.* 8 (2012) 3436–45.

[145] S.M. Dang, S. Gerecht-Nir, J. Chen, J. Itskovitz-Eldor, P.W. Zandstra, Controlled, Scalable Embryonic Stem Cell Differentiation Culture, *Stem Cells*. 22 (2004) 275–282.

[146] N. Rahman, K.A. Purpura, R.G. Wylie, P.W. Zandstra, M.S. Shoichet, The use of vascular endothelial growth factor functionalized agarose to guide pluripotent stem cell aggregates toward blood progenitor cells., *Biomaterials*. 31 (2010) 8262–70.

[147] L. Li, A.E. Davidovich, J.M. Schloss, U. Chippada, R.R. Schloss, N. a Langrana, et al., Neural lineage differentiation of embryonic stem cells within alginate microbeads., *Biomaterials*. 32 (2011) 4489–97.

[148] M. Chayosumrit, B. Tuch, K. Sidhu, Alginate microcapsule for propagation and directed differentiation of hESCs to definitive endoderm., *Biomaterials*. 31 (2010) 505–14.

[149] N. Wang, G. Adams, L. Buttery, F.H. Falcone, S. Stolnik, Alginate encapsulation technology supports embryonic stem cells differentiation into insulin-producing cells., *J. Biotechnol.* 144 (2009) 304–12.

[150] S. Fang, Y. Qiu, L. Mao, X. Shi, D. Yu, Y. Ding, Differentiation of embryoid-body cells derived from embryonic stem cells into hepatocytes in alginate microbeads in vitro., *Acta Pharmacol. Sin.* 28 (2007) 1924–30.

[151] J.P. Magyar, M. Nemir, E. Ehler, N. Suter, J.C. Perriard, H.M. Eppenberger, Mass production of embryoid bodies in microbeads., *Ann. N. Y. Acad. Sci.* 944 (2001) 135–43.

[152] M.A. Kinney, R. Saeed, T.C. McDevitt, Systematic analysis of embryonic stem cell differentiation in hydrodynamic environments with controlled embryoid body size., *Integr. Biol.* 4 (2012) 641–50.

[153] K. Watanabe, M. Ueno, D. Kamiya, A. Nishiyama, M. Matsumura, T. Wataya, et al., A ROCK inhibitor permits survival of dissociated human embryonic stem cells., *Nat. Biotechnol.* 25 (2007) 681–6.

[154] T.C. Doetschman, H. Eistetter, M. Katz, W. Schmidt, R. Kemler, The in vitro development of blastocyst-derived embryonic stem cell lines: formation of visceral yolk sac, blood islands and myocardium., *J. Embryol. Exp. Morphol.* 87 (1985) 27–45.

[155] C. Stabler, K. Wilks, A. Sambanis, I. Constantinidis, The effects of alginate composition on encapsulated TC3 cells, *Biomaterials*. 22 (2001) 1301–1310.

[156] E.K. Purcell, A. Singh, D.R. Kipke, Alginate composition effects on a neural stem cell-seeded scaffold., *Tissue Eng. Part C. Methods*. 15 (2009) 541–50.

[157] B. Thu, P. Bruheim, T. Espevik, O. Smidsrød, P. Soon-Shiong, G. Skjåk-Braek, Alginate polycation microcapsules I. Interaction between alginate and polycation., *Biomaterials*. 17 (1996) 1031–40.

[158] B. Thu, P. Bruheim, T. Espevik, O. Smidsrød, P. Soon-Shiong, G. Skjåk-Braek, Alginate polycation microcapsules. II. Some functional properties., *Biomaterials*. 17 (1996) 1069–79.

[159] P.L. Chang, G. Hortelano, D.E. Awrey, M. Tse, Growth of recombinant fibroblasts in alginate microcapsules., *Biotechnol. Bioeng.* 43 (1994) 925–33.

[160] S. Cheng, I. Constantinidis, A. Sambanis, Use of Glucose-Responsive Material to Regulate Insulin Release From Constitutively Secreting Cells, *Biotechnol. Bioeng.* 93 (2006) 1–10.

[161] D. Li, J. Zhou, F. Chowdhury, J. Cheng, N. Wang, F. Wang, Role of mechanical factors in fate decisions of stem cells, *Regen. Med.* 6 (2011) 229–240.

[162] W. Zhang, S. Zhao, W. Rao, J. Snyder, J.K. Choi, J. Wang, et al., A Novel Core-Shell Microcapsule for Encapsulation and 3D Culture of Embryonic Stem Cells., *J. Mater. Chem. B. Mater. Biol. Med.* 2013 (2013) 1002–1009.

[163] Q.-L. Ying, A. Smith, Defined Conditions for Neural Commitment and Differentiation, *Methods Enzymol.* 365 (2003) 327–341.

[164] Q.-L. Ying, J. Wray, J. Nichols, L. Batlle-Morera, B. Doble, J. Woodgett, et al., The ground state of embryonic stem cell self-renewal., *Nature*. 453 (2008) 519–23.

[165] V. Tropepe, S. Hitoshi, C. Sirard, T.W. Mak, J. Rossant, D. van der Kooy, Direct neural fate specification from embryonic stem cells: a primitive mammalian neural stem cell stage acquired through a default mechanism., *Neuron*. 30 (2001) 65–78.

[166] R.L. Carpenedo, C.Y. Sargent, T.C. McDevitt, Rotary suspension culture enhances the efficiency, yield, and homogeneity of embryoid body differentiation., *Stem Cells*. 25 (2007) 2224–34.

[167] P.R. Baraniak, M.T. Cooke, R. Saeed, M. a. Kinney, K.M. Fridley, T.C. McDevitt, Stiffening of human mesenchymal stem cell spheroid microenvironments induced by incorporation of gelatin microparticles, *J. Mech. Behav. Biomed. Mater.* (2012) 1–9.

[168] M.W. Pfaffl, A new mathematical model for relative quantification in real-time RT-PCR., *Nucleic Acids Res.* 29 (2001) e45.

[169] P. De Vos, B. De Haan, R. Van Schilfgaarde, Effect of the alginate composition on the biocompatibility of alginate-polylysine microcapsules, *Biomaterials*. 18 (1997) 273–278.

[170] S.H. Capone, M. Dufresne, M. Rechel, M.-J. Fleury, A.-V. Salsac, P. Paullier, et al., Impact of Alginate Composition: From Bead Mechanical Properties to Encapsulated HepG2/C3A Cell Activities for In Vivo Implantation., *PLoS One*. 8 (2013) e62032.

[171] E. Alsberg, K.W. Anderson, a Albeiruti, R.T. Franceschi, D.J. Mooney, Cell-interactive alginate hydrogels for bone tissue engineering., *J. Dent. Res.* 80 (2001) 2025–2029.

[172] G.A. King, A.J. Dougulis, P. Faulkner, F.A. Goosen, Alginate-Polylysine Microcapsules of Controlled Membrane Molecular Weight Cutoff for Mammalian Cell Culture Engineering, *Biotechnol. Prog.* 3 (1987) 231–240.

[173] A. Banerjee, M. Arha, S. Choudhary, R.S. Ashton, S.R. Bhatia, D. V Schaffer, et al., The influence of hydrogel modulus on the proliferation and differentiation of encapsulated neural stem cells., *Biomaterials*. 30 (2009) 4695–9.

[174] E.-S. Chan, T.-K. Lim, W.-P. Voo, R. Pogaku, B.T. Tey, Z. Zhang, Effect of formulation of alginate beads on their mechanical behavior and stiffness, *Particuology*. 9 (2011) 228–234.

[175] M.S. Shoichet, R.H. Li, M.L. White, S.R. Winn, Stability of hydrogels used in cell encapsulation: An in vitro comparison of alginate and agarose., *Biotechnol. Bioeng.* 50 (1996) 374–81.

[176] J.F. Markusen, C. Mason, D. a Hull, M. a Town, A.B. Tabor, M. Clements, et al., Behavior of adult human mesenchymal stem cells entrapped in alginate-GRGDY beads., *Tissue Eng.* 12 (2006) 821–30.

[177] P. Navarro, N. Festuccia, D. Colby, A. Gagliardi, N.P. Mullin, W. Zhang, et al., OCT4/SOX2-independent Nanog autorepression modulates heterogeneous Nanog gene expression in mouse ES cells., *EMBO J.* 31 (2012) 4547–62.

[178] S. Muñoz Descalzo, P. Rué, J. Garcia-Ojalvo, A. Martinez Arias, Correlations between the levels of Oct4 and Nanog as a signature for naïve pluripotency in mouse embryonic stem cells., *Stem Cells*. 30 (2012) 2683–91.

[179] F. Faunes, P. Hayward, S.M. Descalzo, S.S. Chatterjee, T. Balayo, J. Trott, et al., A membrane-associated β-catenin/Oct4 complex correlates with ground-state pluripotency in mouse embryonic stem cells., *Development*. 140 (2013) 1171–83.

[180] J. Wu, E.S. Tzanakakis, Contribution of stochastic partitioning at human embryonic stem cell division to NANOG heterogeneity., *PLoS One*. 7 (2012) e50715.

[181] A. V Ngangan, J.C. Waring, M.T. Cooke, C.J. Mandrycky, T.C. McDevitt, Soluble factors secreted by differentiating embryonic stem cells stimulate exogenous cell proliferation and migration., *Stem Cell Res. Ther.* 5 (2014) 26.

[182] C.Y. Sargent, G.Y. Berguig, T.C. McDevitt, Cardiomyogenic differentiation of embryoid bodies is promoted by rotary orbital suspension culture., *Tissue Eng. Part A.* 15 (2009) 331–42.

[183] S. Tohyama, F. Hattori, M. Sano, T. Hishiki, Y. Nagahata, T. Matsuura, et al., Distinct Metabolic Flow Enables Large-Scale Purification of Mouse and Human Pluripotent Stem Cell-Derived Cardiomyocytes, *Cell Stem Cell*. 12 (2012) 1–11.

[184] C.L. Bauwens, R. Peerani, S. Niebruegge, K. a Woodhouse, E. Kumacheva, M. Husain, et al., Control of human embryonic stem cell colony and aggregate size heterogeneity influences differentiation trajectories., *Stem Cells*. 26 (2008) 2300–10.

[185] Y.-S. Hwang, B.G. Chung, D. Ortmann, N. Hattori, H.-C. Moeller, A. Khademhosseini, Microwell-mediated control of embryoid body size regulates embryonic stem cell fate via differential expression of WNT5a and WNT11., *Proc. Natl. Acad. Sci.* 106 (2009) 16978–83.

[186] J.C. Mohr, J. Zhang, S.M. Azarin, A.G. Soerens, J.J. de Pablo, J.A. Thomson, et al., The microwell control of embryoid body size in order to regulate cardiac differentiation of human embryonic stem cells., *Biomaterials*. 31 (2010) 1885–93.

[187] M.L. Shuler, F. Kargi, Bioprocess Engineering: Basic Concepts, 2nd ed., Prentice Hall, 2002.

[188] J.M. Reichert, Metrics for antibody therapeutics development, *MAbs*. 2 (2010) 695–700.

[189] F.M. Wurm, Production of recombinant protein therapeutics in cultivated mammalian cells, *Nat. Biotechnol.* 22 (2004) 1393–1398.

[190] P.R. Baraniak, T.C. McDevitt, Stem cell paracrine actions and tissue regeneration, *Regen. Med.* 5 (2010) 121–143.

[191] C. Tran, M.S. Damaser, Stem cells as drug delivery methods: Application of stem cell secretome for regeneration, *Adv. Drug Deliv. Rev.* 82-83 (2015) 1–11.

[192] J. Doorn, G. Moll, K. Le Blanc, C. Van Blitterswijk, J. De Boer, Therapeutic Applications of Mesenchymal Stromal Cells: Paracrine Effects and Potential Improvements, *Tissue Eng. Part B.* 18 (2012) 101–115.

[193] A. Caplan, Why are MSCs therapeutic? New data: new insight, *J. Pathol.* 217 (2009) 318–324.

[194] M.R. Placzek, I.-M. Chung, H.M. Macedo, S. Ismail, T. Mortera Blanco, M. Lim, et al., Stem cell bioprocessing: fundamentals and principles., *J. R. Soc. Interface*. 6 (2009) 209–32.

[195] N. Liu, R. Zang, S.-T. Yang, Y. Li, Stem cell engineering in bioreactors for large-scale bioprocessing, *Eng. Life Sci.* (2013) n/a–n/a.

[196] M.A. Kinney, C.Y. Sargent, T.C. McDevitt, The Multiparametric Effects of Hydrodynamic Environments on Stem Cell Culture, *Tissue Eng. Part B.* 17 (2011) 249–262.

[197] J.A. King, W.M. Miller, Bioreactor development for stem cell expansion and controlled differentiation., *Curr. Opin. Chem. Biol.* 11 (2007) 394–8.

[198] M.R. Koller, S.G. Emerson, B.O. Palsson, Large-scale expansion of human stem and progenitor cells from bone marrow mononuclear cells in continuous perfusion cultures., *Blood*. 82 (1993) 378–84.

[199] W.J. Fong, H.L. Tan, A. Choo, S.K.W. Oh, Perfusion cultures of human embryonic stem cells., *Bioprocess Biosyst. Eng.* 27 (2005) 381–7.

[200] S.K.W. Oh, W.J. Fong, Y. Teo, H.L. Tan, J. Padmanabhan, A.C.P. Chin, et al., High density cultures of embryonic stem cells., *Biotechnol. Bioeng.* 91 (2005) 523–33.

[201] D. Yeo, A. Kiparissides, J.M. Cha, C. Aguilar-Gallardo, J.M. Polak, E. Tsiridis, et al., Improving embryonic stem cell expansion through the combination of perfusion and Bioprocess model design., *PLoS One*. 8 (2013) e81728.

[202] F. Coletti, S. Macchietto, N. Elvassore, Mathematical Modeling of Three-Dimensional Cell Cultures in Perfusion Bioreactors, *Ind. Eng. Chem. Res.* 45 (2006) 8158–8169.

[203] C. Kontoravdi, S.P. Asprey, E.N. Pistikopoulos, A. Mantalaris, Application of Global Sensitivity Analysis to Determine Goals for Design of Experiments: An

Example Study on Antibody-Producing Cell Cultures, *Biotechnol. Prog.* 21 (2005) 1128–1135.

[204] M.L. Acosta, A. Sánchez, F. García, A. Contreras, E. Molina, Analysis of kinetic, stoichiometry and regulation of glucose and glutamine metabolism in hybridoma batch cultures using logistic equations, *Cytotechnology*. 54 (2007) 189–200.

[205] G. Schmid, C.R. Wilke, H.W. Blanch, Continuous hybridoma suspension cultures with and without cell retention: kinetics of growth, metabolism and product formation., *J. Biotechnol.* 22 (1992) 31–40.

[206] N. Templeton, J. Dean, P. Reddy, J.D. Young, Peak antibody production is associated with increased oxidative metabolism in an industrially relevant fed-batch CHO cell culture, *Biotechnol. Bioeng.* 110 (2013) 2013–2024.

[207] B.P. Jena, Molecular machinery and mechanism of cell secretion., *Exp. Biol. Med.* 230 (2005) 307–319.

[208] W. Nickel, Unconventional secretion: an extracellular trap for export of fibroblast growth factor 2, *J. Cell Sci.* 120 (2007) 2295–2299.

[209] W. Nickel, M. Seedorf, Unconventional Mechanisms of Protein Transport to the Cell Surface of Eukaryotic Cells, *Annu. Rev. Cell Dev. Biol.* 24 (2008) 287–308.

[210] I. Prudovsky, A. Mandinova, R. Soldi, C. Bagala, I. Graziani, M. Landriscina, et al., The non-classical export routes: FGF1 and IL-1 point the way, *J. Cell Sci.* 116 (2003) 4871–4881.

[211] T.L. Burgess, R.B. Kelly, Constitutive and regulated secretion of proteins., *Annu. Rev. Cell Biol.* 3 (1987) 243–293.

[212] H.L. Waldum, P.M. Kleveland, E. Brenna, I. Bakke, G. Qvigstad, T.C. Martinsen, et al., Interactions between gastric acid secretagogues and the localization of the gastrin receptor, *Scand. J. Gastroenterol.* 44 (2009) 390–393.

[213] H. Zhou, X. Wang, W.K.W. Ko, A.O.L. Wong, Evidence for a Novel Intrapituitary Autocrine/Paracrine Feedback Loop Regulating Growth Hormone Synthesis and Secretion in Grass Carp Pituitary Cells by Functional Interactions between Gonadotrophs and Somatotrophs, *Endocrinology*. 145 (2004) 5548–5559.

[214] K.A. Magri, M.R. Benedict, D.Z. Ewton, J.R. Florini, Negative Feedback Regulation of Insulin-Like Growth Factor-II Gene Expression in Differentiating Myoblasts in Vitro, *Endocrinology*. 135 (1994) 53–62.

[215] K. Watanabe, Y. Hasegawa, H. Yamashita, K. Shimizu, Y. Ding, M. Abe, et al., Vasohibin as an endothelium-derived negative feedback regulator of angiogenesis, *J. Clin. Invest.* 114 (2004) 898–907.

[216] B. a Hesser, X.H. Liang, G. Camenisch, S. Yang, D. a Lewin, R. Scheller, et al., Down syndrome critical region protein 1 (DSCR1), a novel VEGF target gene that regulates expression of inflammatory markers on activated endothelial cells, *Hemostasis, Thromb. Vasc. Biol.* 104 (2004) 149–158.

[217] I.B. Lobov, R. a Renard, N. Papadopoulos, N.W. Gale, G. Thurston, G.D. Yancopoulos, et al., Delta-like ligand 4 (Dll4) is induced by VEGF as a negative regulator of angiogenic sprouting., *Proc. Natl. Acad. Sci. U. S. A.* 104 (2007) 3219–3224.

[218] K. Blagovic, L.Y. Kim, J. Voldman, Microfluidic Perfusion for Regulating Diffusible Signaling in Stem Cells, *PLoS One*. 6 (2011) e22892.

[219] C.E. Murry, G. Keller, Differentiation of embryonic stem cells to clinically relevant populations: lessons from embryonic development., *Cell*. 132 (2008) 661–80.

[220] R.J. Cole, R.G. Edwards, J. Paul, Cytodifferentiation and embryogenesis in cell colonies and tissue cultures derived from ova and blastocysts of the rabbit., *Dev. Biol.* 13 (1966) 385–407.

[221] A. Beenken, M. Mohammadi, The FGF family: biology, pathophysiology and therapy., *Nat. Rev. Drug Discov.* 8 (2009) 235–53.

[222] D.L. Coutu, J. Galipeau, Roles of FGF signaling in stem cell self-renewal, senescence and aging., *Aging (Albany. NY).* 3 (2011) 1–14.

[223] P. Ducy, G. Karsenty, The family of bone morphogenetic proteins., *Kidney Int.* 57 (2000) 2207–2214.

[224] V. Hwa, Y. Oh, R.G. Rosenfeld, The Insulin-Like Growth Factor-Binding Protein (IGFBP) Superfamily, *Endocr. Rev.* 20 (1999) 761–787.

[225] G.J. Allan, D.J. Flint, K. Patel, Insulin-like growth factor axis during embryonic development, *Reproduction*. 122 (2001) 31–39.

[226] P. Anversa, Aging and longevity: the IGF-1 enigma., *Circ. Res.* 97 (2005) 411–4.

[227] A. Salminen, K. Kaarniranta, Insulin/IGF-1 paradox of aging: regulation via AKT/IKK/NF-kappaB signaling., *Cell. Signal.* 22 (2010) 573–7.

[228] C.Y. Logan, R. Nusse, The Wnt signaling pathway in development and disease., *Annu. Rev. Cell Dev. Biol.* 20 (2004) 781–810.

[229] H. Clevers, Wnt/B-Catenin Signaling in Development and Disease, *Cell*. 127 (2006) 469–480.

[230] S.C. Bendall, C. Hughes, J.L. Campbell, M.H. Stewart, P. Pittock, S. Liu, et al., An enhanced mass spectrometry approach reveals human embryonic stem cell growth factors in culture., *Mol. Cell. Proteomics*. 8 (2009) 421–32.

[231] A. Farina, C. D'Aniello, V. Severino, D.F. Hochstrasser, A. Parente, G. Minchiotti, et al., Temporal proteomic profiling of embryonic stem cell secretome during cardiac and neural differentiation., *Proteomics*. 11 (2011) 3972–82.

[232] P. Sarkar, S. Randall, D. Muddiman, B. Rao, Targeted proteomics of the secretory pathway reveals the secretome of mouse embryonic fibroblasts and human embryonic stem cells, *Mol. Cell. Proteomics*. 11 (2012) 1829–1839.

[233] B. Bhattacharya, J. Cai, Y. Luo, T. Miura, J. Mejido, S.N. Brimble, et al., Comparison of the gene expression profile of undifferentiated human embryonic stem cell lines and differentiating embryoid bodies., *BMC Dev. Biol.* 5 (2005) 22.

[234] F.C. Mansergh, C.S. Daly, A.L. Hurley, M. a Wride, S.M. Hunter, M.J. Evans, Gene expression profiles during early differentiation of mouse embryonic stem cells., *BMC Dev. Biol.* 9 (2009) 5.

[235] D.L. Kelly, a Rizzino, DNA microarray analyses of genes regulated during the differentiation of embryonic stem cells., *Mol. Reprod. Dev.* 56 (2000) 113–123.

[236] R. Nair, A. V Ngangan, M.L. Kemp, T.C. McDevitt, Gene Expression Signatures of Extracellular Matrix and Growth Factors During Embryonic Stem Cell Differentiation, *PLoS One*. 7 (2012) e42580.

[237] A. Mohyeldin, T. Garzón-Muvdi, A. Quiñones-Hinojosa, Oxygen in stem cell biology: a critical component of the stem cell niche., *Cell Stem Cell*. 7 (2010) 150–61.

[238] M. Gassmann, J. Fandrey, S. Bichet, M. Wartenberg, H.H. Marti, C. Bauer, et al., Oxygen supply and oxygen-dependent gene expression in differentiating embryonic stem cells., *Proc. Natl. Acad. Sci. U. S. A.* 93 (1996) 2867–72.

[239] H.-J. Lim, J. Han, D.-H. Woo, S.-E. Kim, S.-K. Kim, H.-G. Kang, et al., Biochemical and morphological effects of hypoxic environment on human embryonic stem cells in long-term culture and differentiating embryoid bodies., *Mol. Cells*. 31 (2011) 123–32.

[240] J.O.A. Forsythe, B. Jiang, N. V Iyer, F. Agani, S.W. Leung, Activation of Vascular Endothelial Growth Factor Gene Transcription by Hypoxia-Inducible Factor 1, *Mol. Cell. Biol.* 16 (1996) 4604–4613.

[241] Q. Ke, M. Costa, Hypoxia-Inducible Factor-1 (HIF-1), *Mol. Pharmacol.* 70 (2006) 1469–1480.

[242] D. Evseenko, Y. Zhu, K. Schenke-Layland, J. Kuo, B. Latour, S. Ge, et al., Mapping the first stages of mesoderm commitment during differentiation of human embryonic stem cells., *Proc. Natl. Acad. Sci. U. S. A.* 107 (2010) 13742–7.

[243] K.A. Purpura, A.M. Bratt-Leal, K.A. Hammersmith, T.C. McDevitt, P.W. Zandstra, Systematic engineering of 3D pluripotent stem cell niches to guide blood development., *Biomaterials*. 33 (2012) 1271–80.

[244] X. Lian, C. Hsiao, G. Wilson, K. Zhu, L.B. Hazeltine, S.M. Azarin, et al., Robust cardiomyocyte differentiation from human pluripotent stem cells via temporal modulation of canonical Wnt signaling., *Proc. Natl. Acad. Sci. U. S. A.* 109 (2012) E1848–57.

[245] J.L. Wilson, M.A. Najia, R. Saeed, T.C. McDevitt, Alginate encapsulation parameters influence the differentiation of microencapsulated embryonic stem cell aggregates., *Biotechnol. Bioeng.* 111 (2014) 618–31.

[246] E. Csaszar, D.C. Kirouac, M. Yu, W. Wang, W. Qiao, M.P. Cooke, et al., Rapid Expansion of Human Hematopoietic Stem Cells by Automated Control of Inhibitory Feedback Signaling, *Cell Stem Cell*. 10 (2012) 218–229.

[247] B. a Nsiah, T. Ahsan, S. Griffiths, M. Cooke, R.M. Nerem, T.C. McDevitt, Fluid shear stress pre-conditioning promotes endothelial morphogenesis of embryonic stem cells within embryoid bodies., *Tissue Eng. Part A.* 20 (2014) 954–65.

[248] M.A. Kinney, R. Saeed, T.C. McDevitt, Mesenchymal morphogenesis of embryonic stem cells dynamically modulates the biophysical microtissue niche., *Sci. Rep.* 4 (2014) 4290.

[249] S.F. Kingsmore, Multiplexed protein measurement: technologies and applications of protein and antibody arrays., *Nat. Rev. Drug Discov.* 5 (2006) 310–320.

[250] H. Yousef, M.J. Conboy, H. Mamiya, M. Zeiderman, D. V Schaffer, I.M. Conboy, Mechanisms of action of hESC-secreted proteins that enhance human and mouse myogenesis, 6 (2014) 602–620.

[251] H. Huynh, J. Zheng, M. Umikawa, C. Zhang, R. Silvany, S. Iizuka, et al., IGF binding protein 2 supports the survival and cycling of hematopoietic stem cells, *Blood*. 118 (2011) 3236–3244.

[252] H. Huynh, S. Iizuka, M. Kaba, O. Kirak, J. Zheng, H.F. Lodish, et al., Insulin-Like Growth Factor-Binding Protein 2 Secreted by a Tumorigenic Cell Line Supports Ex Vivo Expansion of Mouse Hematopoietic Stem Cells, *Stem Cells*. 26 (2008) 1628–1635.

[253] C.C. Zhang, M. Kaba, S. Iizuka, H. Huynh, H.F. Lodish, Angiopoietin-like 5 and IGFBP2 stimulate ex vivo expansion of human cord blood hematopoietic stem cells as assayed by NOD / SCID transplantation, *Blood*. 111 (2008) 3415–3424.

[254] N. Kosaka, H. Sakamoto, M. Terada, T. Ochiya, Pleiotropic function of FGF-4: Its role in development and stem cells, *Dev. Dyn.* 238 (2009) 265–276.

[255] S.-C. Choi, S.-J. Kim, J.-H. Choi, C.-Y. Park, W.-J. Shim, D.-S. Lim, Fibroblast growth factor-2 and -4 promote the proliferation of bone marrow mesenchymal stem cells by the activation of the PI3K-Akt and ERK1/2 signaling pathways., *Stem Cells Dev.* 17 (2008) 725–736.

[256] Y.W. Eom, J.-E. Oh, J.I. Lee, S.K. Baik, K.-J. Rhee, H.C. Shin, et al., The role of growth factors in maintenance of stemness in bone marrow-derived mesenchymal stem cells., *Biochem. Biophys. Res. Commun.* 445 (2014) 1–7.

[257] J. Farré, S. Roura, C. Prat-Vidal, C. Soler-Botija, A. Llach, C.E. Molina, et al., FGF-4 increases in vitro expansion rate of human adult bone marrow-derived mesenchymal stem cells., *Growth Factors*. 25 (2007) 71–76.

[258] J. Reinders, U. Lewandrowski, J. Moebius, Y. Wagner, A. Sickmann, Challenges in mass spectrometry-based proteomics, *Proteomics*. 4 (2004) 3686–3703.

[259] R. Aebersold, M. Mann, Mass spectrometry-based proteomics., *Nature*. 422 (2003) 198–207.

[260] J.A. Burdick, G. Vunjak-Novakovic, Engineered microenvironments for controlled stem cell differentiation., *Tissue Eng. Part A*. 15 (2009) 205–19.

[261] H. Geiger, G. de Haan, M.C. Florian, The ageing haematopoietic stem cell compartment., *Nat. Rev. Immunol.* 13 (2013) 376–89.

[262] W.B. Ershler, J. Ross, J.L. Finlay, N.T. Shahidi, Bone-marrow microenvironment defect in congenital hypoplastic anemia, *N. Engl. J. Med.* 302 (1980) 1321–1327.

[263] Y. Dror, M.H. Freedman, Shwachman-Diamond syndrome: An inherited preleukemic bone marrow failure disorder with aberrant hematopoietic progenitors and faulty marrow microenvironment., *Blood*. 94 (1999) 3048–54.

[264] S. Aizawa, M. Nakano, O. Iwase, M. Yaguchi, M. Hiramoto, H. Hoshi, et al., Bone marrow stroma from refractory anemia of myelodysplastic syndrome is defective

in its ability to support normal CD34-positive cell proliferation and differentiation in vitro., *Leuk. Res.* 23 (1999) 239–46.

[265] E.A. McCulloch, L. Siminovitch, J.E. Till, E.S. Russell, S.E. Bernstein, The Cellular Basis of the Genetically Determined Hemopoietic Defect in Anemic Mice of Genotype Sl/Sld, *Blood*. 26 (1965) 399–410.

[266] J.E. Barker, Sl/Sld hematopoietic progenitors are deficient in situ, *Exp. Hematol.* 22 (1994) 174–177.

[267] J.E. Barker, Early transplantation to a normal microenvironment prevents the development of Steel hematopoietic stem cell defects, *Exp. Hematol.* 25 (1997) 542–547.

[268] C. a. Collins, I. Olsen, P.S. Zammit, L. Heslop, A. Petrie, T. a. Partridge, et al., Stem cell function, self-renewal, and behavioral heterogeneity of cells from the adult muscle satellite cell niche, *Cell*. 122 (2005) 289–301.

[269] C. Lepper, T. a Partridge, C.-M. Fan, An absolute requirement for Pax7-positive satellite cells in acute injury-induced skeletal muscle regeneration., *Development*. 138 (2011) 3639–3646.

[270] M.M. Murphy, J. a Lawson, S.J. Mathew, D. a Hutcheson, G. Kardon, Satellite cells, connective tissue fibroblasts and their interactions are crucial for muscle regeneration., *Development*. 138 (2011) 3625–3637.

[271] R. Sambasivan, R. Yao, A. Kissenpfennig, L. Van Wittenberghe, A. Paldi, B. Gayraud-Morel, et al., Pax7-expressing satellite cells are indispensable for adult skeletal muscle regeneration., *Development*. 138 (2011) 3647–3656.

[272] S.D. Gopinath, T. a. Rando, Stem Cell Review Series: Aging of the skeletal muscle stem cell niche, *Aging Cell*. 7 (2008) 590–598.

[273] P. Prasajak, P. Rattananinsruang, K. Chotinantakul, C. Dechsukhum, W. Leeanansaksiri, Embryonic stem cells conditioned medium enhances Wharton's jelly-derived mesenchymal stem cells expansion under hypoxic condition., *Cytotechnology*. 67 (2015) 493–505.

[274] H. Yousef, M.J. Conboy, J. Li, M. Zeiderman, T. Vazin, C. Schlesinger, et al., hESC-secreted proteins can be enriched for multiple regenerative therapies by heparin-binding., *Aging (Albany. NY).* 5 (2013) 357–72.

[275] A. Filby, J. Begum, M. Jalal, W. Day, Appraising the suitability of succinimidyl and lipophilic fluorescent dyes to track proliferation in non-quiescent cells by dye dilution, *Methods*. 82 (2015) 29–37.

[276] S.M. Prasad, M. Czepiel, C. Cetinkaya, K. Smigielska, S.C. Weli, H. Lysdahl, et al., Continuous hypoxic culturing maintains activation of Notch and allows long-term propagation of human embryonic stem cells without spontaneous differentiation., *Cell Prolif.* 42 (2009) 63–74.

[277] I. Rosová, M. Dao, B. Capoccia, D. Link, J. a Nolta, Hypoxic preconditioning results in increased motility and improved therapeutic potential of human mesenchymal stem cells., *Stem Cells*. 26 (2008) 2173–82.

[278] C.C. Tsai, Y.J. Chen, T.L. Yew, L.L. Chen, J.Y. Wang, C.H. Chiu, et al., Hypoxia inhibits senescence and maintains mesenchymal stem cell properties through down-regulation of E2A-p21 by HIF-TWIST, *Blood*. 117 (2011) 459–469.

[279] C. Conte, E. Riant, C. Toutain, F. Pujol, J.F. Arnal, F. Lenfant, et al., FGF2 translationally induced by hypoxia is involved in negative and positive feedback loops with HIF-1α, *PLoS One*. 3 (2008).

[280] L.S. Lu, S.J. Wang, R. Auerbach, In vitro and in vivo differentiation into B cells, T cells, and myeloid cells of primitive yolk sac hematopoietic precursor cells expanded > 100-fold by coculture with a clonal yolk sac endothelial cell line., *Proc. Natl. Acad. Sci. U. S. A.* 93 (1996) 14782–14787.

[281] L. Robb, Cytokine receptors and hematopoietic differentiation., *Oncogene*. 26 (2007) 6715–6723.

[282] K. Kaushansky, Lineage-Specific Hematopoietic Growth Factors, *N. Engl. J. Med.* 354 (2006) 2034–2045.

[283] J.L. Moran, Y. Li, A. a Hill, W.M. Mounts, C.P. Miller, Gene expression changes during mouse skeletal myoblast differentiation revealed by transcriptional profiling., *Physiol. Genomics*. 10 (2002) 103–111.

[284] C.H. Clegg, T. a. Linkhart, B.B. Olwin, S.D. Hauschka, Growth factor control of skeletal muscle differentiation: Commitment to terminal differentiation occurs in G1 phase and is repressed by fibroblast growth factor, *J. Cell Biol.* 105 (1987) 949–956.

[285] T. a Linkhart, C.H. Clegg, S.D. Hauschika, Myogenic differentiation in permanent clonal mouse myoblast cell lines: regulation by macromolecular growth factors in the culture medium., *Dev. Biol.* 86 (1981) 19–30.

[286] T. Uruno, J. Oki, K. Ozawa, K. Miyakawa, H. Ueno, T. Imamura, Distinct regulation of myoblast differentiation by intracellular and extracellular fibroblast growth factor-1., *Growth Factors*. 17 (1999) 93–113.

[287] S. a Coolican, D.S. Samuel, F.J. Mcwade, D.Z. Ewton, J.R. Florini, Cell Biology and Metabolism : The Mitogenic and Myogenic Actions of Insulin-like Growth Factors Utilize Distinct Signaling Pathways The Mitogenic and Myogenic Actions of Insulin-like Growth Factors Utilize Distinct Signaling Pathways *, *J. Biol. Chem.* 272 (1997) 6653–6662.

[288] M.L. Hribal, J. Nakae, T. Kitamura, J.R. Shutter, D. Accili, Regulation of insulin-like growth factor-dependent myoblast differentiation by Foxo forkhead transcription factors., *J. Cell Biol.* 162 (2003) 535–541.

[289] W.L. Murphy, T.C. McDevitt, A.J. Engler, Materials as stem cell regulators, *Nat. Mater.* 13 (2014).

[290] Y. Shao, J. Sang, J. Fu, On human pluripotent stem cell control: The rise of 3D bioengineering and mechanobiology, *Biomaterials*. 52 (2015) 26–43.

[291] J. Berger, J. Hauber, R. Hauber, R. Geiger, B.R. Cullen, Secreted placental alkaline phosphatase: a powerful new quantitative indicator of gene expression in eukaryotic cells, *Gene*. 66 (1988) 1–10.

[292] B.A. Tannous, Gaussia luciferase reporter assay for monitoring biological processes in culture and in vivo, *Nat. Protoc.* 4 (2009) 582–591.

[293] C. López-Otín, M. a Blasco, L. Partridge, M. Serrano, G. Kroemer, The hallmarks of aging., *Cell*. 153 (2013) 1194–217.

[294] T.A. Rando, Stem cells, ageing and the quest for immortality., *Nature*. 441 (2006) 1080–6.

[295] L. Liu, T.A. Rando, Manifestations and mechanisms of stem cell aging., *J. Cell Biol.* 193 (2011) 257–66.

[296] G. Van Zant, Y. Liang, Hematopoietic Stem Cell Aging , Life Span , and Transplantation, *Stem Cells Transl. Med.* 1 (2012) 651–657.

[297] I. Beerman, W.J. Maloney, I.L. Weissmann, D.J. Rossi, Stem cells and the aging hematopoietic system., *Curr. Opin. Immunol.* 22 (2010) 500–6.

[298] F. Li, F. Jin, a Freitas, P. Szabo, M.E. Weksler, Impaired regeneration of the peripheral B cell repertoire from bone marrow following lymphopenia in old mice., *Eur. J. Immunol.* 31 (2001) 500–5.

[299] L. a Warren, D.J. Rossi, Stem cells and aging in the hematopoietic system., *Mech. Ageing Dev.* 130 (2009) 46–53.

[300] A. Nakamura-Ishizu, T. Suda, Aging of the hematopoietic stem cells niche., *Int. J. Hematol.* 100 (2014) 317–25.

[301] A. Waterstrat, G. Van Zant, Effects of aging on hematopoietic stem and progenitor cells., *Curr. Opin. Immunol.* 21 (2009) 408–13.

[302] J.N.P. Smith, L.M. Calvi, Current Concepts in Bone Marrow Microenvironmental Regulation of Hematopoietic Stem and Progenitor Cells., *Stem Cells*. 31 (2013) 1044–1050.

[303] W. Wagner, P. Horn, S. Bork, A.D. Ho, Aging of hematopoietic stem cells is regulated by the stem cell niche., *Exp. Gerontol.* 43 (2008) 974–80.

[304] D.-M. Su, D. Aw, D.B. Palmer, Immunosenescence: a product of the environment?, *Curr. Opin. Immunol.* 25 (2013) 498–503.

[305] A. V Ergen, N.C. Boles, M. a Goodell, Rantes/Ccl5 influences hematopoietic stem cell subtypes and causes myeloid skewing., *Blood*. 119 (2012) 2500–9.

[306] S.R. Tuljapurkar, T.R. McGuire, S.K. Brusnahan, J.D. Jackson, K.L. Garvin, M. a Kessinger, et al., Changes in human bone marrow fat content associated with changes in hematopoietic stem cell numbers and cytokine levels with aging., *J. Anat.* 219 (2011) 574–81.

[307] S.J. Morrison, A.M. Wandycz, K. Akashi, A. Globerson, I.L. Weissman, The aging of hematopoietic stem cells, *Nat. Med.* 2 (1996) 1011–1016.

[308] D.E. Harrison, C.M. Astle, J.W. Doubleday, Cell lines from old immunodeficient donors give normal responses in young recipients, *J. Immunol. (Baltimore, Md. 1950)*. 118 (1977) 1223–1227.

[309] D. Ogden, H. Micklem, The Fate of Serially Transplated Bone Marrow Cell Populations from Young and Old Donors, *Transplantation*. 22 (1976) 287–293.

[310] Y. Liang, G. Van Zant, S.J. Szilvassy, Effects of aging on the homing and engraftment of murine hematopoietic stem and progenitor cells, *Blood*. 106 (2005) 1479–1487.

[311] G. Van Zant, K. Scott-Micus, B. Thompson, R. Fleischman, S. Perkins, Stem cell quiescence/activation is reversible by serial transplantation and is independent of stromal cell genotype in mouse aggregation chimeras, *Exp. Hematol.* 20 (1992) 470–475.

[312] A.S. Brack, T. a. Rando, Intrinsic Changes and Extrinsic Influences of Myogenic Stem Cell Function During Aging, *Stem Cell Rev.* 3 (2007) 226–237.

[313] J.M. Taylor-Jones, R.E. McGehee, T. a. Rando, B. Lecka-Czernik, D. a. Lipschitz, C. a. Peterson, Activation of an adipogenic program in adult myoblasts with age, *Mech. Ageing Dev.* 123 (2002) 649–661.

[314] J. V. Chakkalakal, K.M. Jones, M.A. Basson, A.S. Brack, The aged niche disrupts muscle stem cell quiescence, *Nature*. (2012).

[315] A. V Molofsky, S.G. Slutsky, N.M. Joseph, S. He, R. Pardal, J. Krishnamurthy, et al., Increasing p16INK4a expression decreases forebrain progenitors and neurogenesis during ageing., *Nature*. 443 (2006) 448–452.

[316] J. Nishino, I. Kim, K. Chada, S.J. Morrison, Hmga2 Promotes Neural Stem Cell Self-Renewal in Young but Not Old Mice by Reducing p16Ink4a and p19Arf Expression, *Cell*. 135 (2008) 227–239.

[317] V.M. Renault, V. a. Rafalski, A. a. Morgan, D. a. M. Salih, J.O. Brett, A.E. Webb, et al., FoxO3 Regulates Neural Stem Cell Homeostasis, *Cell Stem Cell*. 5 (2009) 527–539.

[318] H.G. Kuhn, H. Dickinson-Anson, F.H. Gage, Neurogenesis in the dentate gyrus of the adult rat: age-related decrease of neuronal progenitor proliferation., *J. Neurosci.* 16 (1996) 2027–2033.

[319] L. Bondolfi, F. Ermini, J.M. Long, D.K. Ingram, M. Jucker, Impact of age and caloric restriction on neurogenesis in the dentate gyrus of C57BL/6 mice, *Neurobiol. Aging*. 25 (2004) 333–340.

[320] a. Y. Maslov, Neural Stem Cell Detection, Characterization, and Age-Related Changes in the Subventricular Zone of Mice, *J. Neurosci.* 24 (2004) 1726–1733.

[321] M. Okamoto, K. Inoue, H. Iwamura, K. Terashima, H. Soya, M. Asashima, et al., Reduction in paracrine Wnt3 factors during aging causes impaired adult neurogenesis., *FASEB J.* 25 (2011) 3570–82.

[322] P. Bert, Experiences et Considerations Sur la Greffe Animale, *J. Anat. Physiol.* 1 (1864) 69–87.

[323] C. Mccay, F. Pope, W. Lunsford, G. Sperling, P. Sambhavaphol, Parabiosis between Old and Young Rats, *Gerontologia*. 1 (1957) 7–17.

[324] I.M. Conboy, T.A. Rando, Heterochronic parabiosis for the study of the effects of aging on stem cells and their niches, *Cell Cycle*. 11 (2012) 2260–2267.

[325] Y. Sun, W. Li, Z. Lu, R. Chen, J. Ling, Q. Ran, et al., Rescuing replication and osteogenesis of aged mesenchymal stem cells by exposure to a young extracellular matrix, *FASEB J.* 25 (2011) 1474–1485.

[326] C.P. Ng, A.R. Mohamed Sharif, D.E. Heath, J.W. Chow, C.B. Zhang, M.B. Chan-Park, et al., Enhanced ex vivo expansion of adult mesenchymal stem cells by fetal mesenchymal stem cell ECM, *Biomaterials*. 35 (2014) 4046–4057.

[327] Y. Zhang, D. Wang, K. Cao, M. Chen, X. Yang, Y. Tao, Rat Induced Pluripotent Stem Cells Protect H9C2 Cells from Cellular Senescence via a Paracrine Mechanism, *Cardiology*. 128 (2014) 43–50.

[328] H.J. Lee, E.G. Lee, S. Kang, J.-H. Sung, H.-M. Chung, D.H. Kim, Efficacy of microneedling plus human stem cell conditioned medium for skin rejuvenation: a randomized, controlled, blinded split-face study., *Ann. Dermatol.* 26 (2014) 584–91.

[329] K. Landin-Wllhelmsen, L. Wllhelmsen, G. Lappast, T. Rosen, G. Lindstedt, P.-A. Lundberg, et al., Serum insulin-like growth factor I in a random population sample of men and women: relation to age, sex, smoking habits, coffee consumption and physical activity, blood pressure and concentrations of plasma lipids, fibrinogen, parathyroid hormone and oste, *Clin. Endocrinol. (Oxf).* 41 (1994) 351–357.

[330] M.R. Rosen, Are stem cells drugs? The regulation of stem cell research and development., *Circulation*. 114 (2006) 1992–2000.

[331] M. Rincon, R. Muzumdar, G. Atzmon, N. Barzilai, The paradox of the insulin/IGF-1 signaling pathway in longevity, *Mech. Ageing Dev.* 125 (2004) 397–403.

[332] H.M. Brown-Borg, Hormonal control of aging in rodents: The somatotropic axis, *Mol. Cell. Endocrinol.* 299 (2009) 64–71.

[333] A. Musarò, C. Giacinti, G. Borsellino, G. Dobrowolny, L. Pelosi, L. Cairns, et al., Stem cell-mediated muscle regeneration is enhanced by local isoform of insulin-like growth factor 1., *Proc. Natl. Acad. Sci. U. S. A.* 101 (2004) 1206–10.

[334] a Musarò, K. McCullagh, a Paul, L. Houghton, G. Dobrowolny, M. Molinaro, et al., Localized Igf-1 transgene expression sustains hypertrophy and regeneration in senescent skeletal muscle., *Nat. Genet.* 27 (2001) 195–200.

[335] P. Cohen, I.A.N. Ocrant, P.J. Fielder, E.K. Nelly, S.E. Gargosky, C.I. Deal, et al., INSULIN-LIKE GROWTH FACTORS (IGFs): IMPLICATIONS FOR AGING IGFBP-1 IGFBP-2 IGFBP-3 IGFBP-4 IGFBP-5 IGFBP-6 Insulin [], 17 (1992) 335–342.

[336] P. Cohen, P. Fielder, Y. Hasegawa, H. Frisch, L. Giudice, R. Rosenfeld, Clinical aspects of insulin-like growth factor binding proteins, *Acta Endocrinol.* 124 (1991) 74–85.

[337] L.R. Donahue, S.J. Hunter, a P. Sherblom, C. Rosen, Age-related changes in serum insulin-like growth factor-binding proteins in women, *J Clin Endocrinol Metab*. 71 (1990) 575–579.

[338] E.S. Tzanakakis, D.J. Hess, D. Sielaff, W. Hu, Extracorporeal Tissue Engineered Liver-Assist Devices, *Annu. Rev. Biomed. Eng.* 02 (2000) 607–32.

[339] J. Rozga, F. Williams, M.S. Ro, D.F. Neuzil, T.D. Giorgio, G. Backfisch, et al., Development of a bioartificial liver: properties and function of a hollow-fiber module inoculated with liver cells., *Hepatology*. 17 (1993) 258–65.

[340] N.L. Sussman, M.G. Chong, T. Koussayer, D.E. He, T. a Shang, H.H. Whisennand, et al., Reversal of fulminant hepatic failure using an extracorporeal liver assist device., *Hepatology*. 16 (1992) 60–5.

[341] J. Gerlach, N. Schnoy, J. Vienken, M. Smith, P. Neuhaus, Comparison of hollow fibre membranes for hepatocyte immobilisation in bioreactors, *Int. J. Artif. Organs*. 19 (1996) 610–16.

[342] G.D. Wells, M.M. Fisher, M. V Sefton, Microencapsulation of viable hepatocytes in HEMA-MMA microcapsules: a preliminary study., *Biomaterials*. 14 (1993) 615–20.

[343] C. Zh, S. Zq, O. Gm, S. Am, Microencapsulated hepatocytes for bioartificial liver support., 12 (1988) 388–393.

[344] F.J. Wu, M. V Peshwa, F.B. Cerra, W.S. Hu, Entrapment of hepatocyte spheroids in a hollow fiber bioreactor as a potential bioartificial liver., *Tissue Eng.* 1 (1995) 29–40.

[345] F.J. Wu, J.R. Friend, A. Lazar, H.J. Mann, R.P. Remmel, F.B. Cerra, et al., Hollow fiber bioartificial liver utilizing collagen-entrapped porcine hepatocyte spheroids, *Biotechnol. Bioeng.* 52 (1996) 34–44.

[346] S.L. Nyberg, R. a Shatford, W.D. Payne, W.S. Hu, F.B. Cerra, Primary culture of rat hepatocytes entrapped in cylindrical collagen gels: an in vitro system with application to the bioartificial liver. Rat hepatocytes cultured in cylindrical collagen gels., *Cytotechnology*. 10 (1992) 205–15.

[347] B. David, M. Dufresne, M.-D. Nagel, C. Legallais, In vitro assessment of encapsulated C3A hepatocytes functions in a fluidized bed bioreactor., *Biotechnol. Prog.* 20 (2004) 1204–12.

[348] S.M. Coward, C. Legallais, B. David, M. Thomas, Y. Foo, D. Mavri-Damelin, et al., Alginate-encapsulated HepG2 Cells in a Fluidized Bed Bioreactor Maintain Function in Human Liver Failure Plasma, *Artif. Organs*. 33 (2009) 1117–1126.

[349] G. Lv, L. Zhao, A. Zhang, W. Du, Y. Chen, C. Yu, et al., Bioartificial liver system based on choanoid fluidized bed bioreactor improve the survival time of fulminant hepatic failure pigs., *Biotechnol. Bioeng.* 108 (2011) 2229–36.

[350] P. Wolf, The nature and significance of platelet products in human plasma., *Br. J. Haematol.* 13 (1967) 269–288.

[351] X.O. Breakefield, R.M. Frederickson, R.J. Simpson, Gesicles: Microvesicle "Cookies" for Transient Information Transfer Between Cells, *Mol. Ther.* 19 (2011) 1574–1576.

[352] G. Raposo, W. Stoorvogel, Extracellular vesicles: Exosomes, microvesicles, and friends, *J. Cell Biol.* 200 (2013) 373–383.

[353] C. Tetta, S. Bruno, V. Fonsato, M.C. Deregibus, G. Camussi, The role of microvesicles in tissue repair, *Organogenesis*. 7 (2011) 105–115.

[354] H. Valadi, K. Ekström, A. Bossios, M. Sjöstrand, J.J. Lee, J.O. Lötvall, Exosome-mediated transfer of mRNAs and microRNAs is a novel mechanism of genetic exchange between cells, *Nat. Cell Biol.* 9 (2007) 654–659.

[355] P.J. Quesenberry, M.S. Dooner, J.M. Aliotta, Stem cell plasticity revisited: The continuum marrow model and phenotypic changes mediated by microvesicles, *Exp. Hematol.* 38 (2010) 581–592.

[356] G. Camussi, M.C. Deregibus, C. Tetta, Paracrine/endocrine mechanism of stem cells on kidney repair: role of microvesicle-mediated transfer of genetic information., *Curr. Opin. Nephrol. Hypertens.* 19 (2010) 7–12.

[357] S. Gatti, S. Bruno, M.C. Deregibus, a. Sordi, V. Cantaluppi, C. Tetta, et al., Microvesicles derived from human adult mesenchymal stem cells protect against ischaemia-reperfusion-induced acute and chronic kidney injury, *Nephrol. Dial. Transplant.* 26 (2011) 1474–1483.

[358] M.Z. Ratajczak, M. Kucia, T. Jadczyk, N.J. Greco, W. Wojakowski, M. Tendera, et al., Pivotal role of paracrine effects in stem cell therapies in regenerative medicine: can we translate stem cell-secreted paracrine factors and microvesicles into better therapeutic strategies?, *Leukemia*. 26 (2012) 1166–1173.

[359] J. Ratajczak, K. Miekus, M. Kucia, J. Zhang, R. Reca, P. Dvorak, et al., Embryonic stem cell-derived microvesicles reprogram hematopoietic progenitors: evidence for horizontal transfer of mRNA and protein delivery., *Leukemia*. 20 (2006) 847–56.

[360] A. Yuan, E.L. Farber, A.L. Rapoport, D. Tejada, R. Deniskin, N.B. Akhmedov, et al., Transfer of MicroRNAs by Embryonic Stem Cell Microvesicles, *PLoS One*. 4 (2009) e4722.

[361] D. Katsman, E.J. Stackpole, D.R. Domin, D.B. Farber, Embryonic stem cell-derived microvesicles induce gene expression changes in Müller cells of the retina., *PLoS One*. 7 (2012) e50417.

[362] W.W. Stewart, H.E. Swaisgood, Characterization of calcium alginate pore diameter by size-exclusion chromatography using protein standards, *Enzyme Microb. Technol.* 15 (1993) 922–927.

[363] R. Glicklis, L. Shapiro, R. Agbaria, J.C. Merchuk, S. Cohen, Hepatocyte behavior within three-dimensional porous alginate scaffolds, *Biotechnol. Bioeng.* 67 (2000) 344–353.

[364] R. Yao, R. Zhang, J. Luan, F. Lin, Alginate and alginate/gelatin microspheres for human adipose-derived stem cell encapsulation and differentiation., *Biofabrication*. 4 (2012) 025007.

[365] T.Y. Hui, K.M.C. Cheung, W.L. Cheung, D. Chan, B.P. Chan, In vitro chondrogenic differentiation of human mesenchymal stem cells in collagen microspheres: influence of cell seeding density and collagen concentration., *Biomaterials*. 29 (2008) 3201–12.

[366] M.H. Hettiaratchi, T. Miller, J.S. Temenoff, R.E. Guldberg, T.C. McDevitt, Heparin microparticle effects on presentation and bioactivity of bone morphogenetic protein-2., *Biomaterials*. 35 (2014) 7228–38.

[367] T. Miller, M.C. Goude, T.C. McDevitt, J.S. Temenoff, Molecular engineering of glycosaminoglycan chemistry for biomolecule delivery., *Acta Biomater.* 10 (2014) 1705–19.

[368] C. Lee, I. Chu, Characterization of Modified Alginate-Poly-L-Lysine Microcapsules, *Artif. Organs*. 21 (1997) 1002–1006.

[369] N. Annabi, J.W. Nichol, X. Zhong, C. Ji, S. Koshy, A. Khademhosseini, et al., Controlling the Porosity and Microarchitecture of Hydrogels for Tissue Engineering, *Tissue Eng. Part B Rev.* 16 (2010) 371–383.

[370] K. Hayashi, S.M.C.D.S. Lopes, F. Tang, M.A. Surani, Dynamic equilibrium and heterogeneity of mouse pluripotent stem cells with distinct functional and epigenetic states., *Cell Stem Cell*. 3 (2008) 391–401.

[371] Y. Toyooka, D. Shimosato, K. Murakami, K. Takahashi, H. Niwa, Identification and characterization of subpopulations in undifferentiated ES cell culture., *Development*. 135 (2008) 909–18.

[372] T. Graf, M. Stadtfeld, Heterogeneity of embryonic and adult stem cells., *Cell Stem Cell*. 3 (2008) 480–3.

[373] S.R. Hough, A.L. Laslett, S.B. Grimmond, G. Kolle, M.F. Pera, A continuum of cell states spans pluripotency and lineage commitment in human embryonic stem cells., *PLoS One*. 4 (2009) e7708.

[374] C. Chazaud, Y. Yamanaka, T. Pawson, J. Rossant, Early lineage segregation between epiblast and primitive endoderm in mouse blastocysts through the Grb2-MAPK pathway., *Dev. Cell*. 10 (2006) 615–24.

[375] T. Enver, M. Pera, C. Peterson, P.W. Andrews, Stem cell states, fates, and the rules of attraction., *Cell Stem Cell*. 4 (2009) 387–97.

[376] J. Silva, A. Smith, Capturing pluripotency., *Cell*. 132 (2008) 532–6.

[377] T. Enver, S. Soneji, C. Joshi, J. Brown, F. Iborra, T. Orntoft, et al., Cellular differentiation hierarchies in normal and culture-adapted human embryonic stem cells., *Hum. Mol. Genet.* 14 (2005) 3129–40.

[378] A. Leahy, J.-W. Xiong, F. Kuhnert, H. Stuhlmann, Use of developmental marker genes to define temporal and spatial patterns of differentiation during embryoid body formation., *J. Exp. Zool.* 284 (1999) 67–81.

[379] G. Keller, Embryonic stem cell differentiation: emergence of a new era in biology and medicine., *Genes Dev.* 19 (2005) 1129–55.

[380] A.A. Sajini, L. V Greder, J.R. Dutton, J.M.W. Slack, Loss of Oct4 expression during the development of murine embryoid bodies., *Dev. Biol.* 371 (2012) 170–179.

[381] W. Risau, H. Sariola, H.G. Zerwes, J. Sasse, P. Ekblom, R. Kemler, et al., Vasculogenesis and angiogenesis in embryonic-stem-cell-derived embryoid bodies., *Development*. 102 (1988) 471–8.

[382] M. Esner, J. Pachernik, A. Hampl, P. Dvorak, Targeted disruption of fibroblast growth factor receptor-1 blocks maturation of visceral endoderm and cavitation in mouse embryoid bodies., *Int. J. Dev. Biol.* 46 (2002) 817–25.

[383] H. Wichterle, I. Lieberam, A. Jeffery, T.M. Jessell, Directed Differentiation of Embryonic Stem Cells into Motor Neurons ES Cell-Derived Motor Neurons, *Cell*. 110 (2002) 385–397.

[384] C. Xu, S. Police, N. Rao, M.K. Carpenter, Characterization and Enrichment of Cardiomyocytes Derived From Human Embryonic Stem Cells, *Circ. Res.* 91 (2002) 501–508.

[385] E.S. Ng, R.P. Davis, L. Azzola, E.G. Stanley, A.G. Elefanty, Forced aggregation of defined numbers of human embryonic stem cells into embryoid bodies fosters robust, reproducible hematopoietic differentiation., *Blood*. 106 (2005) 1601–3.

[386] S.J. Kattman, T.L. Huber, G.M. Keller, Multipotent flk-1+ cardiovascular progenitor cells give rise to the cardiomyocyte, endothelial, and vascular smooth muscle lineages., *Dev. Cell*. 11 (2006) 723–32.

[387] A.P. Van Winkle, I.D. Gates, M.S. Kallos, Mass Transfer Limitations in Embryoid Bodies during Human Embryonic Stem Cell Differentiation., *Cells. Tissues. Organs*. 196 (2012) 34–47.

[388] S.-H. Hong, T. Werbowetski-Ogilvie, V. Ramos-Mejia, J.B. Lee, M. Bhatia, Multiparameter comparisons of embryoid body differentiation toward human stem cell applications., *Stem Cell Res.* 5 (2010) 120–30.

[389] S. Niebruegge, C.L. Bauwens, R. Peerani, N. Thavandiran, S. Masse, E. Sevaptisidis, et al., Generation of human embryonic stem cell-derived mesoderm and cardiac cells using size-specified aggregates in an oxygen-controlled bioreactor., *Biotechnol. Bioeng.* 102 (2009) 493–507.

[390] B. Valamehr, S.J. Jonas, J. Polleux, R. Qiao, S. Guo, E.H. Gschweng, et al., Hydrophobic surfaces for enhanced differentiation of embryonic stem cell-derived embryoid bodies, *Proc. Natl. Acad. Sci.* 105 (2008) 14459–14464.

[391] J.M. Messana, N.S. Hwang, J. Coburn, J.H. Elisseeff, Z. Zhang, Size of the embryoid body influences chondrogenesis of mouse embryonic stem cells, *J. Tissue Eng. Regen. Med.* 2 (2008) 499–506.

[392] Y.Y. Choi, B.G. Chung, D.H. Lee, A. Khademhosseini, J.-H. Kim, S.-H. Lee, Controlled-size embryoid body formation in concave microwell arrays., *Biomaterials*. 31 (2010) 4296–303.

[393] T. Schroeder, Long-term single-cell imaging of mammalian stem cells, *Nat. Methods*. 8 (2011) S30–S35.

[394] J.F. Zhong, Y. Chen, J.S. Marcus, A. Scherer, S.R. Quake, C.R. Taylor, et al., A microfluidic processor for gene expression profiling of single human embryonic stem cells., *Lab Chip*. 8 (2008) 68–74.

[395] J.P. Jung, J.M. Squirrell, G.E. Lyons, K.W. Eliceiri, B.M. Ogle, Imaging cardiac extracellular matrices: a blueprint for regeneration., *Trends Biotechnol.* 30 (2012) 233–40.

[396] D.G. Buschke, D.J. Hei, K.W. Eliceiri, B.M. Ogle, Screening Approaches for Stem Cells, in: R. Gorodetsky (Ed.), Stem Cell-Based Tissue Repair, Royal Society of Chemistry, 2010: pp. 55–140.

[397] K. Chung, J. Wallace, S.-Y. Kim, S. Kalyanasundaram, A.S. Andalman, T.J. Davidson, et al., Structural and molecular interrogation of intact biological systems, *Nature*. 497 (2013) 332–337.

[398] K. Chung, C. a Rivet, M.L. Kemp, H. Lu, Imaging single-cell signaling dynamics with a deterministic high-density single-cell trap array, *Anal. Chem.* 83 (2011) 7044–52.

[399] V.A. Maltsev, J. Rohwedel, J. Hescheler, A.M. Wobus, Embryonic stem cells differentiate in vitro into cardiomyocytes representing sinusnodal, atrial and ventricular cell types., *Mech. Dev.* 44 (1993) 41–50.

[400] M. Schuldiner, R. Eiges, A. Eden, O. Yanuka, J. Itskovitz-Eldor, R.S. Goldstein, et al., Induced neuronal differentiation of human embryonic stem cells., *Brain Res.* 913 (2001) 201–5.

[401] A. Singh, S. Suri, T. Lee, J.M. Chilton, M.T. Cooke, W. Chen, et al., Adhesion strength–based, label-free isolation of human pluripotent stem cells, *Nat. Methods*. 10 (2013) 438–444.

[402] P.B. Lillehoj, H. Tsutsui, B. Valamehr, H. Wu, C.-M. Ho, Continuous sorting of heterogeneous-sized embryoid bodies., *Lab Chip*. 10 (2010) 1678–82.

[403] H.-W. Wu, R.-C. Hsu, C.-C. Lin, S.-M. Hwang, G.-B. Lee, An integrated microfluidic system for isolation, counting, and sorting of hematopoietic stem cells., *Biomicrofluidics*. 4 (2010).

[404] W.-T. Fung, A. Beyzavi, P. Abgrall, N.-T. Nguyen, H.-Y. Li, Microfluidic platform for controlling the differentiation of embryoid bodies., *Lab Chip*. 9 (2009) 2591–5.

[405] M. Khoury, A. Bransky, N. Korin, L.C. Konak, G. Enikolopov, I. Tzchori, et al., A microfluidic traps system supporting prolonged culture of human embryonic stem cells aggregates., *Biomed. Microdevices*. 12 (2010) 1001–8.

[406] S. Cui, Y. Liu, W. Wang, Y. Sun, Y. Fan, A microfluidic chip for highly efficient cell capturing and pairing., *Biomicrofluidics*. 5 (2011) 32003–320038.

[407] I. Kumano, K. Hosoda, H. Suzuki, K. Hirata, T. Yomo, Hydrodynamic trapping of Tetrahymena thermophila for the long-term monitoring of cell behaviors., *Lab Chip*. 12 (2012) 3451–3457.

[408] A. Lawrenz, F. Nason, J.J. Cooper-White, Geometrical effects in microfluidic-based microarrays for rapid, efficient single-cell capture of mammalian stem cells and plant cells., *Biomicrofluidics*. 6 (2012) 2411201–2411217.

[409] V. Lecault, M. Vaninsberghe, S. Sekulovic, D.J.H.F. Knapp, S. Wohrer, W. Bowden, et al., High-throughput analysis of single hematopoietic stem cell proliferation in microfluidic cell culture arrays., *Nat. Methods*. 8 (2011) 581–6.

[410] S.L. Faley, M. Copland, D. Wlodkowic, W. Kolch, K.T. Seale, J.P. Wikswo, et al., Microfluidic single cell arrays to interrogate signalling dynamics of individual, patient-derived hematopoietic stem cells., *Lab Chip*. 9 (2009) 2659–64.

[411] S.A. Kobel, O. Burri, A. Griffa, M. Girotra, A. Seitz, M.P. Lutolf, Automated analysis of single stem cells in microfluidic traps., *Lab Chip*. 12 (2012) 2843–9.

[412] C. Buhlmann, T. Preckel, S. Chan, G. Luedke, M. Valer, A New Tool for Routine Testing of Cellular Protein Expression : Integration of Cell Staining and Analysis of Protein Expression on a Microfluidic Chip-Based System, *J. Biomol. Tech.* 14 (2003) 119–127.

[413] M. Wu, T.D. Perroud, N. Srivastava, C.S. Branda, K.L. Sale, B.D. Carson, et al., Microfluidically-unified cell culture, sample preparation, imaging and flow cytometry for measurement of cell signaling pathways with single cell resolution., *Lab Chip*. 12 (2012) 2823.

[414] A.K. White, M. VanInsberghe, O.I. Petriv, M. Hamidi, D. Sikorski, M. a Marra, et al., High-throughput microfluidic single-cell RT-qPCR., *Proc. Natl. Acad. Sci.* 108 (2011) 13999–4004.

[415] J.P. Glotzbach, M. Januszyk, I.N. Vial, V.W. Wong, A. Gelbard, T. Kalisky, et al., An information theoretic, microfluidic-based single cell analysis permits identification of subpopulations among putatively homogeneous stem cells., *PLoS One*. 6 (2011) e21211.

[416] E. Sachlos, D.T. Auguste, Embryoid body morphology influences diffusive transport of inductive biochemicals: a strategy for stem cell differentiation., *Biomaterials*. 29 (2008) 4471–80.

[417] D.E. White, M.A. Kinney, T.C. McDevitt, M.L. Kemp, Spatial pattern dynamics of 3D stem cell loss of pluripotency via rules-based computational modeling, *PLoS Comput. Biol.* 9 (2013) e1002952.

VITA

JENNA L. WILSON

Jenna was born in Lodi, California. She attended public schools in the Roseburg Public School District in Roseburg, Oregon, and received an honors B.S. in Bioengineering from Oregon State University in Corvallis, Oregon in 2010 before coming to Georgia Tech to pursue a doctorate in Bioengineering. Jenna enjoys cooking (and eating), traveling, playing nerdy tabletop RPGs, and spending time with her human and animal family.